DIAGENESIS AND POROSITY DEVELOPMENT OF MISSION CANYON RESERVOIR INTERVAL IN 07 43B POOL, PIERSON FIELD, MANITOBA

A Thesis

Submitted to

The Faculty of Graduate Studies

The University of Manitoba

In Partial Fulfillment

of the Requirements for the Degree

Master of Science

---

by

© Mushfique Ahmed

ISBN 0-315-33824-5

DIAGENESIS AND POROSITY DEVELOPMENT OF MISSION CANYON RESERVOIR INTERVAL IN 07 43B POOL, PIERSON FIELD, MANITOBA

BY

MUSHFIQUE AHMED

A thesis submitted to the Faculty of Graduate Studies of the University of Manitoba in partial fulfillment of the requirements of the degree of

MASTER OF SCIENCE

ABSTRACT

The 07 43B pool is in the northeastern part of the Pierson field located in southwestern Manitoba. This pool is situated within the subcrop of Mississippian MC-3a beds which constitute the producing zone. The MC-3a beds can be correlated with beds in the adjacent Waskada area of southwestern Manitoba.

In the study area, the MC-3a beds represent a carbonate tidal flat complex. Four lithofacies have been identified. These are: algal, vadolite, bioclastic grainstone and peloidal grainstone facies. Except for the vadolite facies, all other facies refer to depositional environments. The vadolite is likely to have formed from subaerial exposure in a strandline environment during early diagenesis.

Diagenetic alteration has been broadly divided into early and late. The early diagenesis is characterized principally by biological diagenesis, formation of vadolite, and calcite cementation. The late stage of diagenesis includes dolomitization, anhydritization, the formation of other authigenic minerals, compaction, pressure solution, fracturing, and leaching. A relative chronology of these events has been reconstructed which, in general, shows considerable overlap of the diagenetic processes.

The development of porosity is not true facies selective. Late diagenetic processes have been inferred to control the preservation of primary porosity as well as the

development of leached porosity and minor intercrystalline porosity. However, facies with higher primary porosity (e.g, vadolite) are more likely to show higher porosity development, and consequently represent the principal reservoir facies. Oil has been found in the traps of primarily structural origin; this is true with the limitation of updip and/or lateral facies change involving porosity development.

TABLE OF CONTENTS

CHAPTER PAGE

LIST OF FIGURES

LIST OF TABLES

LIST OF PLATES

ACKNOWLEDGEMENT

The author extends his sincere gratitude to his advisor Dr. W.M. Last for the advice and aid given in the preparation of this manuscript.

The author is grateful to S.P. Halabura and the Manitoba Mines Branch for permission to work in the government core storage facilities at the University of Manitoba.

Special thanks to Dr. R.J. Elias for his aid in identifying microfossils.

The author is indebted to Dr. A.C. Turnock for his assistance in identifying minerals in thin sections, and photographic assistance. Photographic assistance by R. Pryhitko and R. McCauley is also acknowledged.

Special thanks must be given to B. Hansen, M. Rogers, and W. Morningstar for their constructive comments and suggestions.

The author wishes to acknowledge the financial support provided by the Canadian Commonwealth Scholarship and Fellowship Committee.

Lastly, thanks to Brenda Lye, who typed this manuscript.

CHAPTER 1

INTRODUCTION

1.1 Location

The Pierson oil field is situated in the extreme southwest corner of the Province of Manitoba lying about 23 km north of the Canadian - United States border, and about 9 km east of Manitoba - Saskatchewan border (Fig. 1). It is located within Townships 2 and 3, Ranges 28 and 29 WPM.

The 07 43B pool (also known as MC-3aB pool), is the largest of the Pierson field pools, and is located in the northeastern part of the field. This pool, confined to Township 3 and Ranges 28 and 29 WPM, is within the Mississippian MC-3a subcrop (Fig. 2). The discovery well of this pool at 13-17-3-28 W1 was drilled by King Resources Ltd. and Partners in 1965.

1.2 Purpose of Study

The purpose of this study is to provide a geologic assessment of the producing interval MC-3a beds, in the 07 43B pool, Pierson field. The objectives were to:

1. Illustrate the stratigraphic relationships of the MC-3a beds.
2. Describe the trapping mechanisms of hydrocarbon.
3. Identify the depositional facies.
4. Document the sequence of diagenetic events.
5. Explain the development of porosity.

NOTICE/AVIS

PAGE(S) Fig. 1 IS/ARE EST/SONT filmed IN SECTIONS

PLEASE WRITE TO THE AUTHOR FOR INFORMATION, OR CONSULT THE ARCHIVAL COPY HELD IN THE DEPARTMENT OF ARCHIVES AND SPECIAL COLLECTIONS, ELIZABETH DAFOE LIBRARY, UNIVERSITY OF MANITOBA, WINNIPEG, MANITOBA, CANADA, R3T 2N2.

VEUILLEZ ECRIRE A L'AUTEUR POUR LES RENSEIGNEMENTS OU VEUILLEZ CONSULTER L'EXEMPLAIRE DONT POSSEDE LE DEPARTEMENT DES ARCHIVES ET DES COLLECTIONS SPECIALES, BIBLIOTHEQUE ELIZABETH DAFOE, UNIVERSITE DU MANITOBA, WINNIPEG, MANITOBA, CANADA, R3T 2N2.

Fig. 1 Location map of the study area. (After Pool Location Map, Petroleum Branch, Department of Energy and Mines, Manitoba, 1983).

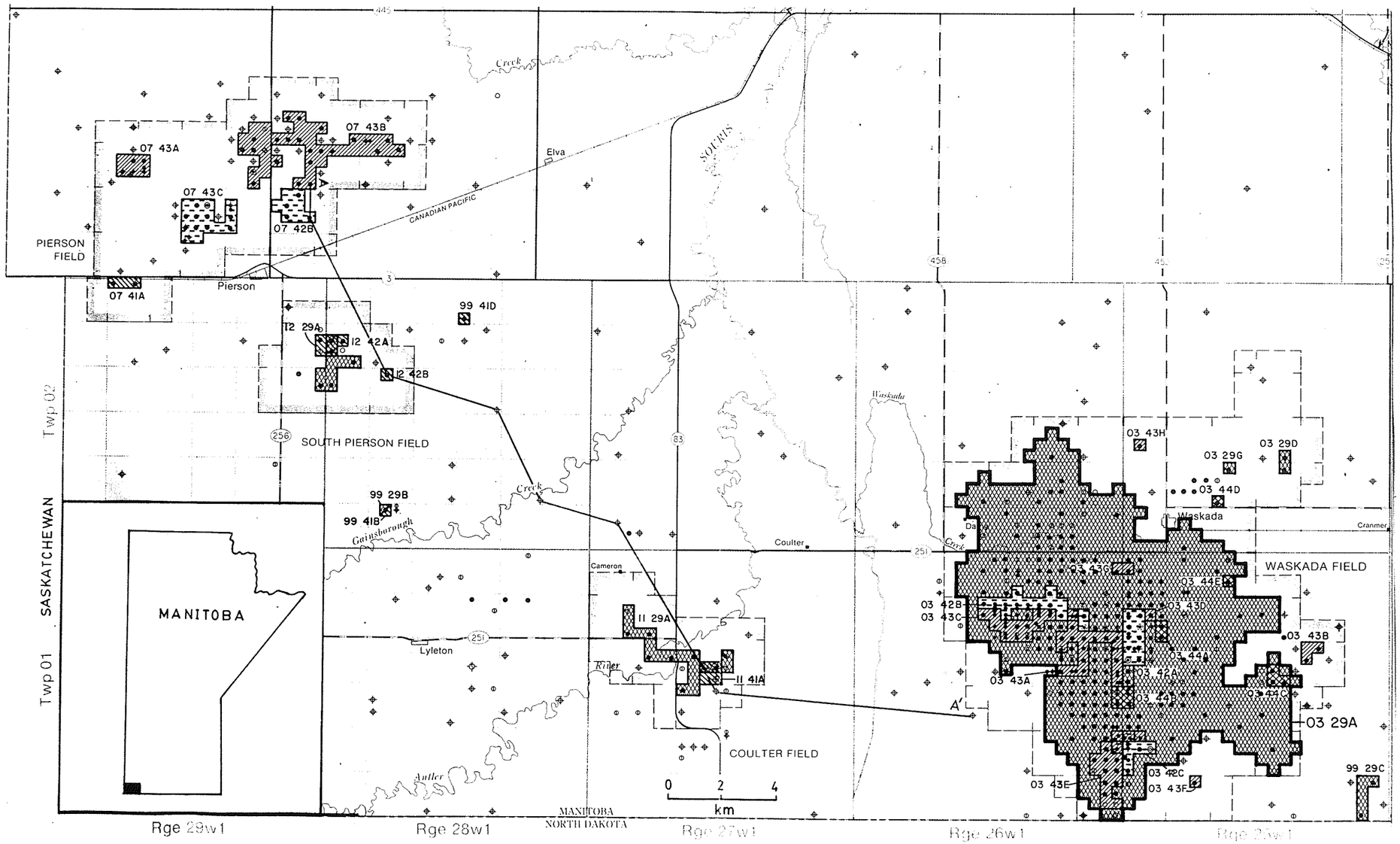
07 43B
07 43A
07 43C
07 42B
PIERSON FIELD
07 41A
Pierson
CANADIAN PACIFIC
Elva
SOURIS
Creek
99 41D
12 29A
12 42A
12 42B
SOUTH PIERSON FIELD
99 29B
99 41B
Gainsborough
Creek
Coulter
Cameron
11 29A
11 41A
Lyleton
Antler
COULTER FIELD
0 2 4
km
Waskada
03 43H
03 29D
03 29G
03 44D
Cranmer
WASKADA FIELD
03 43G
03 44E
03 42B
03 43C
03 43D
03 43B
03 44B
03 42A
03 43A
03 44C
03 29A
03 42C
03 43E
03 43F
99 29C
A'
MANITOBA
Twp 02
Twp 01
SASKATCHEWAN
MANITOBA
NORTH DAKOTA
Rge 29w1
Rge 28w1
Rge 27w1
Rge 26w1
Rge 25w1

Fig. 1

Fig. 2 Mission Canyon subcrop-southwestern Manitoba (After Halabura, 1984)

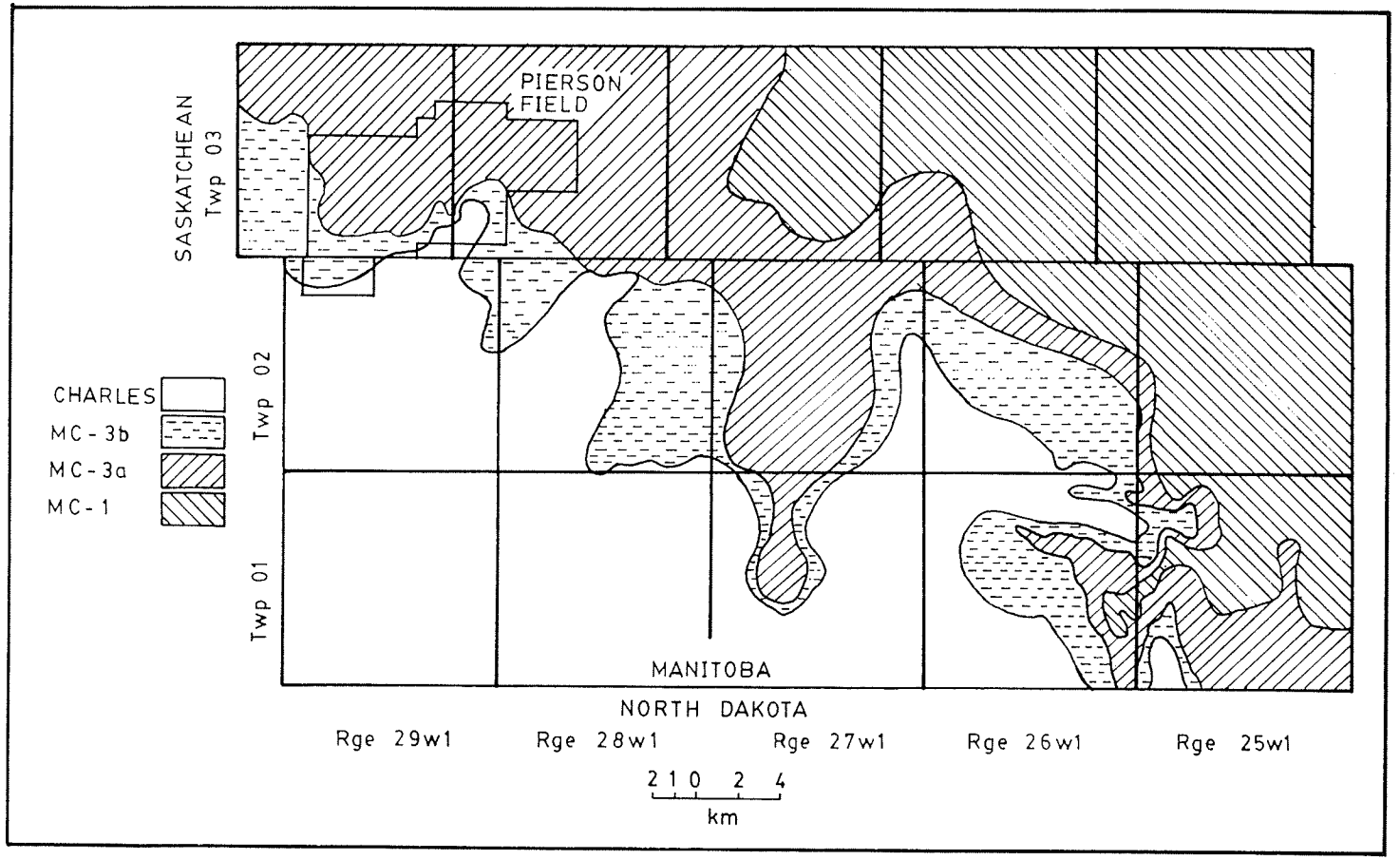
PIERSON
FIELD
SASKATCHEAN
Twp 03
Twp 02
Twp 01
CHARLES
MC-3b
MC-3a
MC-1
MANITOBA
NORTH DAKOTA
Rge 29w1
Rge 28w1
Rge 27w1
Rge 26w1
Rge 25w1
2 1 0 2 4
km

Fig·2

1.3 Methods of Study

All available cores of studied pool were examined and sampled. These are: 1-18-3-28 W1 (17.98 m), 3-20-2-28 W1 (10.67 m), 2-13-3-29 W1 (7.67 m), 14-13-3-29 W1 (8.13 m) and 15-13-3-29 W1 (7.92 m). Geophysical logs from the wells were also examined.

Stratigraphic and structural data were presented in the form of cross-sections, structure contour maps and isopach map.

To study the sedimentary petrography polished representative slabs from the drill cores were examined both parallel and perpendicular to the stratification under a binocular microscope. A total of 144 thin sections were prepared from the rock plaquettes cut both parallel and perpendicular to stratification from the slabs, and stained with Alazarin Red S. The thin sections were studied under a Leitz Wetzlar SM-LUX-POL microscope and lithologic logs were prepared from the obtained data. Photomicrographs of prepared thin sections and polished core slabs as well as photographs of polished core slabs were taken to document the data.

Porosity and permeability data from core analysis were available for two studied drilled cores. For the rest of the cores estimation of porosity was carried out microscopically.

To show the interrelationships of various parameters responsible for the development of porosity a correlation

matrix was prepared using data from the section below the altered zone in 1-18-3-28 W1 well. The determinations of amount of dolomite rhombs and anhydrite as well as dolomite rhomb size was carried out microscopically. The mean and the standard deviation of dolomite rhomb size were calculated on the basis of measurements of twenty randomly selected dolomite crystals along the long diagonals of the rhombs.

1.4 Previous Work

McCabe (1959) in his regional stratigraphic study first covered the Pierson area. Later McCabe (1963) discussed the stratigraphic and structural factors responsible for the oil accumulation in the MC-3a beds in the Pierson field. These works were published before the discovery of the 07 43B pool. Ghazar (1978) undertook a reconnaissance study to evaluate the hydrocarbon potential in the Pierson area. The only other work is a detailed stratigraphic and sedimentological study of the MC-3 Member in this area by Halabura (1984). These studies provided specific information relevant to the present study.

Previous studies of the Mission Canyon sequence in adjoining areas gave rise to a number of different predictions regarding the porosity development. Gerhard et al. (1978) suggested that permeability of the Frobisher-Alida beds producing in the Glenburn field (northeastern Williston Basin), North Dakota is associated with early diagenetic strandline vadose pisolite. This coated-grain

facies was previously regarded as oolite formed in agitated water of submarine shoals on a platform edge far away basinward from the shoreline. Elliot (1982) and McCulloch-Smith (1984) working on the Haas field (northeastern Williston Basin), North Dakota and the Woodnorth field, southwestern Manitoba respectively concluded that most porosity was secondary or secondarily enlarged and resulted from leaching of calcite during later diagenesis. Lindsay (1982), Lindsay and Roth (1982), and Lindsay and Kendall (1984, quoted by Elliot, 1982), in their study on Little Knife field (central Williston Basin), North Dakota related the development of porosity to early diagenetic anhydrite replacement of skeletal fragments followed by dolomitization of the muddy matrix, and late diagenetic anhydrite leaching. These contrasting scenarios may reflect either regional differences or different interpretations of similar processes due to lack of sufficient data.

1.5 Regional Geology

Southwestern Manitoba constitutes the northeastern corner of the Williston Basin (Fig. 3). The Williston Basin encompasses an area of about 160,934 sq. km with its centre in northwestern North Dakota (McCabe, 1959).

The Williston Basin may be defined as an autogeosyncline of Kay (1951) or an intracratonic basin of Krumbein and Sloss (1951) (Laird, 1956).

It had been tectonically active from Ordovician to

Fig. 3 Outline map of the Williston Basin (After McCabe 1959).

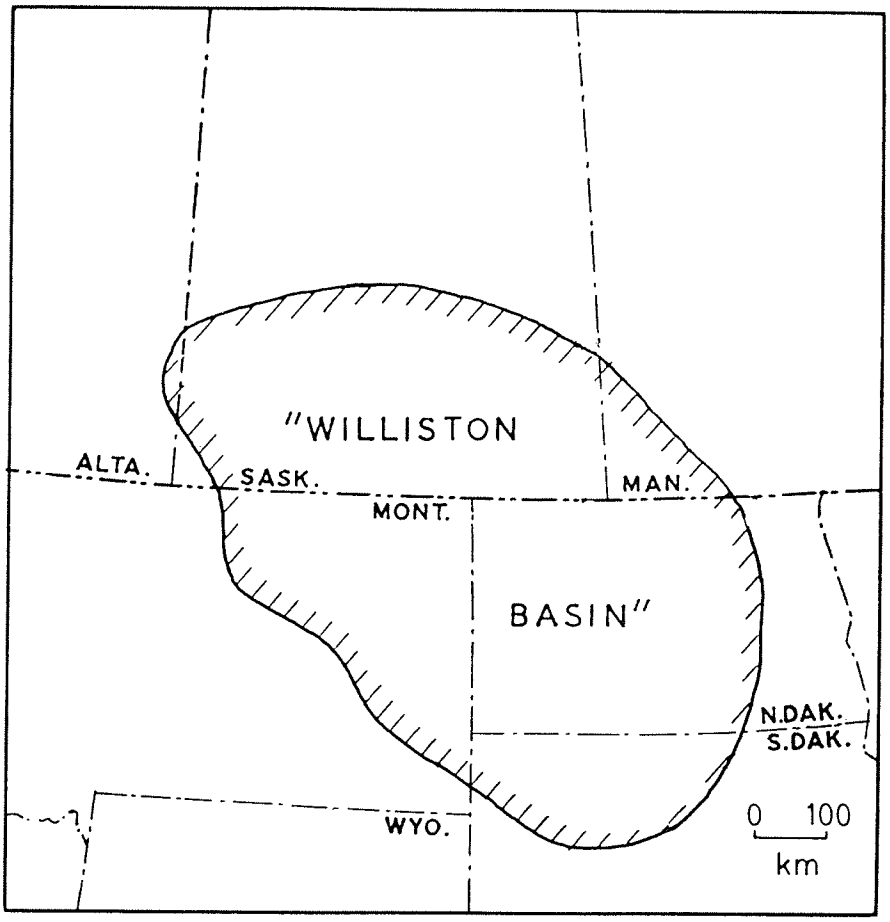

Fig. 3

Cretaceous time and, hence, was the principal feature governing the pattern of sedimentation in this region during this time (McCabe, 1971).

Two gross lithologic sequences are present in southwestern Manitoba:

1. The lower Paleozoic sequences composed almost entirely of carbonate rocks.
2. The upper Mesozoic and Cenozoic sequences consisting mainly of shale and sandstone.

These two sequences are separated by a pronounced angular unconformity (Fig. 4) which results in the burial of the entire Mississippian system as well as the upper part of the Devonian beneath the overlapping Mesozoic strata. Consequently, an irregular series of northwest trending subcrop belts developed beneath the Jurassic strata.

The Mississippian system in southwestern Manitoba consists of four formations. These are, from bottom to top: Bakken, Lodgepole, Mission Canyon, and Charles Formations (Fig. 5).

The Bakken Formation consists of two highly radioactive black shales separated by grey variegated calcareous sandstones, siltstones or dolomites, and conformably overlies upper Devonian strata (Ghazar, 1978). This formation is one of the three significant source rocks for hydrocarbon in the Williston Basin (Williams, 1974).

The Lodgepole Formation rests conformably on the Bakken Formation, and is composed of argillaceous, cherty,

Fig. 4 Cross-section - southwestern Manitoba. (After McCabe, 1963).

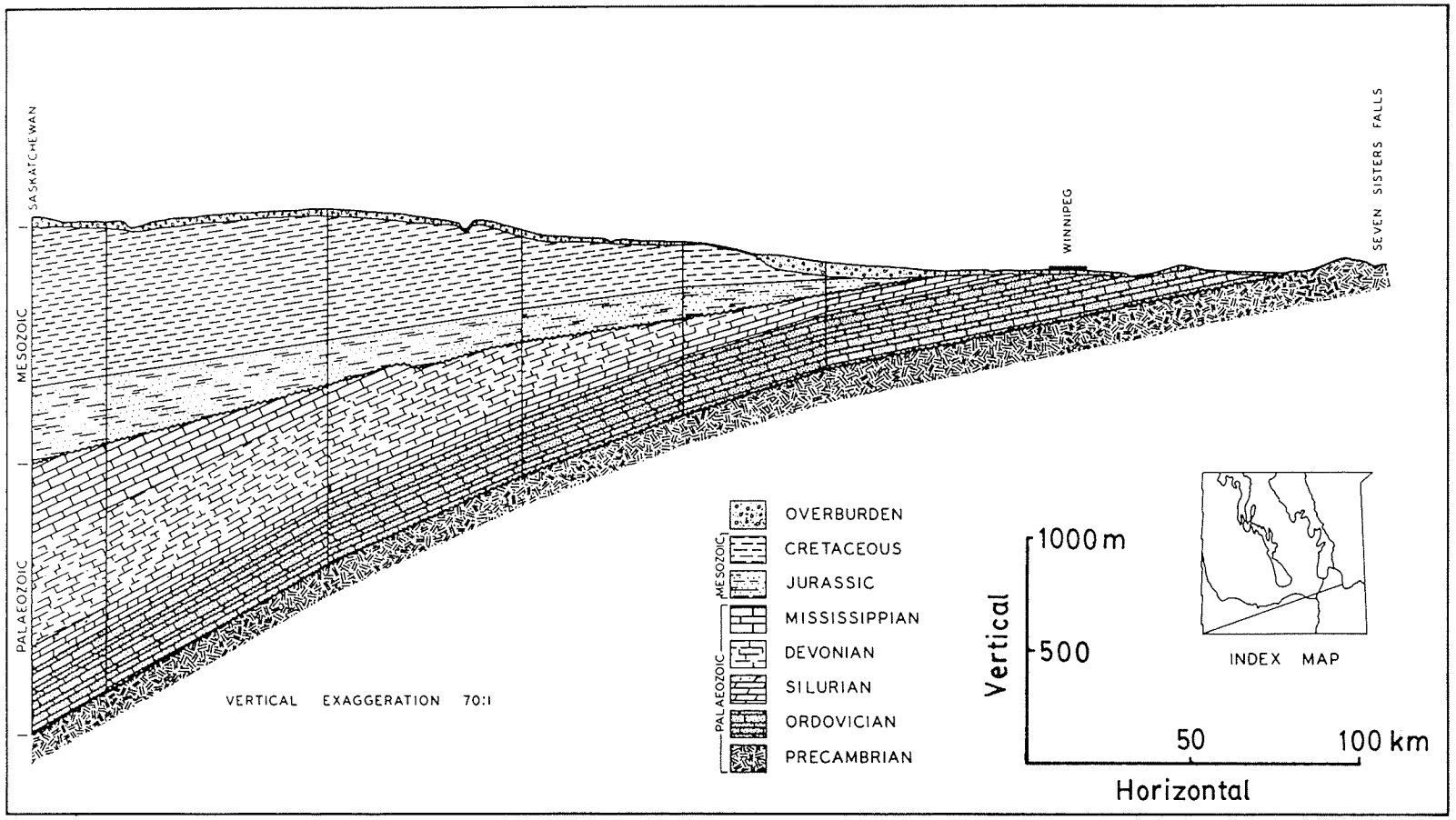
SASKATCHEWAN
MESOZOIC
PALAEOZOIC
WINNIPEG
SEVEN SISTERS FALLS
VERTICAL EXAGGERATION 70:1
OVERBURDEN
CRETACEOUS
JURASSIC
MISSISSIPPIAN
DEVONIAN
SILURIAN
ORDOVICIAN
PRECAMBRIAN
MESOZOIC
PALAEOZOIC
1000 m
500
Vertical
INDEX MAP
50
100 km
Horizontal

Fig. 4

NOTICE/AVIS

PAGE(S) Fig. 5 IS/ARE EST/SONT filmed in sections

PLEASE WRITE TO THE AUTHOR FOR INFORMATION, OR CONSULT THE ARCHIVAL COPY HELD IN THE DEPARTMENT OF ARCHIVES AND SPECIAL COLLECTIONS, ELIZABETH DAFOE LIBRARY, UNIVERSITY OF MANITOBA, WINNIPEG, MANITOBA, CANADA, R3T 2N2.

VEUILLEZ ECRIRE A L'AUTEUR POUR LES RENSEIGNEMENTS OU VEUILLEZ CONSULTER L'EXEMPLAIRE DONT POSSEDE LE DEPARTEMENT DES ARCHIVES ET DES COLLECTIONS SPECIALES, BIBLIOTHEQUE ELIZABETH DAFOE, UNIVERSITE DU MANITOBA, WINNIPEG, MANITOBA, CANADA, R3T 2N2.

Fig. 5 Mississippian Correlation and Nomenclature Chart. (After McCabe, 1959).

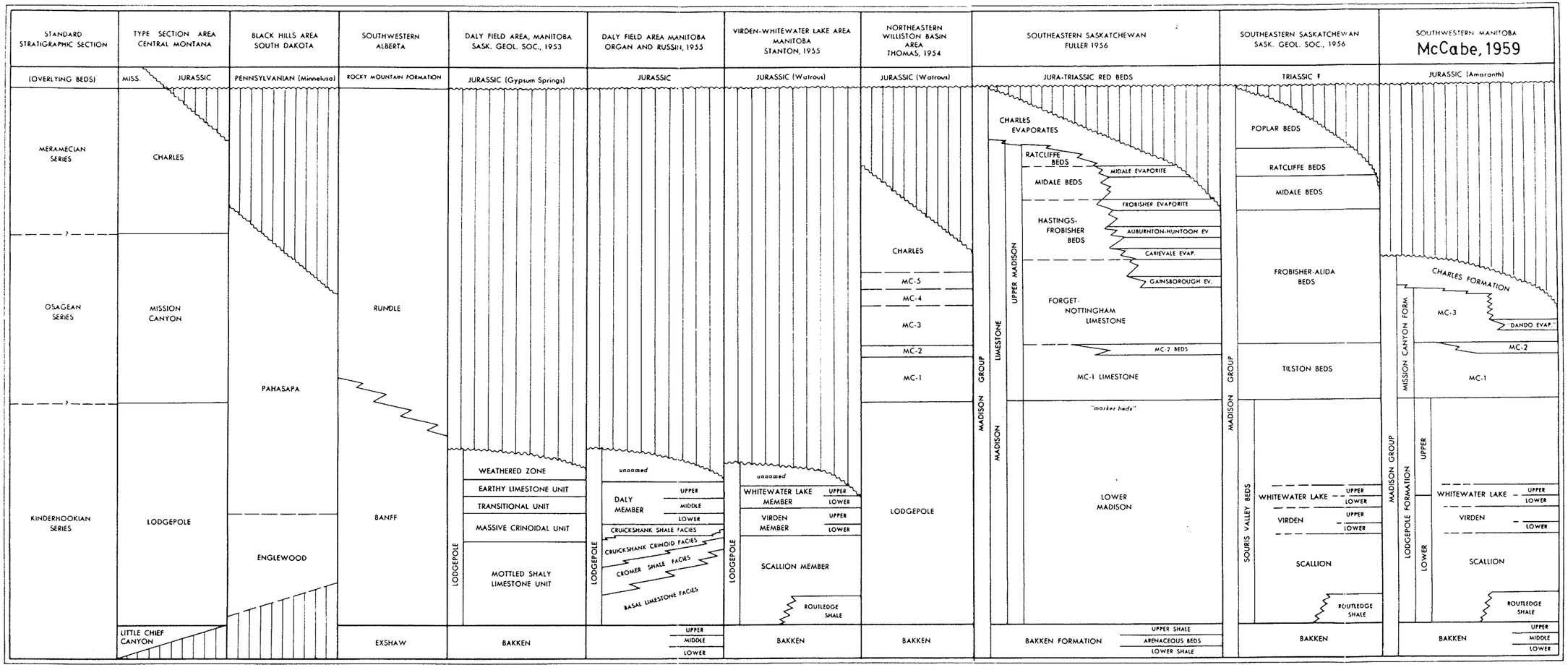
STANDARD STRATIGRAPHIC SECTION
TYPE SECTION AREA CENTRAL MONTANA
BLACK HILLS AREA SOUTH DAKOTA
SOUTHWESTERN ALBERTA
DALY FIELD AREA, MANITOBA SASK. GEOL. SOC., 1953
DALY FIELD AREA MANITOBA ORGAN AND RUSSIN, 1955
VIRDEN-WHITEWATER LAKE AREA MANITOBA STANTON, 1955
NORTHEASTERN WILLISTON BASIN AREA THOMAS, 1954
SOUTHEASTERN SASKATCHEWAN FULLER 1956
SOUTHEASTERN SASKATCHEWAN SASK. GEOL. SOC., 1956
SOUTHWESTERN MANITOBA McCabe, 1959
(OVERLYING BEDS)
MISS.
JURASSIC
PENNSYLVANIAN (Minnelusa)
ROCKY MOUNTAIN FORMATION
JURASSIC (Gypsum Springs)
JURASSIC
JURASSIC (Watrous)
JURASSIC (Watrous)
JURA-TRIASSIC RED BEDS
TRIASSIC ?
JURASSIC (Amaranth)
MERAMECIAN SERIES
CHARLES
OSAGEAN SERIES
MISSION CANYON
KINDERHOOKIAN SERIES
LODGEPOLE
LITTLE CHIEF CANYON
PAHASAPA
ENGLEWOOD
RUNDLE
BANFF
EXSHAW
WEATHERED ZONE
EARTHY LIMESTONE UNIT
TRANSITIONAL UNIT
MASSIVE CRINOIDAL UNIT
MOTTLED SHALY LIMESTONE UNIT
BAKKEN
LODGEPOLE
unnamed
DALY MEMBER
UPPER
MIDDLE
LOWER
CRUICKSHANK SHALE FACIES
CRUICKSHANK CRINOID FACIES
CROMER SHALE FACIES
BASAL LIMESTONE FACIES
BAKKEN
LODGEPOLE
unnamed
WHITEWATER LAKE MEMBER
UPPER
LOWER
VIRDEN MEMBER
UPPER
LOWER
SCALLION MEMBER
ROUTLEDGE SHALE
BAKKEN
LODGEPOLE
CHARLES
MC-5
MC-4
MC-3
MC-2
MC-1
MADISON GROUP
BAKKEN
CHARLES EVAPORATES
RATCLIFFE BEDS
MIDALE BEDS
MIDALE EVAPORITE
FROBISHER EVAPORITE
HASTINGS-FROBISHER BEDS
AUBURNTON-HUNTOON EV.
CARIEVALE EVAP.
GAINSBOROUGH EV.
FORGET-NOTTINGHAM LIMESTONE
MC-2 BEDS
MC-1 LIMESTONE
"marker beds"
LOWER MADISON
LIMESTONE
UPPER MADISON
MADISON
BAKKEN FORMATION
UPPER SHALE
ARENACEOUS BEDS
LOWER SHALE
POPLAR BEDS
RATCLIFFE BEDS
MIDALE BEDS
FROBISHER-ALIDA BEDS
TILSTON BEDS
MADISON GROUP
SOURIS VALLEY BEDS
WHITEWATER LAKE
UPPER
LOWER
VIRDEN
UPPER
LOWER
SCALLION
ROUTLEDGE SHALE
BAKKEN
CHARLES FORMATION
MC-3
DANDO EVAP.
MC-2
MC-1
MISSION CANYON FORM.
MADISON GROUP
LODGEPOLE FORMATION
UPPER
LOWER
WHITEWATER LAKE
UPPER
LOWER
VIRDEN
LOWER
SCALLION
ROUTLEDGE SHALE
BAKKEN
UPPER
MIDDLE
LOWER

Fig. 5

bioclastic limestone with interbedded silty shales (Ghazar, 1978).

The Mission Canyon Formation overlies the Lodgepole Formation conformably. It is composed of bioclastic, oolitic, and algal limestones with intercalations of thin but fairly persistent silty dolomites (Ghazar, 1978).

Conformably resting on the Mission Canyon Formation is a sequence of anhydrite, dolomite, and red and green shales of Charles Formation (Ghazar, 1978).

These Mississippian strata are unconformably overlain by Jurassic Amaranth red beds.

1.6 Stratigraphy of the Study Area

The Mission Canyon Formation has been divided into three members (McCabe, 1959). These are, in the ascending order, MC-1, MC-2, and MC-3 Members.

Ghazar (1978) described the MC-1 Member as consisting of dense, cherty, crinoidal limestones in the basal part through finely granular chalky limestone to oolitic and algal zones in the upper part.

The overlying MC-2 Member is composed of anhydrite and argillaceous, microcrystalline algal dolomite (Ghazar, 1978).

According to Ghazar (1978), the succeeding MC-3 Member is a dense cherty, crinoidal limestone in the basal part to porous oolitic finely comminuted crinoidal limestone in the upper part. The Pierson field produces from MC-3 Member.

The MC-3 Member has been further subdivided into lower

(MC-3a) and upper (MC-3b) intervals with MC-3 marker bed separating them (Halabura, 1984). The producing horizons of the 07 43B pool have been found in the MC-3a beds.

Fig. 6 (Back Pocket) shows correlation of Mission Canyon Formation between the Pierson and Waskada areas.

1.7 Hydrocarbon Traps of the Study Area

Three styles of hydrocarbon trapping, namely, structural-topographic, truncation and facies traps have been found in the study area, and each of these is described below.

1.7.1 Structural-Topographic Traps

The Mississippian erosion surface is characterized by "highs" or "noses" (Fig. 7 and Fig. 1) representing primarily the sites of oil accumulation.

Local thinning of Jurassic red beds (Fig. 8) depicting topographic "highs" is somewhat coincidental with these structures. However, a remarkable resemblance between structure contours on the Mississippian erosion surface and on the top of MC-2 marker has been observed (Fig. 9).

McCabe (1959) suggested that these "highs" on the Mississippian erosion surface are structural, and originated for the most part subsequent to the period of erosion, and prior to, or contemporaneous with, red beds deposition. Alternatively, they may represent principally topographic "highs", created by the differential erosion during the

Fig. 7 Structure contour map (in meters) on Mississippian erosion surface. (After Halabura, 1984).

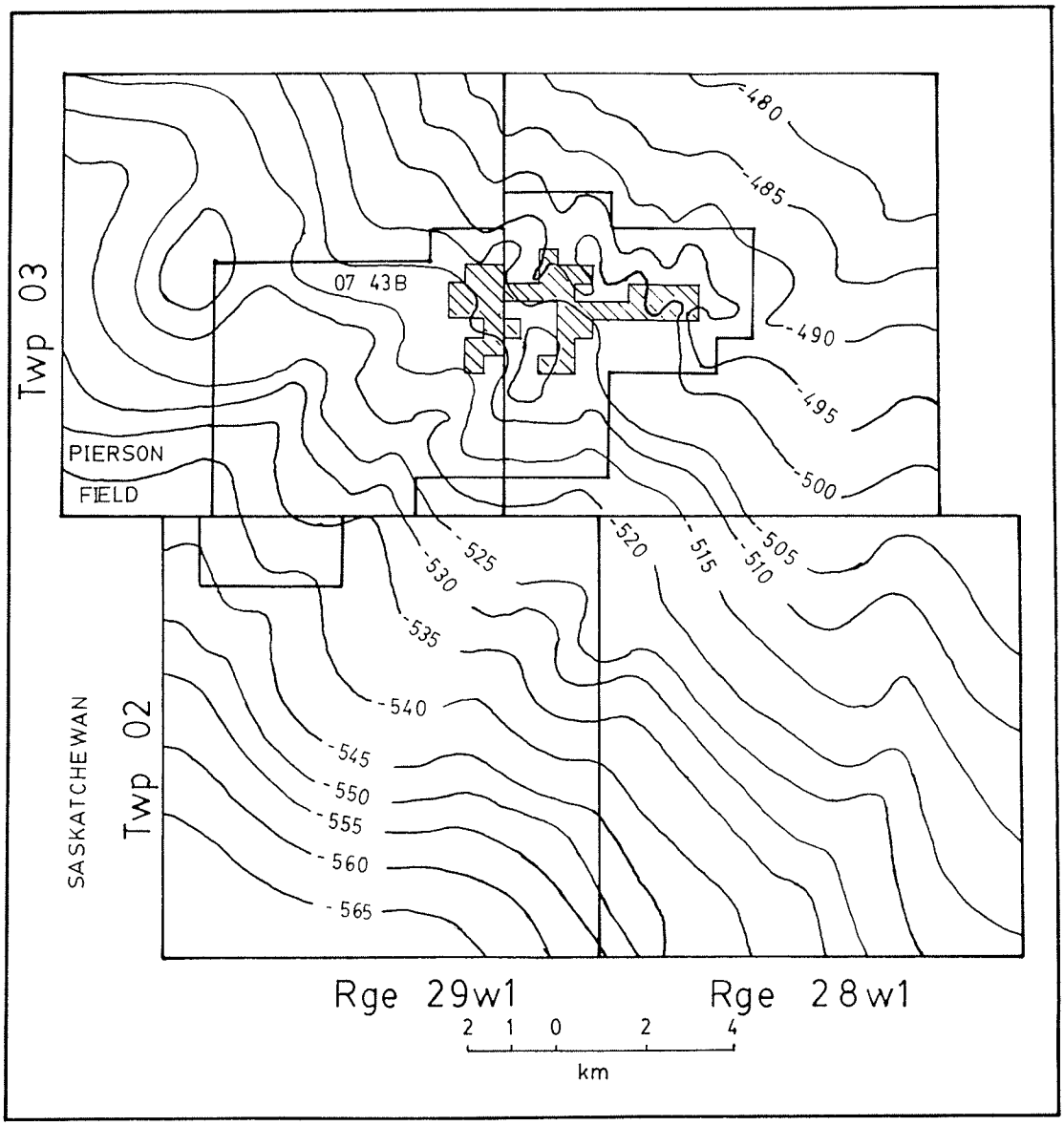
Twp 03
07 43B
PIERSON
FIELD
480
485
490
495
500
505
510
515
520
525
530
535
540
545
550
555
560
565
SASKATCHEWAN
Twp 02
Rge 29w1
Rge 28w1
2 1 0 2 4
km

Fig·7

Fig. 8 Isopach map (in meters) of the Lower Amaranth Formation. (After Halabura, 1984).

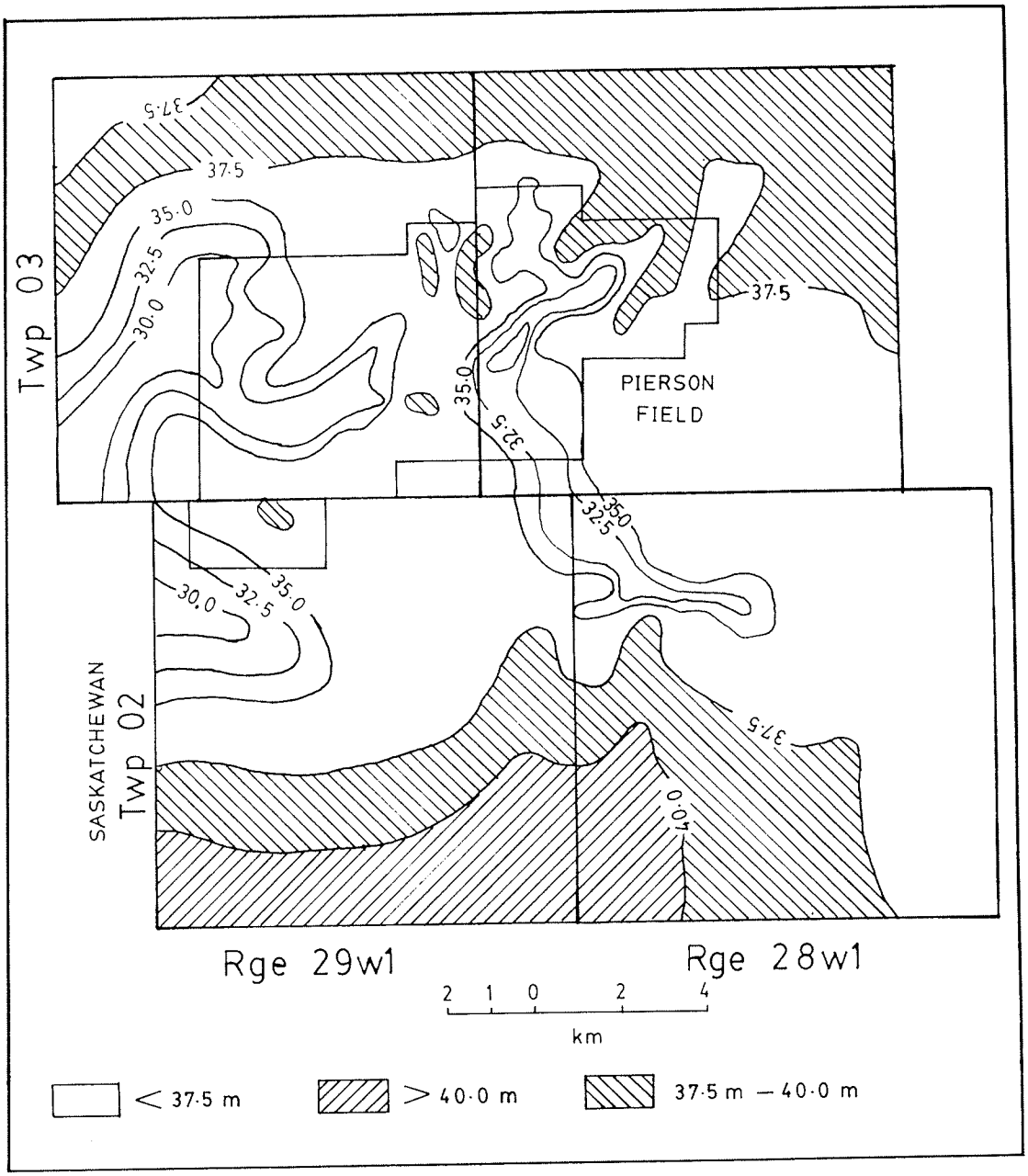
Twp 03
SASKATCHEWAN
Twp 02
PIERSON
FIELD
37·5
35·0
32·5
30·0
Rge 29w1
Rge 28w1
2 1 0 2 4
km
< 37·5 m
> 40·0 m
37·5 m — 40·0 m

Fig. 8

formation of the unconformity surface, that kept a noticeable "memory" of the structures formed earlier.

1.7.2 Truncation Traps

The studied reservoir rocks were truncated by the Mississippian erosion surface, and developed a dolomitized and anhydritized altered zone as a caprock immediately below the unconformity.

However, the distribution of oil accumulations suggest that the traps are primarily structural rather than truncational.

1.7.3 Facies Traps

Rapid facies changes from reservoir rocks to non-reservoir rocks, both updip [Fig. 10 (Back Pocket)] and lateral [Fig. 11 (Back Pocket)], have been observed to control the oil accumulation in the structural traps.

In light of the above discussion, it is believed that the traps are primarily structural; this is true with the limitation of facies changes responsible for distributing porosity and permeability.

Fig. 9 Structure contour map (in meters) on top of MC-2 marker. (After Halabura, 1984).

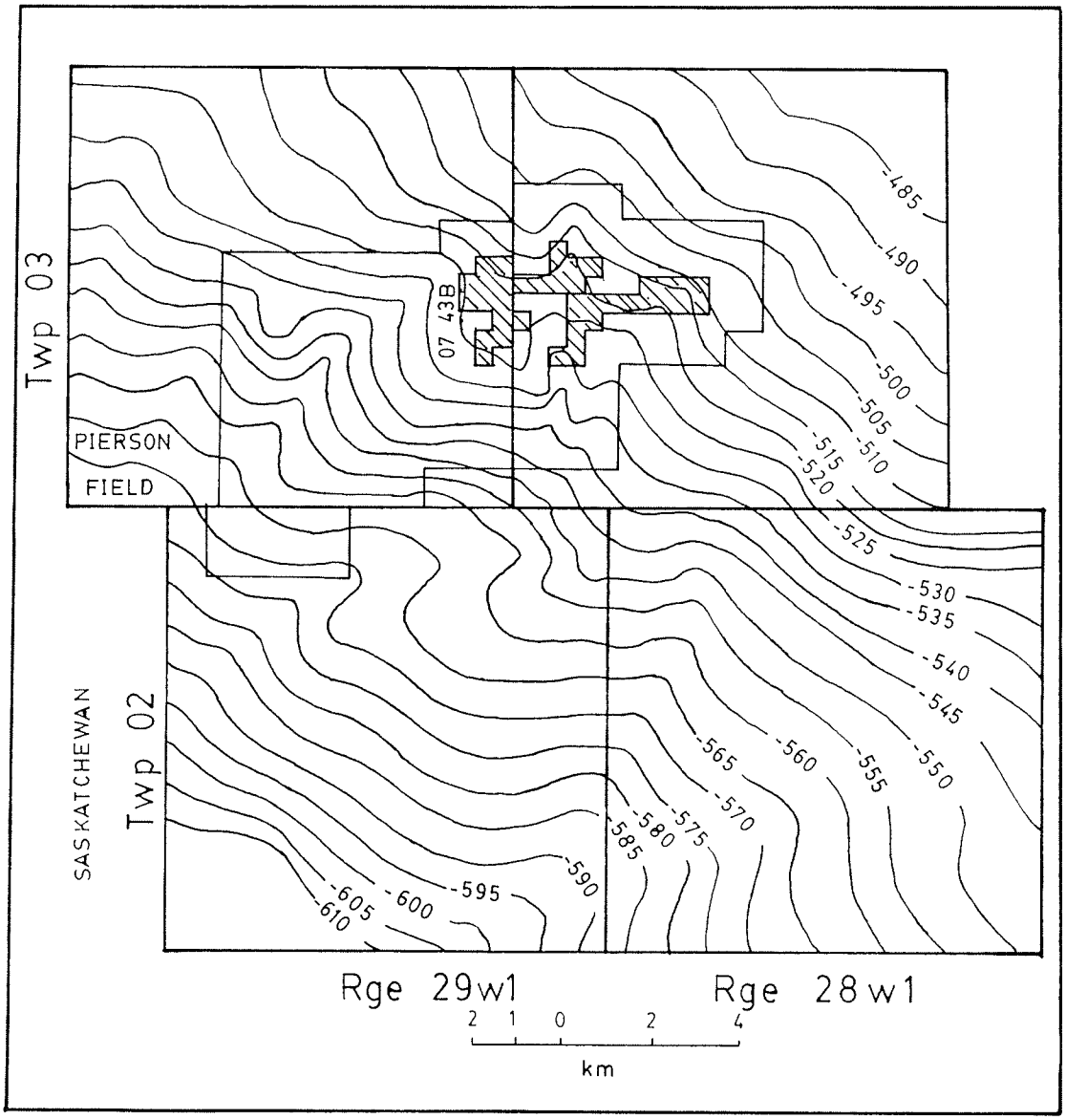
Twp 03
Twp 02
07 43B
PIERSON
FIELD
SASKATCHEWAN
-485
-490
-495
-500
-505
-510
-515
-520
-525
-530
-535
-540
-545
-550
-555
-560
-565
-570
-575
-580
-585
-590
-595
-600
-605
-610
Rge 29w1
Rge 28w1
2 1 0 2 4
km

Fig·9

CHAPTER 2

DEPOSITIONAL ENVIRONMENT

2.1 Description of Lithofacies

Four lithofacies have been recognized in MC-3a rocks in the study area. These are:

1. Stromatolite/cryptalgal laminite/pseudostromata.
2. Vadolite.
3. Bioclastic grainstone.
4. Peloidal grainstone.

Except for vadolite facies which is of early diagenetic origin due to subaerial exposure, all others refer to depositional environment.

2.1.1 Stromatolite/Cryptalgal Laminite/Pseudostromata Facies

This facies comprises the main rock type of the study area. All rocks of this facies are algal in origin and have been subdivided into three subfacies depending on the growth form of algae:

1. Stromatolite: It is characterized by organic structures produced by algae.
2. Cryptalgal laminite: It exhibits algal growth in the form of laminae.
3. Pseudostromata: This rock type is defined in the sense of Wolf (1965) as the product of crustose algae growths: irregular dense patches of granuloid

algal micrite with some detritus. It is a sedimentary term, and not a paleobotanical one.

2.1.1.1 Stromatolite Subfacies

This subfacies is of somewhat restricted development being recognized in 3 out of 5 studied wells. This rock type is composed of stromatolites with infilled sedimented micrite (Plate 1). The stromatolite is mainly LLH type of Logan et al. (1964), i.e., laterally linked hemispheroids (Plate 1-A). SH type (Logan et al. 1964) character - stacked hemispheroids - has also been found in this facies (Plate 1-B; 2).

This rock type is characterized by irregular fenestrae throughout the matrix (Plate 1-B) as well as laminoid fenestrae between stromatolitic laminae (Plate 3-A). It may be termed as an algal mat lofrite as it is characterized by development of fenestrae (Plates 1-B; 3-A) as well as sheet cracks (Plates 3-B; 4-A). This biomat is a product of the growth of blue-green algae (Plate 4-B), probably girvanella (Plate 5-A).

Often pockets of peloids are found to be entrapped in the mat (Plate 5-B). Although fossils are scarce, small amounts of bioclasts of ostracod, dasyclad, foram (Plate 6-A) and brachiopod (Plate 6-B) have been identified. Another minor component of this facies is blue green algal grains (Plate 5-B).

Usually this rock type is buff colored.

2.1.1.2 Cryptalgal Laminite Subfacies

This subfacies constitutes the principal algal rock type. This rock type is composed of mainly micrite and algal peloids bounded by blue-green algae (Plate 7-A).

In well defined sections the algal laminae are represented by planar as well as irregular anastomosing fabric with the former type being predominant (Plate 7). This facies is characterized by laminoid fenestrae (Plate 8-A).

Like the Stromatolitic facies, it also contains a minor amount of bioclasts-ostracod, foram, dasyclad, codiacean algae, gastropod, brachiopod, echinoderm as well as blue-green algal grains.

Upward in the section this subfacies sometimes becomes enriched in terrigeneous argillaceous components.

This rock type is inferred to be the principal depositional facies of the dolomitized and anhydritized altered zone as suggested by the vaguely preserved cryptalgal laminae in the latter (Plate 8-B). Normally it is cream colored, but in the altered zone it assumes a grey buff color characteristic of that zone.

2.1.1.3 Pseudostromata Subfacies

Macroscopically, this subfacies looks like a mudstone having well-defined fenestrae (Plate 9-A) and sheet cracks (Plate 9-B) as well as vertical desiccation cracks (Plate 10-A). The abundance of blue-green algal filaments and renalic

structures (Plate 10-B) speaks for the origin due to crustose algal growth. Microscopically, it is composed of dense patches of granuloid algal micrite.

Like other algal rock types the bioclasts constitute a minor amount and are: ostracod, dasyclad, foram and blue-green algal grains. This rock is bioturbated by mainly vertical burrows (Plate 11). Usually it is buff to buff white colored.

2.1.2 Vadolite Facies

This facies (Plate 12) has not developed throughout the study area. It occurs in three wells, and contributes to the dolomitized and anhydritized altered zone in one well. This facies is composed of vadoids ranging from microscopic microid (peloid size) to pisolite size (up to 1 cm) (Plate 12-B). The vadose origin of the coated grains of this facies and hence the name vadoids are justified by:

1. Occurences of vadose crust and inverse-graded grains (Plate 12).
2. Broken grains due to desiccation fracturing (Plate 13-A).
3. Flattened grains and polygonal fitting among them (Plates 13-B; 14-A).
4. Sharing of the outer laminae, and continuation of outer laminae into the surrounding sediment (Plate 14-B).
5. Perched inclusions in the grains (Plate 15-A).

6. Multistage grains (Plates 13-B; 14-A).
7. Downward thickening of the outer laminae (Plate 15-A).
8. Vertical asymmetry of the grains (Plates 13-B; 14-A; 15-B).
9. Microstalactitic cement (Plate 16).
10. Continuation of radiaxial spar to form the cement (Plate 17-A).

Normally this rock type is buff grey to buff white colored, but in the altered zone it assumes a grey buff color characteristic of that zone. The two extreme types of vadoids are: marine vadoid having radial fabric composed of alternating micrite and radiaxial spar layers, and micritic caliche vadoids (Plates 17-B; 18-A). All gradations between them occur with the predominance of marine vadoid type (Plate 18-A). The nucleii of the vadoids are usually broken vadoids (Plate 13-B) and obscure micritic bodies (Plate 18-B).

2.1.3 Bioclastic Grainstone Facies

This facies is of very restricted development and is found in only one well. It is composed of blue-green algal grains (Plates 22-B; 23-A) (e.g. girvanella) (Plate 23-B), forams (Plate 23-A), dasyclads (Plate 23-B), echinodermal fragments (Plates 22-B; 23-A), and bryozoa (Plate 24-A). A very minor amount is comprised of brachiopods, red algae (Plate 24-B) and rugose corals (Plate 25-A). It is usually buff to grey buff colored (Plate 25-B).

2.1.4 Peloidal Grainstone Facies

The peloids may be categorized into fecal pellets, pseudopelletoids (rounded and sorted carbonate mud reworked by water current), and micritized, rounded and abraded bioclasts (Plate 26-A). The bioclasts include echinodermal fragments, dasyclads and forams. The patchy distribution of the open space structure in this grainstone facies may be suggestive of trapping of the grains by algal crusts (Flugel, 1982). This facies is of restricted development being found in two wells. It is grey buff to tan colored (Plate 26-B).

2.2 Interpretation of Lithofacies

2.2.1 Stromatolite/Cryptalgal Laminite/Pseudostromata Facies

2.2.1.1 Stromatolite Subfacies

Stromatolites are organosedimentary structures formed by binding of fine calcareous mud and silt, detrital grains, and tests of micro-organisms in a sticky algal sheath (Logan et al., 1964).

Modern stromatolites characteristically develop in the intertidal or near-tidal zone. When stromatolite terrain is inundated, fine grained sediments in suspension are bound into laminae by algae. The formation of a stromatolite is a function of location, exposure and tidal amplitude. These factors give rise to a number of different types (Logan et al., 1964).

Type LLH - laterally linked hemispheroids - is typical

of protected intertidal mudflat where wave action is slight, (Logan et al., 1964), which normally coincides with the littoral zone and periodically extends into the supralittoral zone. According to Logan et al. (1964), this type results from one or a combination of the following factors:

1. Lateral growth expansion.
2. Growth over pre-existing irregularities.
3. Relief created by rapid growth in the highs and inhibition of growth in depressions.
4. Gas-evolution under algal mat.

Type SH - stacked hemispheroids - is characteristic of intertidal headlands (Logan et al., 1964). This type develops in the exposed intertidal mudflats where scouring of wave action and other interacting factors inhibit continuous growth of algal mats.

The majority of the stromatolitic structures are compound, i.e., having changed with vertical growth from one type to another with a change of depositional environment.

The stromatolites of the study area correspond to LLH-SH type. This compound type has its modern analogs (e.g., Shark Bay, Western Australia).

It may be inferred that the depositional environment of the stromatolites in the study area fluctuated between protected intertidal flats and exposed intertidal mudflats characterized by wave action. The former environment probably periodically extended into supralittoral zone as suggested by the presence of desiccation cracks in the LLH

type as well.

During storm tides interstructural depressions of the stromatolites are likely to be subjected to sedimentation. The observed predominance of micrite infilling the interstructural area as well as inhibiting the growth of the structure may be attributed to storms or unusually high tides. This also explains the presence of subtidal broken brachiopod bioclasts in the rock.

2.2.1.2 Cryptalgal Laminite Subfacies

This rock type is a product of blue-green algal binding on the tidal flats during the time of inundation. The laminae resulted from micrograding or alternation of peloidal and micritic layers.

According to Wilson (1975, p. 69) this facies is characteristic of tidal ponds. The very minor amount of broken subtidal bioclasts (e.g., brachiopod, echinoderm) found in the rock type may be explained by having been brought to the depositional site during storms or unusually high tides.

2.2.1.3 Pseudostromata Subfacies

Wolf (1965) reported the occurrence of this rock type in the space between distinctly shaped algal colonies.

The bioturbation characteristic of this rock type is believed to be the reason why it is devoid of organosedimentary structures typical of algal mats. The ubiquitous

vertical association with stromatolite [Fig. 12 (Back Pocket)] is suggestive of the fact that this rock type is a homogenized product of parent stromatolites as a result of thorough bioturbation.

2.2.2 Vadolite Facies

The vertical association of this facies [Figs. 12 (Back Pocket); 13] with the algal facies, and, more importantly, the observed gradational contact between these facies (Plates 19; 20-A) point to the fact that the parent sediment was of algal facies. Bioclasts such as ostracods, forams, gastropods and dasyclads, have been found to form the nuclei of some vadoids (Plates 20-B; 21; 22-A), but these are very rare. In line with the above interpretation regarding the origin of this facies, these rare bioclast nuclei may be the ones that were trapped in the original algal rocks.

Normally the vadoids are composed of accretionary growth of alternating laminae of micrite and radiaxial spar. The radial fabric vadoid as well as the radiaxial fabric of microstalactitic cement point to an environment of formation whose modern analog is the coniatolite terrain of Purser and Loreau (1973). In this environment vadoids form by precipitation from any shallow hypersaline water in a peritidal environment. The fracturing found in the vadoids may have been caused, as pointed out by Assereto and Folk (1980), by desiccation. These fracturing episodes alternated with vadoid growth (Peryt, 1983).

Fig. 13 Panel diagram constructed from the present study showing lithofacies changes.

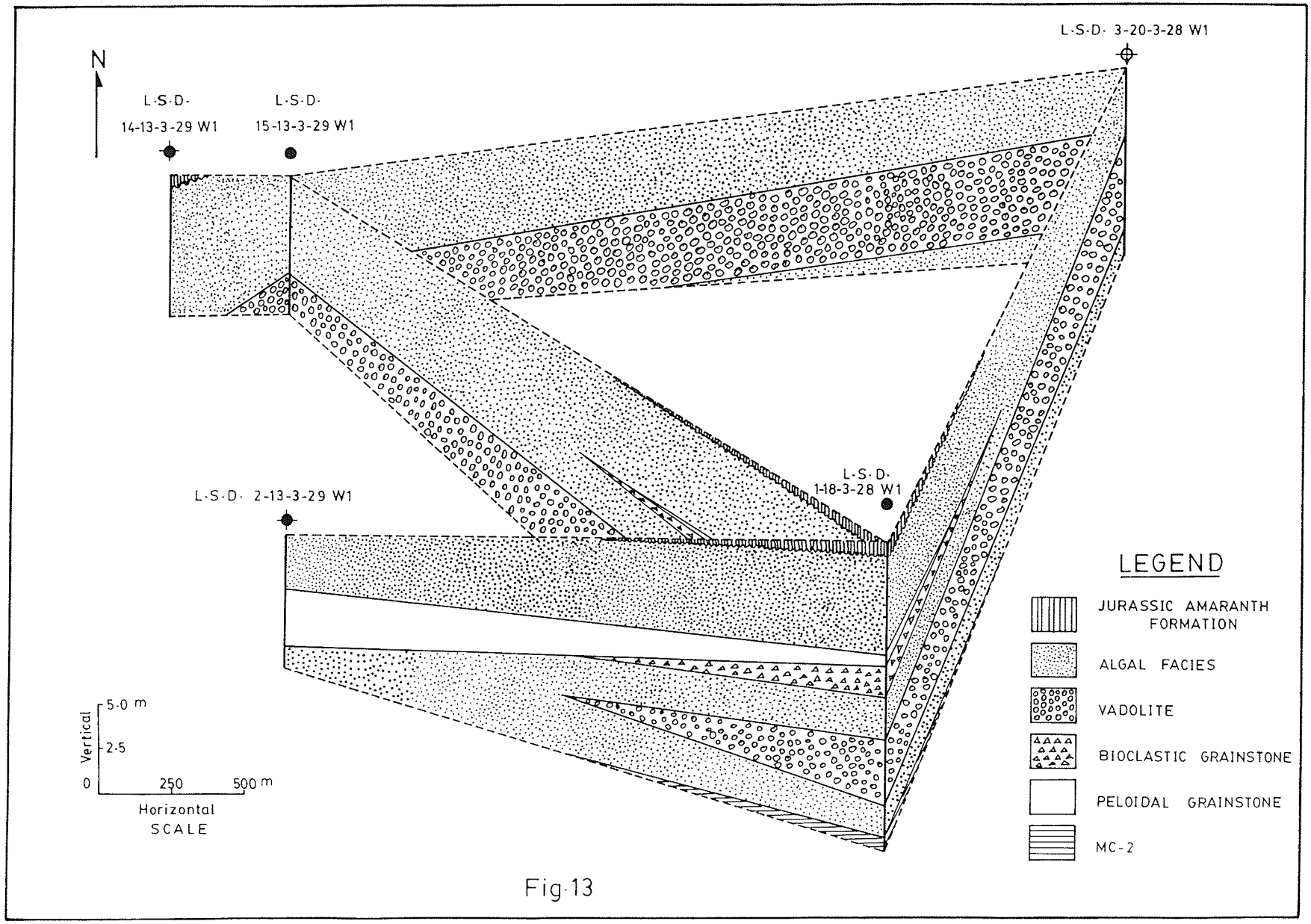
N
L·S·D· 14-13-3-29 W1
L·S·D· 15-13-3-29 W1
L·S·D· 3-20-3-28 W1
L·S·D· 2-13-3-29 W1
L·S·D· 1-18-3-28 W1
LEGEND
JURASSIC AMARANTH FORMATION
ALGAL FACIES
VADOLITE
BIOCLASTIC GRAINSTONE
PELOIDAL GRAINSTONE
MC-2
Vertical
5·0 m
2·5
0
250
500 m
Horizontal
SCALE

Fig·13

On the other hand, Esteban (1976) suggested that micritic vadoids are of caliche origin. However, this postulation has met with objections because of the fact that at least some "caliche vadoids" sensu Esteban have been reported from vadose marine environment (e.g., Burgess, 1983).

Subaerial exposure together with flushing with fresh water is required for vadose compaction of carbonate sediments (Clark, 1980, quoted by Peryt, 1983). According to Peryt (1983), the characteristic feature of this compaction is marked downward intensity, and fitting of the flattened vadoids as a result of dissolution of the vadoid due to their unstable mineralogy (i.e., aragonite and high-Mg calcite). In the Persian Gulf area recent vadoids composed of aragonite and high-Mg calcite form when hypersaline groundwater is pulled up by capillary pressure, but no vadose compaction has been reported, mainly because of absence of freshwater flushing (Peryt, 1983).

It is proposed that the vadoid formation terrain in the study area is a marine vadose one with some freshwater vadose characteristics, since, in a generally hypersaline environment attacks of freshwater can happen (Peryt, 1983), giving rise to the schizohaline environment of Folk and Land (1975).

2.2.3 Bioclastic Grainstone Facies

Cyanophycean and dasycladacean algae are

characteristically found in restricted environments (Wilson, 1975, p. 74).

The presence of Cyanophycean algal grains as the major constituent of the grainstone facies as well as the presence of dasycladacean and forams lead to the inference that this facies developed on a restricted marine shoal. The occurrence of echinodermal fragments as a visible minority and the existence of small amounts of bioclasts comprised of bryozoa, brachiopod and rugose coral may be explained by their transportation into the depositional site during storms. It is noteworthy to mention, however, that the presence of echinodermata, brachiopoda and bryozoa in the restricted environment in the Persian Gulf has been reported by Hughes Clarke and Keij (1973).

2.2.4 Peloidal Grainstone Facies

This rock type develops on the restricted marine shoals characterized by moderate water movement (Flugel, 1982, p. 407). The echinodermal bioclasts found in this facies may be transported into the depositional site during times of storms. However, again it should be noted that Hughes Clarke and Keij (1973) reported the presence of echinodermata in restricted environments in the Persian Gulf.

2.3 Summary of Depositional Environment

The rocks of the study area fall within the "facies of restricted circulation on marine platform" of Wilson (1975,

p. 26). This parallel-to-shore facies belt includes sediments in the whole complex of carbonate tidal flat environments including tidal channels, cut-off lagoons, and coastal ponds with restricted circulation.

Lobue (1982), while appreciating the applicability of Walther's Law on a large scale, such as for transgressive and regressive sequences, suggested that each parallel-to-shore belt, particularly the supratidal and intertidal, is characterized by microfacies that migrate parallel to the overall trend of the facies belt. In fact, in modern carbonate environments of the intertidal zone, lithofacies occur roughly perpendicular to the shoreline rather than parallel to it (Shinn et al., 1969). This model of a tidal flat complex is also applicable to the rocks of the study area.

The study area is characterized by the lithofacies having extremely variable distribution and thickness [Figs. 12 (Back Pocket); 13]. Consequently, detailed correlation becomes difficult. The thick algal facies, which has been found in all studied drill cores, constitutes the main rock type of the inferred tidal flat complex. Other facies show thin and sparse development.

The variability of distribution and thickness of the lithofacies is indicative of the ephemeral nature of the environment. Lobue (1982) related this ephemerality to:

1. Very active tidal channels.
2. Very shallow depositional slope.

These two factors would allow small fluctuations in relative sea level to cause extensive physiographic changes locally giving rise to a dynamic depositional system in the study area.

CHAPTER 3

DIAGENESIS

3.1 Introduction

Two points of view exist among geologists in defining the term "diagenesis" (Larsen & Chillinger, 1967). One school defines diagenesis as embracing all physicochemical, biochemical and physical processes that modify sediments at low temperature and pressure characteristic of near-surface environment during the time span between initial deposition and lithification. The other view regards diagenesis as incorporating all processes including postlithification ones that change sediments up to the point of the commencement of metamorphism. In the present study the latter sense of the term has been taken.

Major diagenetic processes operative in the study area are presented in the following sections.

3.2 Biological Diagenesis

Boring endolithic algae and fungi, and burrowing organisms are instrumental in bringing about biological diagenesis. The resulting features are micritization and sparmicritization, and burrows respectively.

3.2.1 Micritization

Microorganisms such as endolithic algae and fungi, especially in tidal zones, bore mainly into the surface of

bioclasts. The resulting empty tiny boreholes are infilled by micritic aragonite and high-magnesian calcite after the death of the organisms. The exact process of this infilling is not known. According to Bathurst (1976, p. 364) sedimentation into those boreholes (6 μm diameter) is unlikely, and hence precipitation is probably the mechanism. The precipitation of micritic aragonite or high-magnesian calcite in the micro-tube is believed to occur in a special physico-chemical environment characterized by sea water enriched in organic compounds released during bacterial decomposition of algae or fungi. Micritization can also occur by micrite calcification of the organisms responsible for boring (Kobluck and Risk, 1977) as well as borewall alterations caused by recrystallization (Windwall, 1968; Kendall and Skipwith, 1969).

The above phenomenon, known as micritization, is probably temperature-dependent (Gunatilaka, 1976). It is presently taking place in marine phreatic zone (Longman, 1980).

Micritization takes place centripetally. Micrite coatings around the grains results from incomplete micritization (Bathurst, 1966), whereas completely micritized grains possess no traces of skeletal microstructure and may become rounded or subrounded to be called peloids (Swinchatt, 1965). In the study area this process mainly gave rise to completely micritized bioclasts.

3.2.2 Sparmicritization

Kahle (1977) first described an early diagenetic process in detail whereby sparry calcite cement is converted into micrite by degrading recrystallization, and coined the term sparmicritization for it.

According to Kahle, minor sparmicritization is caused by micrite calcification of endolithic algae or fungi, or by micrite precipitation into the empty borings after the death of the organisms. Most sparmicritization, however, occurs as a result of micritization by borewall alteration. It is a dissolution-precipitation phenomenon whereby dissolution of sparry calcite cement takes place with concomitant precipitation of micrite. The requisites for such sparmicritization are:

1. Slow but steady flow of groundwater.
2. Groundwater enriched in organic matter released by the bacterial decomposition of algae or fungi.

According to Kahle (1977), sparmicritization can occur in vadose as well as in marine diagenetic environments and is more common than previously realized because of:

1. Small size of algal and fungal endoliths.
2. The endoliths were believed to be restricted to allochems (e.g. Bathurst, 1966).

In the study area, sparmicritization is observed in the algal facies, and is believed to have taken place in the vadose zone as equant calcite filling fenestrae and desiccation voids has been sparmicritized (Plate 27-A).

3.2.3 Burrowing

Burrows are only observed in the pseudostromata subfacies. Burrowing is an early diagenetic process that homogenizes the sediments, and is caused by mud-eating and grazing organisms (e.g., worms, mollusks) in their search for food and protection.

In the drill cores, tubular sediment filled structures differing in color from the adjacent sediment were interpreted as burrows (Plate 11-A). These burrows show orientations which are dominantly vertical (Plate 11-B), typical for burrows that develop in partly lithified intertidal sediments, as opposed to horizontal orientations characteristically found in subtidal sediments (Frey in Perkins, 1971, quoted by Wilson, 1975, p. 84).

3.3 Chemical Diagenesis

Chemical diagenesis incorporates the majority of diagenetic processes observed in the MC-3a beds. These processes are: calcite cementation, neomorphism, formation of dolomite, anhydrite, and other authigenic minerals, leaching, and pressure solution.

3.3.1 Calcite Cementation

Cementation is the formation of new crystals into pre-existing voids of any origin.

In the study area, calcite cement, which is of early diagenetic origin (see section-3.3.1.3), has been observed to be one of the porosity reducers as well as the principal contributor to lithification. The latter attribute is responsible for preservation of some primary porosity in view of the fact that otherwise the rock-framework would have collapsed giving rise to non-porous rocks under burial conditions. In the study area cements precipitated from both marine water and freshwater have been observed.

3.3.1.1 Marine Cement

Fibrous aragonite (later neomorphosed into radiaxial calcite) and high-Mg micritic cement (later neomorphosed into micritic calcite cement) are the two types of marine cements.

Radiaxial calcite cements (Plates 16-B; 27-B; 28-A) have been observed in the vadolite facies and bioclastic grainstone facies. These inclusion-rich cements are characterized by bladed morphology, alignment of C-axis perpendicular to the pore-boundary, and undulose extinction. These cements are believed to represent a neomorphic alteration product of a fibrous precursor (Kendall & Tucker, 1973). The precursors were aragonite fibres (Assereto and Folk, 1976) which had been subjected to aggrading recrystallization in hypersaline waters (Kahle, 1974). These cements have been interpreted to correspond to different subenvironments:

1. Marine phreatic, and

2. Marine vadose.

The high-Mg micritic calcite, however, has formed in the vadose marine zone and is found only in the vadolite facies.

3.3.1.1.1 Marine Phreatic Cement

This cement is found only in bioclastic grainstone forming a minor percentage of the overall cement component of the facies. The phreatic origin is inferred by the uniform (isopachous) distribution around the porewall (Plate 28-A).

It occurs in the intraparticle pores of the bioclasts, e.g., bryozoa, foraminifera. The cause of the paucity of this cement may be explained by:

1. Later freshwater leaching which leaves only the smaller intraparticle pores (Plate 28-A), and/or
2. Water chemistry of the precipitating fluid having inhibitors (Longman, 1980).

3.3.1.1.2 Vadose Marine Cement

Vadose marine cement developed only in the vadolite facies. As discussed in section 2.2.2, the vadolite facies is principally formed in vadose marine environment, this facies formed mainly by the accretionary growth of alternating laminae of high-Mg micritic calcite (later recrystallized into micritic calcite), and sparry laminae of fibrous aragonite (later inverted into radiaxial calcite) (Plate 17-A).

In the vadolite facies radiaxial calcite mosaic has also

been found forming microstalactitic cement (Plate 16).

3.3.1.2 Freshwater Cement

3.3.1.2.1 Freshwater Vadose Cement

The main vadose cement type is the meniscus cement of Dunham (1971). It developed only in the bioclastic grainstone facies (Plate 22-B; 28-B) and is characterized by patchy habit of uneven cementation, as opposed to isopachous/even cementation characteristic of the phreatic zone. The cement preferentially developed in small-scale pores as opposed to easily drained large ones. Grain contact cement is abundant, and shows pore rounding character, especially in the well-developed small-scale pore areas.

The cements are composed of blocky, rather than acicular crystals (Plate 29). This is in agreement with the morphology of the vadose cement produced in a simulated environment in the laboratory by Thorstenson et al. (1971). Freshwater vadose cements are characteristically composed of blunted crystals due to the fact that the water-air interface causes undernourishment of the crystal tips (Dunham, 1971). In the study area, however, the cements show sharp crystal faces. If vadose cement is placed in the phreatic zone euhedral crystal faces will form on the previously blunted crystal (Dunham, 1971). Accordingly, it is likely that the observed sharp termination of the vadose cement grew in the succeeding phreatic zone.

The other type of freshwater vadose cement is micritic

calcite which forms part of the vadolite facies (Plates 17-B; 18-A). This cement is capable of forming as a result of rapid precipitation in this environment (Folk, 1974).

3.3.1.2.2 Syntaxial Overgrowth

Syntaxial overgrowth is commonly found in the bioclastic grainstone facies characteristically developed around echinodermal fragments (Plates 22-B; 29). This cement is typical of freshwater phreatic environment. Syntaxial overgrowth, where present, fills large proportions of the pores - which is suggestive of its faster growth. The rapid rate of growth of this cement is mainly due to the large crystal nucleus (echinodermal fragment) around which it precipitates in optical continuity (Longman, 1980).

3.3.1.2.3 Equant Cement

Equant cement developed mainly in the fenestrae and desiccation cracks of the stromatolite and pseudostromata subfacies (Plate 30-A). A minor amount of it is also found in the bioclastic grainstone facies. This pore filling cement shows coarsening toward the centre of the pore (Plate 30-A) which is characteristic of early freshwater phreatic diagenesis (Longman, 1980).

3.3.1.3 Timing of Cementation

All the calcite cements observed in the study area are products of early diagenesis before burial. In the

bioclastic grainstone facies the meniscus cement is found to be enclosed by syntaxial overgrowths which, in turn, are enclosed by equant calcite cement (Plate 29). Hence, the meniscus cement is inferred to be first to precipitate, followed by syntaxial overgrowth, and finally equant calcite. No break has been observed in this freshwater cement stratigraphy.

The marine phreatic cement, however, is leached and then overlain by equant calcite cement (Plate 30-B). This observed break in the cement stratigraphy with marine phreatic cement below and freshwater cement above is suggestive of earlier growth of the former.

The marine vadose cement as well as freshwater vadose micritic cement forming the vadolite facies presumably developed early in the diagenetic history.

3.3.2 Neomorphism

Folk (1965, p. 21) defined neomorphism as:

> "All transformation between one mineral and itself or a polymorph - whether inversion or recrystallization, whether the new crystals are larger or smaller or simply differ in shape from the previous ones."

A number of neomorphic changes are identified in the study area.

Borewall alteration associated with micritization is a neomorphic process that occurred immediately after deposition

when the sediments were still in the marine phreatic environment. With the advent of freshwater phreatic environment, inversion of aragonite that survived leaching, and recrystallization of high-magnesian calcite gave rise to calcite as the neomorphic product.

As the freshwater phreatic environment continued some micrite suffered aggrading neomorphism. This aggrading neomorphism is sparse, and developed mainly in the algal grains converting the micrite calcified algal filament into microspar (4 – 10 μm) with some pseudospar (> 10 μm) (Plate 5-A). However, all bryozoan fragments that are present as a minor component of bioclastic grainstone are converted into microspar with some pseudospar due to this aggrading neomorphism (Plate 24-A).

Borewall alteration associated with sparmicritization observed in the algal facies (Plate 27-A) is inferred to be due to degrading neomorphism which converts equant calcite cement into micrite. This is believed to have occurred in the freshwater vadose environment succeeding the freshwater phreatic one early in the diagenetic history.

Aggrading neomorphism of early marine fibrous aragonite cement in a hypersaline environment brought about the formation of radiaxial calcite cement (Plate 27-B). The precise time of the aggrading neomorphism giving rise to radiaxial calcite is not documented in the literature. Kendall and Tucker (1973), on petrographic grounds, suspected that this transformation "occurred at some (perhaps

considerable) time after burial of the sediment".

3.3.3 Formation of Dolomite and Anhydrite

3.3.3.1 Formation of Altered Zone

The altered zone, i.e., the zone of complete dolomitization with anhydrite bands, occurs where the Mississippian subcrop is overlain by Jurassic Watrous Red Beds or evaporites (Kendall, 1975). This zone developed immediately below the Mississippian unconformity which constitutes an effective caprock that can be readily identified on logs by a low sonic reading (interval transit time, ΔT) as well as a high resistivity kick immediately below the Jurassic Amaranth Red Beds.

Fuller (1956a, b), Fuzesy (1960, 1966), Martin (1966) and Miller (1972) believed that the altered zone is genetically related to the Mississippian unconformity (Fig.-14A). However, Kendall (1975) considers their hypothesis inadequate as it fails to explain the thickness pattern of the altered zone as well as the development of the zone under Watrous cover only.

McCabe (1959) found that there exists an inverse relationship in southwestern Manitoba between the altered zone thickness and the thickness of Jurassic Amaranth Red Beds. This relationship is observed to be valid in the study area. The same relationship has been observed by McCamis (1958, quoted by Kendall, 1975) in the Mississippian subcrop region of neighboring Saskatchewan. He also noted that the

Fig. 14 Diagramatic north-south sections through south-eastern Saskatchewan illustrating various hypotheses suggested for the origin of the altered zone. (From Kendall, 1975).

Fig. 15 Stability fields of gypsum and anhydrite at 101.3 KPa total pressure. (From Berner, 1971, after Hardie, 1967).

Fig. 16 Stability fields of gypsum (G) and anhydrite (A) as a function of temperature and pressure. The G-A curves with negative slope correspond to cases where pressure on the solutes is lithostatic and that on the surrounding water is hydrostatic. The G-A curves with positive slope is for the pure lithostatic situation. The geothermal gradient is Grand Saline Dome, Texas. (From Berner, 1971, after McDonald, 1953, and Hardie, 1967).

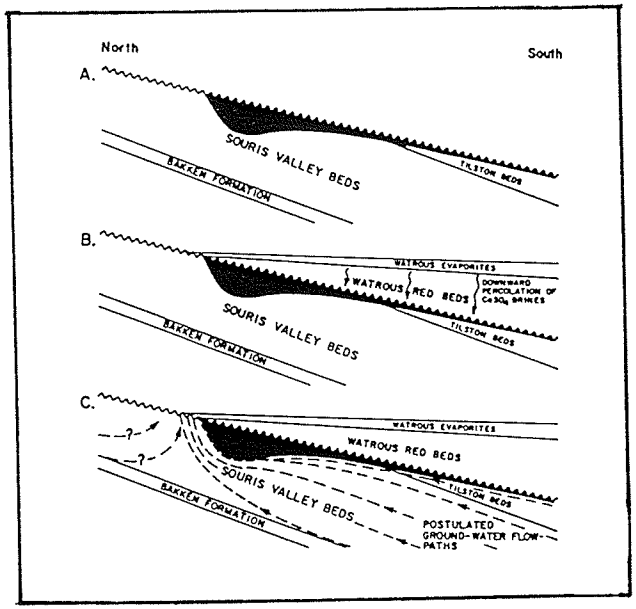

Fig.14

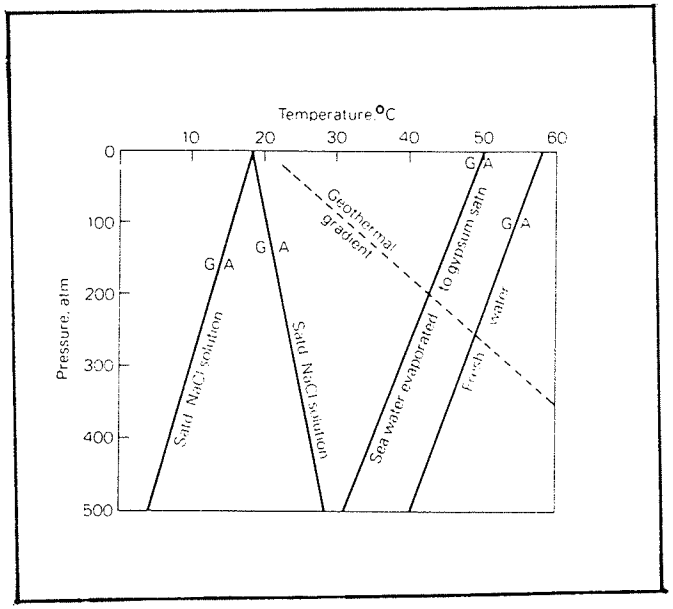

Fig.16

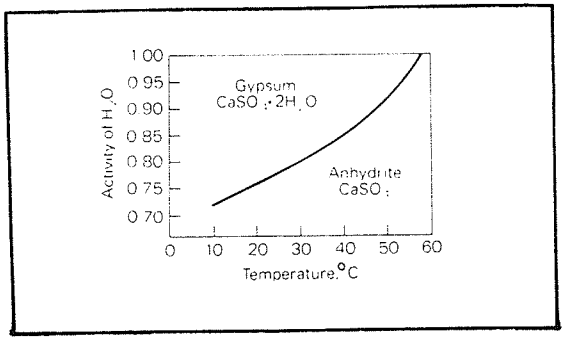

Fig.15

altered zone was absent beyond the limit of Watrous Formation. McCamis postulated that the formation of the altered zone postdated the deposition of red beds. It occurred contemporaneous with Upper Watrous (Watrous Evaporite) deposition when Mg^{++} and $CaSO_4$-rich brine percolated through the red beds into the uppermost Mississippian carbonates (Fig.-14B).

Kendall (1975) gave the points against the downward percolation hypothesis of Berg (1956) and McCamis (1958):

1. Watrous Red Beds are not permeable enough for the downward percolation of brine suggested for alteration.
2. Downward percolation of brine would have converted the uppermost Mississippian carbonates into an impermeable superficial layer which would prevent further alteration.
3. The thick altered zone in the Broadview area (McCamis' study area) reflects contact with brine derived from below rather than from above.

Kendall (1975) himself developed a hypothesis for the formation of this altered zone (Fig.-14C). According to this hypothesis groundwater carrying the ions required for the formation of the altered zone originated during or after the Watrous deposition in the more central portion of the Williston Basin. These groundwaters were driven out by compaction and were forced by the impermeable Watrous red beds to flow northward beneath the Mississippian

unconformity.

These groundwaters trapped within the northward thinning Mississippian sediments between upper overstepping Watrous red beds and the lower impermeable Bakkan Formation gave rise to thicker altered zones.

Kendall's (1975) hypothesis seems to be most logical in dealing with the genesis of altered zones in the Mississippian subcrop region of Williston Basin. However, in view of the fact that in southwestern Manitoba red beds are quite porous (Hansen, Personal Communication, 1984), the hypothesis of percolation of hypersaline brine from above is believed to be a major component for the formation of the altered zone in the study area.

The presence of irregular patches, blebs and stringers of dolomite in anhydrite bands (Plate 31), the occurrence of replacement anhydrite (Plate 32-A), and the fracture infilling of anhydrite (Plate 32-B) in the dolomitic matrix clearly demonstrate that dolomitization pre-dated anhydritization.

3.3.3.2 Types of Dolomite

In the study area dolomite may be divided into two categories:

1. Microcrystalline dolomite:

   Microcrystalline dolomite is observed in all facies below the altered zone. It developed as diffuse small scale patches within the

microcrystalline calcite forming both micritized grains (Plate 21-B) and carbonate mud (Plate 33-A) as well as an intimate mixture with microcrystalline calcite (Plate 33-B).

2. Crystalline dolomite:

a. Dirty dolomite rhombs:

These finely to medium crystalline rhombs are characterized by inclusions of black insoluble residue as much as 20% of the crystals and appear brownish under microscope (Plate 34-A). The extinction is not sharp; some rhombs show discernible zoning with no apparent change in dirtiness (Plate 34). Xenotopic to hypidiotopic tight interlock of these rhombs (Plate 34-A) that resulted from the advancement of dolomitization beyond the point of crystal inhibition, constitute the altered zone. These crystalline dolomites also occur constituting part of scattered clusters of rhombs (Plate 35-A) as well as dispersed individuals in the matrix of microcrystalline calcite with some small-scale patches of microcrystalline dolomite in the section below the altered zone (Plate 34-B). Here the rhombs assume euhedral shape (Plate 34-B). However, the quantity of this type decreases with the increase in depth below the altered zone.

b. Limpid dolomite rhombs:

In the sections below the altered zone, clear white sparry limpid dolomite rhombs occur as do the dirty ones (Plate 35-B). The quantity of these crystalline dolomite, however, increases with the increase in the depth below the altered zone.

c. Incipient dolomite rhombs:

These dolomite rhombs are characterized by very faint, nearly imperceptible extinction and very 'granular' appearance (Plates 33-A; 35-B; 36-A). They are always associated with microcrystalline dolomite with both of them being bounded by rhombic outline. Mattes and Mountjoy (1980) reported this type of dolomite and named it "mosaic dolomite".

3.3.3.3 Formation of Dolomite

Microcrystallinity of dolomite is characteristic of primary or penecontemporaneous dolomite such as occurs at present in Coorong Lagoon, Persian Gulf, Bahama Banks. Consequently, the microcrystalline dolomite in the study area is thought to be a very early product.

The two most commonly accepted ways of forming dolomite, suggested by Folk and Land (1975), are:

1a. Sabkha model.

i. Supratidal flooding, or

ii. Evaporative pumping; or

b. Seepage reflux.

2a. Near-surface environment characterized by hyper-saline brines subject to periodic mixing with freshwater - the schizohaline environment;

b. Mixing of shallow-subsurface highly saline brine with fresh water;

c. Mixing of normal seawater or its connate equivalent with meteoric water; and

d. Mg-purging by meteoric water from Mg-calcite during early diagenesis.

Dolomite is also believed to be precipitating directly from hypersaline lakes, e.g., Coorong area South Australia (von der Borch et al., 1964).

In the study area, the textural property of the pene-contemporaneous dolomite, i.e., the diffuse small scale patches within the microcrystalline calcite is suggestive of Mg-purging as the principal mechanism of formation. According to Stehli & Hower (1961), unconsolidated mixtures of aragonite and high-Mg calcite give rise to cemented limestone composed of low-magnesian calcite having local concentrations of dolomite. Folk and Land (1975) recognized the formation of minor amounts of dolomite confined to Mg-calcite allochems or their internal pores. However, the inferred formation of vadolite dictates the principal mechanism for this facies to be schizohaline.

The incipient dolomite rhombs recognized by Mattes and

Mountjoy (1980) ("mosaic dolomite") was interpreted to be secondary replacement dolomite because of its observed inconsistency with penecontemporaneous dolomite on geochemical grounds. But geochemical data alone is not enough to confirm the genesis of a dolomite. According to Land (1980), ancient dolomites are geochemically very different from their modern analogs.

Petrographic study reveals that all possible gradations exist among microcrystalline dolomite, incipient dolomite rhombs and dolomite rhombs (both dirty and limpid) (Plates 35-B; 36-A) as well as between microcrystalline calcite and dolomite rhombs (both dirty and limpid) (Plates 35-B; 36-A). Hence, the inferred processes are neomorphism of microcrystalline dolomite to dolomite rhombs via incipient dolomite and secondary replacement of microcrystalline calcite to dolomite rhombs respectively.

With regard to neomorphism of microcrystalline dolomite it is as likely to occur as replacement of normal marine carbonate in a later diagenetic realm (Land, 1980).

Along stylolites and grain contact sutures mosaics of finely crystalline dirty to clear euhedral dolomite rhombs have been observed. In the majority of rock types, the presence of a large amount of dolomite rhombs elsewhere in the rock suggests that the formation of dolomite was independent of these pressure solution features. Accordingly, dolomites along pressure solution features (Plate 36-B) have been inferred as a cumulate product, i.e.,

accumulating as less-soluble residue, rather than a reactate, i.e., formed along these surfaces during pressure solution. However, in the stromatolitic and pseudostromata subfacies, where overall the amount of dolomite rhombs is usually very low, a large amount of dolomite rhombs has been observed adjacent to stylolites. This is likely to be a reactate. According to Wanless (1979) the magnesium required for this type of dolomitization is of local origin. Zenger and Dunham (1980), however, called for further testing of this hypothesis.

Dolomite in this study has also been found to have formed partially (Plate 37-A) or completely (Plate 37-B) by replacing calcite cement. It also occurs as late pore lining cement (Plate 38-A).

Dolomitization in the cores of this study is pervasive as opposed to fabric selective. This may be because of neomorphic contribution of the penecontemporaneous microcrystalline dolomite. A significant amount of crystalline dolomite was formed by the neomorphism of microcrystalline dolomite. These dolomite rhombs have the dispersed distribution of their precursors (see section-3.3.3.2).

In light of the above discussion formation of dolomite in the study area is believed to have taken place by the following processes:

1. Penecontemporaneous replacement to form micro-crystalline dolomite which later underwent

neomorphism giving rise to crystalline dolomite.

2. Secondary replacement by hypersaline brines that brought about the formation of an altered zone. This process constitutes the principal phase of dolomitization in the study area, and is responsible for the formation of all dolomites in the altered zone together with some below it.
3. Secondary replacement due to mixing of the near-surface water with hypersaline brine because, as suggested by Folk and Land (1975), dilute water is necessary for the formation of limpid dolomite. This probably has taken place since the commencement of Cenozoic erosion.
4. Secondary replacement due to pressure solution which is responsible for the formation of a minor amount of dolomite along some of the stylolites.

3.3.3.4 Types of Anhydrite

Anhydrite was observed in the altered zone as well as in the rest of the section below it. Primarily there are two types of anhydrite:

1. Grey white (Plates 12-A; 31-A).
2. Brown colored (Plate 7-B).

The grey white anhydrite can further be divided into two types on the basis of their occurrence as:

a. Bands of anhydrite (Plate 31).

b. Void-filling anhydrite (Plates 32-B; 38-B; 39-A).

The brown anhydrite may also be divided into two categories:

a. Xenotopic to hypidiotopic (Plates 39-B; 40-A).

b. Poikilotopic (Plates 32-A; 40-B).

The grey white bands of anhydrite are restricted to the altered zone only, whereas the others occur throughout the section in the study area.

Translucent grey white bands of anhydrite bounded by well defined, more or less parallel sides as much as 38 cm thick occur in the altered zone. These bands are inferred to be clustered nodules having displacement or compactional origin in a host rock where individual nodules had been squeezed against one another.

Although this anhydrite is relatively free from carbonate material, irregular patches, blebs, and stringers of host dolomite (Plate 31-B) have been found to "float" in it suggesting nodular growth. This mosaic nodular anhydrite shows characteristic tightly interlocking fabric of needle-like to tubular crystals (Plate 31-B).

However, this type of anhydrite grades into replacement type along its margin with host dolomite.

Void-filling translucent grey white anhydrite is found mainly in fractures as well as in moldic pores (Plate 41-A) and in the leached stylolites (Plate 41-B). The anhydrite crystals occur as clear individuals (Plate 41-A) filling the pre-existing space; however in larger voids the development

of aggregates of clear tabular crystals (Plates 32-B; 38-B; 39-A) are also found. The void-filling anhydrite exhibits transition to replacement type along the margin of the voids.

Murray (1964) defined replacement anhydrite as having formed within the rock and occupying the space previously occupied by other minerals and fine pore space. This is a dissolution-precipitation phenomenon, i.e., simultaneous dissolution of parent rock and precipitation of the anhydrite. However, the dissolution is often incomplete as suggested by the relicts of the replaced material. The characteristic brown color is imparted to the replacement anhydrite by this included material.

Crystal habit of the replacement anhydrite is often controlled by that of the material being replaced. This situation results in the formation of mainly xenotopic to hypidiotopic replacement anhydrite composed of crystals which show all gradation from rectangular habit characteristic of anhydrite to rhombic habit pseudomorphic after dolomite (Plates 39-B; 40-A). Although this type of anhydrite is found to replace bioclasts as noted by various researchers (e.g., Murray, 1964), replacement of other grains and matrix as well has been found.

Poikilotopic replacement anhydrite found in the study area are presumably formed when the area being replaced has fine pore space connected enough to allow the growth of single crystals. Enclosed in the poikilotopes are marginally corroded dolomite rhombs having the same order of size as

those of the matrix and patches of matrix (Plate 32-A) as well as corroded equant calcite cement (Plate 40-B) (in the stromatolite and pseudostromata subfacies). The distribution of enclosed material within this anhydrite shows that the enclosed material is not in three-dimensional contact, and consequently are not capable of forming a pore-system by themselves. Hence, they are the leftover particles remaining within the replacement anhydrite. This type of anhydrite develops mainly in the fenestrae of the algal facies which were earlier filled with calcite cement and partially (stromatolite and pseudostromata) or completely (cryptalgal laminite subfacies) dolomitized. The reason for this fabric selectivity is probably due to the fact that the required minimum connection of the fine pores is more likely to be present in these fenestrae than in the matrix.

3.3.3.5 Formation of Anhydrite

The stability of anhydrite and gypsum is mainly controlled by the temperature and salinity (a_{H_2O}) (Berner, 1971). Fig. 15 shows the stability fields of anhydrite and gypsum as a function of temperature and a_{H_2O}, but the thermodynamic predictions are not consistent with the experimental results. Murray (1964) reported precipitation of gypsum rather than anhydrite during evaporation of seawater at temperature range of 50° - 80°C. Gypsum can be readily converted to anhydrite in the laboratory; but even in the presence of anhydrite seeds direct precipitation cannot

be achieved (Hardie, 1967). Thus gypsum is metastable in highly saline waters.

On reaction kinetic grounds Conley & Bundy (1958) concluded that primary precipitation of anhydrite is highly improbable because:

1. Gypsum is capable of crystallizing in its metastable state.
2. Activators present in the seawater such as Na_2SO_4 and K_2SO_4 causes immediate hydration of precipitated anhydrite crystallites into gypsum at temperatures below 42°C.

In the field also, metastable assemblages of halite and gypsum in modern sediments is relatively common (Phleger, 1969). But, Kinsman (1969) reported anhydrite from the sabkhas of the Trucial Coast of Arabia which shows primary anhydrite in the interstices between pseudomorphic anhydrite. Berner (1971), however, suggested that both of the anhydrite types mentioned by Kinsman can be the dehydration product of primarily precipitated gypsum.

Most of the ancient evaporites buried to a considerable depth are composed of anhydrite rather than gypsum which is in agreement with thermodynamic predictions. Fig. 16 shows the stability fields of anhydrite and gypsum as a function of temperature and pressure. This figure depicts that the intersection between the geothermal gradient curve and the P-T equilibrium curve for seawater evaporated to gypsum saturation is at P = 20.3 MPa which is equivalent to a depth

of about 830 meters. The intersection representing the gypsum-anhydrite transition depth decreases with the increase in concentration of the brine. As pointed out by Murray (1964), the value of the depth of intersection must be a minimum since the rate of change of gypsum to anhydrite as a function of subsidence is not known. Thus the deepest observed gypsum in the field at a depth of about 1060 m (Murray, 1963) can be shown to be consistent with these predictions.

In light of the above discussion, most of the anhydrite in the study area, if not all, is the replacement product of gypsum due to progressive burial into the stability field of anhydrite. In his study of Mississippian altered zone anhydrite of southeastern Saskatchewan, Kendall (1975) arrived at similar conclusions inferring from the regional considerations that at one time the anhydrite zone was buried to a level considerably deeper (well within the anhydrite stability field) than that at the present time.

3.3.3.6 Gypsification

Anhydrite of the study area is associated with gypsum. This gypsum is found in all types of anhydrite and contributes about 15% of the total evaporites.

Usually, the gypsum shows the same crystal habit as does the anhydrite of respective types (Plates 3Z-B; 38-B; 39-A). It also exhibits fibrous habit in the vadolite facies (Plate 4Z-A).

This gypsum may be unreplaced precipitated gypsum suggesting incomplete anhydritization or gypsification of the replacement anhydrite. However, corroded anhydrite grains found in the gypsum crystals (Plates 32-B; 39-A; 42-B) point to the second option. As inferred by Kendall (1975) for the northernmost part of the anhydritized zone of southeastern Saskatchewan, the gypsum of the study area is believed to be formed as a result of partial hydration of anhydrite in the stability field of gypsum due to erosion and unloading since the Tertiary. A similar conclusion had been arrived at by Zakus (1967) for the gypsification of anhydrite in the anhydritized zone of Mississippian Whitewater Lake Member of the southwestern Manitoba.

3.3.4 Dedolomitization

In the calcitic dolostone immediately below the altered zone in the section, calcite occurs as dispersed crystals that enclose corroded dolomite rhombs (Plate 43). Some calcite crystals are found to be pseudomorphs after dolomite rhombs (Plate 44-A). These clearly suggest that the calcite crystals are dedolomites, i.e., a replacement product of dolomite.

For there to be dedolomitization a solution with high Ca/Mg ratio is required (Blatt et al., 1980, p. 531). Accordingly, this phenomenon in the study area is believed to have occurred hand in hand with the leaching of calcium sulphates due to percolation of groundwater through vertical

fractures mainly due to erosion and uplift since the Tertiary.

Although dedolomites occur mainly in the calcitic dolostone immediately below the altered zone, they are found in minor amount elsewhere in the section below the altered zone. Concentration of dedolomitization in the former portion of the section can be explained by the characteristic high intercrystalline porosity causing exposure of very high surface area to calcifying fluid.

3.3.5 Other Authigenic Minerals

3.3.5.1 Hematite

Black hematite has been observed disseminated in the matrix, along laminae and within the bioclasts and vadoids (Plates 21-B; 44-B; 45-A).

The disseminated nature is believed to be suggestive of pre-lithification origin. The source of the iron is assumed to be organic iron compound present in the deposited sediments. Hematite is stable under relatively high Eh and high pS^{--}. In order to form hematite the original sediment was likely to be relatively free from metabolizable organic matter otherwise iron would be reduced by iron-reducing bacteria or H_2S produced by sulphate-reducing bacteria. This is in agreement with the observed lack of pre-lithification disseminated pyrite in the drill cores. However, percolation of iron-bearing fluid during initial stages of deposition of the Amarath red beds (Young, 1973) may also be a contributor

to hematization.

Hematite is also observed as cumulate along stylolites.

3.3.5.2 Pyrite

Brass yellow to dark colored pyrite occurs as patches mainly in the secondary voids (Plates 45-B; 46-A) and intercrystalline pores (Plate 46-B). Some pyrite is also found to partially fill fractures (Plate 47-A).

The characteristic association with oil suggest that pyrite formation post-dated oil migration (Plate 35-A). Three principal factors for the formation of pyrite are:

1. Concentration and reactivity of iron compounds present in the sediment.
2. Availability of dissolved sulphate.
3. Concentration of metabolizable organic compounds.

The second and third requirements are fulfilled by abundant calcium sulphate in the sediment and migrated oil respectively. The source of reactive iron is believed to be hematite formed earlier.

The pyrite formation is inferred to pre-date pressure solution as it is found as cumulate along the stylolite.

3.3.5.3 Limonite

Yellow limonite has been observed often associated with pyrite (Plate 45-B). It is characterized by diffuse occurrence within pyrite patches.

McCulloch-Smith (1984) proposed that it may be an

oxidation product of iron sulphide. She also noted that the documentation of this type of mechanism is not present in the literature.

It is possible that pyrite may be converted into limonite later in an oxidizing environment created by the oxygen-rich percolating groundwater through vertical conduits due to uplift since the Tertiary.

3.3.5.4 Silica

Silica is found only in the argillaceous dolostone developed in the 2-13-3-29 W1 well at the top of the section.

Most of the silica present is detrital quartz grains which is a constituent of the depositional facies - cryptalgal laminite. Some silica occurs as fracture filling (Plate 47-B) and void filling (Plate 48-A) cement. These are identified as chalcedony by their characteristic fibrous extinction (Plate 48-A).

Infilling of fractures and voids in the altered zone indicates that the formation of this chalcedony post-dated dolomitization.

The formation of silica is favored by a relatively low pH and low temperature. Hence, it is thought to be very late in the diagenetic history when the combination of pH and temperature became low enough as a result of percolation of CO_2-charged groundwater through vertical fractures due to uplift since the Tertiary.

The source of silica is believed to be original detrital

quartz which went into solution under the preceeding environment characterized by higher pH and temperature, and saturated the pore water.

3.3.6 Leaching

Leaching of the rocks of the study area was likely to have taken place during the exposure in the pre-Jurassic erosion period as suggested by Berg (1956) for the Lodgepole subcrop in the Virden area, Manitoba. Groundwaters percolated through the Mississippian subcrop resulting in the leaching of the limestone. The percolating groundwaters penetrated downdip from the pre-Middle Jurassic outcrop. Fractures resulting from pre-erosional structural movement were also likely to have contributed to this process by guiding the leaching waters into the formation.

There is also a later phase of leaching presumably due to erosion and unloading in this region since the Tertiary (Kendall, 1975). This leaching resulted in preferential dissolution of calcite in the dolomite matrix and removal of calcium sulphates. The percolating waters associated with leaching are believed to be responsible for dedolomitization and gypsification. The fracture systems related to the Devonian salt solution also constitute pathways for the leaching waters.

3.3.7 Pressure Solution

Pressure solution is caused by compaction in deep burial

stage (see section-3.4). The principal style in the cores is sutured-seam solution of Wanless (1977) which gave rise to stylolites and grain-contact sutures immediately adjacent to them. Using the terminology of Logan and Semeniuk (1976, cited by Flugel, 1978), configuration of individual stylolites and patterns of stylolite sets will be discussed in the next paragraph.

Four types of stylolite configurations have been observed:

1. Transitional between peak high amplitude and columner (Plate 19-A).
2. Irregular (Plate 48-B).
3. Peaks low amplitude (Plate 49-A).
4. Hummocky (Plate 10-A).

Although stylolites have been developed mainly as individuals, some occur as sets. Two types of sets have been found:

1. Conjugate set of peaks low amplitude (Plate 49-B).
2. Irregular anastomosing sets of hummocky with peaks low amplitude (Plate 10-A).

Stylolites characteristically developed within the facies as well as along the facies boundary in the section below the altered zone. In the altered zone no stylolites have been observed probably because of the compaction inhibition property of dolomitization (see section-3.4). However, an anastomosing swarm of fine clay seams (Plate 50), developed as a result of non-sutured grain solution (Wanless,

1977), has been found in an argillaceous dolostone within this zone in one wall.

The dolomite concentrated along the stylolites as well as grain-contacts is mainly cumulate which suggests that stylolite formation post-dates the principal phase of dolomitization. Occurrences of pyrite and hematite as cumulates also point to their formation prior to the growth of stylolites. Dead oil along some stylolites (Plate 48-B) indicates that stylolites post-date oil migration.

3.4 Compaction

Compaction may be defined as the phenomenon whereby bulk volume of the rock decreases due to mechanical processes that result in grain deformation or closer packing and pressure solution (Flugel, 1978).

Presumably, the limestone in the study area suffered some compaction immediately after deposition. Zankl (1969) noted that in the first few tens of centimeters of burial, coarse-grained carbonates suffer nominal compaction in comparison to substantial compaction experienced by fine-grained carbonates.

However, Flugel (1978) pointed out that many carbonates experience relatively little compaction or are only subjected to deep burial compaction. The only early diagenetic compaction that has been observed in the study area is the vadose compaction in the vadolite facies (see section 2.2.2). Subaerial exposure as well as flushing with freshwater is

required for vadose compaction of carbonate sediments. As a result of this compaction, the rock structure becomes packed: the grain contacts become fitting due to selective dissolution. The vadose compaction occurs because of the unstable mineralogy of the sediments.

In the drill cores, the prominent signature of deep burial compaction has been observed mainly in the form of stylolite and immediately adjacent grain-contact sutures due to pressure solution (Plate 36-B). The bioclastic grainstone facies, which is devoid of stylolites, shows the alternative effect of compaction via grain deformation in the form of breakage of some grains (Plate 45-A) and rare stressed delicate brachiopod shells (Plate 24-B).

Except for these sparse features, the section appears to have undergone insignificant compaction. This seems to be mainly due to the lithification as a result of early diagenetic cementation. It is to be noted that the altered zone shows no development of pressure solution features except for one anastomosing swarm of fine clay seams (Plate 50) in an argillaceous dolostone. This is because of the probable compaction inhibition property of dolomitization suggested by Flugel (1978).

3.5 Fracturing

All cores examined show fractures which are mainly vertical, having lengths up to one metre. The fractures are usually infilled with anhydrite (Plate 12-A). All of the

fractures in the altered zone are infilled with anhydrite, whereas the section below the altered zone exhibits open fractures as well.

Fractures with oil stain (Plate 26-B) and fractures partially infilled with pyrite (Plate 47-A) have also been observed in the section below the altered zone.

The fracturing event is a post-lithification one. In the study area it is not confined within a single period. Petrographic evidence shows that the upper limit of the time range for the fracturing episodes is post gypsification (Plate 50-B).

The fracturing is mainly associated with slump faulting (Milne & Nickoloff, 1955) and slump folds (McCabe, 1963) due to the removal of underlying Devonian Prairie Evaporite and subsequent collapse of the overlying strata. McCulloch-Smith (1984) postulated intermittent salt solution in this region occurring over a long period of time ranging from at least Middle Cretaceous to Mississippian.

Significant fracturing also occurred due to pre-erosional structural movement related to Mississippian unconformity (Berg, 1956) as well as erosion and unloading since the Tertiary.

3.6 Summary of Diagenesis

The large number of diagenetic environments, the variability of products in each one, and the possible repetitive nature of them make the chronology of diagenetic

events very complex. However, sufficient evidence usually exists for interpreting major events, from which a workable diagenetic sequence can be constructed (Longman, 1980). Table 1 shows relative chronology of the principal diagenetic events in the sediments of the study area as a function of time.

All sediments composed of Mg-calcite and aragonite were first deposited in a shallow-water environment. In the algal facies syndepositional burrowing of the stromatolites was the first stage of diagenesis. This resulted in the formation of pseudostromata. With the advent of a freshwater phreatic environment aragonite was subjected to dissolution. The Mg-calcite and aragonite that survived were recrystallized and inverted respectively to calcite. Mg-purging resulted in the formation of microcrystalline dolomite. Equant calcite cements formed in the fenestrae and desiccation cracks. The rocks were then exposed to a freshwater vadose environment where sparmicritization took place.

In the marine phreatic environment bioclastic grainstone first experienced diagenesis. Micritization of bioclasts, and formation of early marine cement took place before the facies passed into a freshwater vadose zone where meniscus cementation occurred. The succeeding freshwater phreatic environment caused the growth of syntaxial overgrowth cement followed by equant calcite cement. The change from a marine to freshwater environment also brought about dissolution of some aragonite, neomorphism of Mg-calcite and survived

TABLE 1 RELATIVE CHRONOLOGY OF THE IMPORTANT DIAGENETIC EVENTS IN THE SEDIMENTS OF THE STUDY AREA.

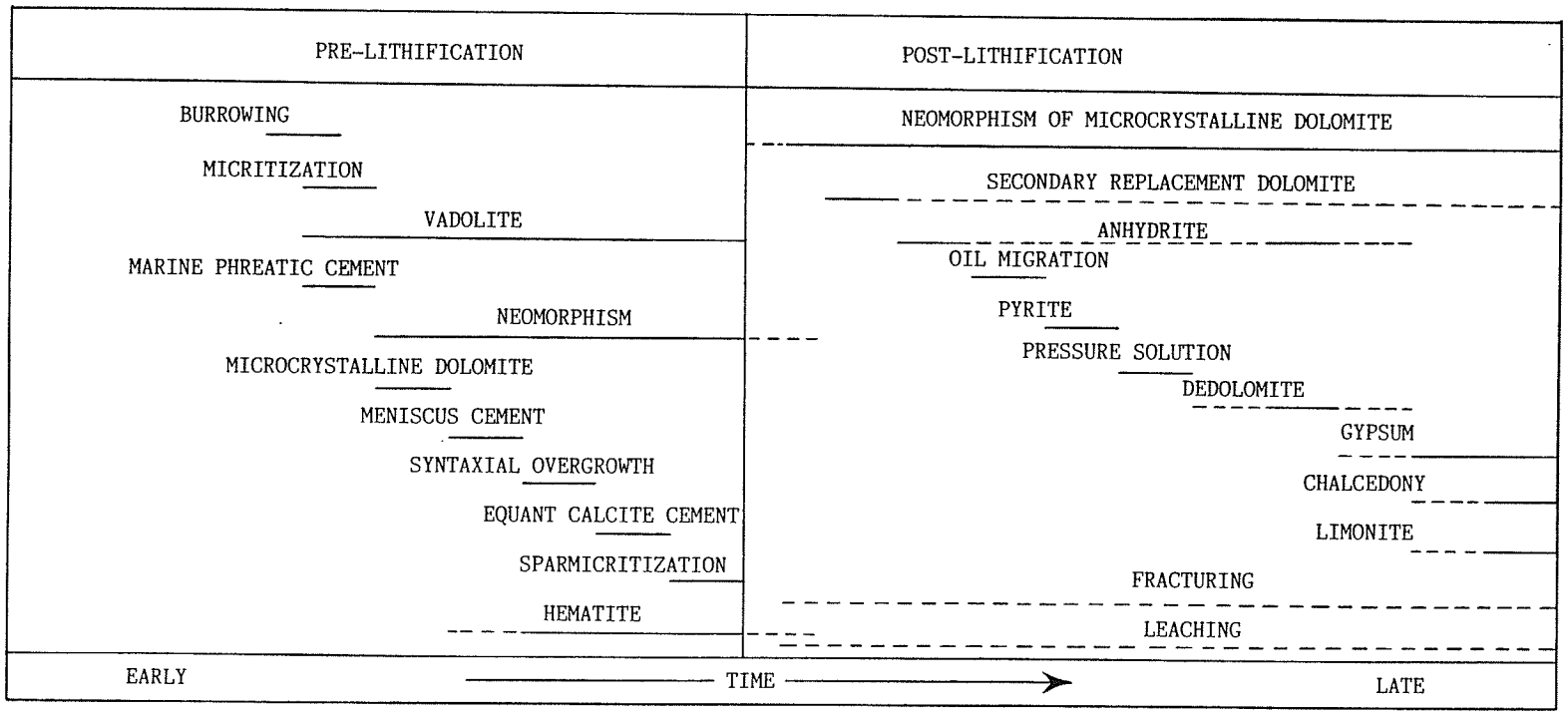

aragonite into calcite, and formation of microcrystalline dolomite due to Mg-purging. Micrite calcified filaments of algal grains as well as bryozoa were neomorphosed into microspar with some pseudospar.

The peloidal grainstone facies underwent micritization in the marine phreatic environment. With the commencement of a freshwater phreatic environment, leaching of some aragonite, neomorphism of Mg-calcite and survived aragonite into calcite, and the formation of microcrystalline dolomite as a result of Mg-purging took place. Although this facies is characterized by a lack of calcite cement, it is believed that early diagenetic cementation must have taken place, otherwise the framework of this grainstone would have collapsed giving rise to tight, non-porous rock under burial conditions. This early cement was likely to be completely leached later in the diagenetic history.

The algal facies is believed to be the parent rock type of the early diagenetic vadolite facies. Subaerial exposure of this facies in the supratidal regime caused the schizohaline environment that brought about the formation of vadolite. Microcrystalline dolomite formed as one of the characteristic products of this environment. The freshwater contributing to this environment is thought to be responsible for the precipitation of some micritic calcite, inversion of Mg-calcite into calcite and formation of minor amounts of microcrystalline dolomite due to Mg-purging as well as vadose compaction.

The only authigenic mineral formed mainly during the early diagenesis is hematite. Organic iron compounds in the deposited sediment are regarded as the source. The sediments are thought to be relatively free from metabolizible organic matter in order to maintain the required physico-chemical conditions.

These early diagenetic events constitute the pre-lithification stage. Following this the rocks of the studied section passed into the post-lithification late diagenesis realm.

The rocks were uplifted prior to the erosion during pre-Jurassic time, to be truncated at the erosion surface on which Amaranth sedimentation took place. Hypersaline brines from both a more basin-central portion of the Williston basin during or after Amaranth deposition as well as from above during the formation of Amaranth Evaporite are responsible for the principal phase of dolomitization. This phase brought about the formation of all dolomite in the altered zone as well as some below this zone.

Formation of dolomite in the section below the altered zone is also attributed to neomorphism of microcrystalline dolomite and mixing of freshwater with hypersaline brine as well as to pressure solution. The neomorphism of microcrystalline dolomite is believed to have been operative throughout the late diagenetic realm. The mixing of freshwater with hypersaline brine however, is interpreted to have taken place mainly after the commencement of Cenozoic

erosion.

The formation of pyrite is inferred to be post-oil migration. The hydrocarbon served as the metabolizible organic matter while already formed hematite constituted the source of iron.

Pressure solution in the study area is post-pyrite formation in view of the fact that along with dolomite, hematite and dead oil, pyrite occurs as a cumulate along the stylolites.

Most of the anhydrite formed immediately after the principal phase of dolomitization. This phase of anhydrite formation predates oil migration as suggested by the oil-stained anhydrite in some modified primary pores (Plate 51). After the commencement of Cenozoic erosion, however, a minor amount of void-filling anhydrite formed in the fractures as well as in the moldic pores and in the leached stylolites. The source material for the formation of this anhydrite is presumably the earlier formed anhydrite. Dedolomitization occurred contemporaneously with the later phase of anhydrite formation. This is because, at that time, the environment was characterized by a solution having high Ca/Mg ratio required for dedolomitization.

Since Tertiary time the section again has been subjected to uplift. Gypsification occurred by the hydration of anhydrite when the rocks reentered the gypsum stability field. This uplifting is also responsible for the creation of the environment of silicification in order to form

chalcedony and conversion of pyrite into limonite in an oxygen-rich environment.

The processes of fracturing and leaching are interpreted as multistage ones that have been operative throughout the late diagenesis.

The relative chronology of the above mentioned important diagenetic events (Table 1) shows, in general, considerable overlap.

CHAPTER 4

DEVELOPMENT OF POROSITY

4.1 Introduction

Murray (1960) pointed out that many hydrocarbon accumulations in carbonate rocks are controlled directly by the facies change involving capillary properties of the rock, and indirectly by structural factors.

Carbonate rocks are very susceptible to diagenesis. The development of porosity and permeability in these rocks results from the interaction between the original sediments and diagenetic processes (Wilson, 1980).

Moore (1979) believed that the utilization of the depositional model as an exploration tool is not a valid working strategy for carbonate rocks in view of the fact that the preservation of primary porosity as well as the development of secondary leached porosity, and inter-crystalline porosity associated with subsequent dolomitization are governed by diagenesis. In the case of preservation of primary porosity, the distribution of the pore space is likely to be controlled by the presence or absence of porefill cement, rather than a change of depositional facies (Moore, 1979).

4.2 Pore Types

The main type of voids in the study area are modified primary pores which include interparticle type in the

vadolite (Plate 52-A), peloidal grainstone (Plate 26-A), and bioclastic grainstone facies (Plates 22-B; 23-A), and fenestrae (Plate 9-A) and desiccation cracks (Plate 4-A) in the algal facies.

The modifications of these pores involved both reduction and enlargement. The reduction is mainly caused by calcite cementation during early diagenesis followed by infilling of anhydrite later in the diagenetic history. Enlargement was principally due to leaching of calcite cement as well as anhydrite. This solution enlargement was sometimes operative to the extent of creating vuggy porosity (Plate 52-B) out of the interparticle pores (Plates 23-A; 52-A) and fenestrae, and channel porosity (Plate 33-B) out of desiccation cracks.

Other important types of porosity are intercrystalline, moldic, and solution enlarged intraparticle porosity.

Intercrystalline porosity (Plate 53-A) associated with dolomitization often developed in a thin band of rocks immediately below the altered zone.

Moldic pores are created by preferential dissolution of calcite in the dolomite matrix as well as leaching of anhydrite. These mineral selective pores may be either fabric selective in giving rise to vadomoldic ones (Plates 38-A; 53-B) or microscopic molds (Plate 41-A) independent of textural elements. However, a trace amount of moldic porosity is contributed by biomoldic pores (Plate 54) which are interpreted to have formed by preferential dissolution of aragonite within the bioclast in the freshwater regime during

early diagenesis.

Leached intraparticle pores within the bioclasts (Plate 23-A) are mainly restricted to the bioclastic grainstone facies where they are one of the contributors to the porosity.

Fractures (Plate 52-A) in the study area are also an important porosity type. Although they constitute little of the gross porosity, fractures, combined with matrix porosities, are likely to raise the effective porosity of the rocks considerably.

In the drill cores leached stylolites (Plate 36-B) have been found to be a very minor type of porosity.

4.3 Porosity As A Function of Dolomitization

During dolomitization magnesium is derived from the replacing fluid; calcium may be thought to come from this fluid where it is replaced by dissolution of calcium carbonate rock (Blatt et al., 1980, p. 530). Over 57% of $CaCO_3$ by volume of the replaced rock is required to supply sufficient calcium to produce a solid dolomite (Murray, 1960; Weyl, 1960).

According to Weyl (1960), carbonate must be added to the system in order for dolomitization to occur because natural waters contain small amounts of total CO_2 as compared to Ca^{++} and Mg^{++}.

Based on the source of carbonate, dolomitization may be categorized into:

1. Local source dolomitization where carbonate is derived from the rock itself that is being replaced.
2. Distant source dolomitization where carbonate is derived from other rocks.

In the former case porosity creation will occur. The final product of this dolomitization will have porosity which is equal to the porosity of the original calcium carbonate rock, plus 12 - 13% of the volume of the replaced solid due to the fact that dolomite has a molar volume 12 - 13% smaller than calcite. Here inhibition of dolomite growth occurs as a result of exhaustion of calcium carbonate.

In the latter type, where carbonate is derived from other rocks, porosity will decrease at first due to the volume for volume growth of dolomite. This will continue up to a point when the volume of $CaCO_3$ is no longer sufficient to supply enough calcium for dolomitization. Accordingly, when the dolomitization attains a high degree (>50% dolomite) excess dissolution of calcite will begin to maintain sufficient supply of calcium and consequently porosity will start increasing. Murray (1960) noted that the relationship of porosity and degree of dolomitization in the Midale beds (3 - 90% dolomite content), Midale field, Saskatchewan, can be alternatively explained in this manner.

Powers (1962) found that, when dolomitization became >90% in Arabian Upper Jurassic carbonate reservoir rocks, porosity and permeability began decreasing.

The mode of dolomite crystal growth has been proposed as a reason for the change in porosity and permeability with increasing dolomite content (Wardlaw, 1979). Dolomites, consisting of euhedral crystals that resulted from the growth of dolomite rhombs limited by the contact of adjacent rhombs, have high porosity and permeability. If the growth of dolomite goes beyond the contact inhibition stage, crystals become more and more euhedral forming compromise, interlocking boundaries, and the resulting rock will be non-porous.

Murray's (1960) observations in the Midale beds does not appear to hold true in this study area in general because the porosity was subjected to later anhydrite infilling in the present case.

The interrelationships of percentage of dolomite rhombs (DOL), percentage of anhydrite (AN), porosity in percent (PHAI), natural logarithm of the mean dolomite rhomb size in microns (LMEAN), natural logarithm of the standard deviation of dolomite rhomb size in microns (LSD), and natural logarithm of the permeabilities in millidarcy (LKMAX, LK90, and LKV) in the section below the altered zone of the drill core 1-18-3-28 W1 were calculated in the form of a correlation matrix (Table 2).

There seems to be no apparent relationship between the porosity and percentage of dolomite rhombs and standard deviation of the dolomite rhomb size. However, significant positive correlations exist between mean rhomb size and

TABLE - 2

INTERRELATIONSHIP OF PARAMETERS
RESPONSIBLE FOR POROSITY DEVELOPMENT

VARIABLE	N	MEAN	STD DEV	SUM	MINIMUM	MAXIMUM
DOL	10	27.32	18.84	273.16	4.00	57.50
AN	10	5.92	5.01	59.25	1.00	17.50
PHAI	10	12.72	3.77	127.20	6.90	18.00
LMEAN	10	3.49	0.09	34.91	3.36	3.67
LSD	10	0.39	0.18	3.94	0.10	0.71
LKMAX	10	2.49	2.29	24.88	-1.61	5.68
LK90	10	2.25	2.16	22.46	-1.61	4.80
LKV	10	1.17	2.29	11.73	-2.21	4.29

CORRELATION COEFFICIENTS / N = 10

	DOL	AN	PHAI	LMEAN	LSD	LKMAX	LK90	LKV
DOL	1.00	0.52	0.05	0.30	0.26	-0.45	-0.50	-0.20
AN	0.52	1.00	0.48	0.41	0.07	-0.07	-0.10	0.07
PHAI	0.05	0.48	1.00	0.44	0.02	0.43	0.42	0.76
LMEAN	0.30	0.41	0.44	1.00	0.10	0.28	0.26	0.24
LSD	0.26	0.07	0.02	0.10	1.00	-0.44	-0.39	-0.18
LKMAX	-0.45	-0.07	0.43	0.28	-0.44	1.00	0.99	0.78
LK90	-0.50	-0.10	0.42	0.26	-0.39	0.99	1.00	0.76
LKV	-0.20	0.07	0.76	0.24	-0.18	0.78	0.76	1.00

porosity, and mean rhomb size and percentage dolomite rhombs. On the other hand, significant negative correlation exists between percentage of dolomite rhombs and permeability.

In the study area, except for intercrystalline porosity that developed often in the calcitic dolostone immediately below the altered zone, dolomitization has been interpreted to have contributed little to the porosity. The minor amount of porosity associated with the dolomitization is believed to have been formed mainly by preferential dissolution of calcite in the dolomite matrix as a result of leaching.

4.4 Porosity As A Function of Anhydritization

Porosity destruction by anhydrite porosity occlusion is very common in the drill cores. However, anhydrite leaching is believed to be one of the major contributors to present porosity. This dual property of anhydrite as a modifier of porosity was noted by Murray (1960).

The significant positive correlation between percentage of anhydrite and porosity substantiate the important role of anhydrite leaching in bringing about present porosity (Table 2). A significant correlation also exists between porosity and vertical permeability ($r = 0.76$) possibly suggesting the anhydrite leaching in creating porosity occurs as a result of percolation of water through vertical conduits.

4.5 Summary of Porosity Development

All facies in the study area demonstrate some degree of porosity. Yet, no single facies has been found to preserve porosity at all times. Accordingly, development of porosity cannot be categorized as true facies selective. On the contrary, it is inferred that the preservation of primary porosity like the development of leached porosity and minor intercrystalline porosity, was controlled by late diagenetic alterations.

However, facies having more primary porosity (e.g., vadolite) are more likely to show higher porosity development, and consequently they represent the principal reservoir facies.

CHAPTER 5

SUMMARY

The Mississippian MC-3a beds, the producing interval of the studied pool, can be correlated into the adjacent Wascada area.

The trapping mechanism of the study area is primarily structural; this is true with the limitation of the updip and/or lateral facies changes involving porosity development.

In the study area, the MC-3a beds represent a carbonate tidal flat complex. Drill cores show development of four lithofacies. These are: algal, vadolite, bioclastic grainstone and peloidal grainstone facies. Except for the vadolite, all others refer to depositional environments characterized by shoreline features; namely a tidal flat complex. The vadolite is believed to have formed due to subaerial exposure in a strandline environment during early diagenesis. It was previously regarded as oolite by earlier workers (e.g., Ghazar, 1978) formed in agitated water submarine shoals on a platform edge far away from the shoreline towards the basin.

The processes of diagenesis fall under two domains: early and late. The early diagenesis is characterized principally by biological diagenesis, formation of vadolite, and calcite cementation. The late diagenesis includes dolomitization, anhydratization, formation of other authigenic minerals, compaction, pressure solution,

fracturing, and leaching. The relative chronology of the important diagenetic events shows, in general, considerable overlap.

The development of porosity is not true facies selective. Late diagenetic alterations controlled the preservation of primary porosity as well as the development of leached porosity and minor intercrystalline porosity. However, facies with higher primary porosity (e.g., vadolite) is more likely to show higher porosity development, and consequently represent the principal reservoir facies.

Finally, this study may be helpful in selecting areas of high porosity and permeability for future development of the pool. Further studies of this type are recommended using scanning electron microscopy as well.

REFERENCES

Assereto, R.L.A.M. and R.L. Folk, 1976, Bricklike texture and radial rays in Triassic pisolites of Lombardy, Italy: a clue to distinguish aragonitic pisolites, Sed. Geol., V. 16, P. 205-222.

Bathurst, R.G.C., 1966, Boring algae, micrite envelopes, and lithification of molluscan biosparites, Geol. Jour., V. 5, P. 15-32.

----------, 1976, Carbonate sediments and their diagenesis, Elsevier Scientific Publishing Co., Amsterdam Oxford New York, 658 p.

Berg, C.A., 1956, Viden-Roselea and North-Virden fields, Manitoba, First Int. Williston Basin Symposium, P. 84-93.

Berner, R.A., 1971, Principles of chemical sedimentology, Mcgraw-Hill Book Company, 240 p.

Blatt, H., G.V. Middleton and R.C. Murray, 1980, Origin of sedimentary rocks, Prentice-Hall Inc., Englewood Cliffs, New Jersey, 782 p.

Burgess, C.J., 1983, Quarternary pisoids of Lau, Fiji, In Peryt, T.M. (ed.), Coated Grain, Springer-Verlag, New York, P. 488-502.

Clark, D.N., 1980, The sedimentology of the Zechstein 2 carbonate formation of eastern Drenthe, the Netherlands, Contr. sedimentology, V. 9, p. 131-165.

Conely, R.F. and W.M. Bundy, 1958, Mechanism of gypsification Geochem, et Cosmochim Acta, V. 15, P. 57-72.

Department of Energy and Mines, Petroleum Branch, Manitoba, 1983, Pool location map.

Dunham, R.J., 1971, Meniscus cement, In Bricker, O.P. (ed.), Carbonate cements, The John Hopkins University, Studies in Geology, No. 19, P. 297-300.

Elliot, T.L., 1982, Carbonate facies, depositional cycles, and the development of secondary porosity during burial diagenesis: Mission Canyon Formation, Hass field, North Dakota, fourth International Williston Basin Symposium, P. 131-151.

Esteban, M., 1976, Vadose pisolite and caliche, A.A.P.G. Bull., V. 60, P. 2048-2057.

Flugel, E., 1982, Microfacies analysis of limestone, Springer-Verlag, Berlin Heidelberg New York, 633 p.

Folk, R.L., 1965, Some aspects of recrystallization in ancient limestones, In Pray, L.C. and R.C. Murray (eds.), Dolomitization and limestone diagenesis, S.E.P.M. Spec. Pub. 13, P. 14-48.

----------, 1974, The natural history of crystalline calcium carbonate: effect of magnesium content and salinity, Journ. Sed. Pet., v. 44, P. 40-53.

---------- and L.S. Land, 1975, Mg/Ca ratio and salinity: two controls over crystallization of dolomite, A.A.P.G. Bull., V. 59, P. 60-68.

Fuller, J.G.C.M., 1956a, Mississippian rocks and oilfields in southeastern Saskatchewan Dept. Mineral Res. Rep. 19, 72 p.

----------, 1956b, Mississippian rocks in the Saskatchewan portion of the Williston Basin: a review, First Int. Williston Basin Symposium, P. 29-35.

Fuzesy, L.M., 1960, Correlation and subcrops of the Mississippian strata in southeastern and south-central Saskatchewan, Saskatchewan Dept. Mineral Res. Rep. 51, 63 p.

----------, 1966, Geology of the Frobisher-alida beds, southeastern Saskatchewan, Saskatchewan Dept. Mineral Res. Rep. 104, 59 p.

Gerhard, L.C., S.B. Anderson and J. Berg, 1978, Mission Canyon porosity development, Glenburn field, North Dakota Williston Basin, In the economic geology of the Williston Basin, Montana Geol. Soc. 24th Ann. Conference, P. 177-188.

Ghazar, W., 1978, Geological report on hydrocarbon exploration in Pierson area, Manitoba, Openfile report, Petroleum Branch, Department of Energy and Mines, Manitoba.

Gunatilaka, A., 1976, Thallophyte boring and micritization within sands from Connemara, Western Ireland, Jour. Sed. Pet., v. 46, P. 548-554.

Halabura, S.P., 1984, Petroleum geology of the MC-3 Member, Mission Canyon formation, Pierson Field, Manitoba, Openfile report, Petroleum Branch, Department of Energy and Mines, Manitoba.

Hardie, L.A., 1967, The gypsum anhydrite equilibrium at one atmosphere pressure, Amer. Mineralogist, V. 53, P. 171-200.

Hughes Clarke, M.W. and A.J. Keij, 1973, Organisms as producers of carbonate sediment and indicators of environment in the southern Persian Gulf, In Purser, B.H. (ed.), The Persian Gulf, Springer-Verlag, New York Heidelberg Berlin, P. 33-57.

Kahle, C.F., 1974, Ooids from Great Salt Lake, Utah, as an analog for the genesis and diagenesis of ooids in marine limestone, Jour. Sed. Pet., V. 44, P. 30-39.

----------, 1977, Origin of subaerial Holocene calcareous crusts: role of algae, fungi and sparmicritization, Sedimentology, v. 24, P. 413-435.

Kay, G.M., 1951, North American Geosynclines, Geological Society of America, Mem. 48, P. 17.

Kendall, A.C., 1975, Anhydrite replacements of gypsum (satin-spar) veins in the Mississippian caprocks of south-eastern Saskatchewan, Canadian Jour. of Earth Sci. V. 12, P. 1190-1195.

---------- and M.E. Tucker, 1973, Radiaxial fibrous calcite: a replacement after acicular carbonate, Sedimentology, V. 20, P. 365-389.

Kendall, C.G.St.C. and P.A.D.E. Skipwith, 1969, Holocene shallow-water carbonate and evaporite sediments of Khoral Bazam, Abu Dhabi, southwest Persian Gulf, A.A.P.G. Bull., V. 53, P. 841-869.

Kinsman, D.J.J., 1969, Modes of formation, Sedimentary associations, and diagenetic features of shallow-water and supratidal evaporites, A.A.P.G. Bull., V. 53, P. 830-840.

Kobluk, D.R. and M.J. Risk, 1977, Micritization and carbonate grain binding by endolithic algae, A.A.P.G. Bull., V. 61, P. 1069-1082.

Krumbein, N.C. and L.L. Sloss, 1951, Stratigraphy and sedimentation, Freeman and Co., San Francisco, 337 p.

Laird, W.M., 1956, The Williston Basin - a backward look with a view to the future, First International Williston Basin Symposium, P. 14-22.

Land, L.S., 1980, The isotope and trace element geochemistry of dolomite: the state of the art, in Zenger, D.H., J.B. Dunham & R.L. Ethington (eds.), Concepts and models of dolomitization, SEPM, Spec. Pub. No. 28, P. 87-110.

Larsen, G. and G.V. Chillinger, 1967, Concluding remarks on diagenesis, In Larsen, G. and G.V. Chillinger (eds.), Diagenesis in sediments, Developments in Sedimentology 8, Amsterdam, Elsevier Publishing Co., P. 523-524.

Lindsay, R.F., 1982, Anatomy of the dolomitized carbonate reservoir, Mission Canyon Formation, Little Knife field, North Dakota (abs), A.A.P.G. Bull., V. 66, P. 594.

---------- and C.G.St.C. Kendall (1984), Depositional facies, diagenesis, and reservoir character of the Mission Canyon Formation (Mississippian) of the Williston Basin at Little Knife field, North Dakota, In Roehl, P.O. and P.W. Choquette (eds.), Carbonate Petroleum Reservoirs, Springer-Verlag, New York.

---------- and M.S. Roth, 1982, Carbonate and evaporite facies, dolomitization and reservoir distribution of the Mission Canyon Formation, Little Knife field, North Dakota, Fourth International Williston Basin Symposium, P. 153-179.

Lobue, C., 1982, Depositional environment and the diagenesis of the Silurian Interlake Formation, Williston Basin, Western North Dakota, In Christopher, J.E. and J. Kaldi (eds.), Fourth International Williston Basin Symposium, P. 29-42.

Logan, B.W. and V. Semeniuk, 1976, Dynamic metamorphism: process and products in Devonian carbonate rocks, Canning Basin, Western Australia, Geol. Soc. Australia, Spec. Pub. 6, 138 p.

Logan, B.W., R. Rezak and R.N. Ginsburg, 1964, Classification and environmental significance of algal stromatolites, Jour. Geol., V. 72, P. 68-83.

Longman, M.W., 1980, Carbonate diagenetic textures from near-surface diagenetic environments, A.A.P.G. Bull., V. 64, P. 461-487.

Macdonald, G.J.F., 1953, Anhydrite-gypsum equilibrium of the Amer. Jour. of Sci., V. 251, P. 884-898.

Mattes, B.W. and E.H. Mountjoy, 1980, Burial dolomitization of the Upper Devonian buildup, Jasper National Park, Alberta, In Zenger, P.H., J.B. Dunham and R.L.E. Ethington (eds.), Concepts and models of dolomitization, S.E.P.M., Spec. Pub. No. 28, P. 259-297.

Martin, R., 1966, Paleogeomorphology and its application to exploration of oil and gas (with examples from Western Canada), A.A.P.G. Bull., V. 50, P. 2277-2311.

McCabe, H.R., 1959, Mississippian stratigraphy of Manitoba, Manitoba Mines Branch, Pub. 58-1, 99 p.

----------, 1963, Mississippian oil fields of southeastern Manitoba, Manitoba Mines Branch, Pub. 60-5, 50 p., Figures to accompany, 31 p.

----------, 1971, Stratigraphy of Manitoba, an introduction and review: Geol. Assoc. of Canada, Spec. Paper No. 9, P. 167-187.

McCamis, J.G., 1958, Anhydritization in the Mississippian Souris Valley Beds of the Broadview area, Saskatchewan, Unpub. M.Sc. thesis, University of Saskatchewan, Saskatoon, Saskatchewan.

McCulloch-Smith, L.A., 1984, The Woodworth oil field: a diagenetic trap, Unpub. B.Sc. (Hons.) thesis, University of Manitoba, 214 p.

Miller, E.G., 1972, Parkman field, Williston Basin, Saskatchewan, In King, R.E. (ed.), Stratigraphic oil and gas fields, A.A.P.G. Mem. 16 and Soc. Explor. Geophys. Spec. Pub. 10, P. 502-510.

Milne, J.F. and G.D. Nickoloff, 1955, Virden-Roselea shows promise of Manitoba, The Petroleum Engineers, V. 27, No. 2, P. B81-B89.

Moore, C.H., 1979, The fate of primary carbonate porosity during and after burial-diagenetic constraints on the depositional model strategy, A.A.P.G. Continuing Education Course Note Series No. 11, P. A8-A9.

Murray, R.C., 1960, Origin of porosity in carbonate rocks, Jour. Sed. Pet., V. 30, P. 59-84.

----------, 1964, Origin and diagenesis of gypsum and anhydrite, Jour. Sed Pet., 34, P. 512-523.

Perkins, B.F. (ed.), 1971, Trace fossils, a field guide to selected localities in Pennsylvanian, Permian, Cretaceous and Tertiary rocks of Texas and related papers, 147 p., S.E.P.M. Field trip, April 1-3, La. State Univ. Misc. Pub. 71-1.

Peryt, T.M., 1983, Vadoids, In Peryt, T.M. (ed.), Coated Grains, Springer-Verlag, New York, P. 437-450.

Phleger, F.B., 1969, A modern evaporite deposit in Mexico, A.A.P.G. Bull., V. 53, P. 824-829.

Powers, R.W., 1962, Arabian Upper Jurassic carbonate reservoir rocks, In Ham, W.E. (ed.), Classification of Carbonate Rocks, A.A.P.G. Mem. 1, 279 p.

Purser, B.H. and J.P. Loreau, 1973, Aragonitic supratidal encrustations on the Trucial Coast, Persian Gulf, In Purser, B.H. (ed.), The Persian Gulf, Springer-Verlag, New York, P. 343-376.

Rodgers, M., 1984, Petroleum Geology of the Mission Canyon Formation, Waskada field, Open file report, Petroleum Branch, Department of Energy and Mines, Manitoba.

Shinn, E.A., R.M. Lloyd and R.N. Ginsburg, 1969, Anatomy of a modern tidal flat, Andros Island, Bahamas, Jour. Sed. Petrology, V. 39, P. 1202-1222.

Stehli, F.G. and J. Hower, 1961, Mineralogy and early diagenesis of carbonate sediments, Jour. Sed. Pet., V. 31, P. 358-371.

Swinchatt, J.P., 1965, Significance of constituent composition, texture and skeletal breakdown in some recent carbonate sediments, Jour. Sed. Pet., V. 35, P. 71-90.

Thorstenson, D.C., F.T. Mackenzie, and B.L. Ristvet, 1972, Experimental vadose and phreatic cementation of skeletal carbonate sand, Jour. Sed. Pet., V. 42, P. 162-167.

Van der Borch, C.C., M. Rubin and B.J. Skinner, 1964, Modern dolomite from South Australia, Amer. Jour. of Sci., V. 262, P. 1116-1118.

Wanless, H.R., 1979, Limestone response to stress: pressure solution and dolomitization, Jour. Sed. Pet., V. 49, P. 437-462.

Wardlaw, N.C., 1979, Pore systems in carbonate rocks and their influence on hydrocarbon recovery efficiency, A.A.P.G. Continuing Education Note Series No. 11, P. E1-E24.

Weyl, P.K., 1960, Porosity through dolomitization: conservation of mass requirements, Jour. Sed. Pet., V. 30, P. 85-90.

Williams, J.A., 1974, Characterization of oil types in Williston Basin, A.A.P.G. Bull., V. 58, P. 1243-1252.

Wilson, J.L., 1975, Carbonate facies in geologic history, Springer-Verlag, Berlin, 471 p.

----------, 1980, A review of carbonate reservoirs, In Miall, A.D. (ed.), Facts and Principles of World Petroleum Occurrence, C.S.P.G., Mem. 6, P. 95-117.

Windwall, H.D., 1968, The role of high Mg calcite in the preservation of micrite envelopes and textural features of aragonite sediments, Jour. Sed. Pet., V. 38, P. 1320-1325.

Wolf, K.H., 1965, Petrogenesis and paleoenvironment of Devonian algal limestones of New South Wales, Sedimentology, V. 4, P. 113-178.

Young, H.R., 1973, Petrology of the Virden Member of the Lodgepole Formation (Mississippian) in south-western Manitoba, Unpub. Ph.D. thesis, Queens University, Kingston, Ontario, 235 p.

Zakus, P.D., 1967, Sedimentary petrography and stratigraphy of the Mississippian Whitewater Lake Member of southwestern Manitoba, Unpub. M.Sc. thesis, University of Manitoba, Winnipeg, Manitoba, 91 p.

Zankl, H., 1969, Structural and textural evidence of early lithification of fine-grained carbonate rocks, Sedimentology, V. 12, P. 241-256.

Zenger, D.H. and J.B. Dunham, 1980, Concepts and models of dolomitization - an introduction, In Zenger, D.H., J.B. Dunham and R.L. Ethington (eds.), Concepts and models of dolomitization, S.E.P.M., Spec. Pub. No. 28, P. 1-10.

PLATES

NOTICE/AVIS

PAGE(S) plates 1-54 IS/ARE EST/SONT colour photos

PLEASE WRITE TO THE AUTHOR FOR INFORMATION, OR CONSULT THE ARCHIVAL COPY HELD IN THE DEPARTMENT OF ARCHIVES AND SPECIAL COLLECTIONS, ELIZABETH DAFOE LIBRARY, UNIVERSITY OF MANITOBA, WINNIPEG, MANITOBA, CANADA, R3T 2N2.

VEUILLEZ ECRIRE A L'AUTEUR POUR LES RENSEIGNEMENTS OU VEUILLEZ CONSULTER L'EXEMPLAIRE DONT POSSEDE LE DEPARTEMENT DES ARCHIVES ET DES COLLECTIONS SPECIALES, BIBLIOTHEQUE ELIZABETH DAFOE, UNIVERSITE DU MANITOBA, WINNIPEG, MANITOBA, CANADA, R3T 2N2.

PLATE - 1

TEXTURAL ROCK TYPES

A. Photograph showing the erosional contact (1) between the upper bioclastic grainstone facies and lower stromatolite subfacies. The latter is composed of LHH type (2) stromatolite with infilled sedimented micrite. Sample no. 1.61, polished core slab perpendicular to stratification slab. Bar scale equals 1 cm.

B. Photograph showing stromatolite subfacies composed of SH type stromatolite (1) with infilled sedimented micrite. Characteristic irregular fenestrae (2) are abundant. Sample no. 4.43, polished core slab perpendicular to stratification. Bar scale equals 1 cm.

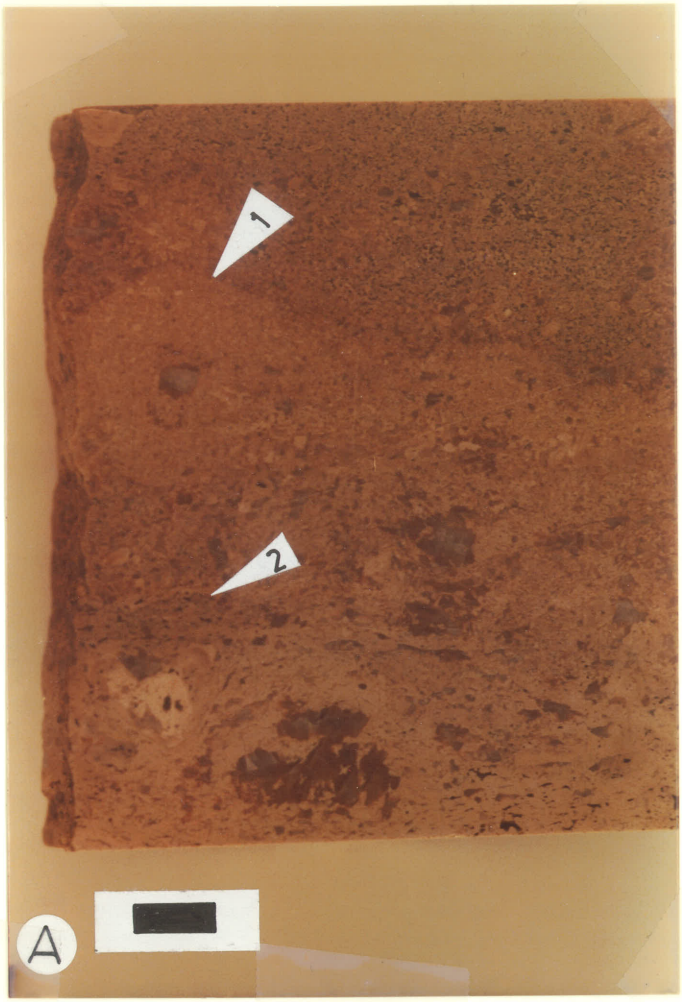
1
2
A

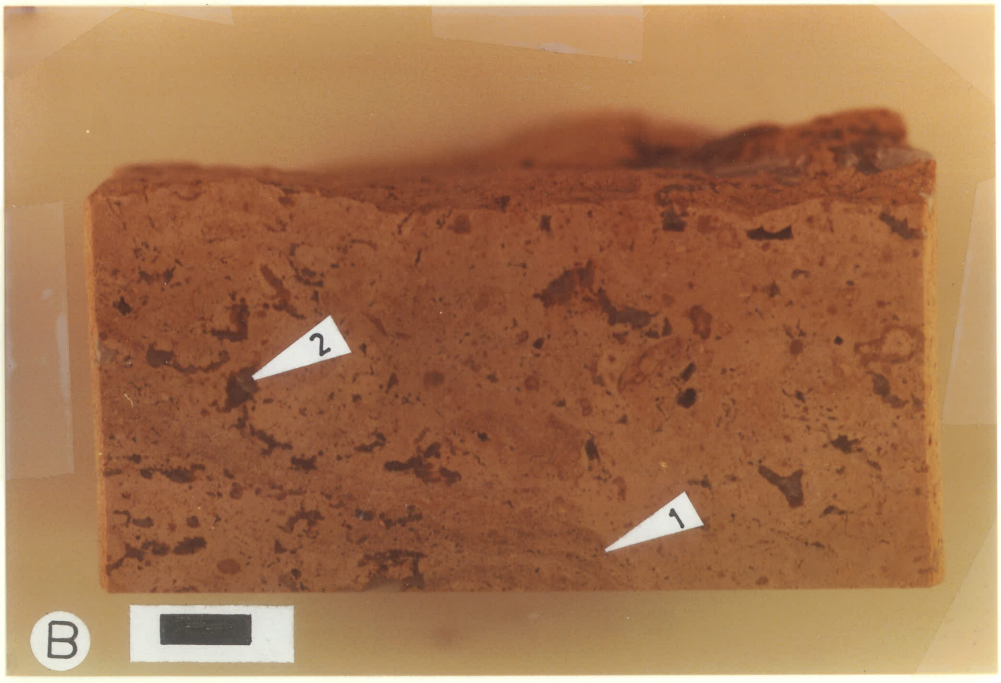
2
1
B

PLATE - 2

TEXTURAL ROCK TYPES

A. Photograph of stromatolite subfacies showing SH type stromatolite. Sample no. 4.41, polished core slab perpendicular to stratification. Bar scale equals 1 cm.

B. Photograph of stromatolite subfacies showing SH type (1) stromatolite. Sample no. 4.41, polished core slab parallel to stratification. Bar scale equals 1 cm.

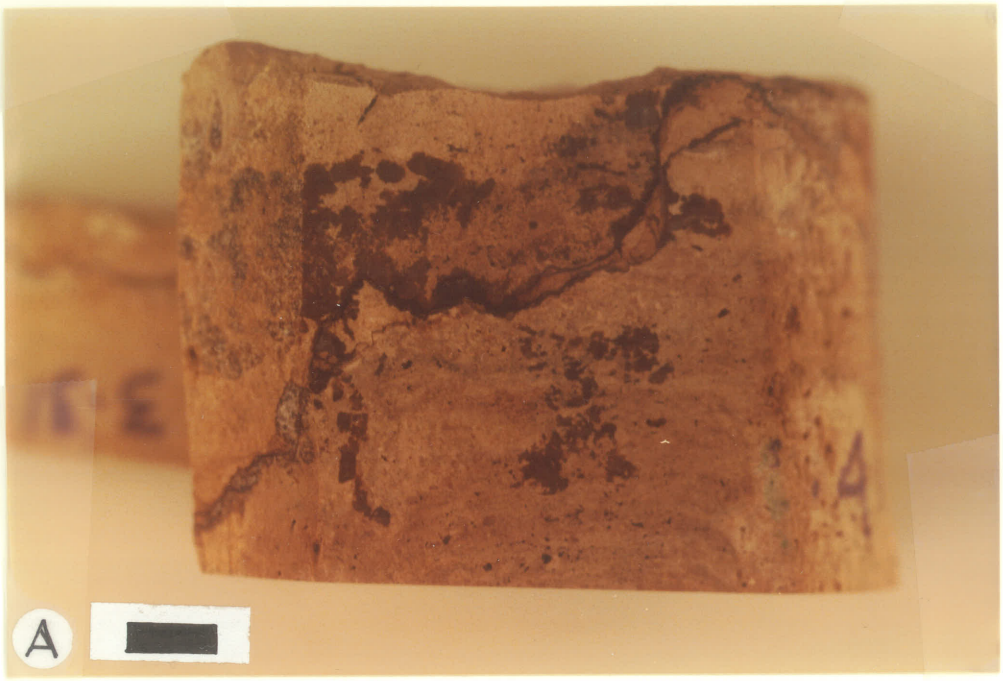
A

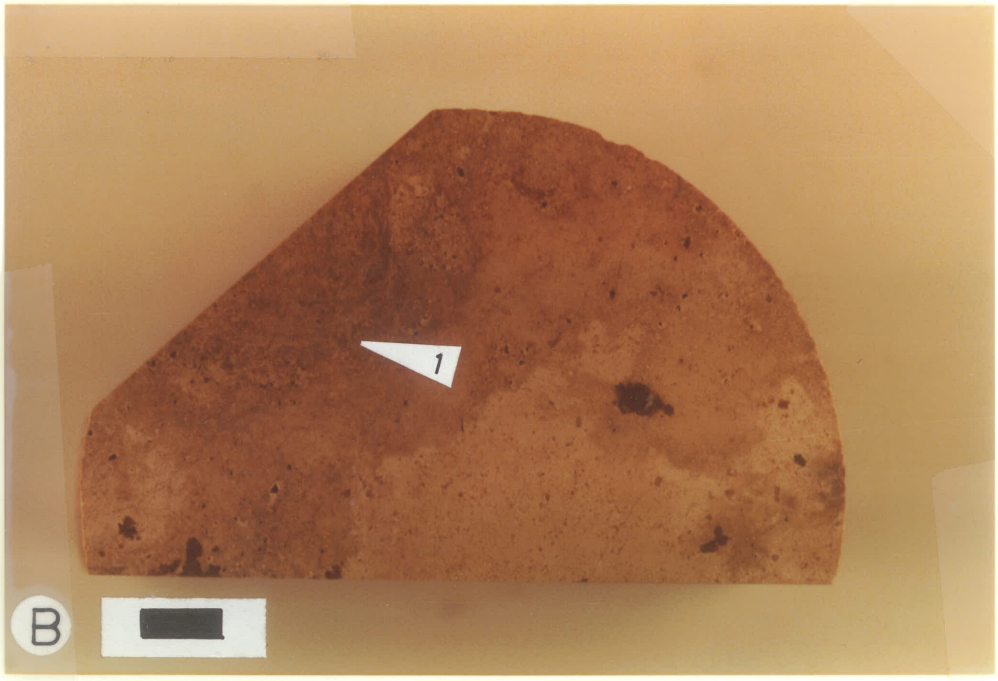
1
B

PLATE - 3

TEXTURAL ROCK TYPES

A. Photomicrograph of stromatolite subfacies showing laminoid fenestrae between stromatolitic laminae. Sample no. 4.43, thin section perpendicular to stratification. Bar scale equals 1.5 mm.

B. Photograph showing erosional contact (1) between upper stromatolite subfacies and lower vadolite facies. The former is characterized by sheet cracks (2). Sample no. 3.52, polished core slab perpendicular to stratification. Bar scale equals 1 cm.

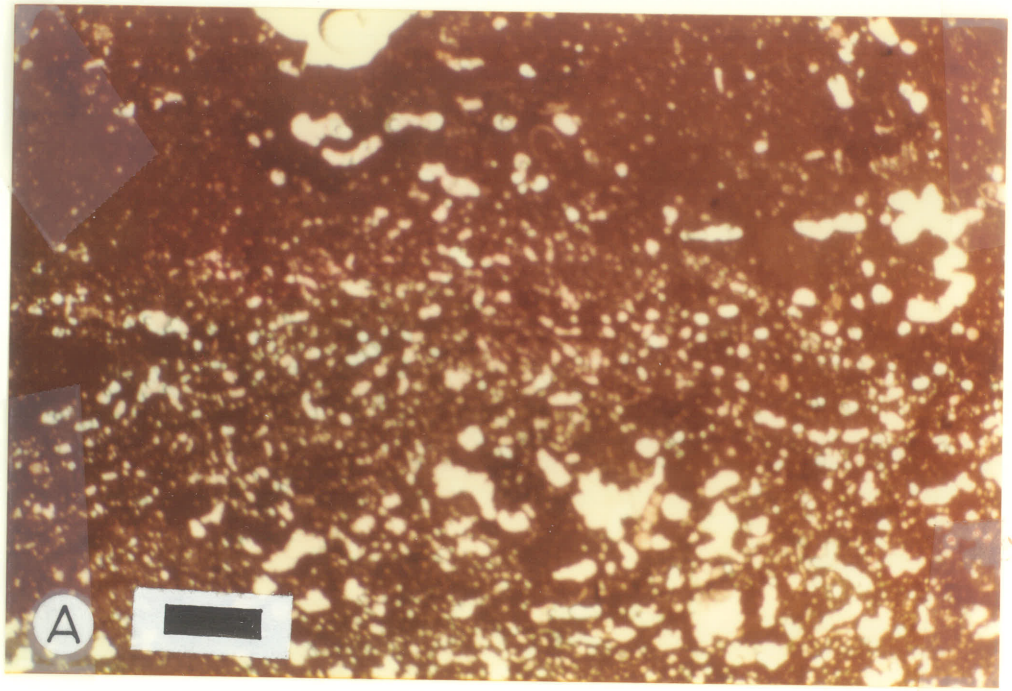
A

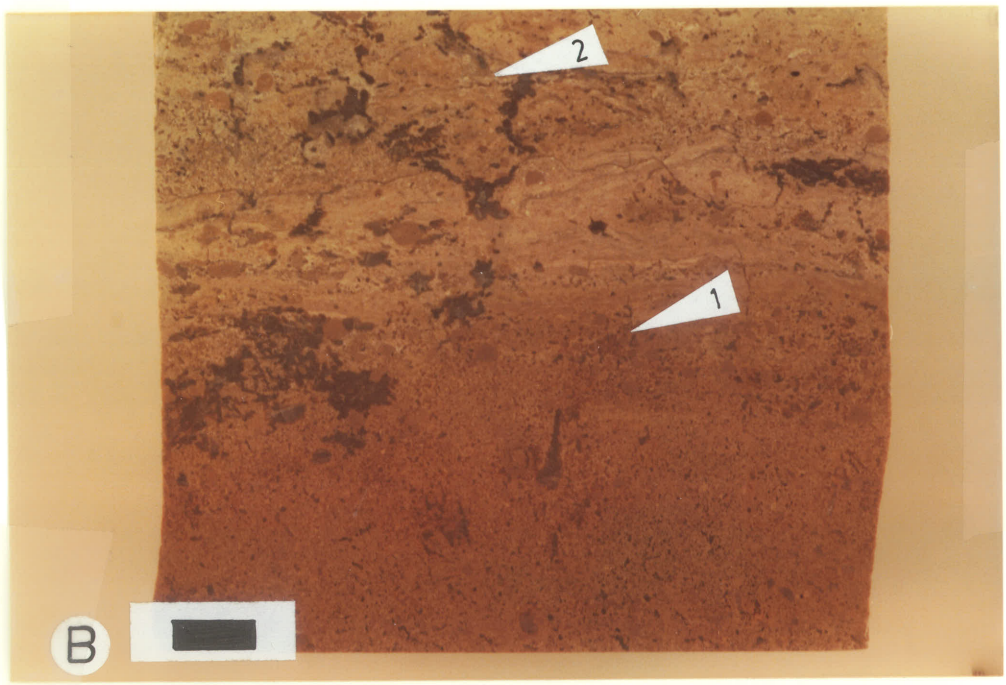
2
1
B

PLATE - 4

TEXTURAL ROCK TYPES

A. Photomicrograph of stromatolite subfacies showing sheet cracks (1) partially infilled with equant calcite cement. Sample no. 4.51, thin section perpendicular to stratification, crossed nicols. Bar scale equals 0.5 mm.

B. Photomicrograph of stromatolitic subfacies showing filaments and renalis structure of encrusting blue-green algae. Sample no. 4.43, thin section perpendicular to stratification, crossed nicols. Bar scale equals 70 microns.

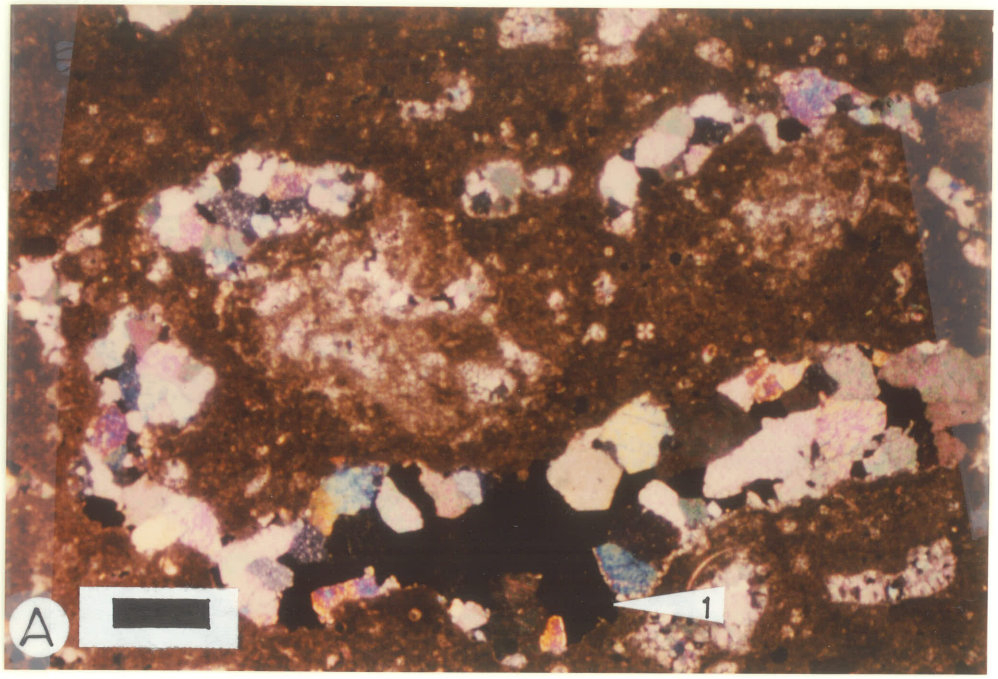
A
1

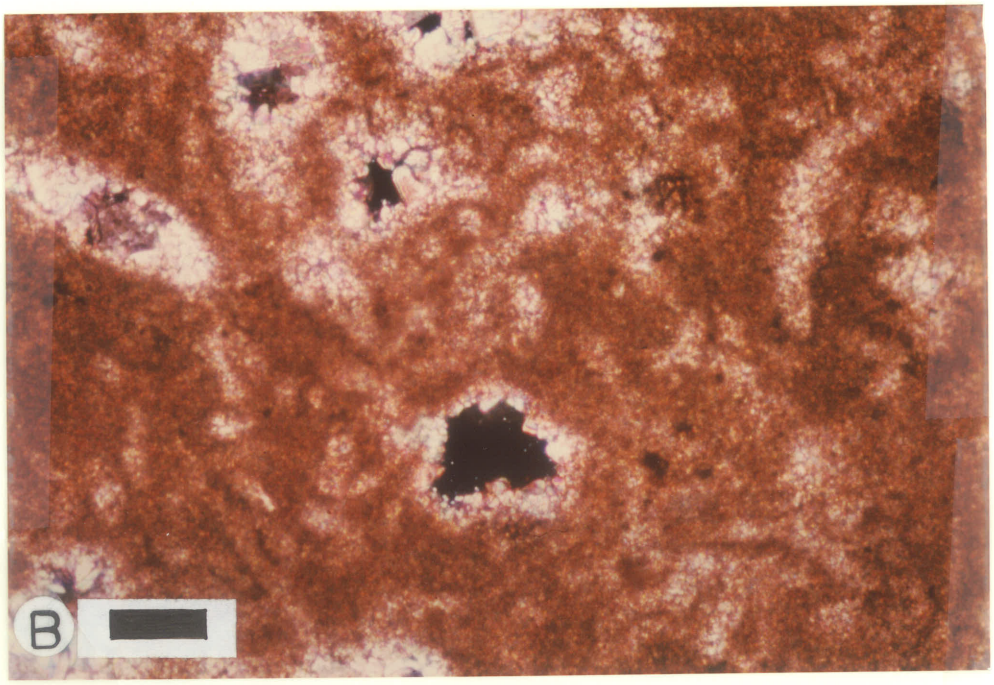
B

PLATE - 5

TEXTURAL ROCK TYPES

A. Photomicrograph of stromatolite subfacies showing Girvanella. The micrite calcified algal filaments (1) have been neomorphosed into microspar with some pseudospar. Sample no. 4.52, thin section perpendicular to stratification. Bar scale equals 0.5 mm.

B. Photomicrograph of stromatolite subfacies showing entrapped peloidal pockets (1) and blue-green algal grains (2). Sample no. 4.52, thin section parallel to stratification. Bar scale equals 0.25 mm.

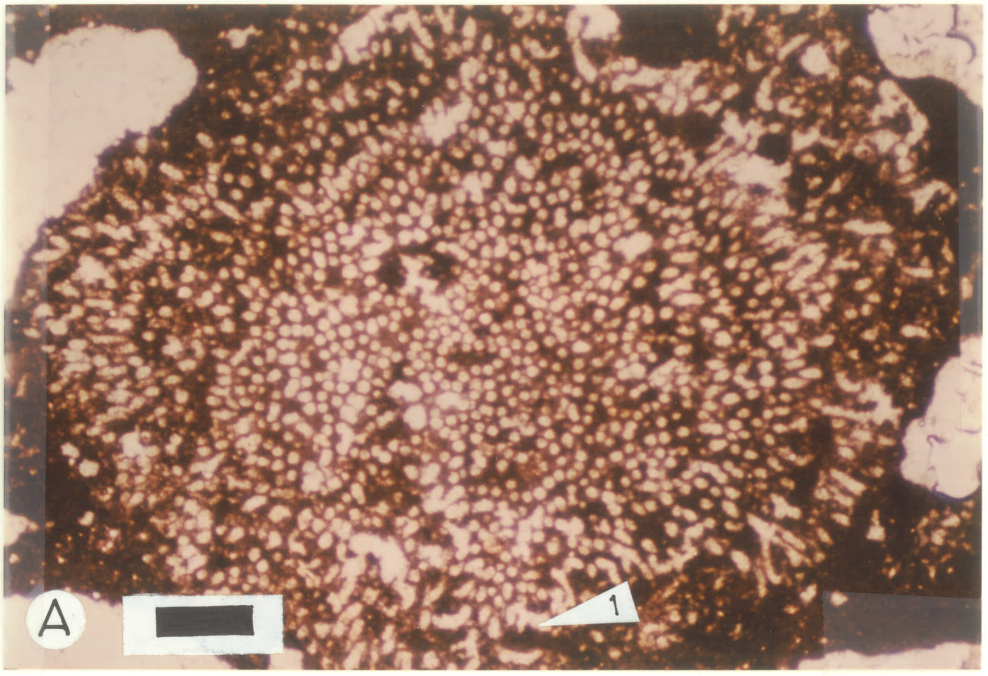
A
1

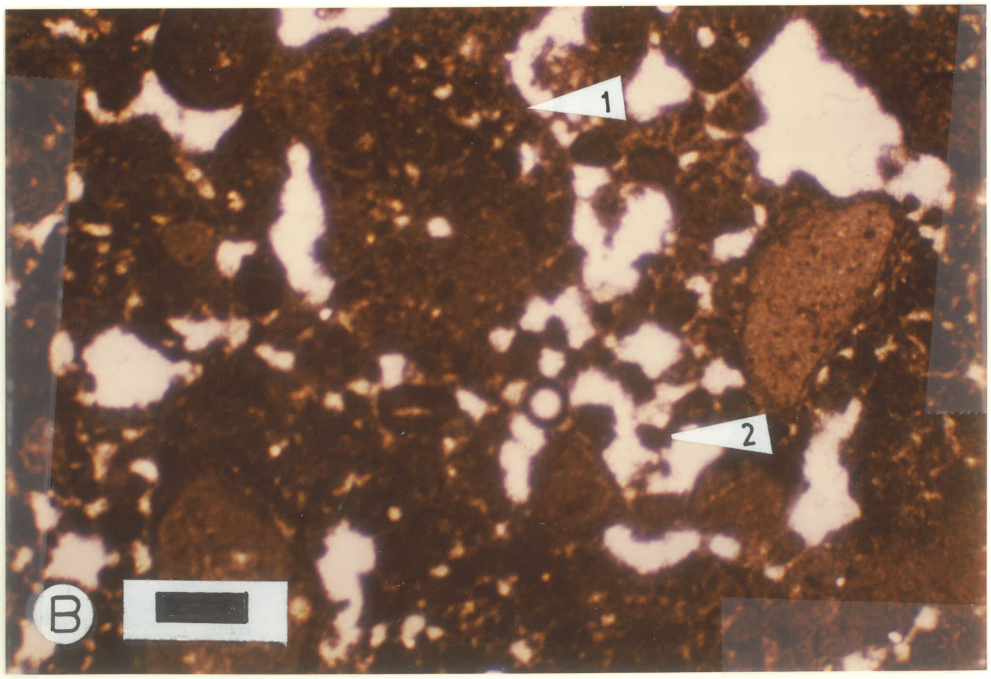
1
2
B

PLATE - 6

TEXTURAL ROCK TYPES

A. Photomicrograph of stromatolite subfacies showing entrapped ostracod (1), dasyclad (2) and foram (3). Sample no. 4.43, thin section parallel to stratification. Bar scale equals to 0.25 mm.

B. Photomicrograph of stromatolite subfacies showing entrapped brachiopod (1). Sample no. 5.32, thin section parallel to stratification. Bar scale equals 0.5 mm.

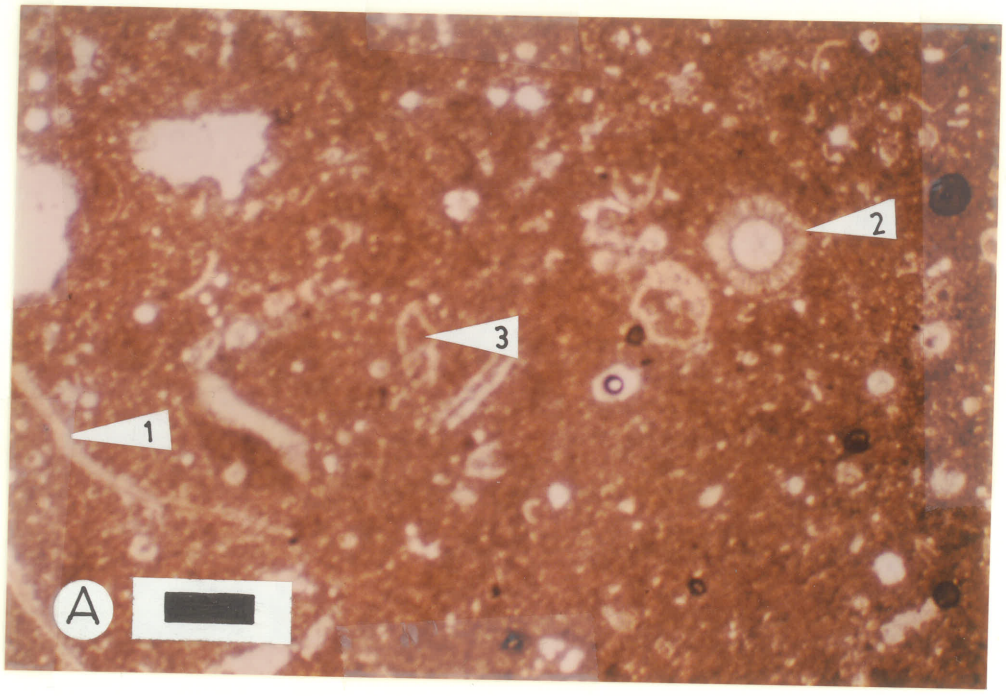
1
2
3
A

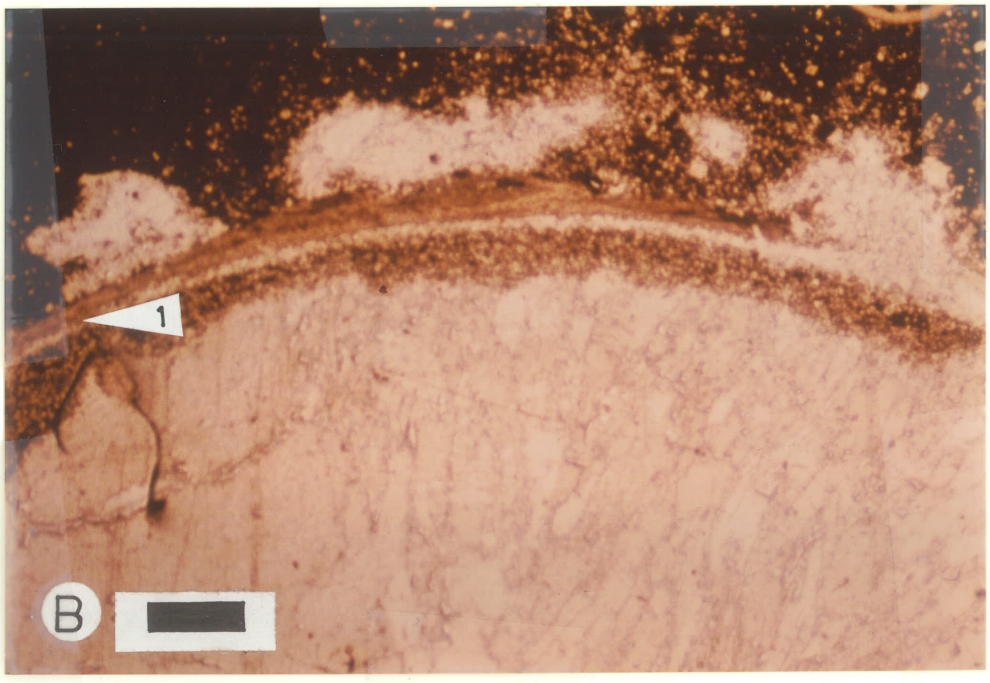
1
B

PLATE - 7

TEXTURAL ROCK TYPES

A. Photomicrograph of cryptalgal laminite subfacies showing algal laminae. Sample no. Z.44, thin section perpendicular to stratification. Bar scale equals 1.5 mm.

B. Photograph of cryptalgal laminite subfacies showing algal laminae and brown replacement anhydrite (1). Sample no. Z.44, polished core slab perpendicular to stratification. Bar scale equals 1 cm.

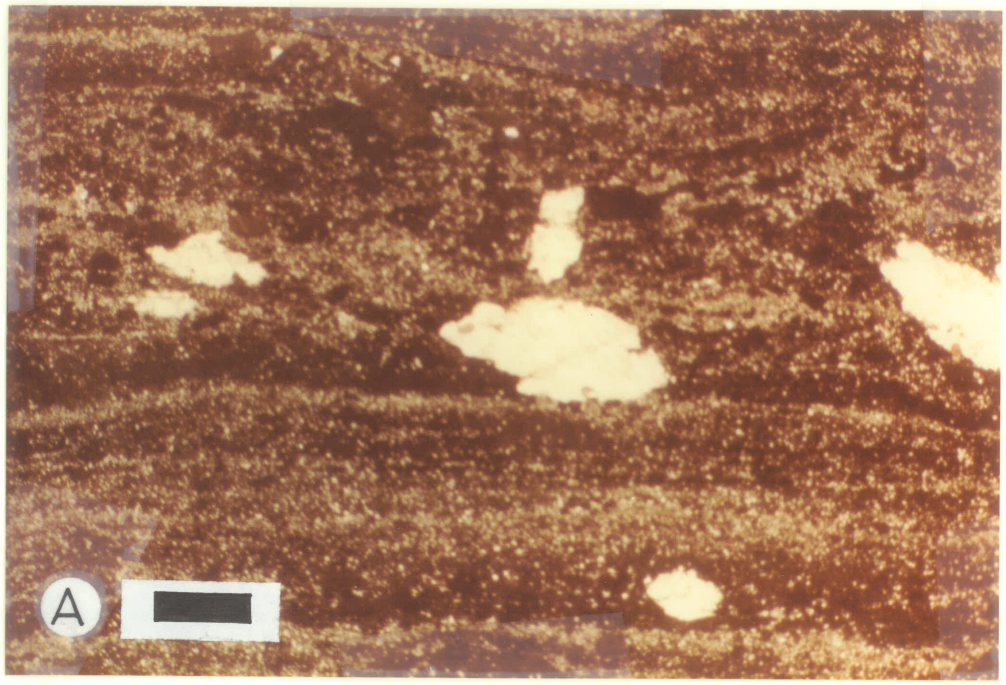
A


1
B

PLATE - 8

TEXTURAL ROCK TYPES

A. Photograph of cryptalgal laminite subfacies showing laminoid fenestrae (1). Sample no. 1.91a, polished core slab perpendicular to stratification. Bar scale equals 1 cm.

B. Photograph of cryptalgal laminite subfacies in the altered zone showing vaguely preserved algal laminae. Sample no. 3.11, polished core slab perpendicular to stratification. Bar scale equals 1 cm.

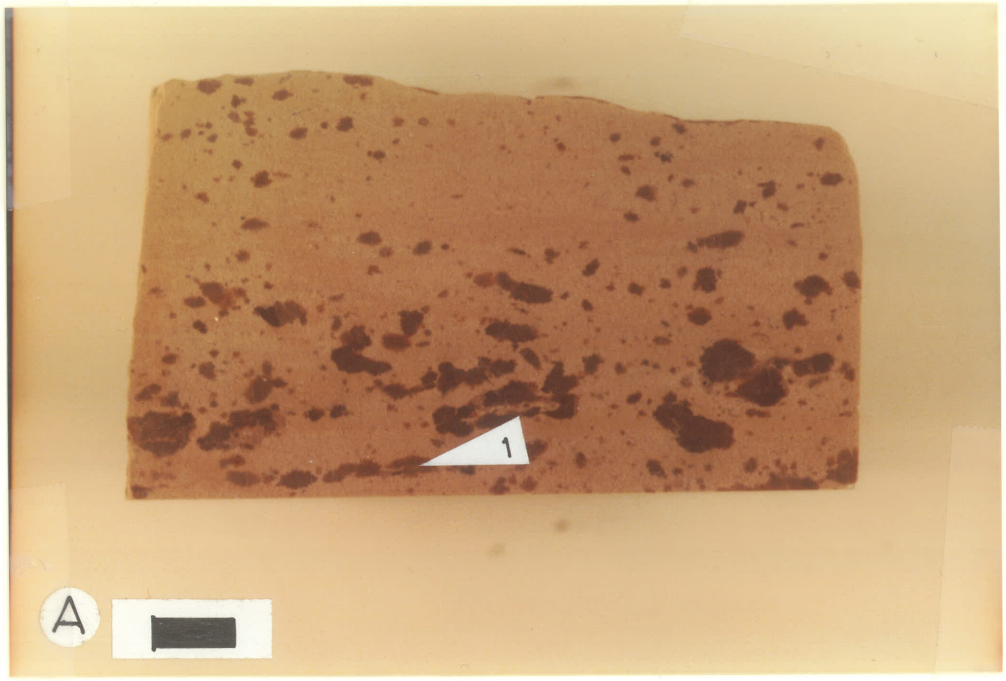
1
A

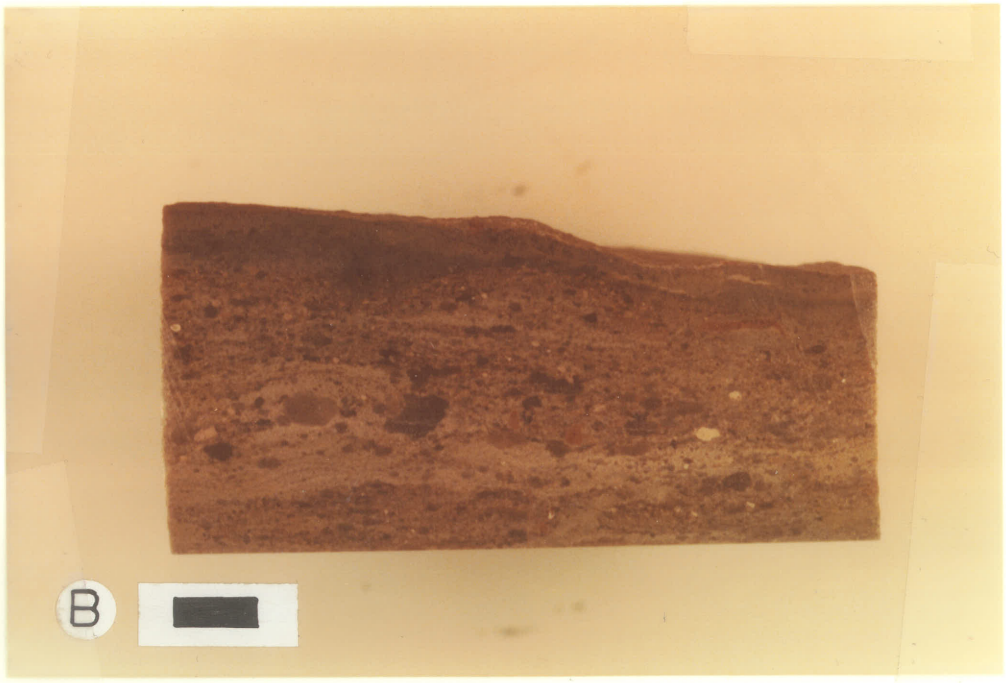
B

PLATE - 9

TEXTURAL ROCK TYPES

A. Photomicrograph of pseudostromata subfacies showing fenestrae (1) partially infilled with equant calcite cement. Sample no. 4.42, thin section parallel to stratification crossed nicols. Bar scale equals 0.5 mm.

B. Photograph of pseudostromata subfacies showing fenestrae (1) and sheet cracks (2). Sample no. 4.42, polished core slab perpendicular to stratification. Bar scale equals 1 cm.

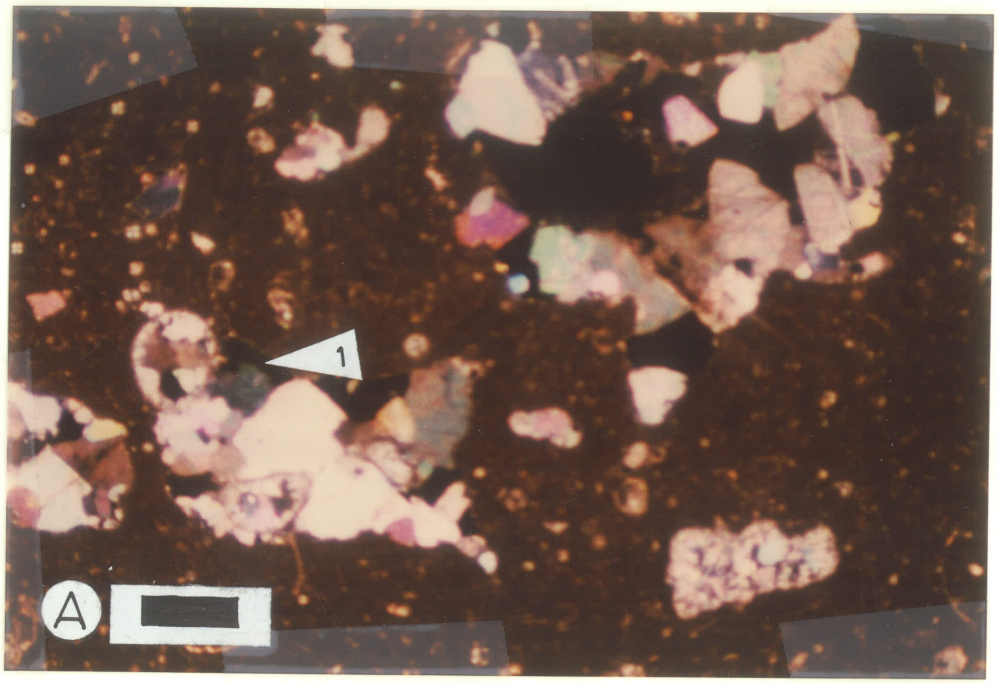
1
A


2
1
B

PLATE - 10

TEXTURAL ROCK TYPES

A. Photograph of pseudostromata subfacies showing vertical desiccation cracks (1), irregular anastomosing set of hummocky (2) and peaks low amplitude stylolites (3). Sample no. 1.62, polished core slab perpendicular to stratification. Bar scale equals 1 cm.

B. Photomicrograph of pseudostromata subfacies showing blue-green algal filaments and renalis structure. Sample no. 4.42, thin section perpendicular to stratification. Bar scale 70 microns.

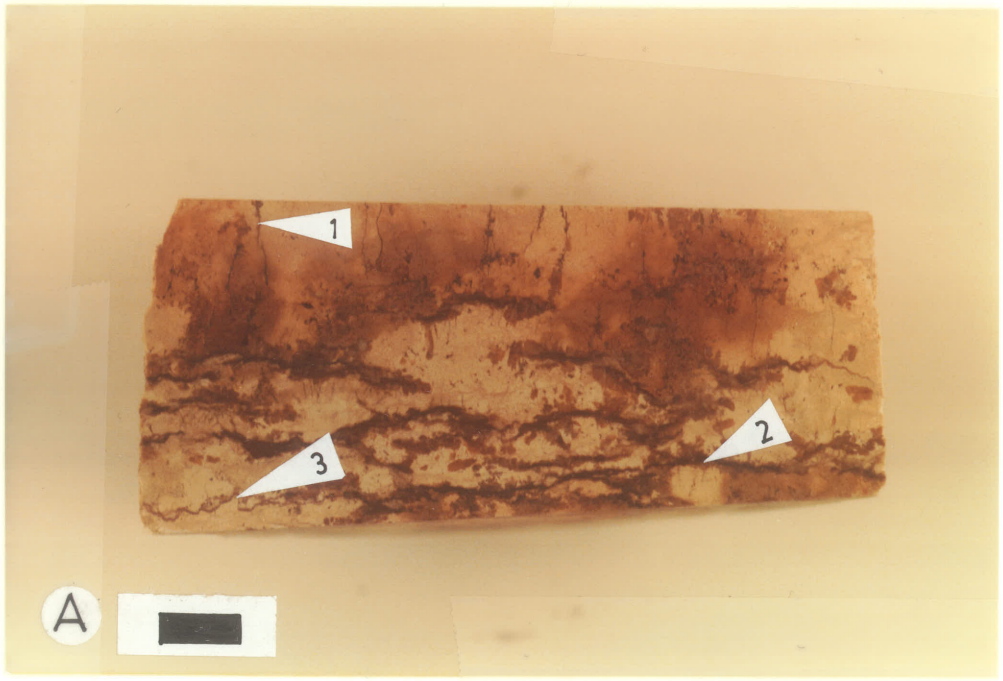
1
2
3
A

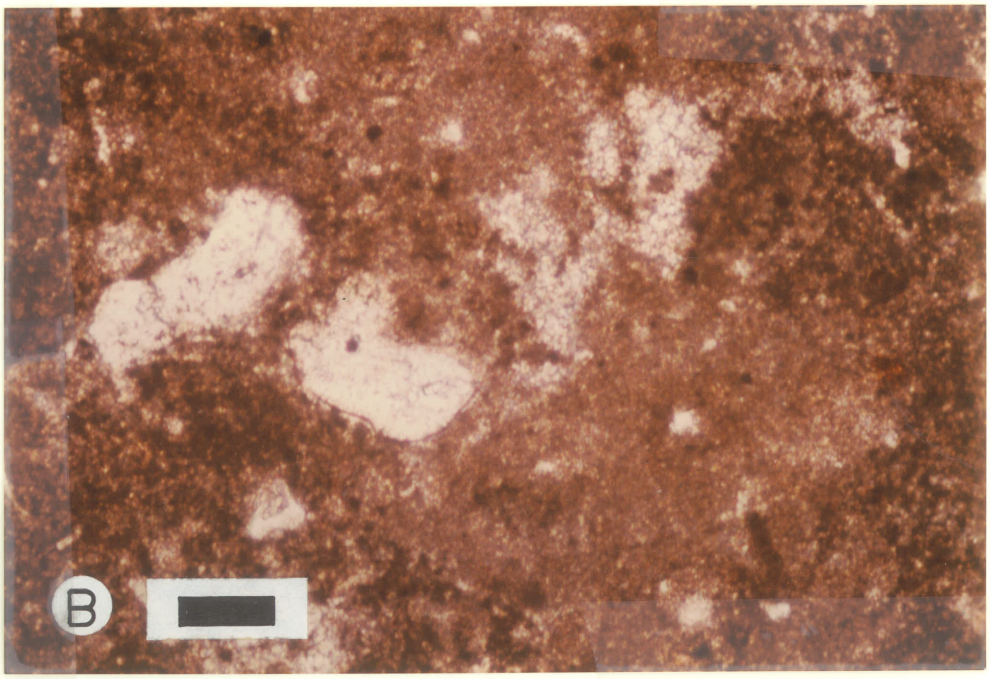
B

PLATE - 11

TEXTURAL ROCK TYPES

A. Photograph of pseudostromata subfacies showing burrows (1). Sample no. 4.40, polished core slab parallel to stratification. Bar scale equals 1 cm.

B. Photograph of pseudostromata subfacies showing the vertical orientation of burrow (1). Sample no. 4.40, polished slab perpendicular to stratification. Bar scale equals 1 cm.

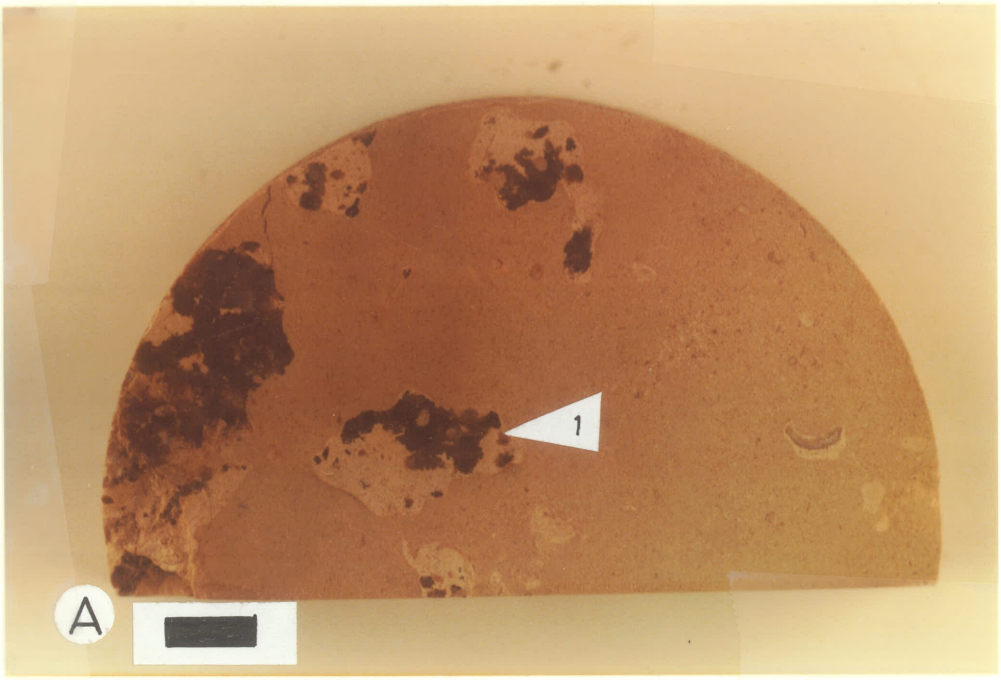
1
A


1
B

PLATE - 12

TEXTURAL ROCK TYPES

A. Photograph of vadolite facies showing vadose crust (1), inverse-graded grains (2), and fracture infilled with grey-white void-filling anhydrite (3). Sample no. 2.34, polished core slab perpendicular to stratification. Bar scale equals 1 cm.

B. Photograph of vadolite facies showing vadose crust (1) and inverse-graded grains (2). Sample no. 5.33, polished core slab perpendicular to stratification. Bar scale equals 1 cm.


1
2
3
A


1
2
B

PLATE - 13

TEXTURAL ROCK TYPES

A. Photomicrograph of vadolite facies showing vadoid coated with alternating laminae of micrite (1) and radiaxial spar (2), then fractured (3) due to desiccation, then recoated with both the laminae, and then again fractured (4). Sample no. 5.34, thin section perpendicular to stratification. Bar scale equals 0.25 cm.

B. Photomicrograph of vadolite facies showing flattened grains (1), sharing of the outer laminae (2), vadoids having broken vadoid as nucleii (3), multistage grain (4), polygonal filling, and vertical asymmetry of the graining. Sample no. 2.34, polished core slab perpendicular to stratification. Bar scale equals 1 mm.

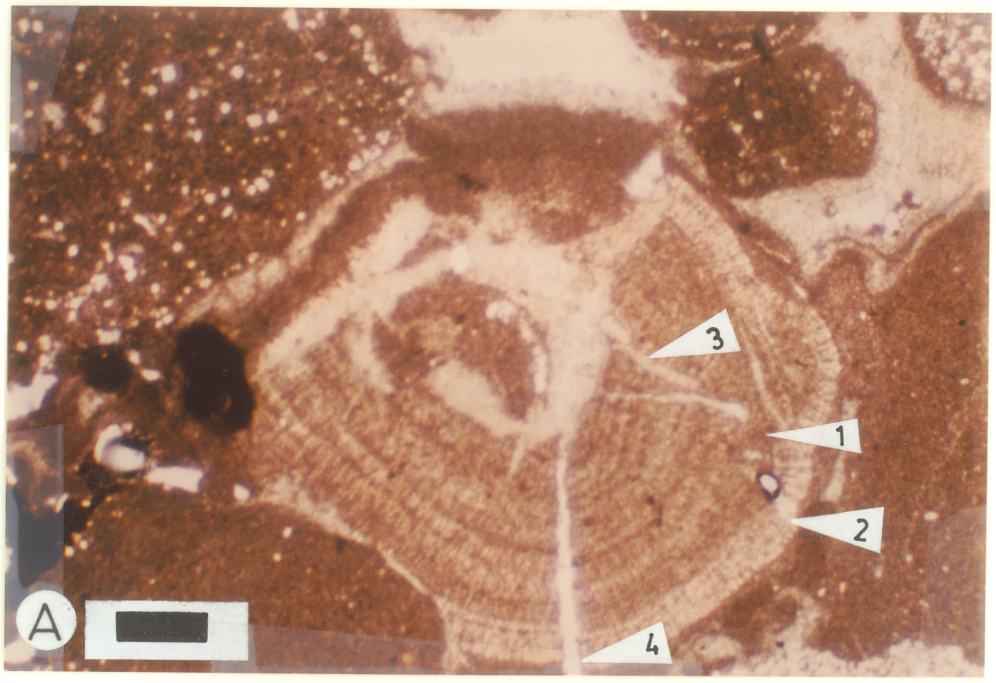
3
1
2
A
4

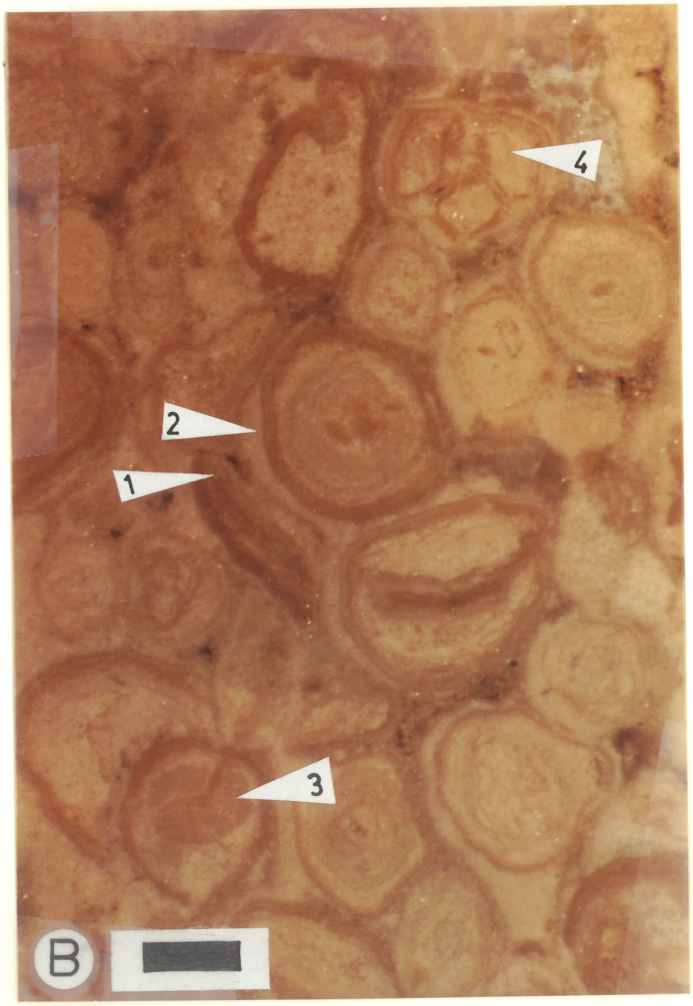
4
2
1
3
B

PLATE - 14

TEXTURAL ROCK TYPES

A. Close up view of Plate 13 Fig. B. Flattened grain (1), sharing of outer laminae (2), multistage grain (3), polygonal fitting, and vertical asymmetry of the grains. Sample no. 2.34, polished core slab perpendicular to stratification. Bar scale equals 0.6 mm.

B. Photomicrograph of vadolite facies showing continuation of outer laminae (1) into the surrounding sediment. Sample no. 5.34, thin section perpendicular to stratification, crossed nicols. Bar scale equals 0.5 mm.

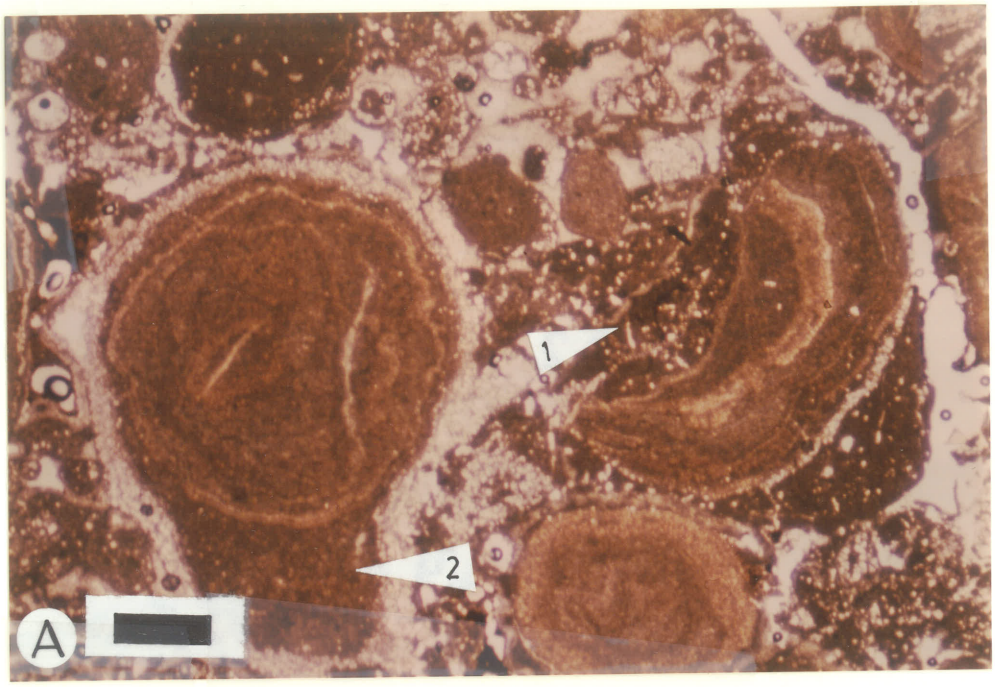
1
2
A

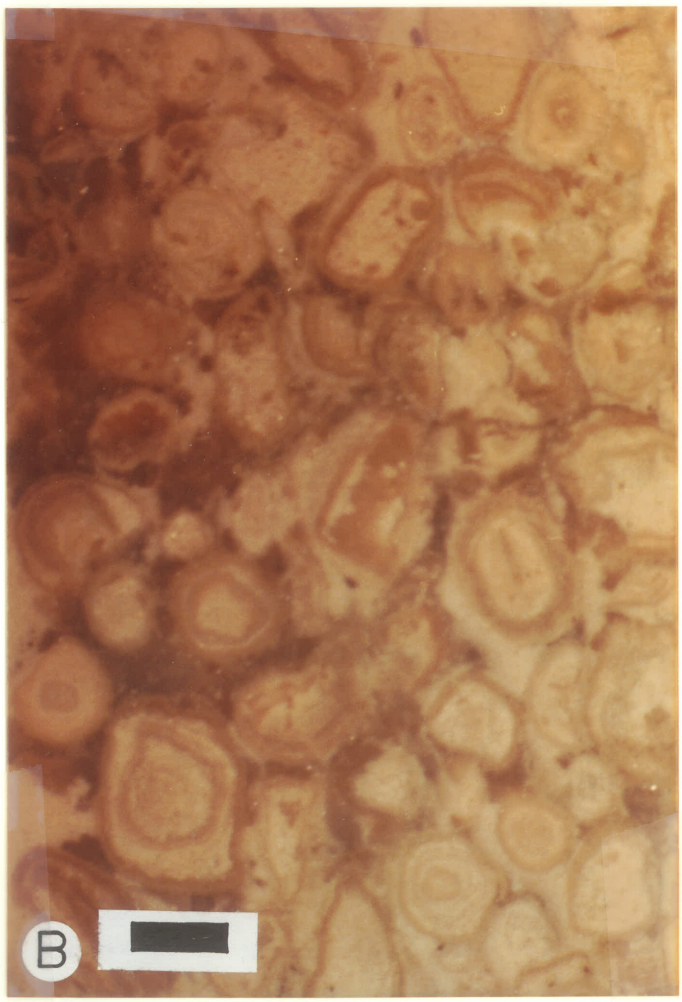
B

PLATE - 15

TEXTURAL ROCK TYPES

A. Photomicrograph of vadolite facies showing perched inclusions (1) in the grains as a result of grading of vadoid laminae into geoptal silt, and downward thickening of the outer laminae of vadoid (2). Sample no. 2.34, thin section perpendicular to stratification. Bar scale equals 0.5 mm.

B. Photomicrograph of vadolite facies showing vertical asymmetry of the grains. Sample no. 2.34, polished core slab perpendicular to stratification. Bar scale equals 1.5 mm.

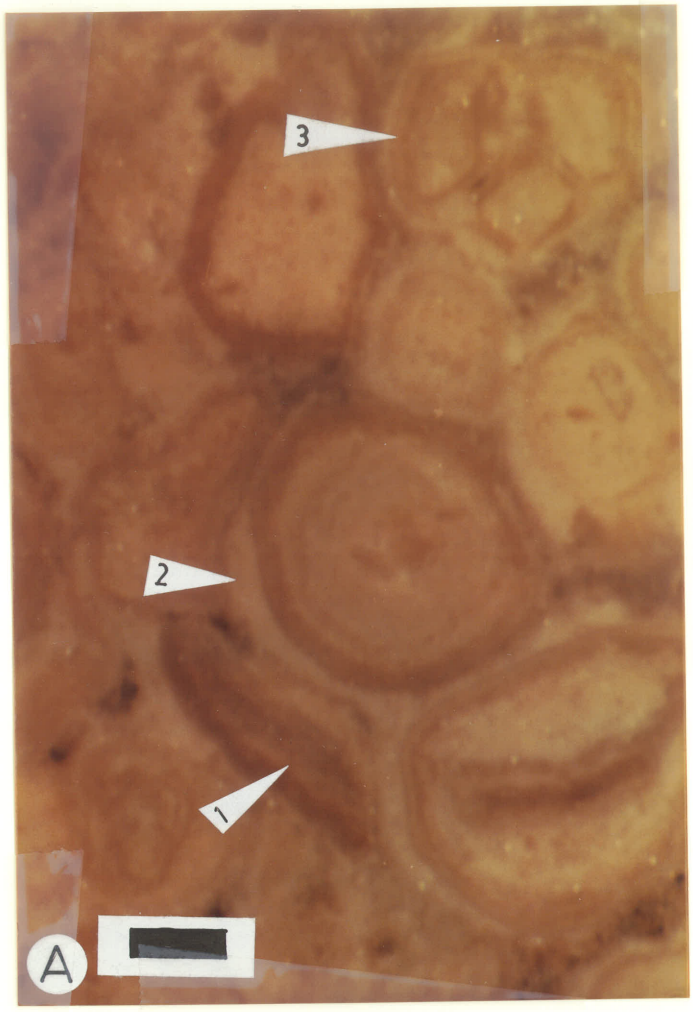
3
2
1
A

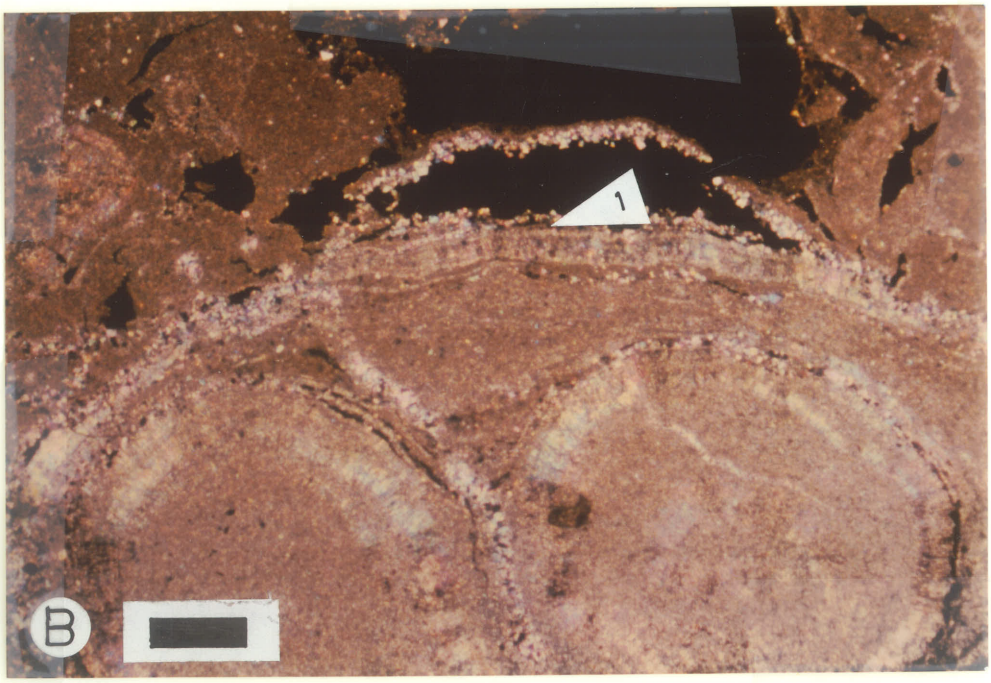
1
B

PLATE - 16

TEXTURAL ROCK TYPES

A. Photomicrograph of vadolite facies showing microstalactitic cement (1). Sample no. 5.34, thin section perpendicular to stratification, crossed nicols. Bar scale equals 0.25 mm.

B. Close up view of Plate 16 Fig. A. Microstalactitic cement composed of radiaxial spar (1). Sample no. 5.34, thin section perpendicular to stratification, crossed nicols. Bar scale equals 70 microns.

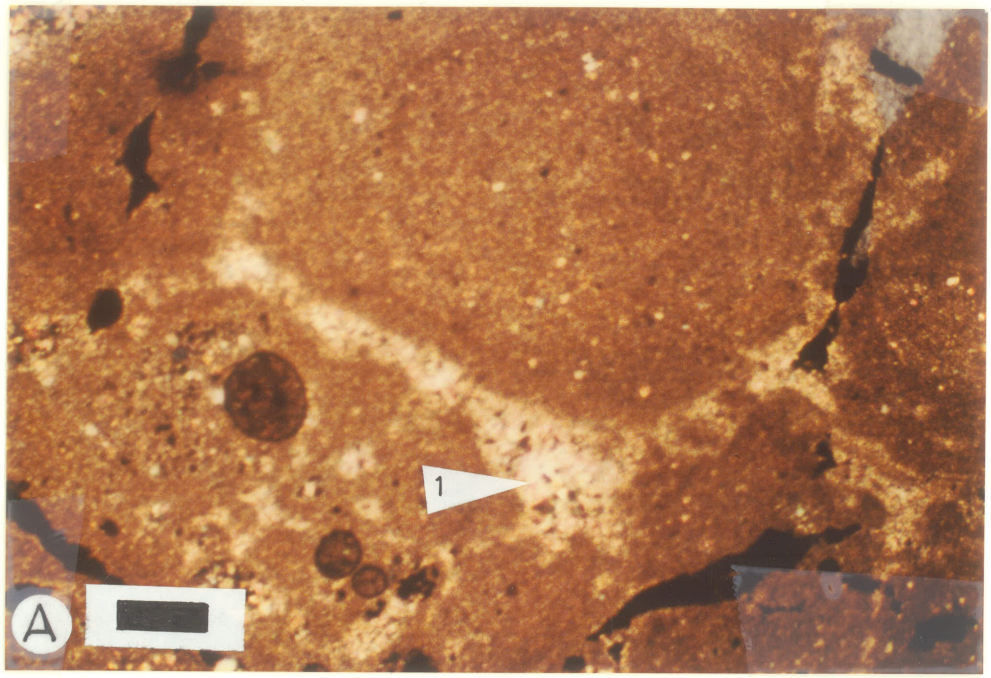
1
A

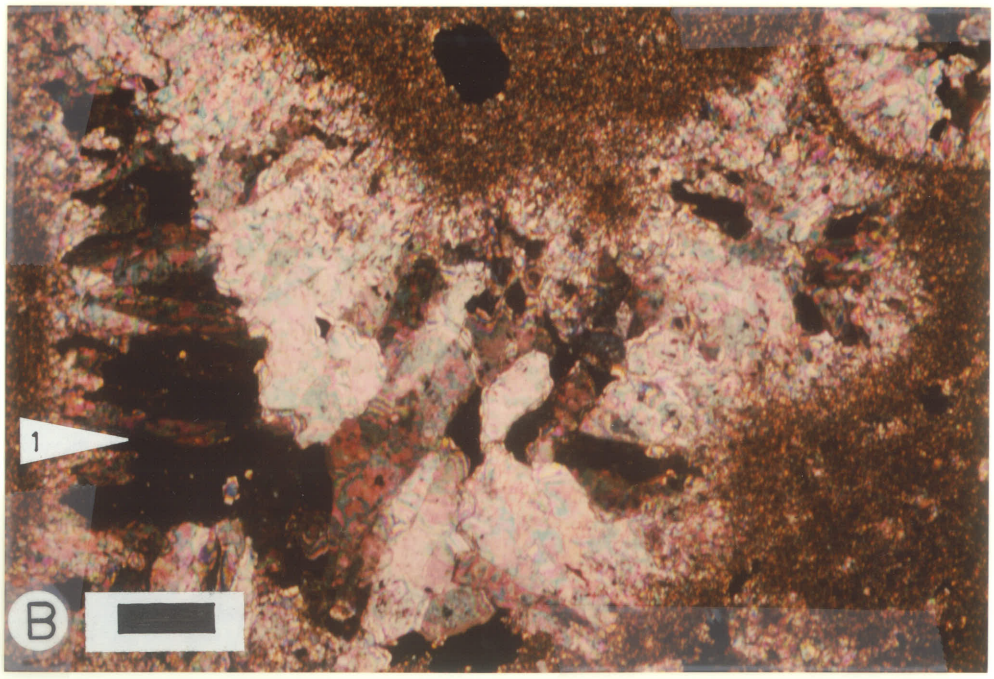
1
B

PLATE - 17

TEXTURAL ROCK TYPES

A. Photomicrograph of vadolite facies showing continuation of radiaxial spar to form the cement (1). Sample no. 5.34, thin section perpendicular to stratification, crossed nicols. Bar scale equals 0.25 mm.

B. Photomicrograph of vadolite facies showing marine vadoid (1) having radial fabric composed of alternating micrite (2) and radiaxial spar (3) laminae, and micritic caliche vadoid (4). Sample no. 5.34, thin section perpendicular to stratification. Bar scale equals 0.25 mm.

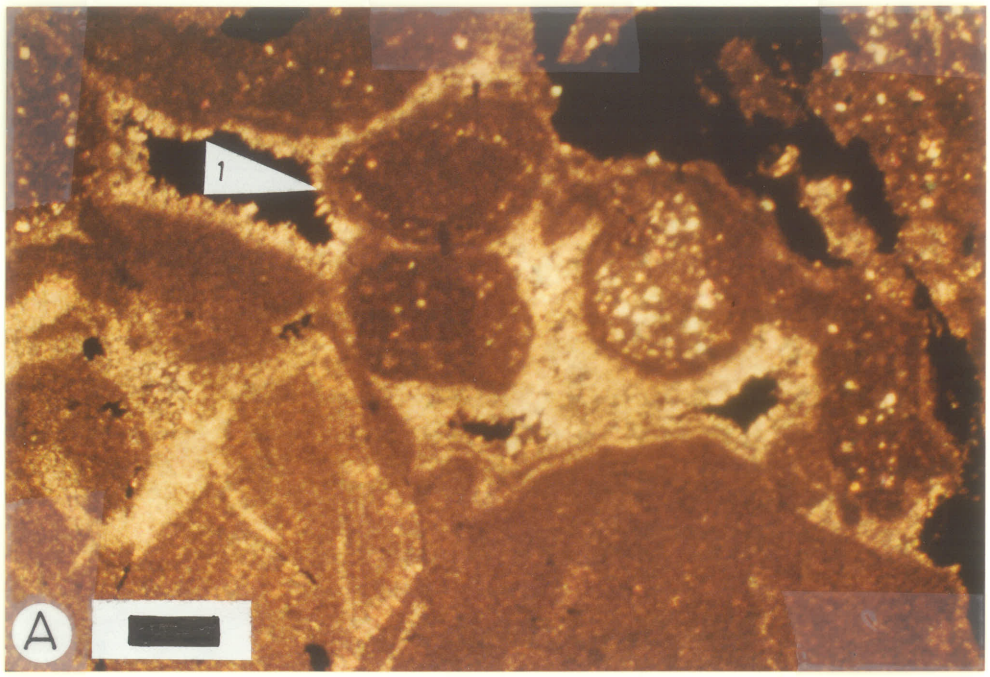
1
A

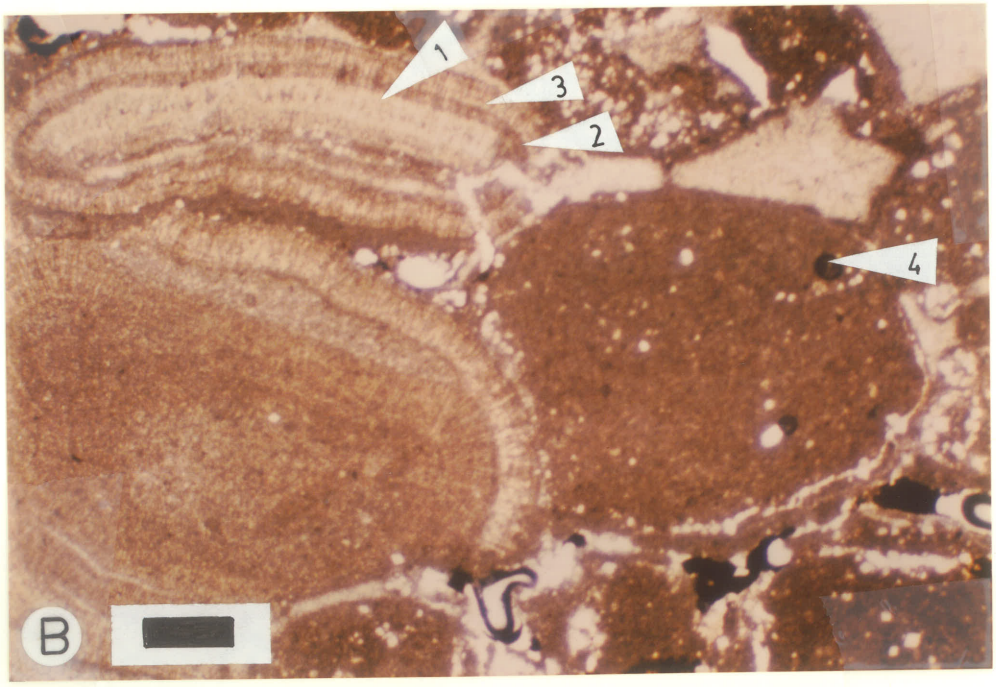
1
3
2
4
B

PLATE - 18

TEXTURAL ROCK TYPES

A. Photomicrograph of vadolite facies showing gradation between marine vadoid (1) and micritic caliche vadoid (2). Sample no. 5.34, thin section perpendicular to stratification. Bar scale equals 1.5 mm.

B. Photomicrograph of vadolite facies showing a vadoid having obscure micritic body as nucleus (1). Sample no. 5.34, thin section perpendicular to stratification. Bar scale equals 0.25 mm.

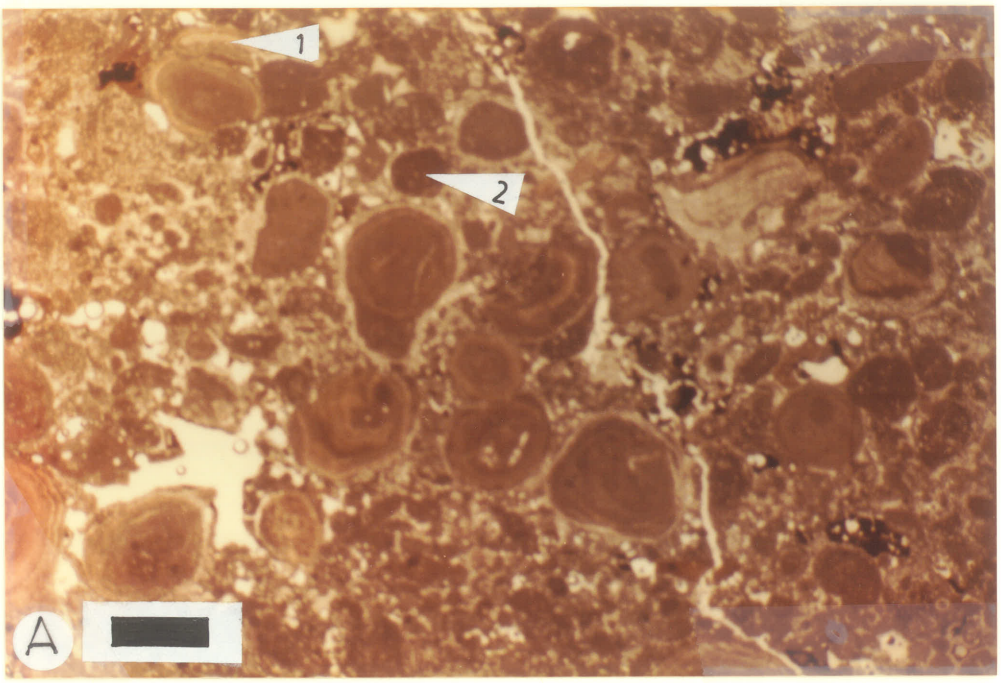
1
2
A

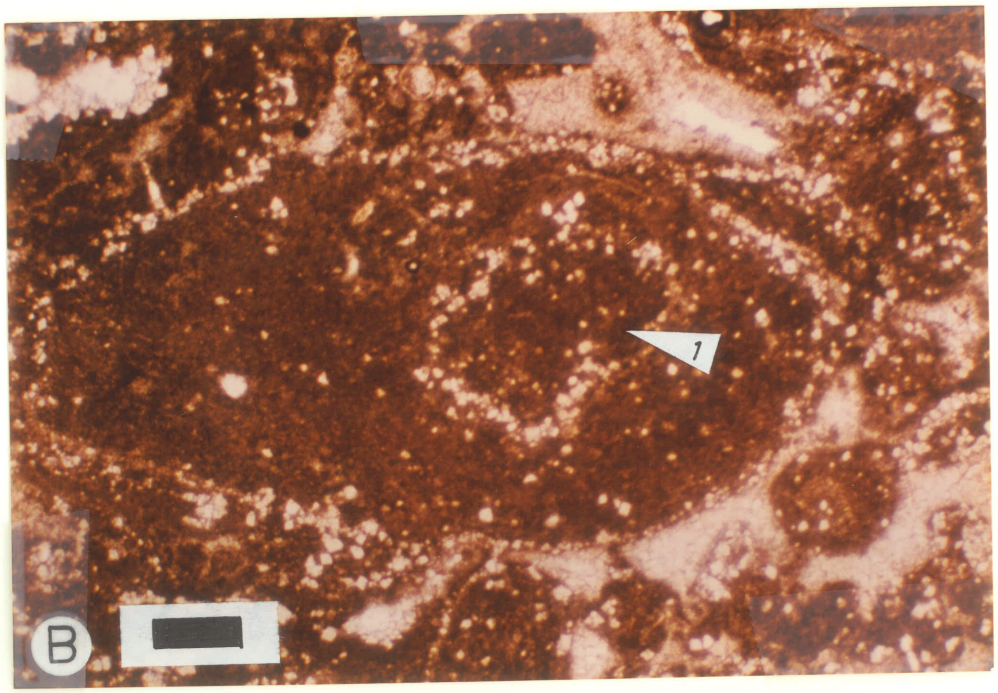
1
B

PLATE - 19

TEXTURAL ROCK TYPES

A. Photograph showing the gradational contact between upper vadolite and lower algal facies; a stylolite (1), which is transitional between peaks high amplitude and columnar types, marks this boundary. Sample no. 2.42, polished core slab perpendicular to stratification. Bar scale equals 1 cm.

B. Photomicrograph showing the gradation contact between upper vadolite and lower algal facies, and the development of first vadoid (1) in this section. Sample no. 2.42, thin section perpendicular to stratification. Bar scale equals 1.5 mm.


1
A

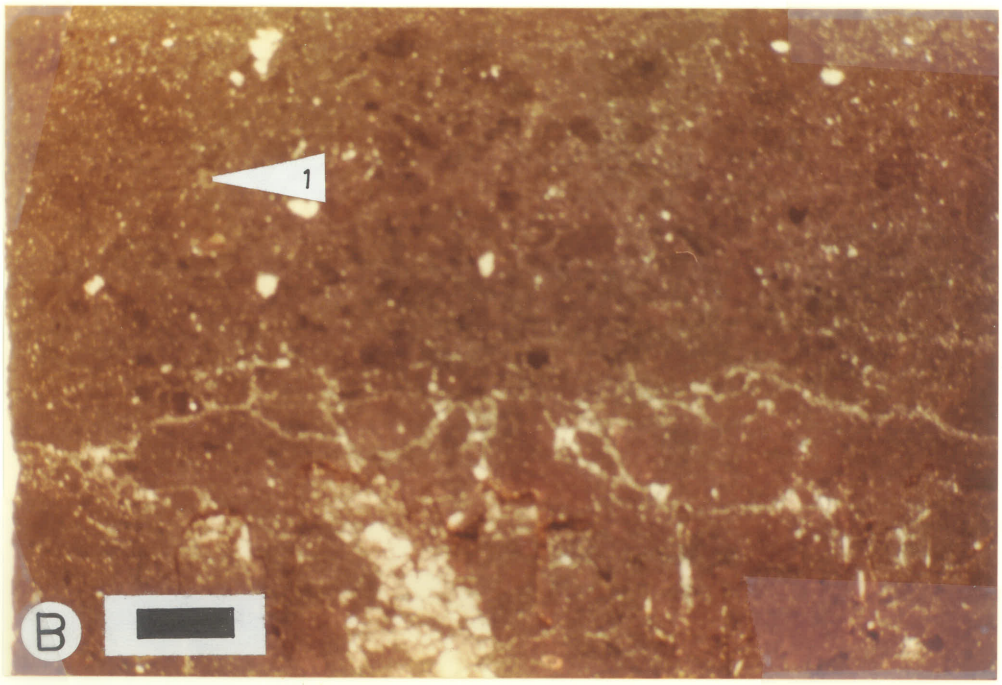
1
B

PLATE - 20

TEXTURAL ROCK TYPES

A. Close up view of Plate 19 Fig. B. The gradational contact between upper vadolite and lower algal facies, and the development of first vadoid (1) in this section. Sample no. 2.42, thin section perpendicular to stratification. Bar scale equals 0.5 mm.

B. Photomicrograph of vadolite facies showing a vadoid having an ostracod (1) as its nucleus. Sample no. 5.33, thin section perpendicular to stratification. Bar scale equals 0.25 mm.

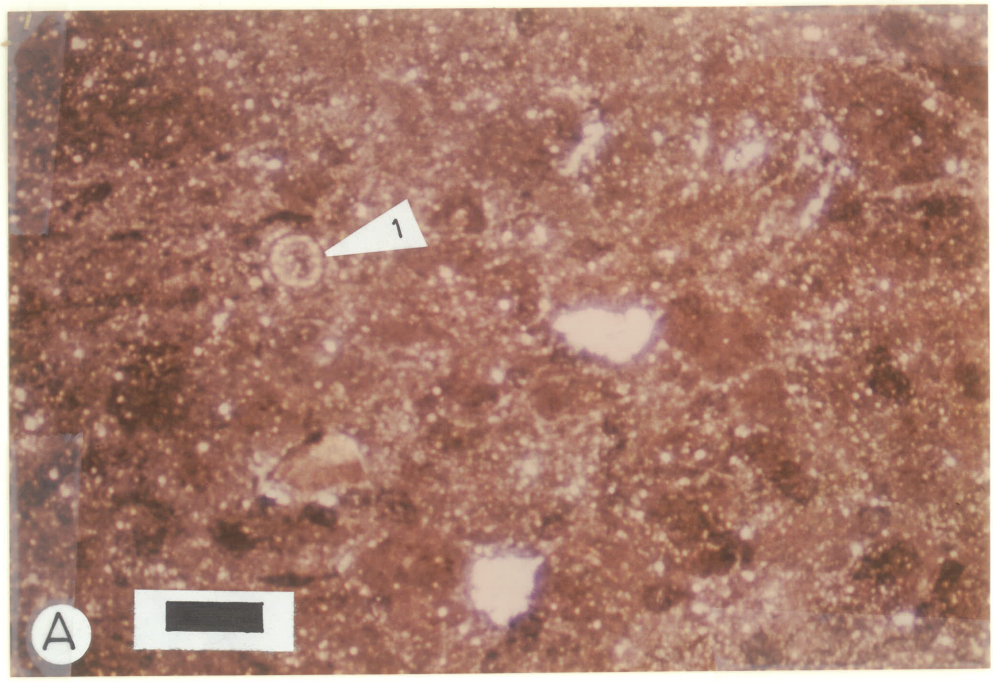
1
A

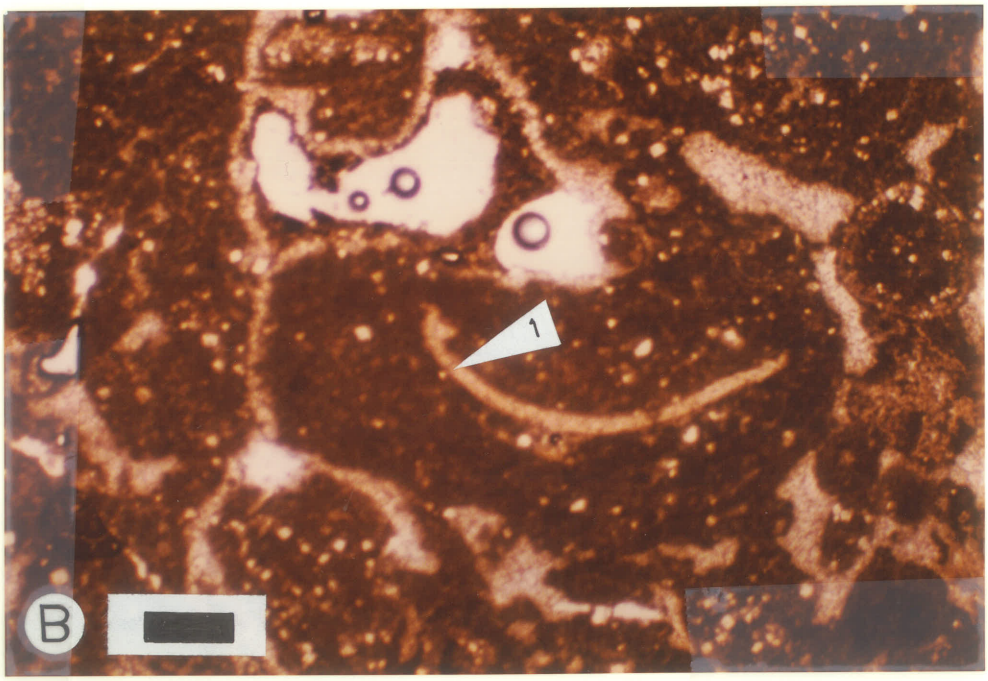
1
B

PLATE - 21

TEXTURAL ROCK TYPES

A. Photomicrograph of vadolite facies showing a vadoid having a foraminifera (1) as its nucleus. Sample no. 5.33, thin section perpendicular to stratification, crossed nicols. Bar scale equals 0.25 mm.

B. Photomicrograph of vadolite facies showing vadoid having a gastropod (1) as its nucleus, small scale patches of microcrystalline dolomite (2) within the grains, and disseminated hematite (3) within the vadoids. Sample no. 5.34, thin section perpendicular to stratification. Bar scale equals 0.5 mm.

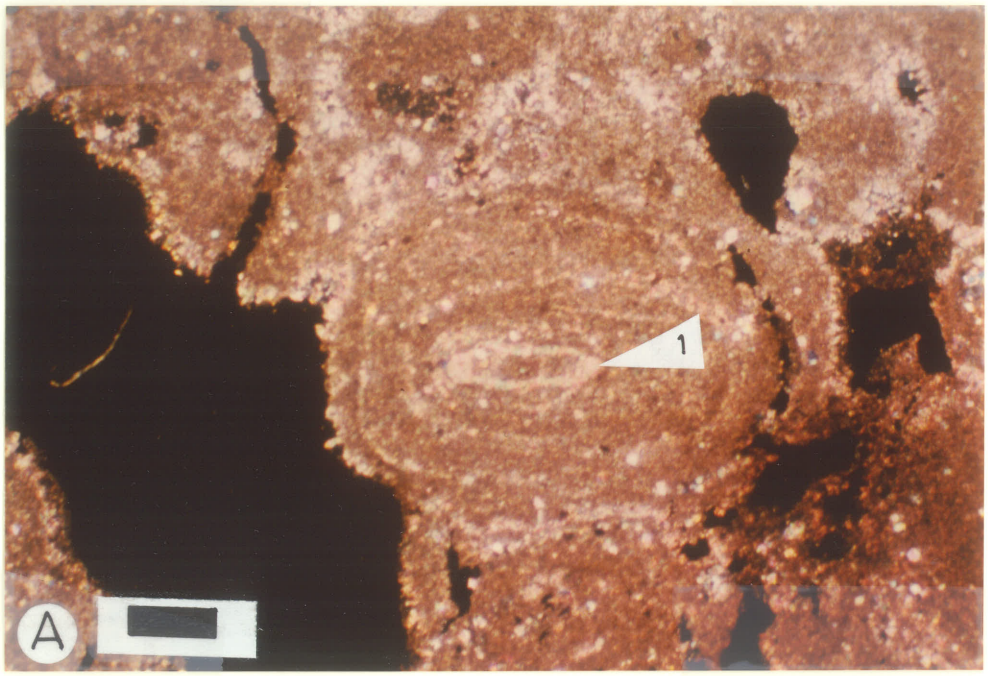
1
A

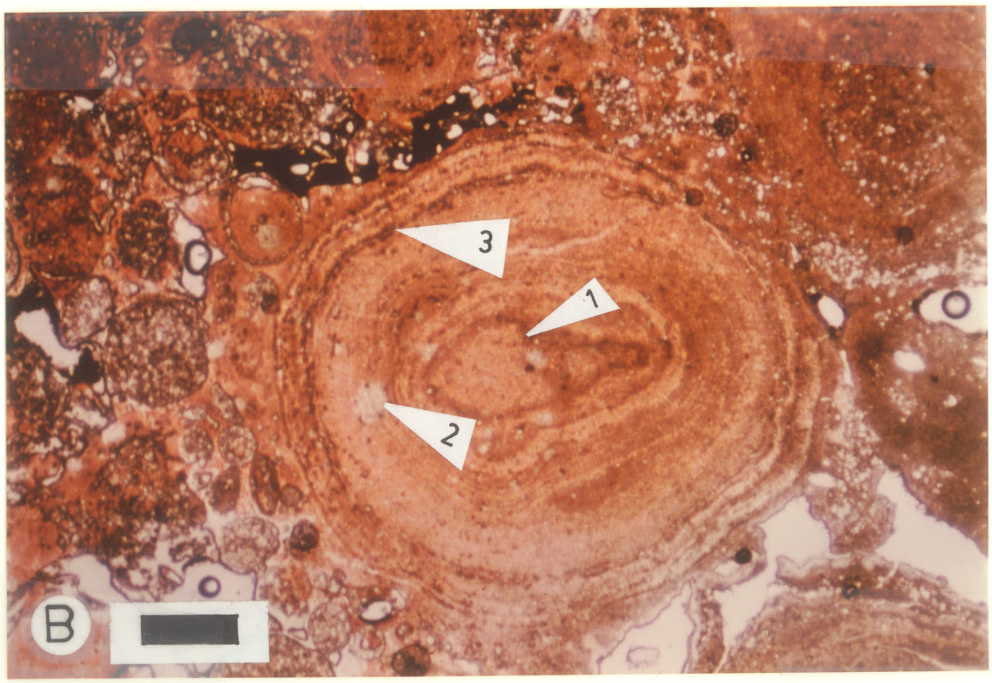
3
1
2
B

PLATE - 22

TEXTURAL ROCK TYPES

A. Photomicrograph of vadolite facies showing a vadoid having a dasyclad (1) as its nucleus. Sample no. 5.33, thin section perpendicular to stratification. Bar scale equals 0.25 mm.

B. Photomicrograph of bioclastic grainstone facies showing algal grains (1), echinodermal fragments (2), meniscus cement (3), syntaxial overgrowth (4), and modified interparticle pores (5). Sample no. 1.61, thin section parallel to stratification, crossed nicols. Bar scale equals 0.25 mm.

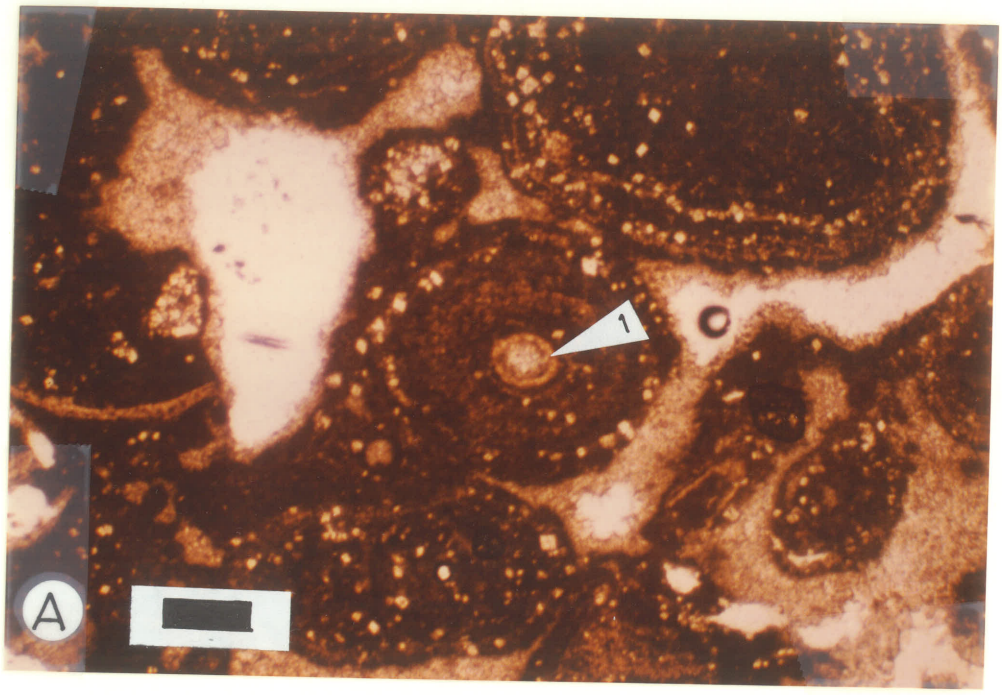
1
A

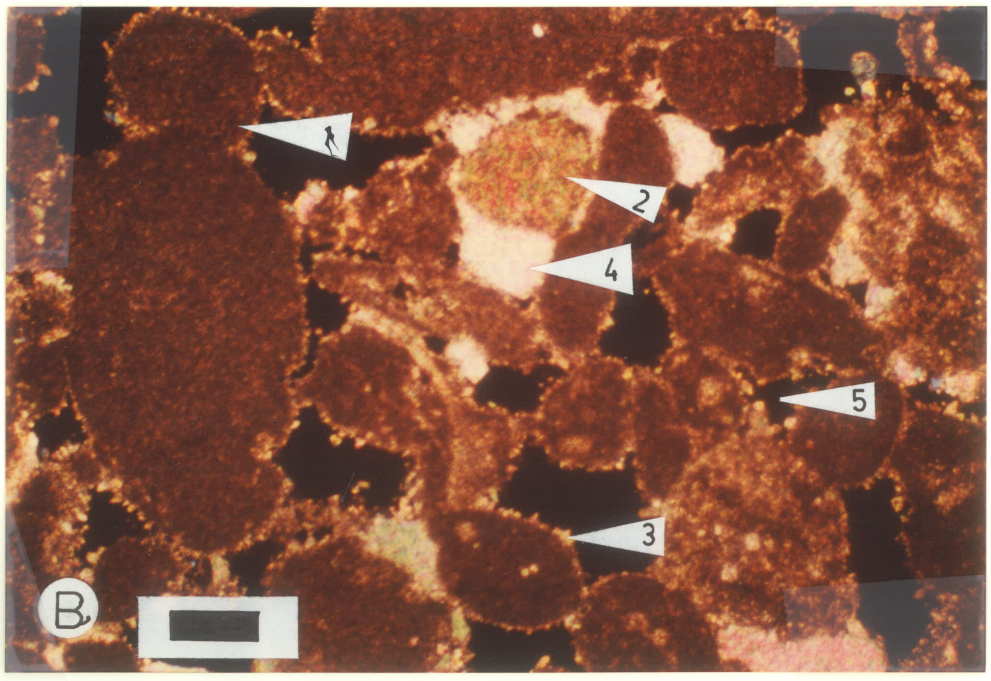
1
2
4
5
3
B

PLATE - 23

TEXTURAL ROCK TYPES

A. Photomicrograph of bioclastic grainstone facies showing algal grains (1), foraminifera (2), echinodermal fragments (3), meniscus cement (4), modified inter-particle pores (5), vuggy pores (6), and leached intraparticle pores within foraminifera (7). Sample no. 1.61, thin section parallel to stratification, crossed nicols. Bar scale equals 0.25 mm.

B. Photomicrograph of bioclastic grainstone facies showing girvanella (1) and dasyclad (2). Sample no. 1.51, thin section parallel to stratification. Bar scale equals 0.5 mm.

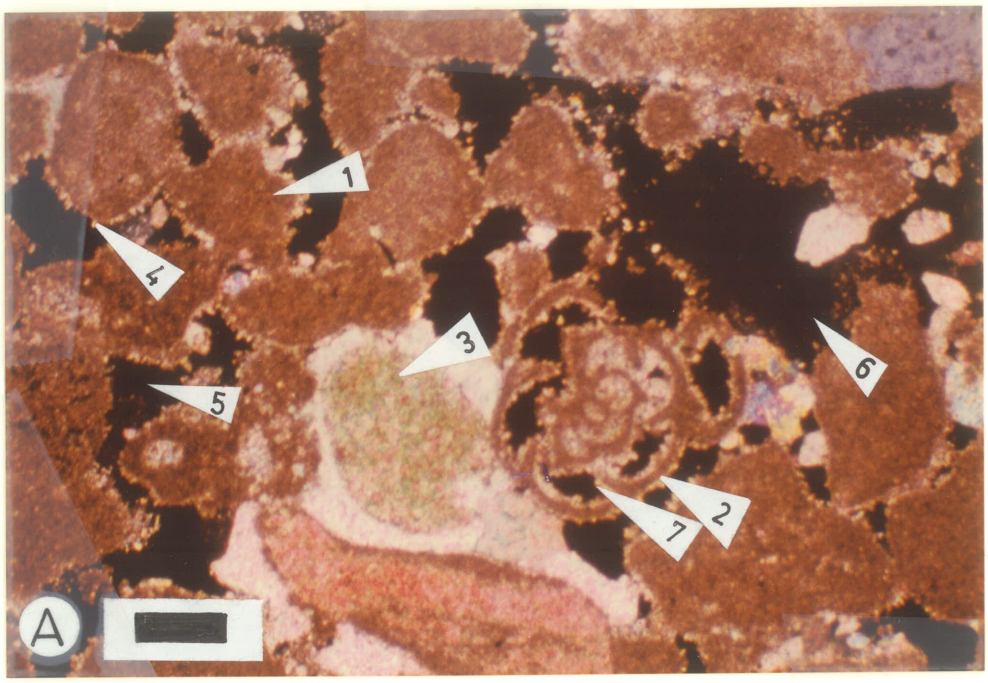
1
4
3
6
5
7
2
A

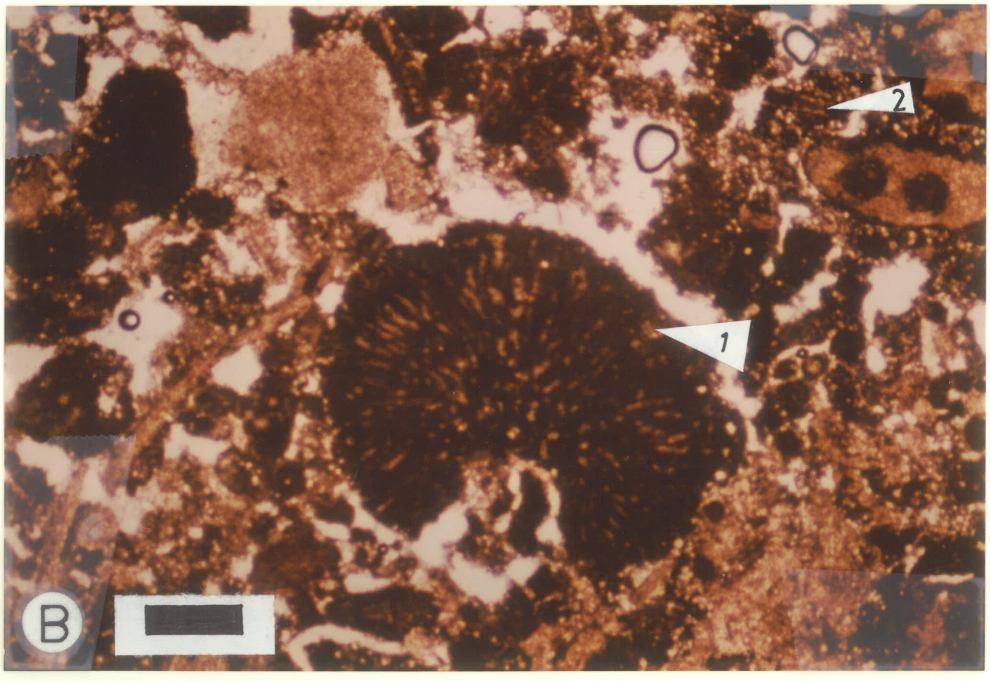
2
1
B

PLATE - 24

TEXTURAL ROCK TYPES

A. Photomicrograph of bioclastic grainstone facies showing bryozoa (1) that has been neomorphosed into microspar with some pseudospar. Sample no. 1.51, thin section parallel to stratification. Bar scale equals 0.5 mm.

B. Photomicrograph of bioclastic grainstone showing stressed brachiopod shell (1), and red algae (2). Sample no. 1.51, thin section perpendicular to stratification. Bar scale equals 0.25 mm.

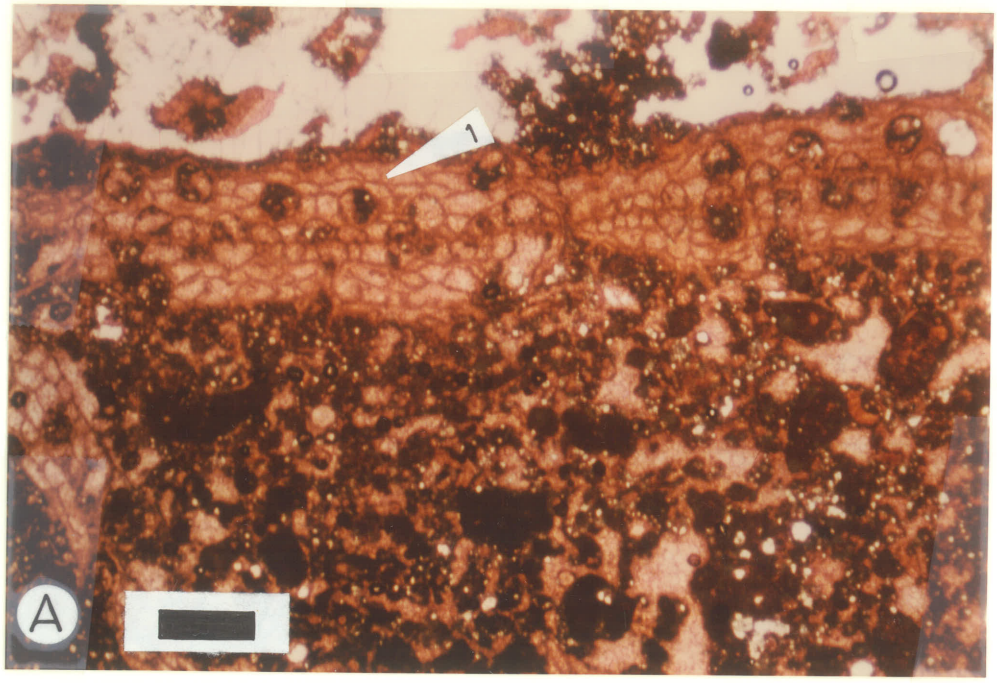
1
A

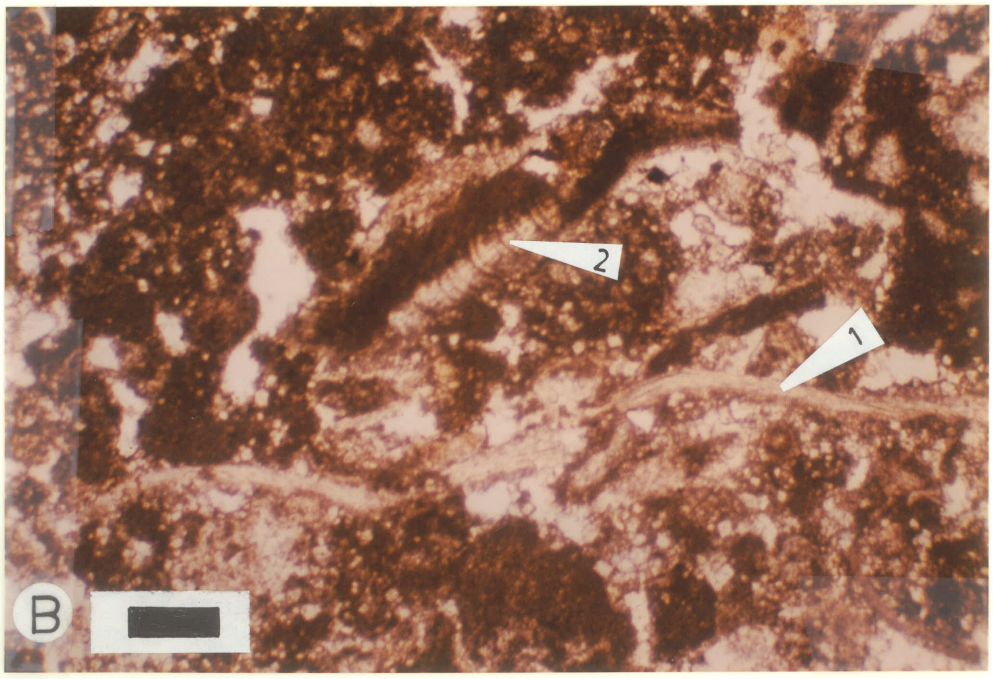
2
1
B

PLATE - 25

TEXTURAL ROCK TYPES

A. Photomicrograph of bioclastic grainstone showing sector of rugose coral. Sample no. 1.51, thin section parallel to stratification, crossed nicols. Bar scale equals 0.25 mm.

B. Photograph showing bioclastic grainstone facies. Sample no. 1.51, polished core slab perpendicular to stratification. Bar scale equals 1 cm.

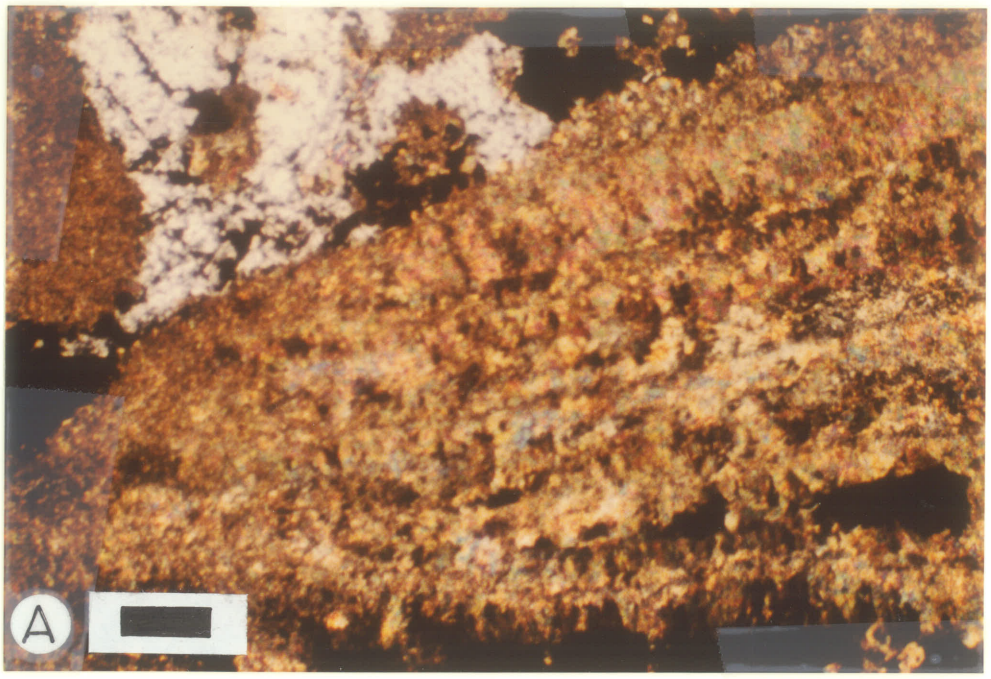
A


B

PLATE - 26

TEXTURAL ROCK TYPES

A. Photomicrograph of peloidal grainstone facies composed of fecal pellets (1), pseudopelletoids (2), and micritized, rounded and abraded bioclasts (3). Modified interparticle pores (4) are abundant. Sample no. 1.41, thin section perpendicular to stratification. Bar scale equals 0.5 mm.

B. Photograph showing peloidal grainstone facies showing fracture with oil stain (1). Sample no. 1.41, polished core slab perpendicular to stratification. Bar scale equals 1 cm.

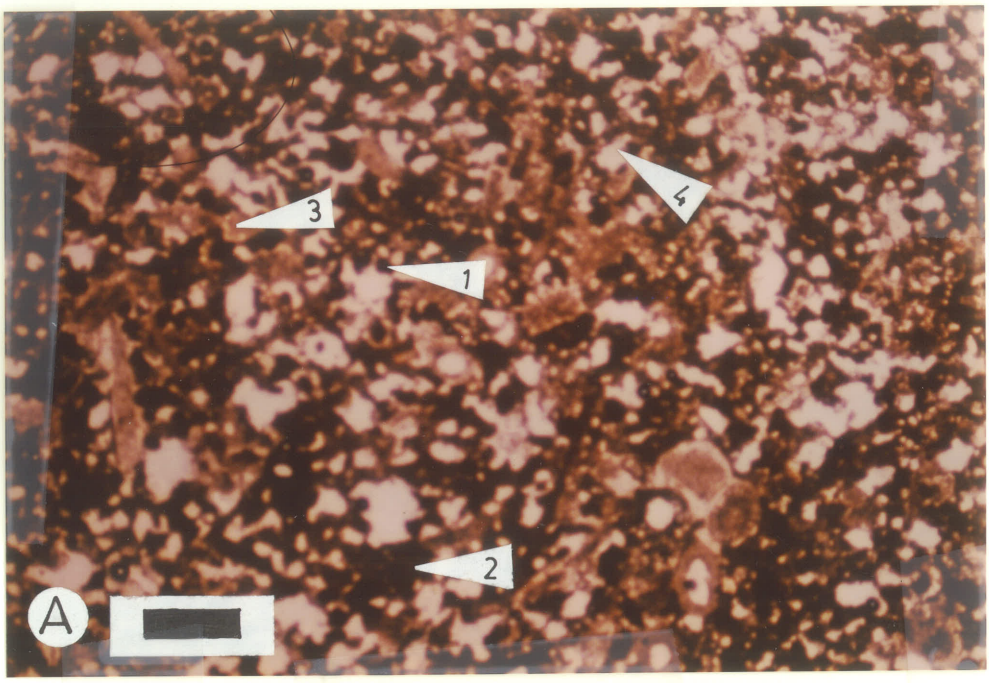
3
4
1
2
A


1
B

PLATE - 27

DIAGENESIS

A. Photomicrograph showing sparmicritization represented by 'spikes' (1) of micrite extending into the sparry calcite cement. Sample no. 4.52, thin section parallel to stratification. Bar scale equals 70 microns.

B. Close up view of Plate 16 Fig. B. Radiaxial calcite cement (1). Sample no. 5.34, thin section perpendicular to stratification, crossed nicols. Bar scale equals 30 microns.

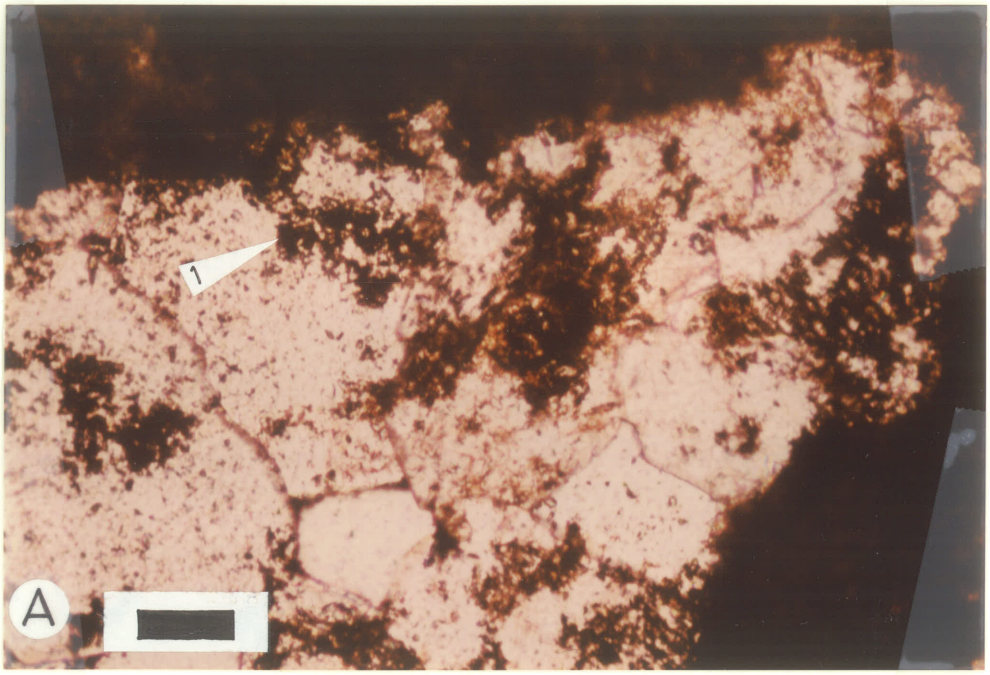
1
A

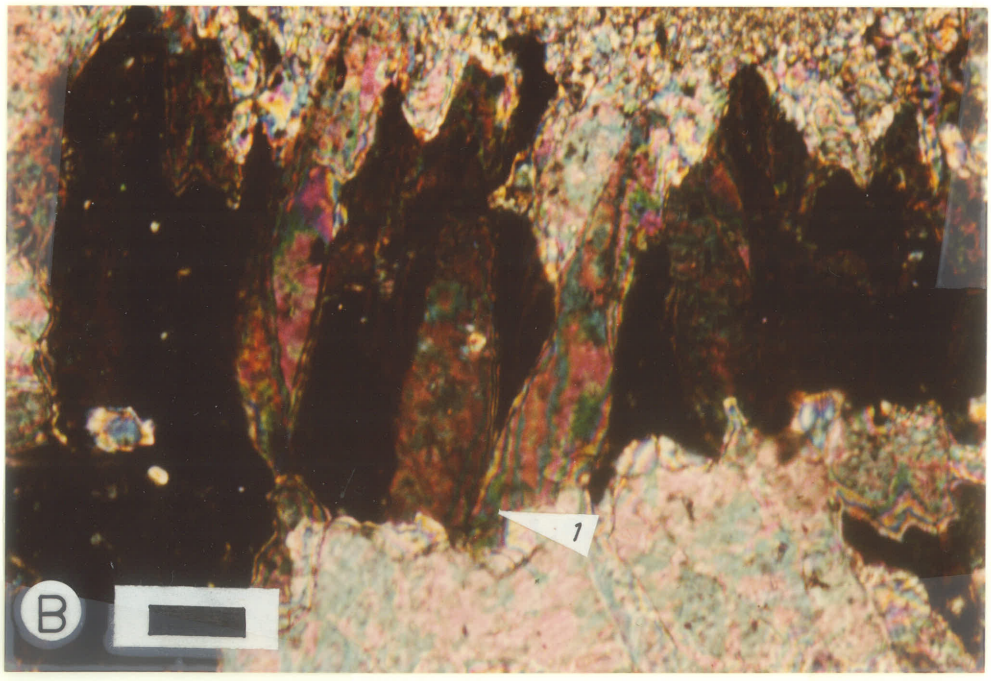
1
B

PLATE - 28

DIAGENESIS

A. Photomicrograph showing bryozoa bound isopachous radiaxial calcite cement (1) overlain unconformably by equant calcite cement (2). Sample no. 1.51, thin section parallel to stratification, crossed nicols. Bar scale equals 0.25 mm.

B. Photomicrograph showing meniscus cement preferentially developed in small-scale interparticle pores (1) as opposed to easily drained large ones (2). Sample no. 1.61, thin section parallel to stratification, crossed nicols. Bar scale equals 0.5 mm.

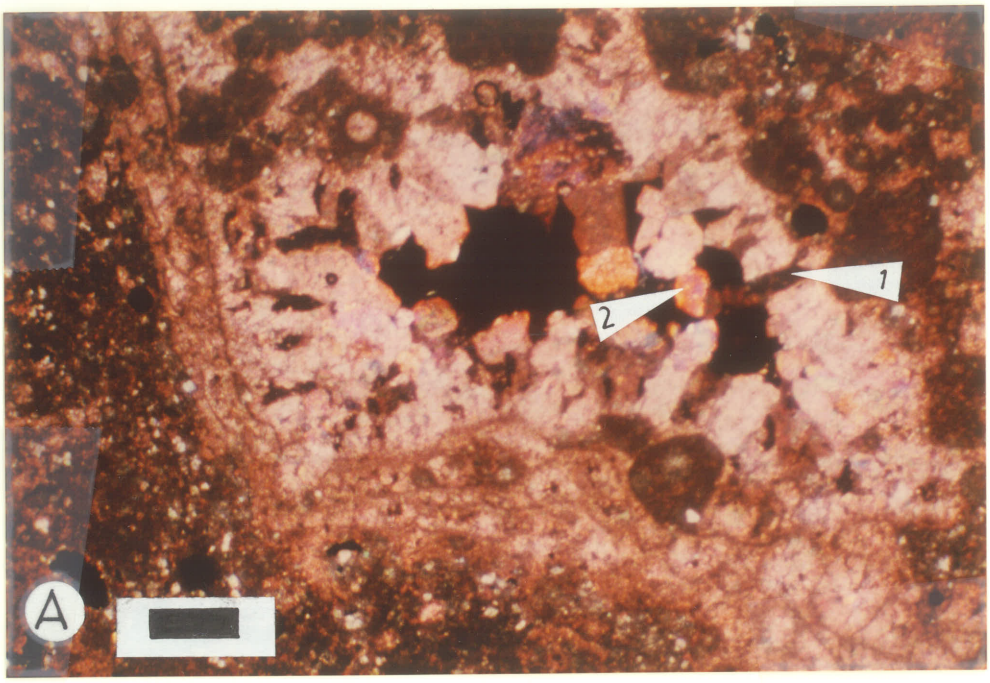
1
2
A

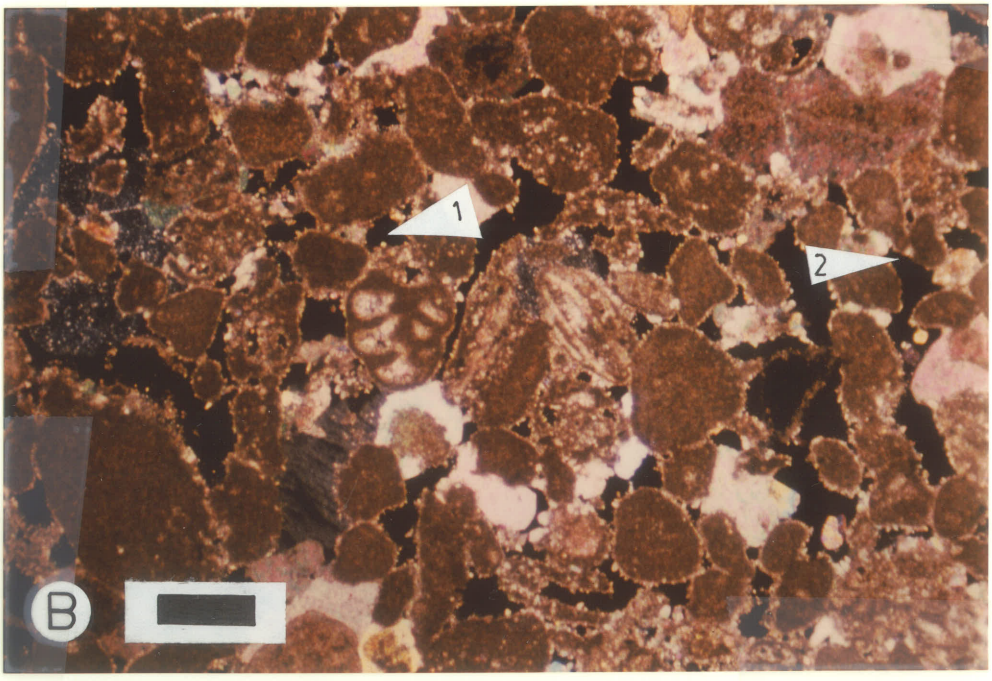
1
2
B

PLATE - 29

DIAGENESIS

A. Photomicrograph showing meniscus cement (composed of blocky crystals (1)) is enclosed by syntaxial overgrowth (2), which is in turn enclosed by equant cement (3). Sample no. 1.61, thin section parallel to stratification, crossed nicols. Bar scale equals 70 microns.

B. Photomicrograph showing meniscus cement (composed of blocky crystals (1)) is enclosed by syntaxial overgrowth (2), which is in turn enclosed by equant cement (3). Sample no. 1.61, thin section parallel to stratification, crossed nicols. Bar scale equals 30 microns.

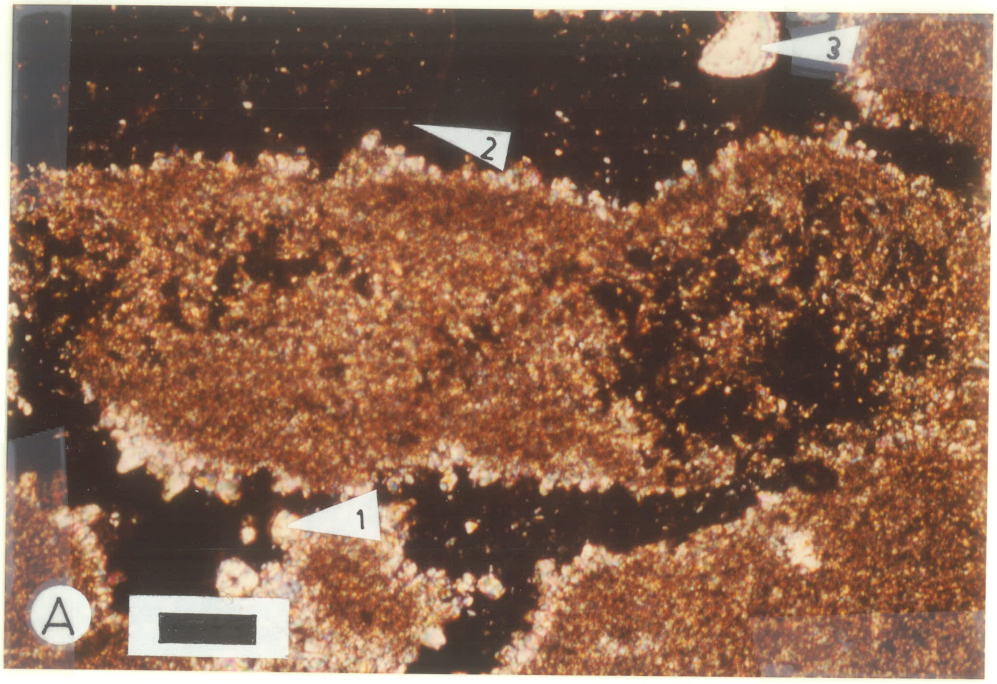
3
2
1
A

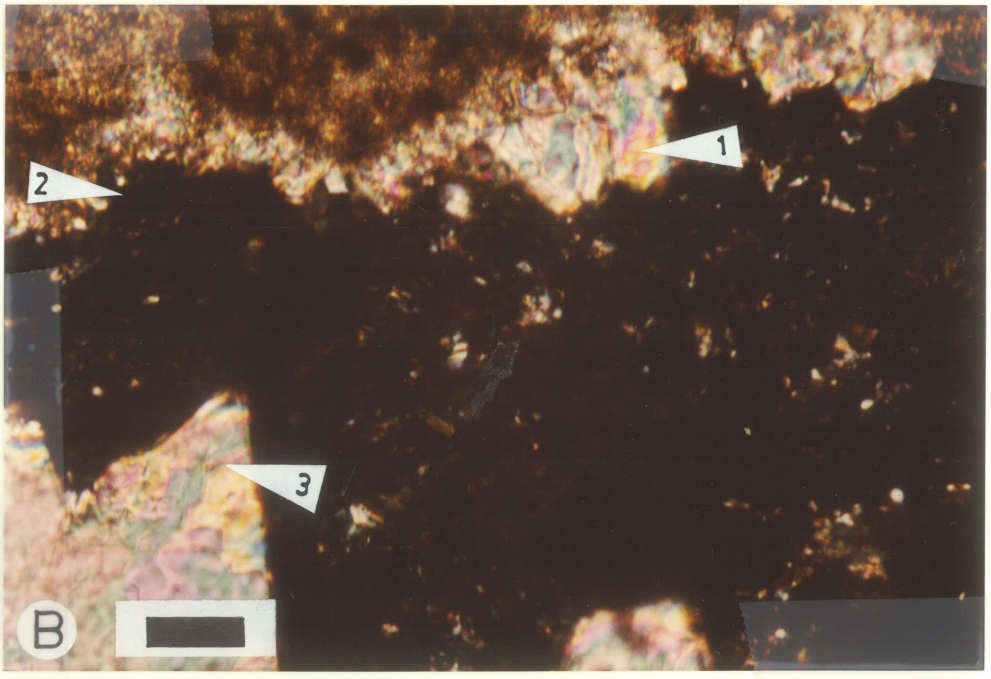
1
2
3
B

PLATE - 30

DIAGENESIS

A. Photomicrograph showing coarsening of equant cement (1) toward the centre of the pore. Sample no. 4.42, thin section perpendicular to stratification, crossed nicols. Bar scale equals 0.25 mm.

B. Close up view of Plate 28 Fig. A. Isopachous radiaxial cement (1) is overlain unconformably by equant cement (2). Sample no. 1.51, thin section parallel to stratification, crossed nicols. Bar scale equals 70 microns.

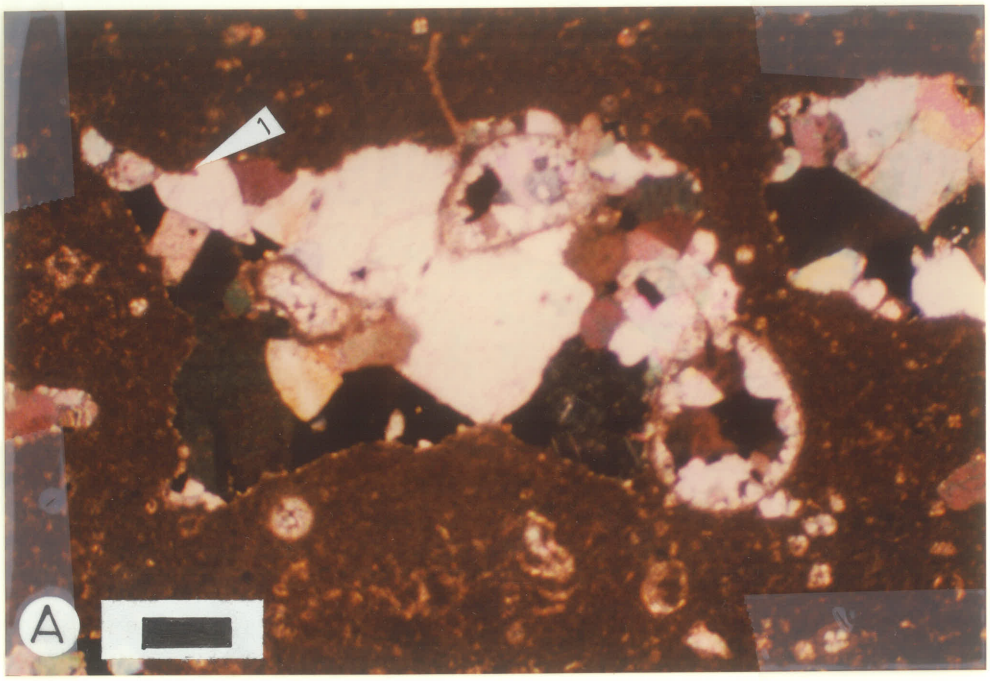
1
A

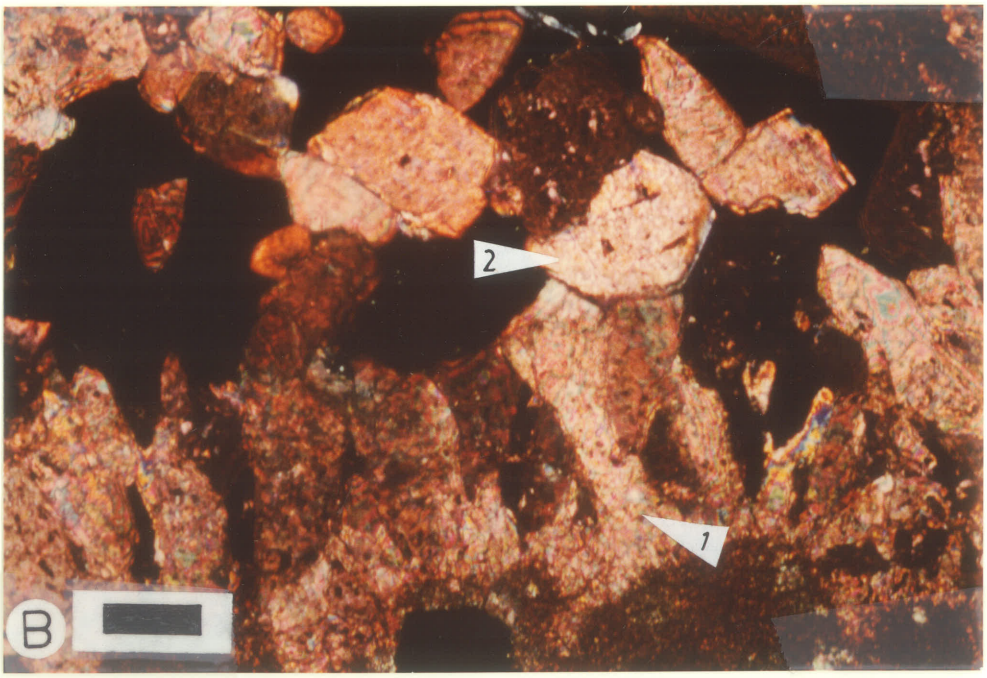
2
1
B

PLATE - 31

DIAGENESIS

A. Photograph of grey white anhydrite from a band of anhydrite in the altered zone showing "floating" patches (1) of parent dolomite. Sample no. 1.21, polished core slab perpendicular to stratification. Bar scale equals 1 cm.

B. Photomicrograph showing mosiac nodular anhydrite (composed of tightly interlocking needle-like to tabular crystals (1)) forming anhydrite bands in the altered zone, and enclosed patches (1) of parent dolomite (2). Sample no. 1.20, thin section perpendicular to stratification, crossed nicols. Bar scale equals 0.25 mm.

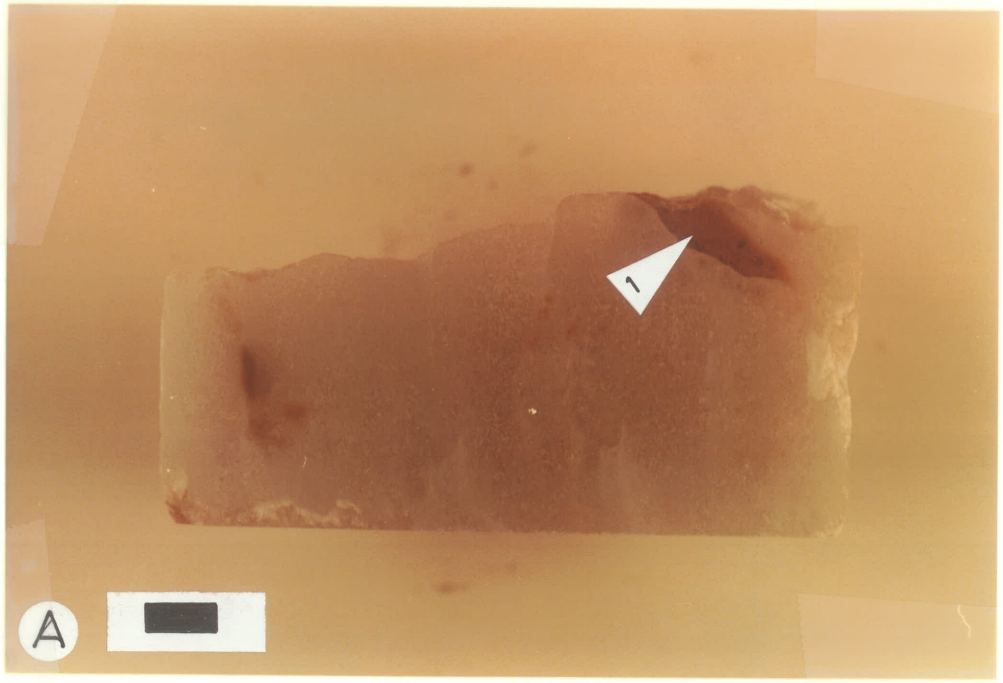
1
A

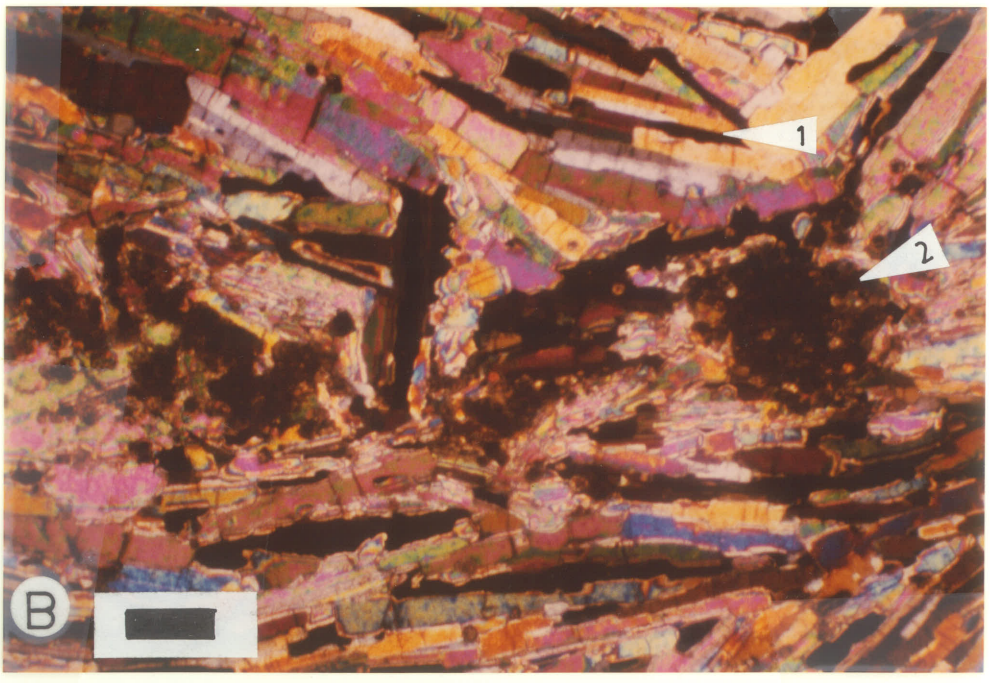
1
2
B

PLATE - 32

DIAGENESIS

A. Photomicrograph showing the development of poikilotopic anhydrite (1) in a fenestrae, and enclosed marginally corroded dolomite rhombs (2) having the same order of size as those of the matrix (3), and enclosed patches (4) of dolomite. Sample no. 2.44, thin section perpendicular to stratification, crossed nicols. Bar scale equals 0.5 mm.

B. Photomicrograph showing void-filling anhydrite (composed of tabular crystals (1)) infilling the fracture in the dolomite matrix, and corroded anhydrite grains (2) in a gypsum crystals (3). Sample no. 4.30, thin section perpendicular to stratification, crossed nicols. Bar scale equals 70 microns.

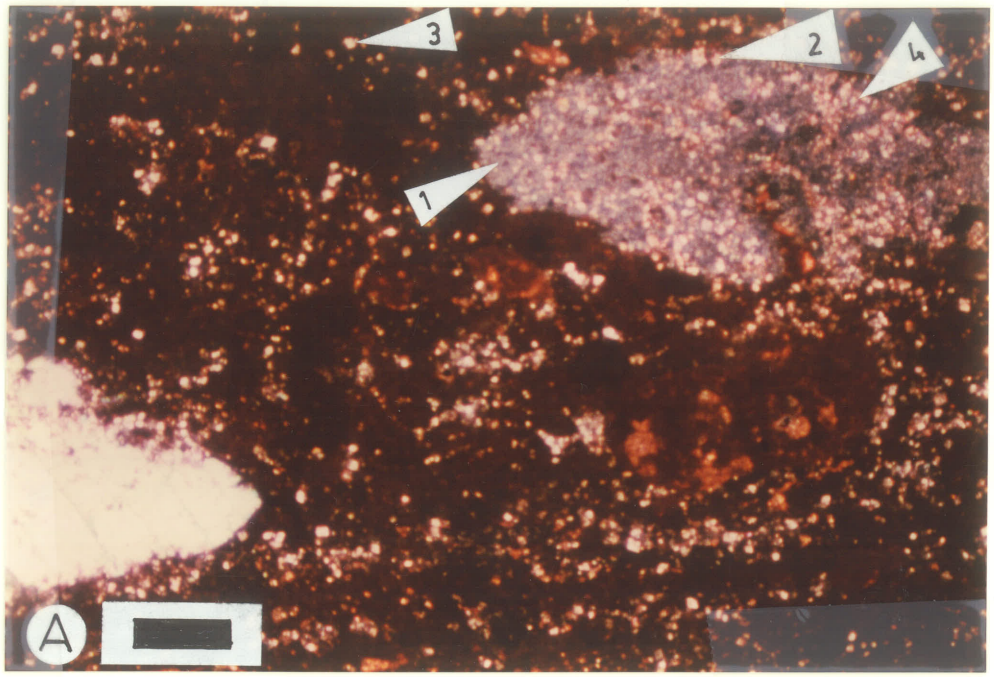
3
2
4
1
A

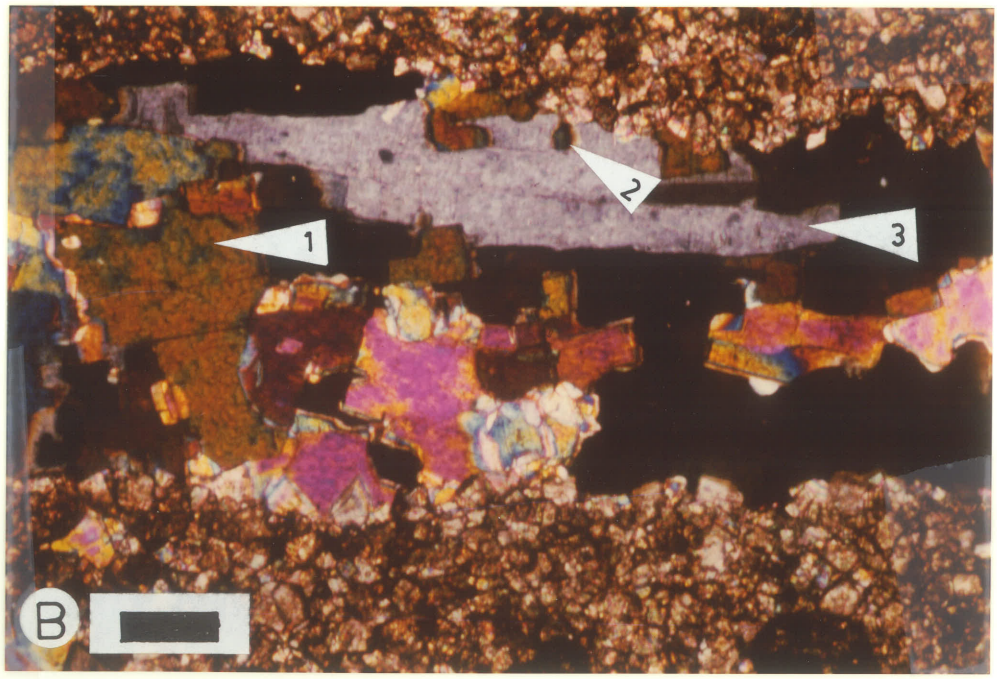
2
1
3
B

PLATE - 33

DIAGENESIS

A. Photomicrograph showing small scale patches of microcrystalline dolomite (1) within microcrystalline calcite (red colored) forming carbonate mud, and incipient dolomite rhombs (2). Sample no. 5.33, thin section perpendicular to stratification. Bar scale equals 30 microns.

B. Photomicrograph showing intimate mixture of microcrystalline dolomite (1) and microcrystalline calcite (red), and channel porosity (2). Sample no. 4.52, thin section perpendicular to stratification, crossed nicols. Bar scale equals 0.5 mm.

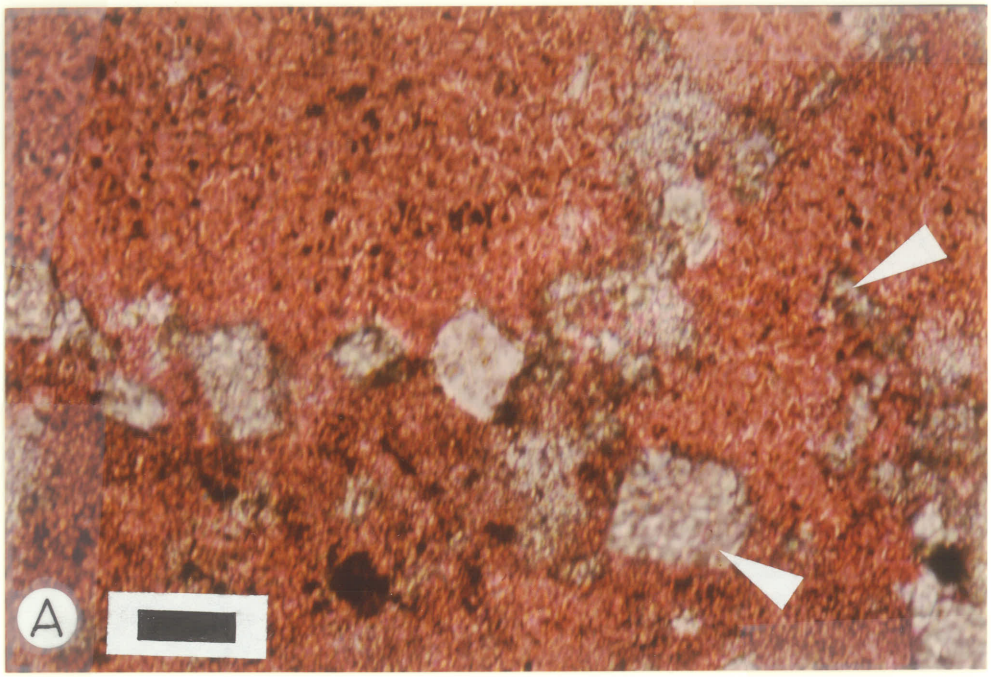
A

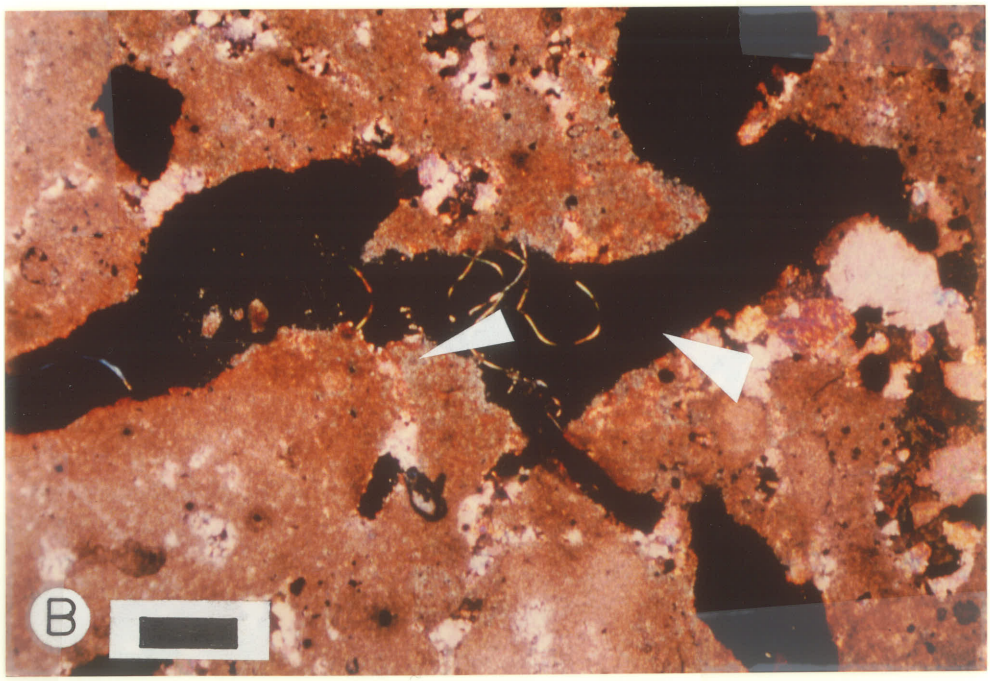
B

PLATE - 34

DIAGENESIS

A. Photomicrograph showing xenotopic to hypodiotopic tight interlock of inclusion-rich dirty dolomite rhombs. Some of the dolomite rhombs exhibit discernible zoning with no apparent change in dirtiness. Sample no. 1.33, thin section perpendicular to stratification. Bar scale equals 10 microns.

B. Photomicrograph showing dirty dolomite rhombs as dispersed euhedral individuals in the matrix of microcrystalline calcite (dark colored) with small scale patches of microcrystalline dolomite (light colored). The dolomite rhombs exhibit discernible zoning with no apparent change in dirtiness. Sample no. 1.41, thin section perpendicular to stratification. Bar scale equals 10 microns.

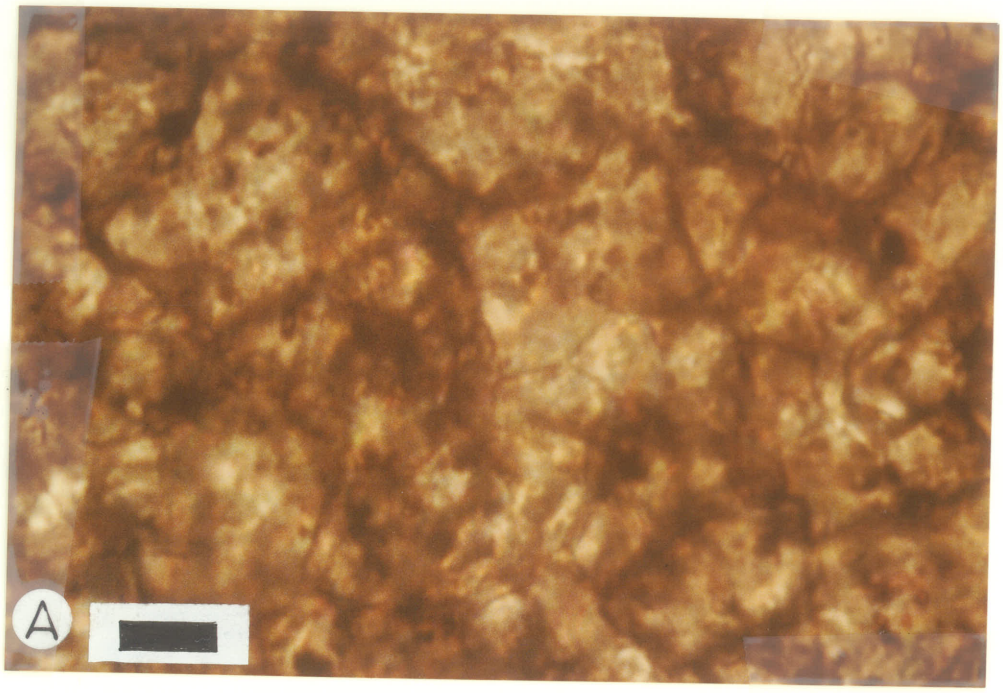
A

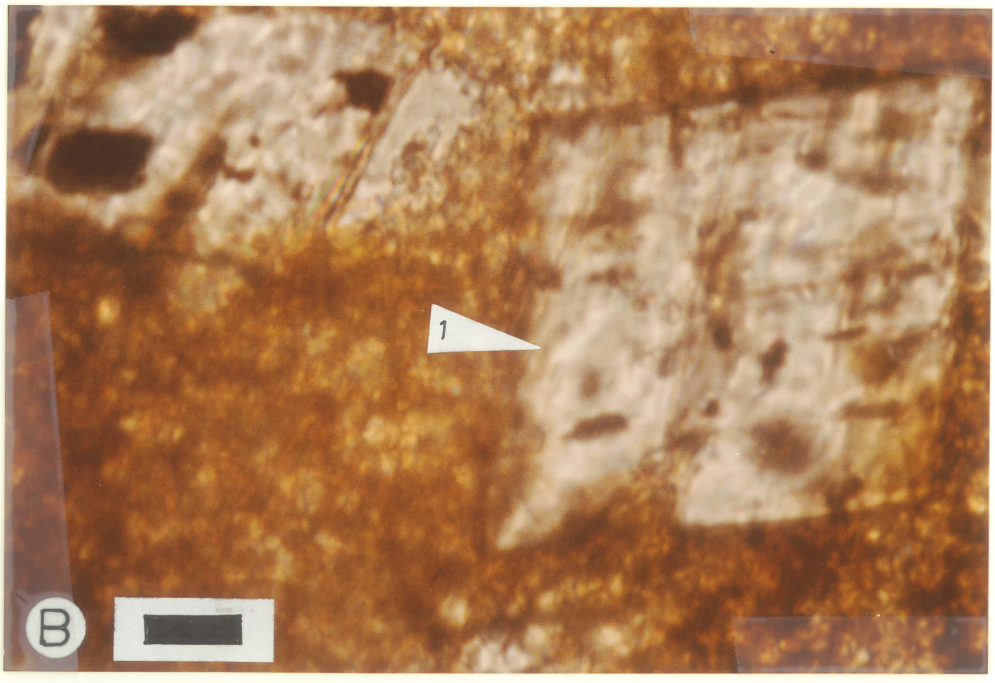
1
B

PLATE - 35

DIAGENESIS

A. Photomicrograph showing dirty dolomite rhombs constituting part of scattered clusters of dolomite rhombs (1), and pyrite (2) and oil (3) in the vug. Sample no. 5.34, thin section perpendicular to stratification. Bar scale equals 0.25 mm.

B. Photomicrograph showing limpid dolomite rhombs (1), incipient dolomite rhombs (2), microcrystalline dolomite (3), and microcrystalline calcite (red colored). Sample no. 2.44, thin section perpendicular to stratification. Bar scale equals 30 microns.

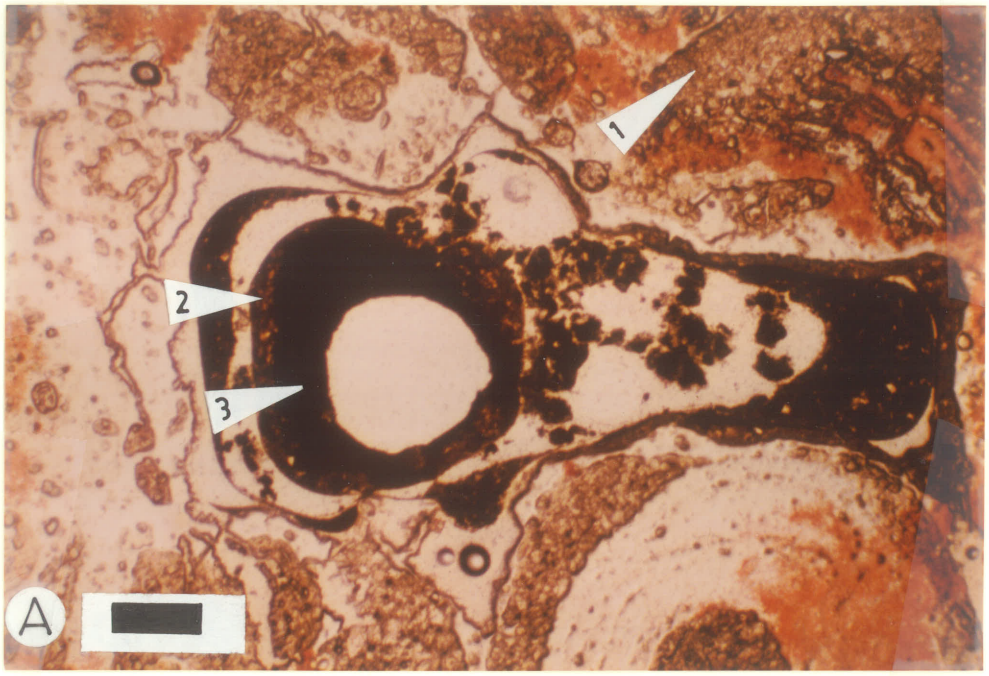
1
2
3
A

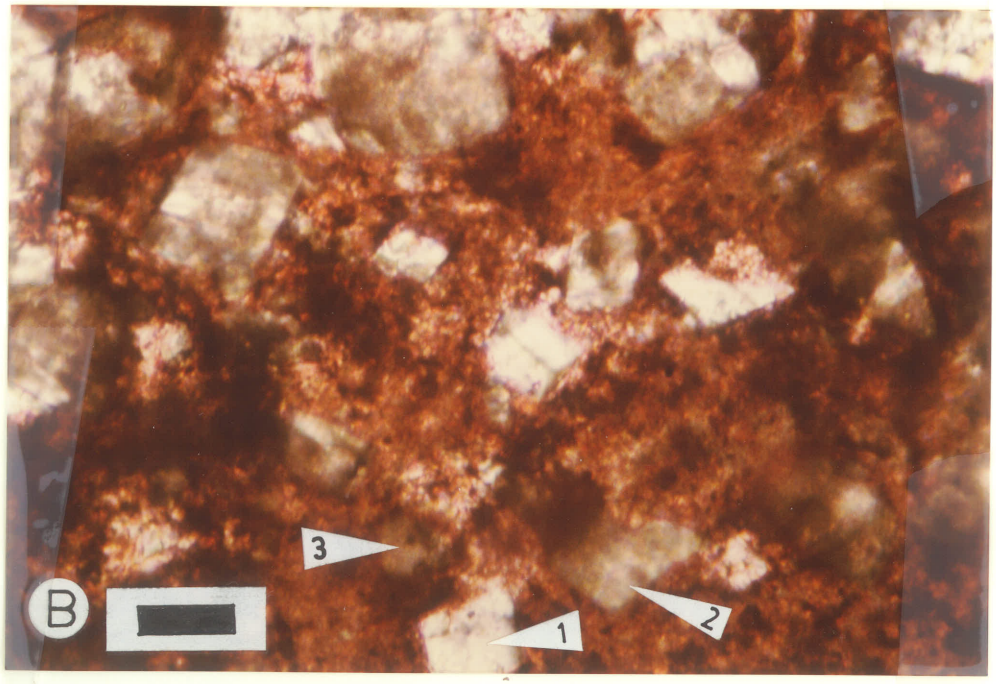
3
1
2
B

PLATE - 36

DIAGENESIS

A. Photomicrograph showing dirty dolomite rhombs (1), incipient dolomite rhombs (2), microcrystalline dolomite (3), and microcrystalline calcite (red colored). Sample no. 5.33, thin section perpendicular to stratification. Bar scale equals 30 microns.

B. Photomicrograph showing development of mosaics rhombs along stylolite (1) and grain contact sutures (2), and leached stylolite (3). Sample no. 1.82, thin section perpendicular to stratification, crossed nicols. Bar scale equals 0.5 mm.

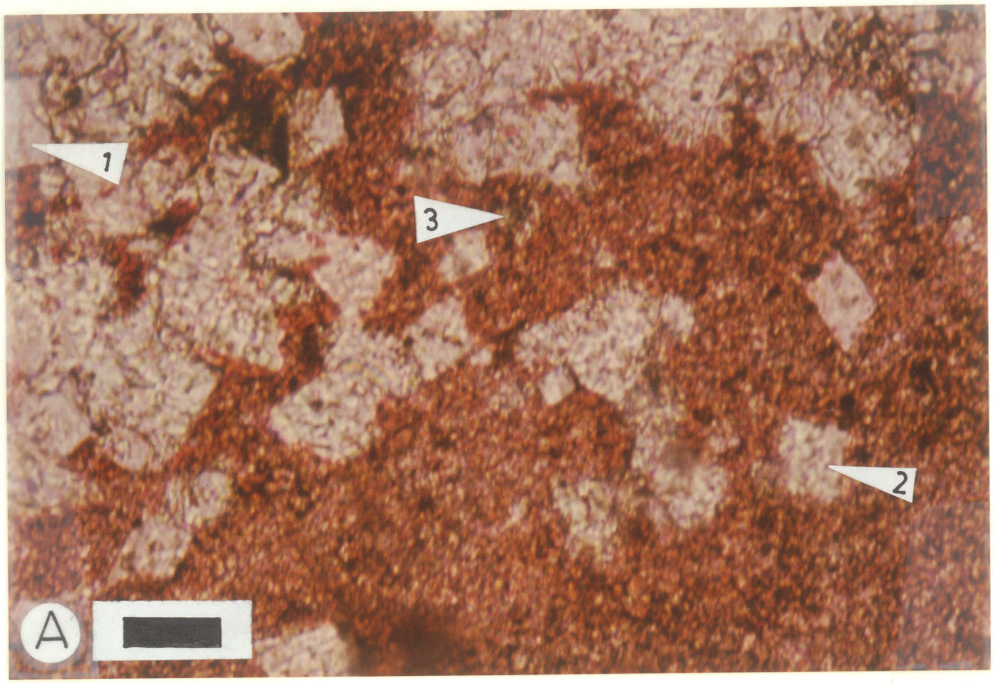
1
3
2
A

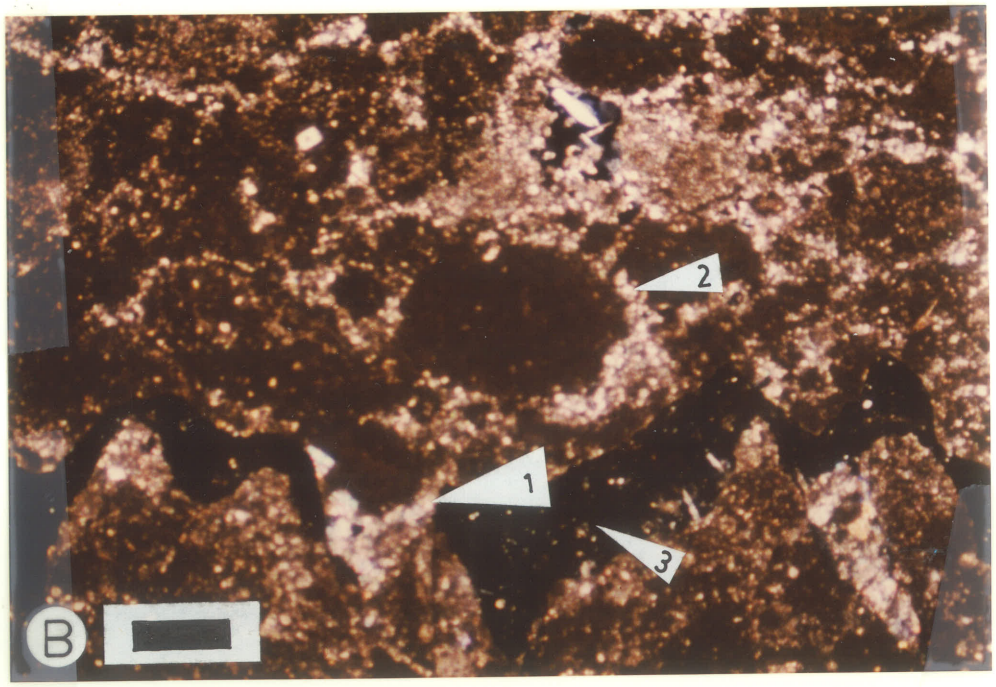
2
1
3
B

PLATE - 37

DIAGENESIS

A. Photomicrograph showing dolomite (1) partially replacing equant calcite cement (2). Sample no. 4.43, thin section perpendicular to stratification, crossed nicols. Bar scale equals 0.25 mm.

B. Photomicrograph showing dolomite (1) completely replacing equant calcite cement. Sample no. 3.11, thin section perpendicular to stratification, crossed nicols. Bar scale equals 30 microns.

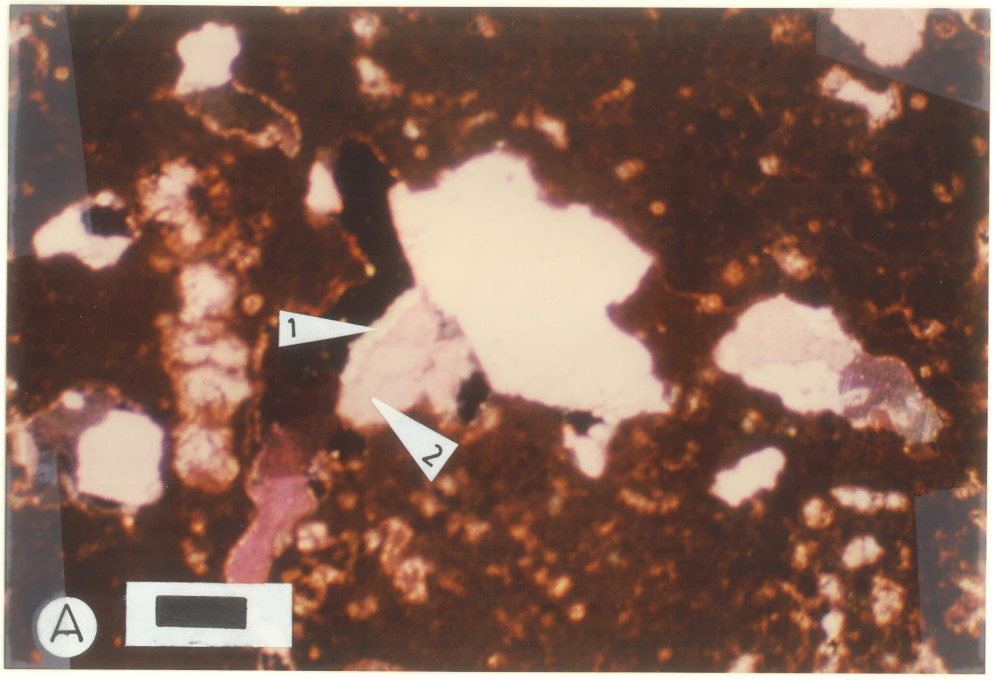
1
2
A

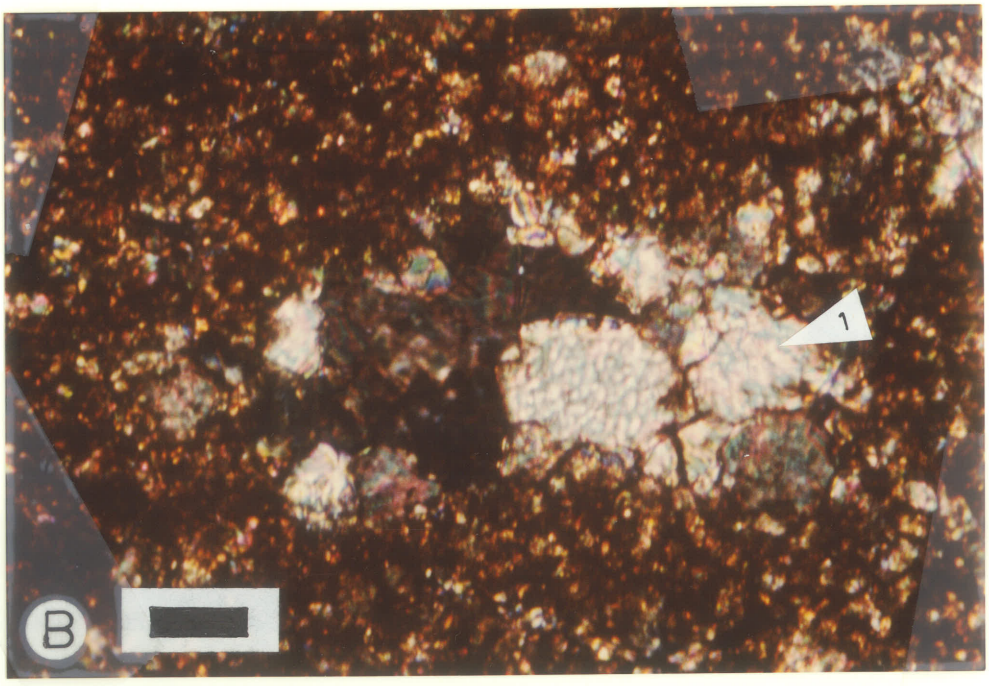
1
B

PLATE - 38

DIAGENESIS

A. Photomicrograph showing geopetal dolomite (1), late pore lining dolomite cement (2) in a vadomoldic pore (3). Sample no. 1.82, thin section perpendicular to stratification, crossed nicols. Bar scale equals 70 microns.

B. Photomicrograph showing void-filling anhydrite composed of tabular crystals (1). Sample no. 2.33, thin section perpendicular to stratification, crossed nicols. Bar scale equals 0.25 mm.

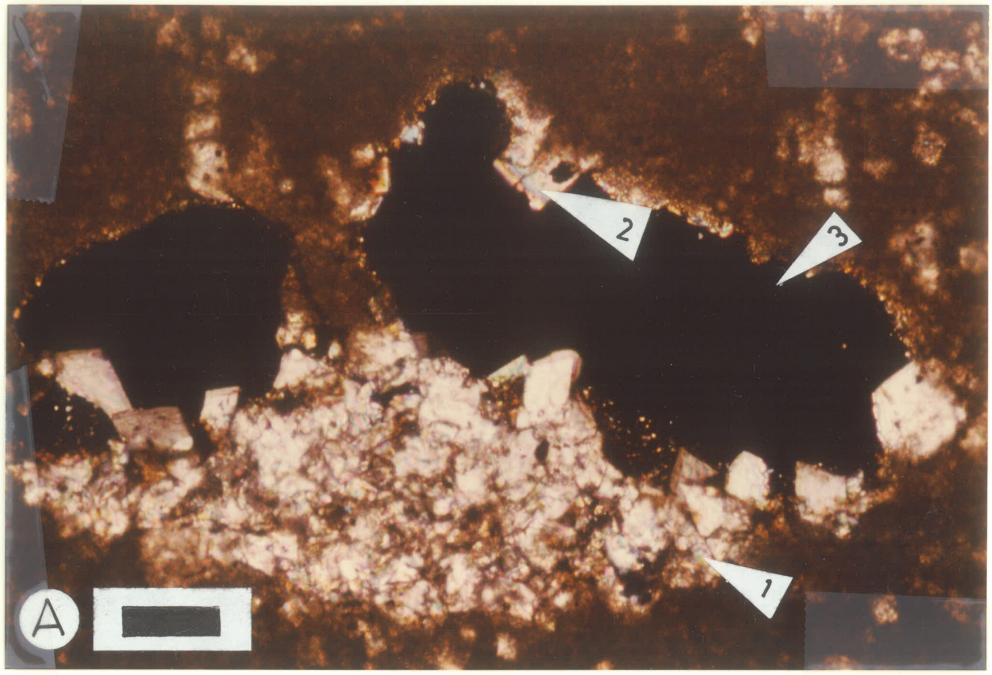
2
3
1
A

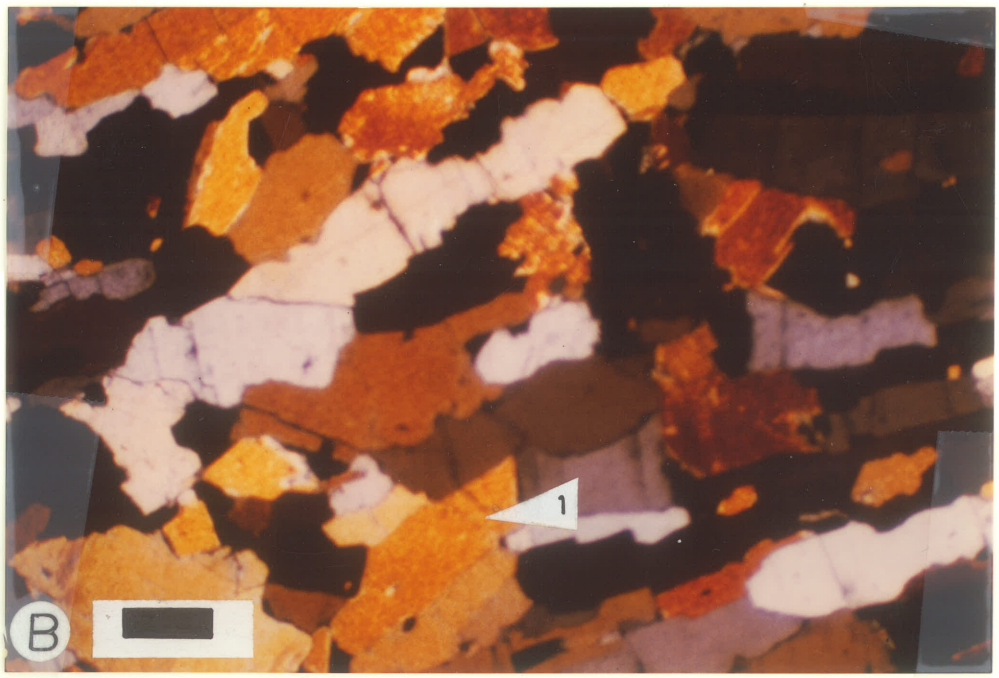
1
B

PLATE - 39

DIAGENESIS

A. Photomicrograph showing void filling anhydrite composed of tabular crystals (1), and corroded anhydrite grains (2) in a gypsum crystal (3). Sample no. 5.34, thin section perpendicular to stratification, crossed nicols. Bar scale equals 70 microns.

B. Photomicrograph showing xenotopic to hypidiotopic replacement anhydrite which exhibits all gradation from rectangular habit (1) to rhombic habit (2) pseudomorphic after parent dolomite. Sample no. 1.11, thin section perpendicular to stratification, crossed nicols. Bar scale equals 0.25 mm.

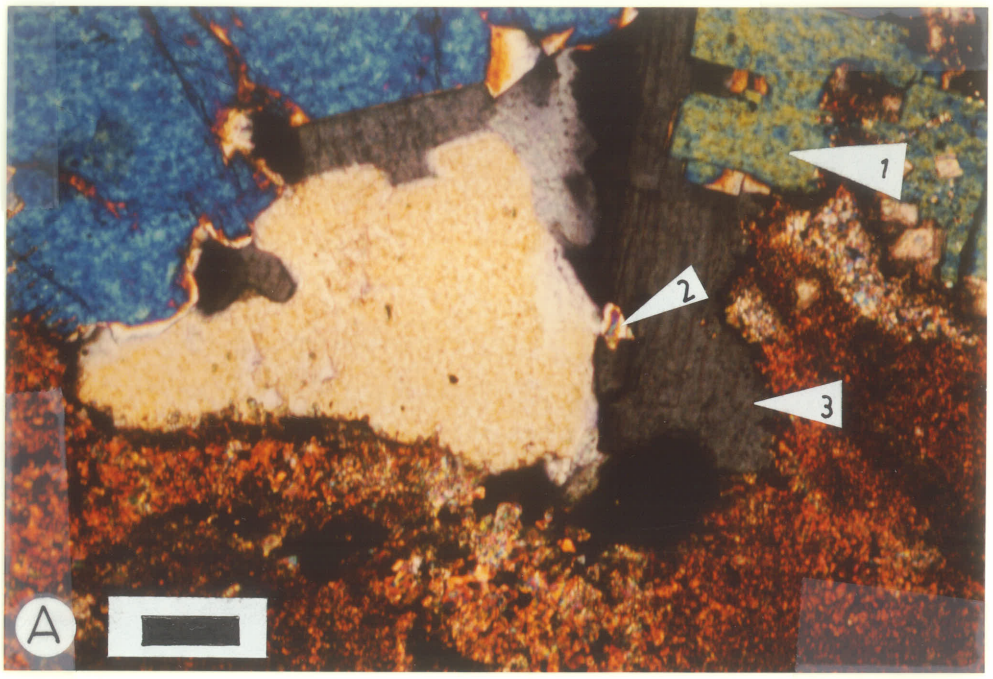
1
2
3
A

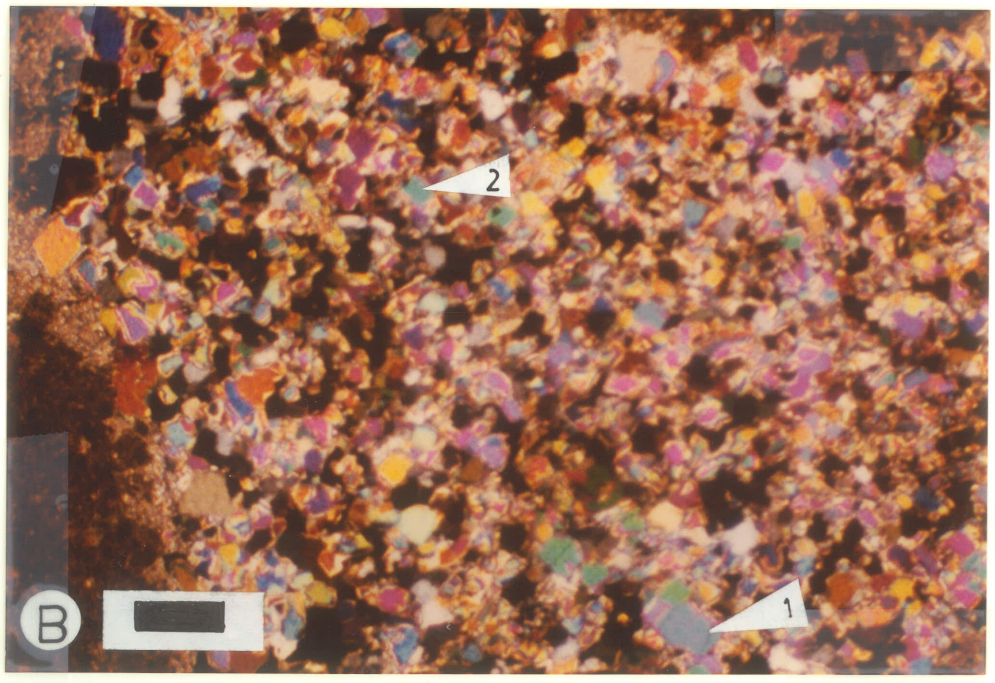
2
1
B

PLATE - 40

DIAGENESIS

A. Close up view of Plate 39 Fig. B. Xenotopic to hypidiotopic replacement anhydrite showing all gradation from rectangular habit (1) to rhombic habit (2) after parent dolomite. Sample no. 1.11, thin section perpendicular to stratification, crossed nicols. Bar scale equals 30 microns.

B. Photomicrograph showing poikilotopic replacement anhydrite (1) enclosing corroded equant calcite cement (1). Sample no. 4.43, thin section perpendicular to stratification. Bar scale equals 0.25 mm.

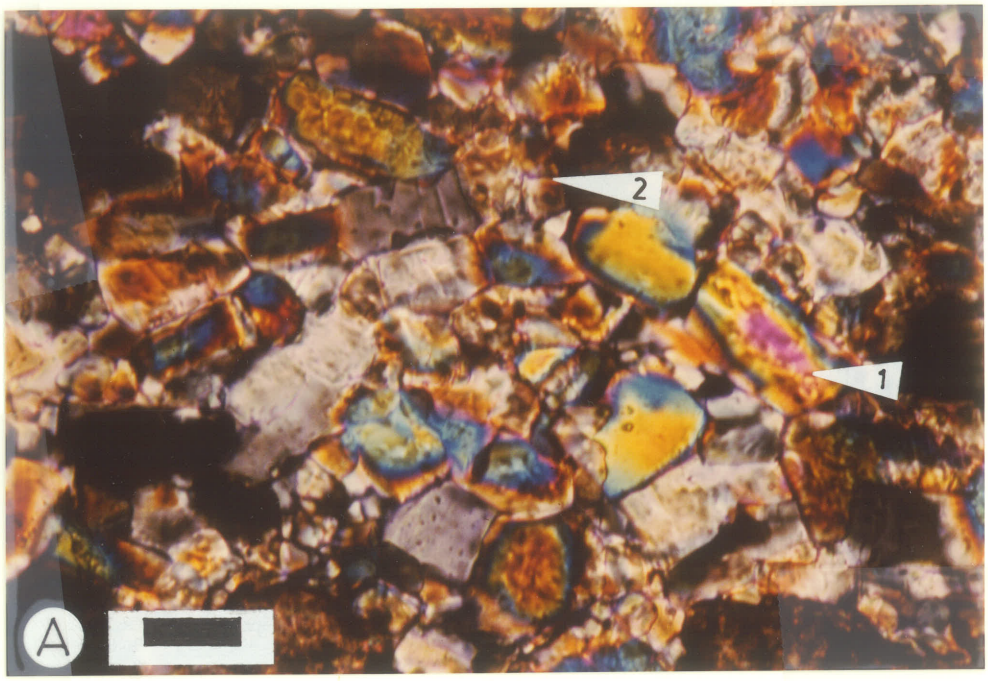
2
1
A

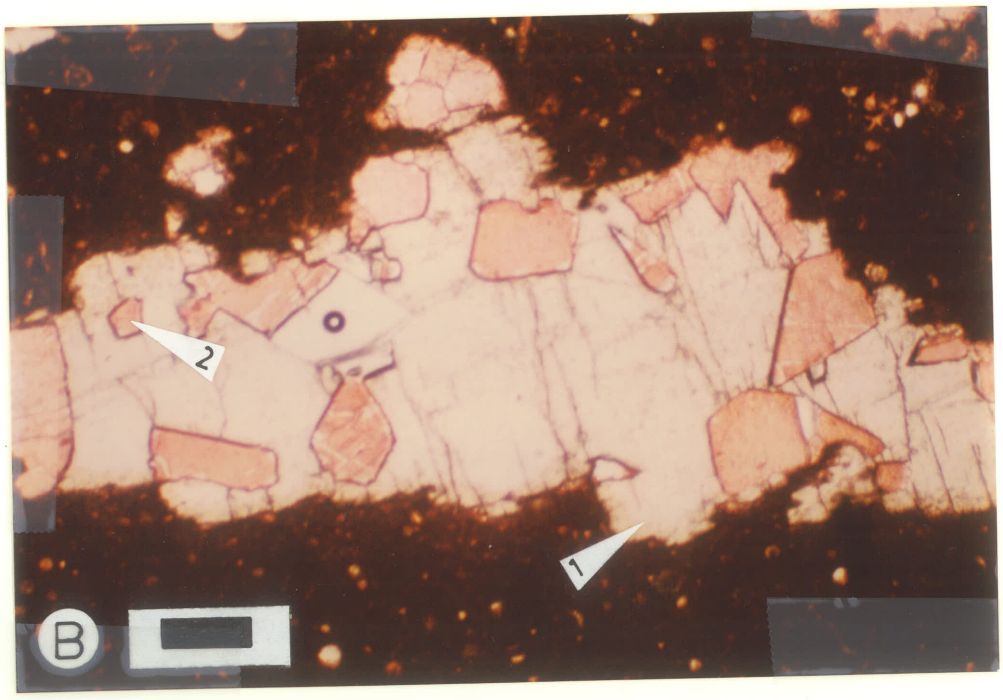
2
1
B

PLATE - 41

DIAGENESIS

A. Photomicrograph showing microscopic moldic pore (1) infilled with void-filling individual anhydrite crystals (2). Sample no. 1.33, thin section perpendicular to stratification, crossed nicols. Bar scale equals 0.25 mm.

B. Photomicrograph showing void filling anhydrite (1) in leached stylolite (2). Sample no. 2.42, thin section perpendicular to stratification, crossed nicols. Bar scale equals 0.5 mm.

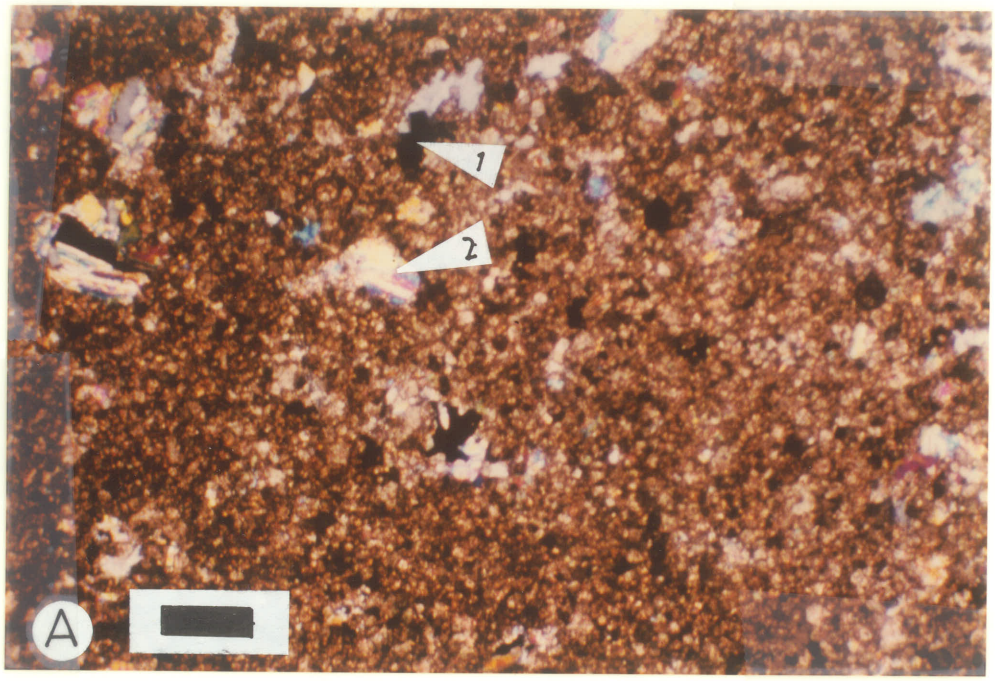
1
2
A

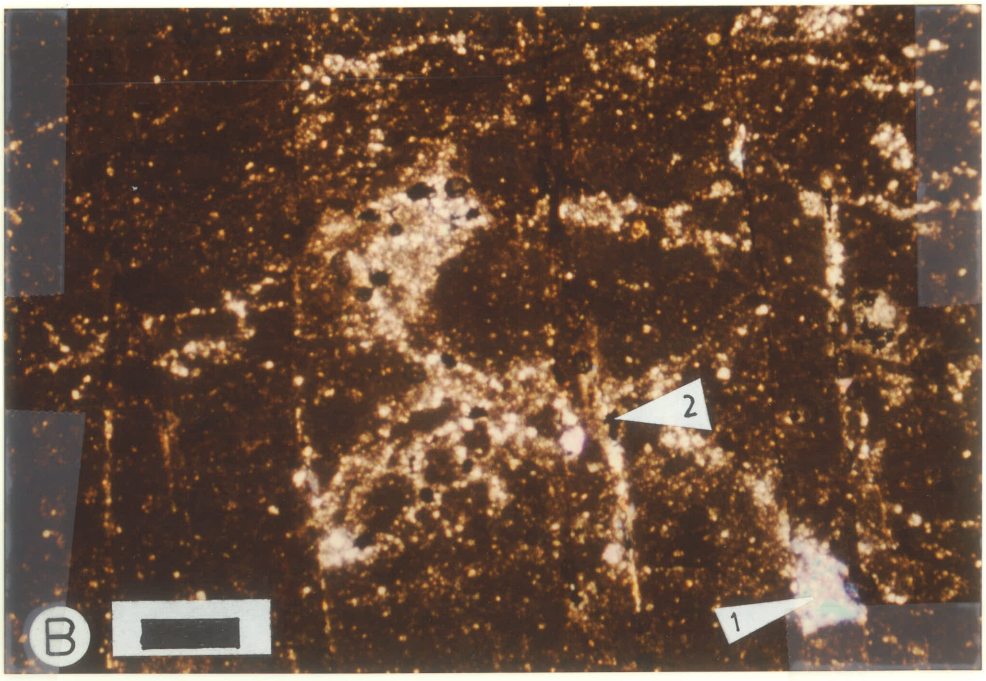
2
1
B

PLATE - 42

DIAGENESIS

A. Photomicrograph showing gypsum of fibrous habit (1). Sample no. 2.22, thin section perpendicular to stratification, crossed nicols. Bar scale equals 70 microns.

B. Photomicrograph of gypsum (1) showing enclosed corroded anhydrite grains (2). Sample no. 1.11, thin section perpendicular to stratification, crossed nicols. Bar scale equals 70 microns.

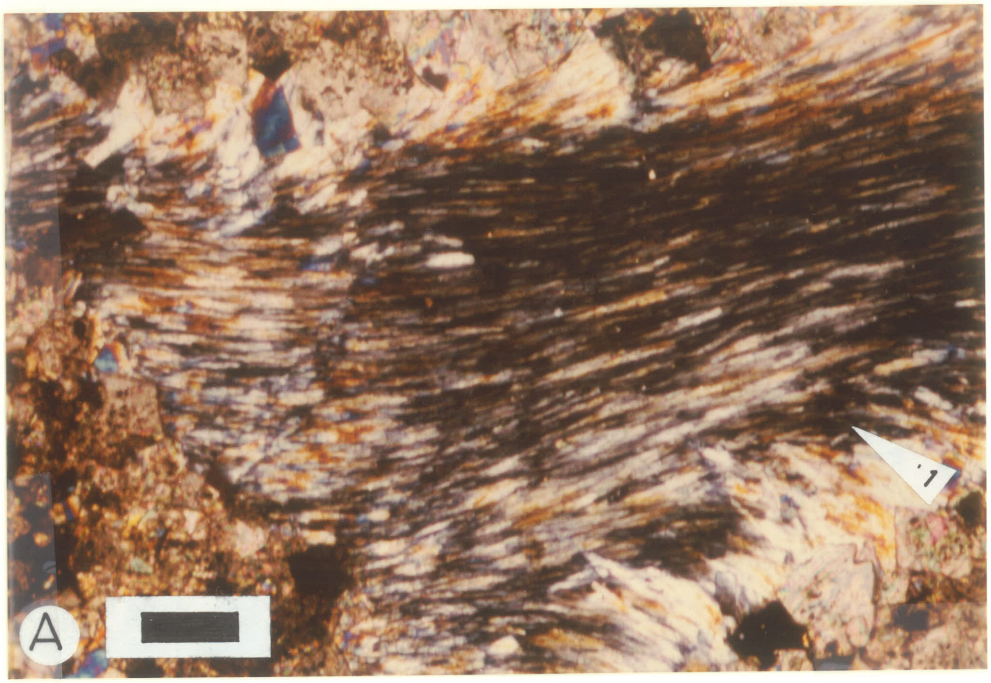
1
A

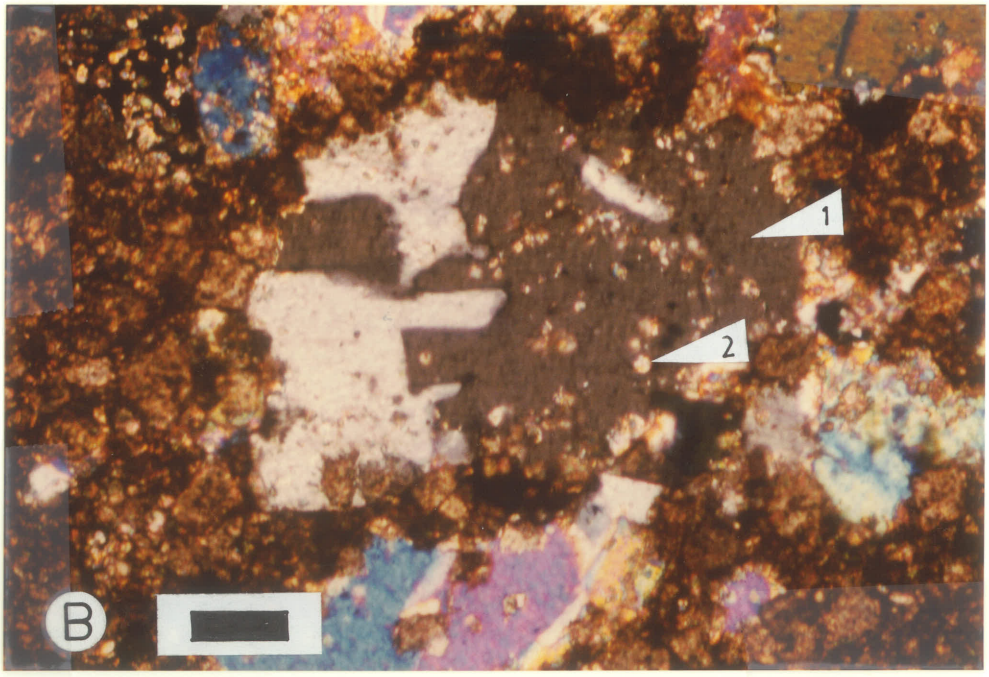
1
2
B

PLATE - 43

DIAGENESIS

A. Photomicrograph showing dispersed dedolomites (1) in calcite dolostone immediately below the altered zone. Dedolomite crystals enclose corroded dolomite rhombs (2). Sample no. 3.20, thin section perpendicular to stratification. Bar scale equals 70 microns.

B. Close up view of Plate 43 Fig. A. Dedolomite crystal enclosed (1) corroded dolomite rhombs (2). Sample no. 3.20, thin section perpendicular to stratification. Bar scale equals 30 microns.

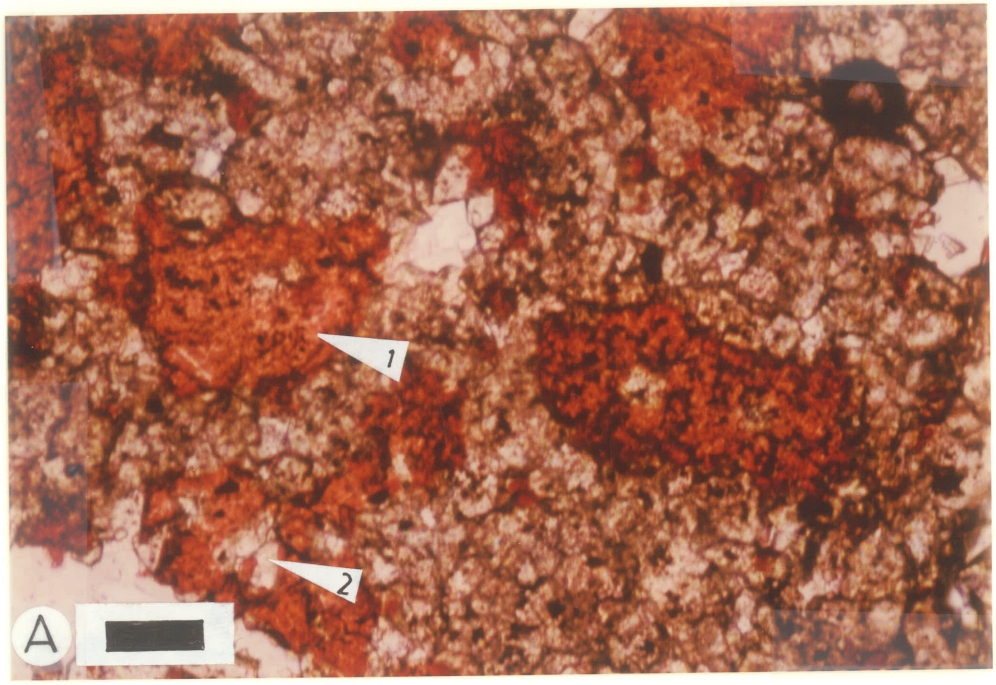
1
2
A

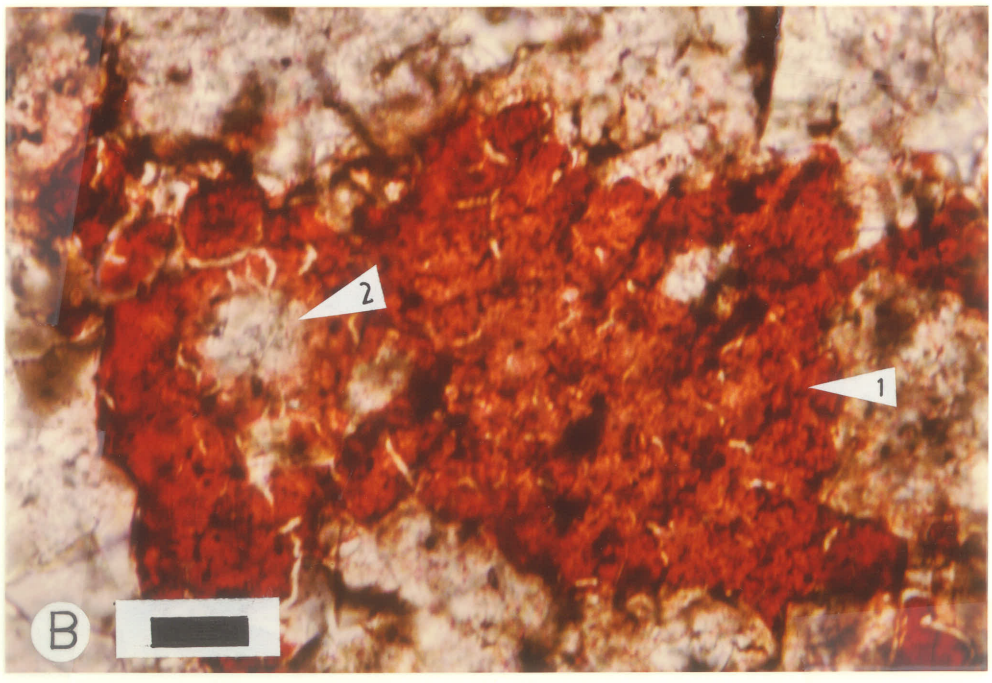
2
1
B

PLATE - 44

DIAGENESIS

A. Photomicrograph showing dedolomite crystals (1) pseudomorphic after dolomite rhombs. Sample no. 3.20 thin section perpendicular to stratification. Bar scale equals 30 microns.

B. Photomicrograph showing disseminated hematite (1) in the matrix. Sample no. 4.30, thin section perpendicular to stratification. Bar scale equals 0.5 mm.

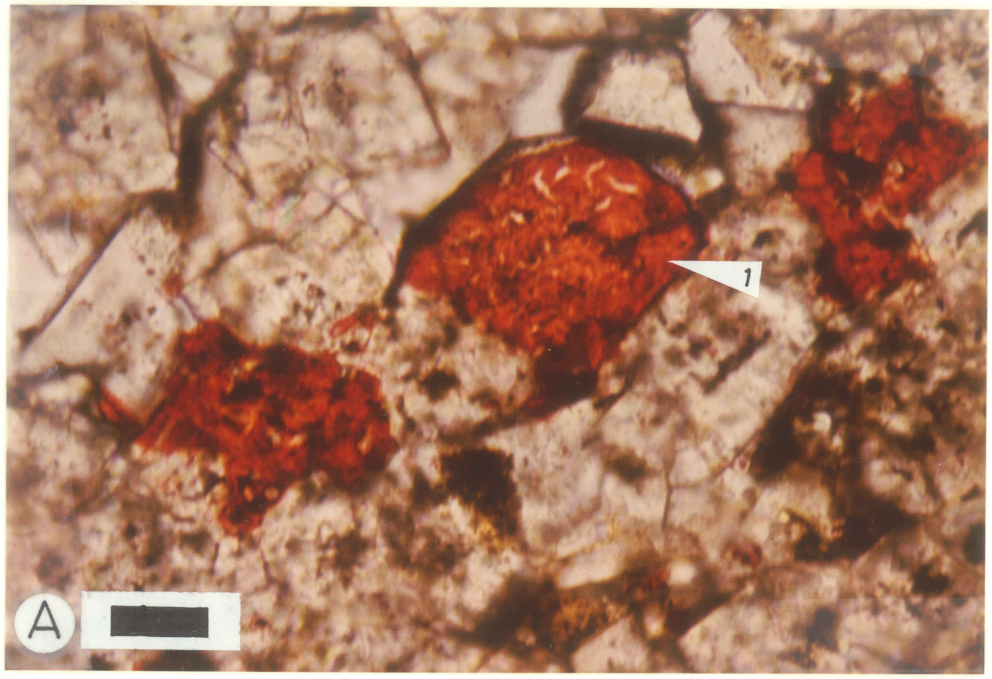
1
A

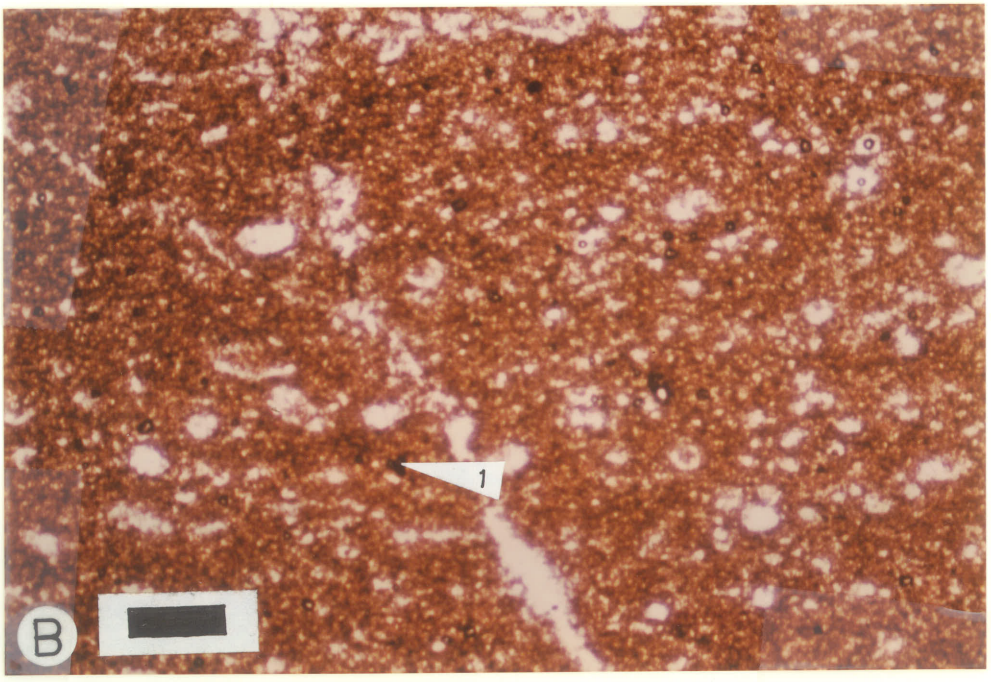
1
B

PLATE - 45

DIAGENESIS

A. Photomicrograph of bioclastic grainstone facies showing disseminated hematite (1) within algal grains and a broken algal grain (2) due to compaction. Sample no. 1.61, thin section parallel to stratification, crossed nicols. Bar scale equals 0.25 mm.

B. Photomicrograph showing patches of pyrite (1) and intimately associated limonite (2) in a secondary void. Sample no. 5.30, thin section perpendicular to stratification. Bar scale equals 30 microns.

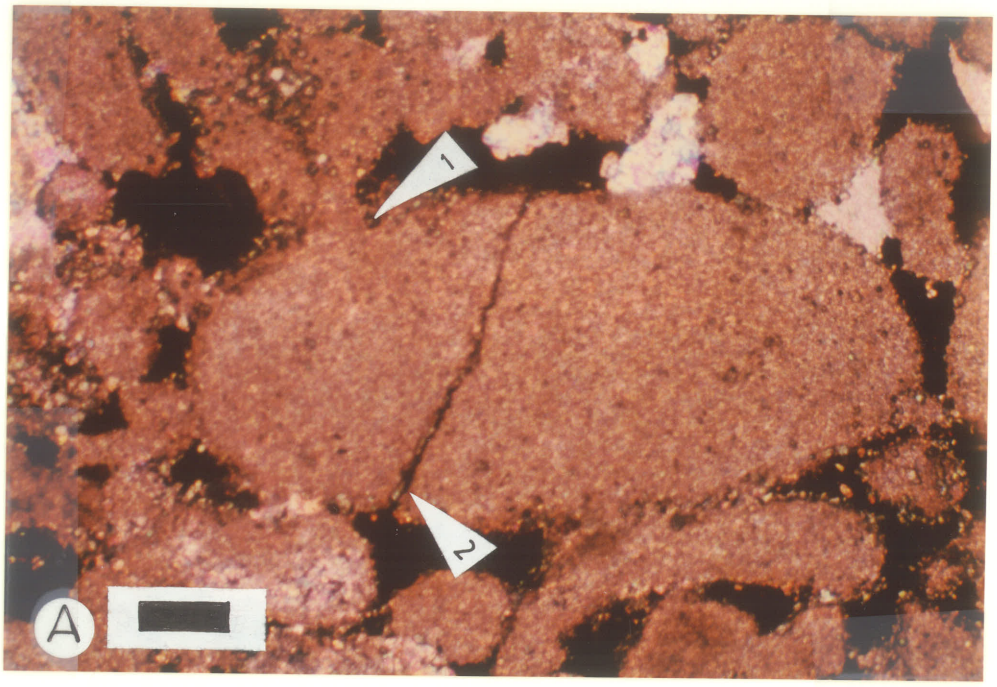
1
2
A

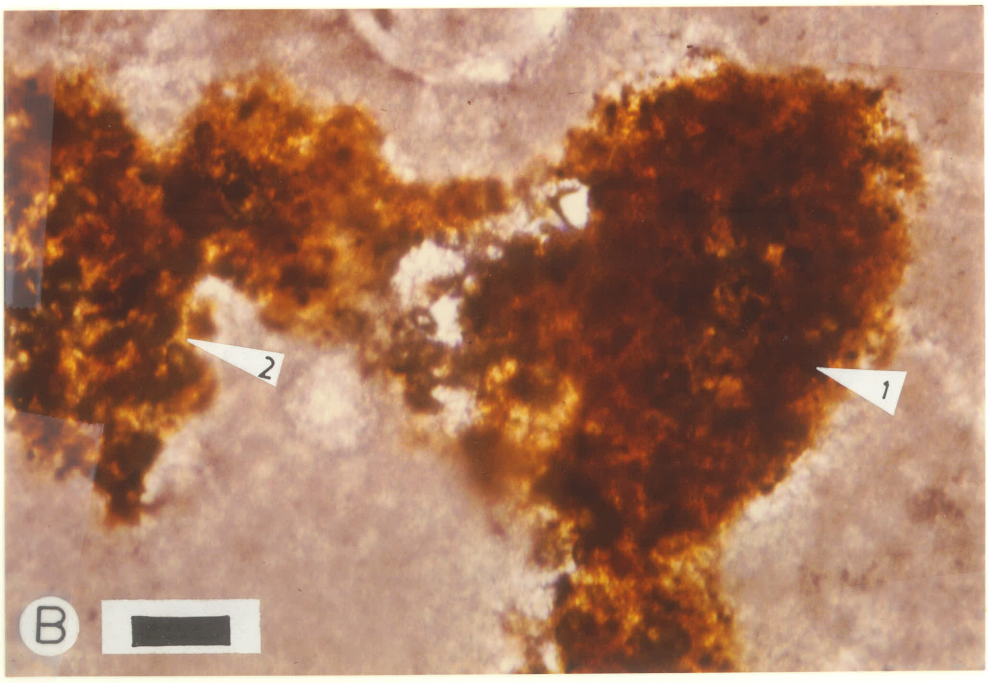
2
1
B

PLATE - 46

DIAGENESIS

A. Photomicrograph showing pyrite grains (1) in a secondary void. Sample no. 4.51, thin section perpendicular to stratification. Bar scale equals 70 microns.

B. Photomicrograph showing development of pyrite (1) in intercrystalline pores. Sample no. 5.21, thin section perpendicular to stratification. Bar scale equals 70 microns.

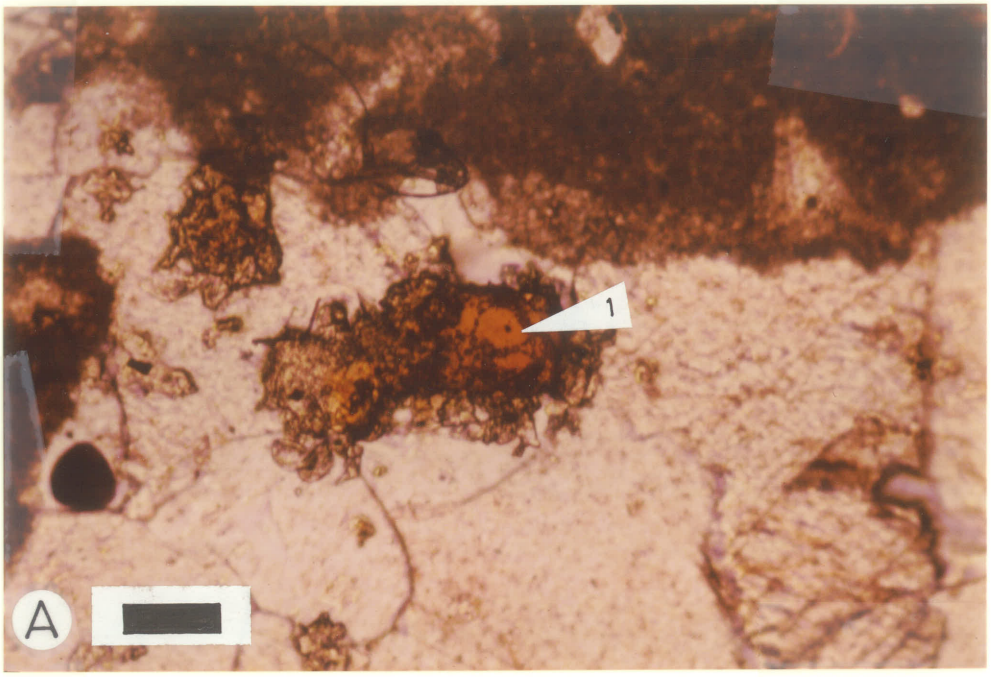
1
A

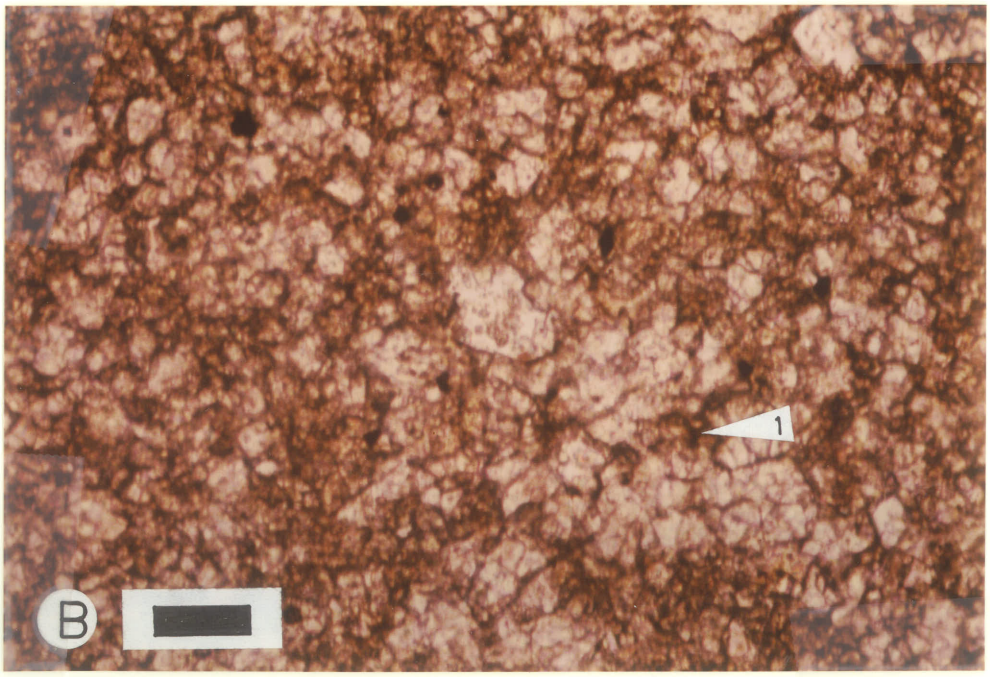
1
B

PLATE - 47

DIAGENESIS

A. Photomicrograph showing pyrite (1) infilling a fracture partially. Sample no. 4.40, thin section perpendicular to stratification, crossed nicols. Bar scale equals 0.5 mm.

B. Photomicrograph showing fracture filling silica cement (1). Sample no. 3.11, thin section perpendicular to stratification, crossed nicols. Bar scale equals 70 microns.

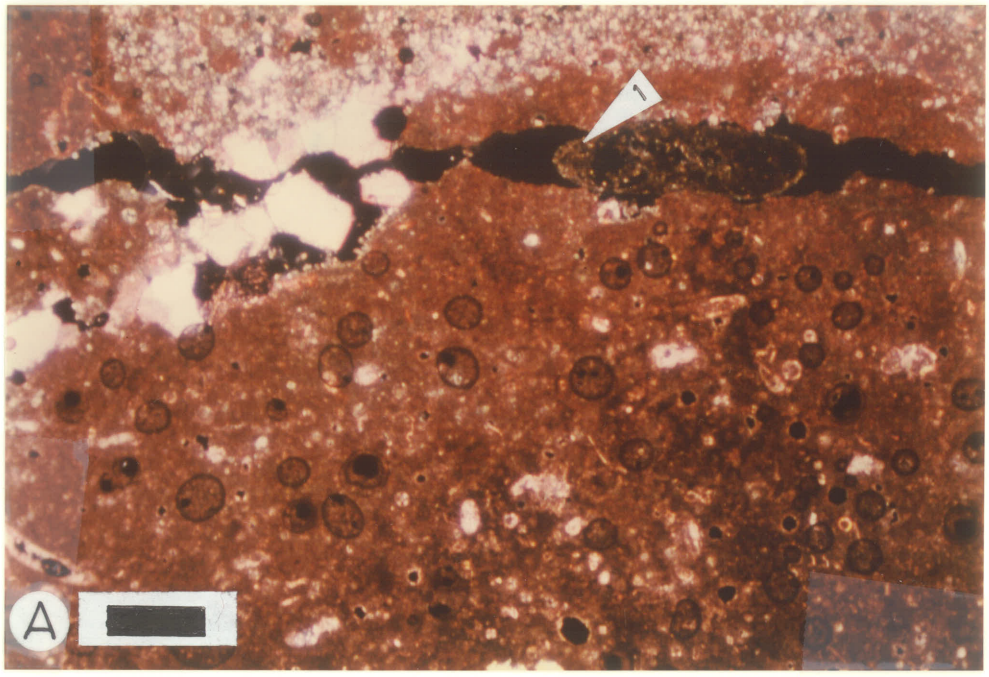
1
A

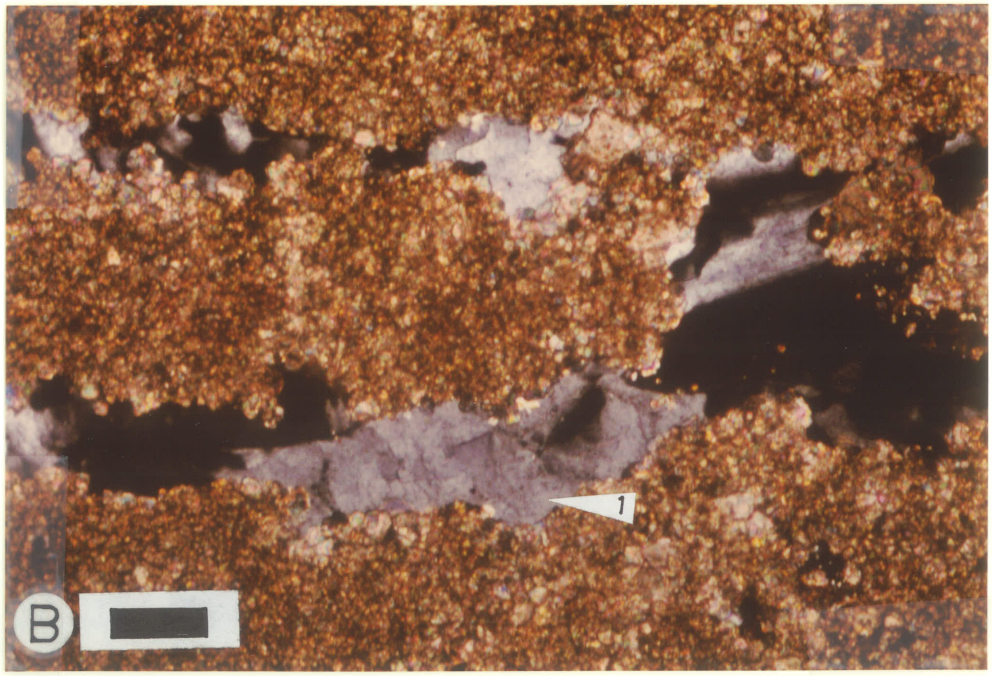
1
B

PLATE - 48

DIAGENESIS

A. Photomicrograph of void-filling silica cement (1) showing fibrous extinction characteristic of Chalcedony. Sample no. 3.11, thin section perpendicular to stratification, crossed nicols. Bar scale equals 70 microns.

B. Photograph showing dead oil (1) along an irregular stylolite (1). Sample no. 4.41, polished core slab perpendicular to stratification. Bar scale equals 1 cm.

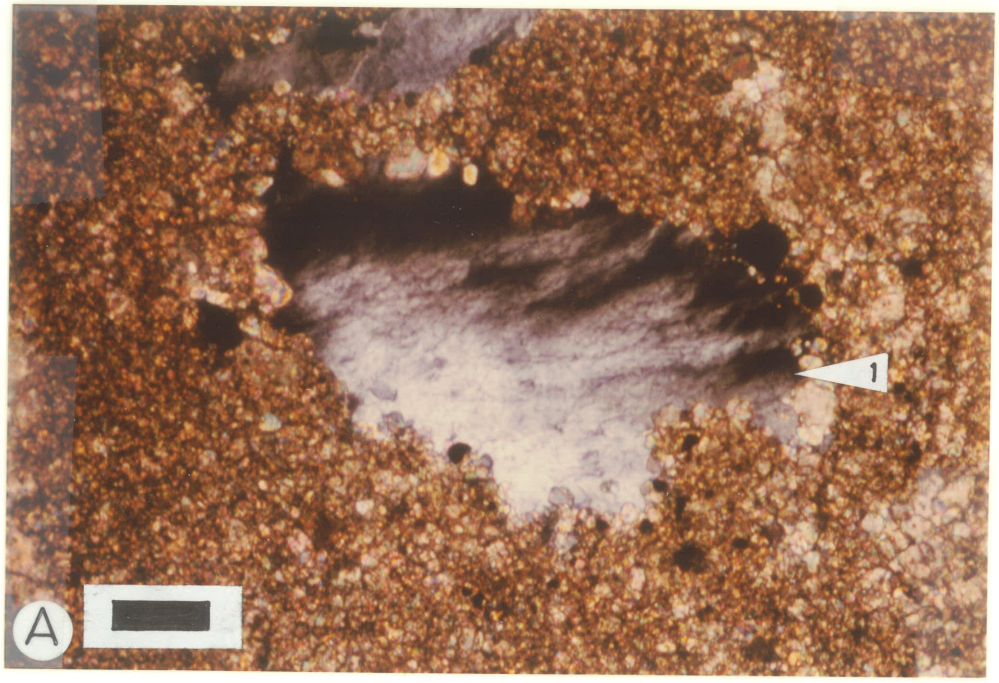
1
A

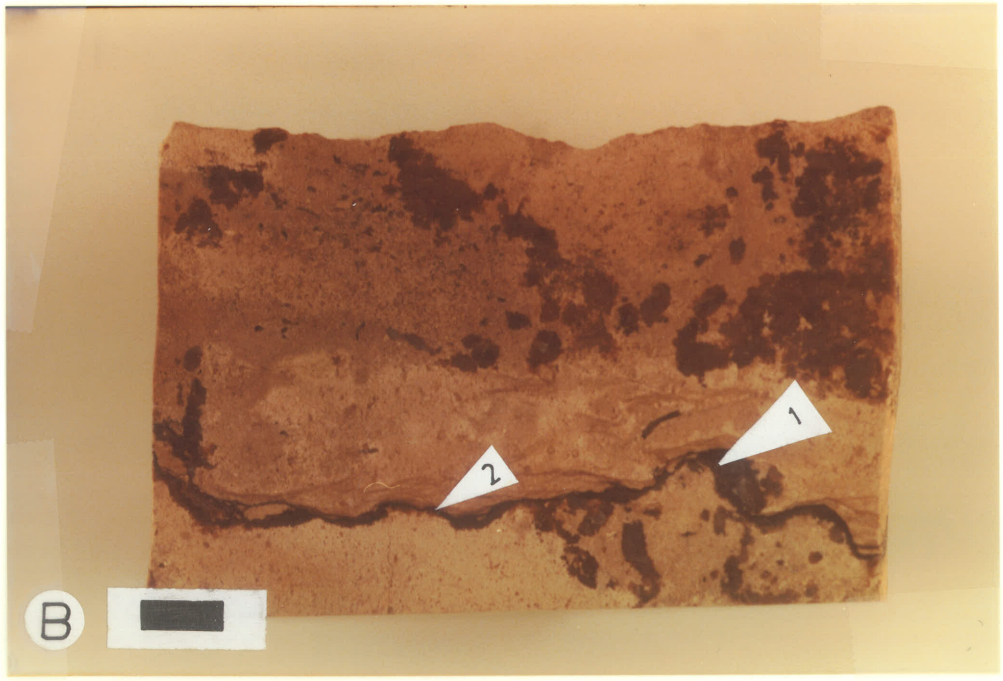
1
2
B

PLATE - 49

DIAGENESIS

A. Photograph showing peaks low amplitude stylolite (1). Sample no. 3.31, polished core slab perpendicular to stratification. Bar scale equals 1 cm.

B. Photograph showing a conjugate set of peaks low amplitude stylolites (1). Sample no. 1.91, polished core slab perpendicular to stratification. Bar scale equals 1 cm.

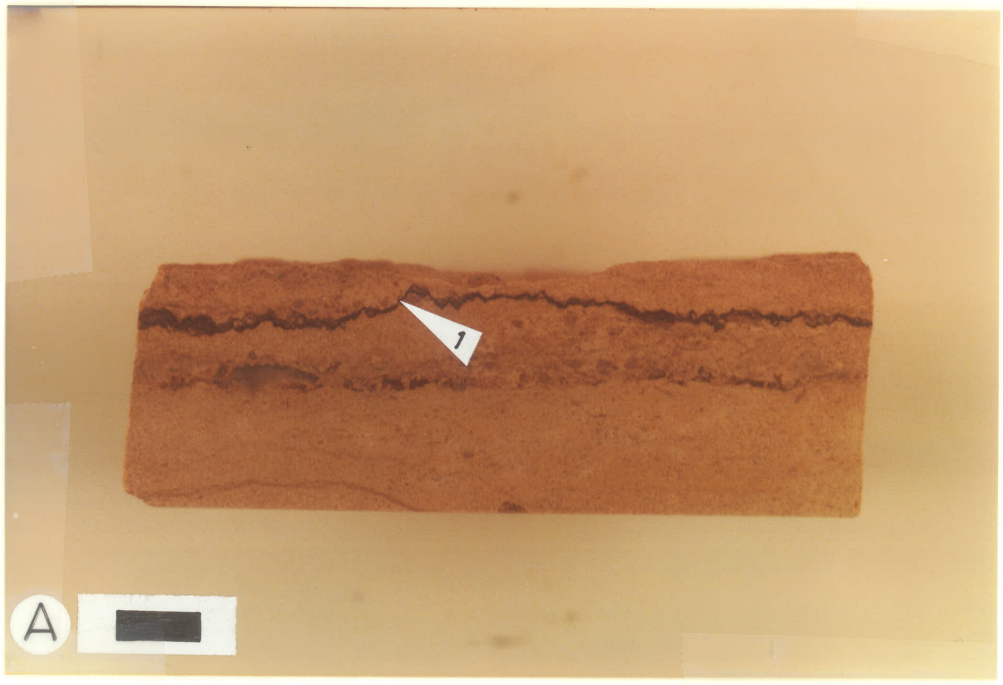
1
A

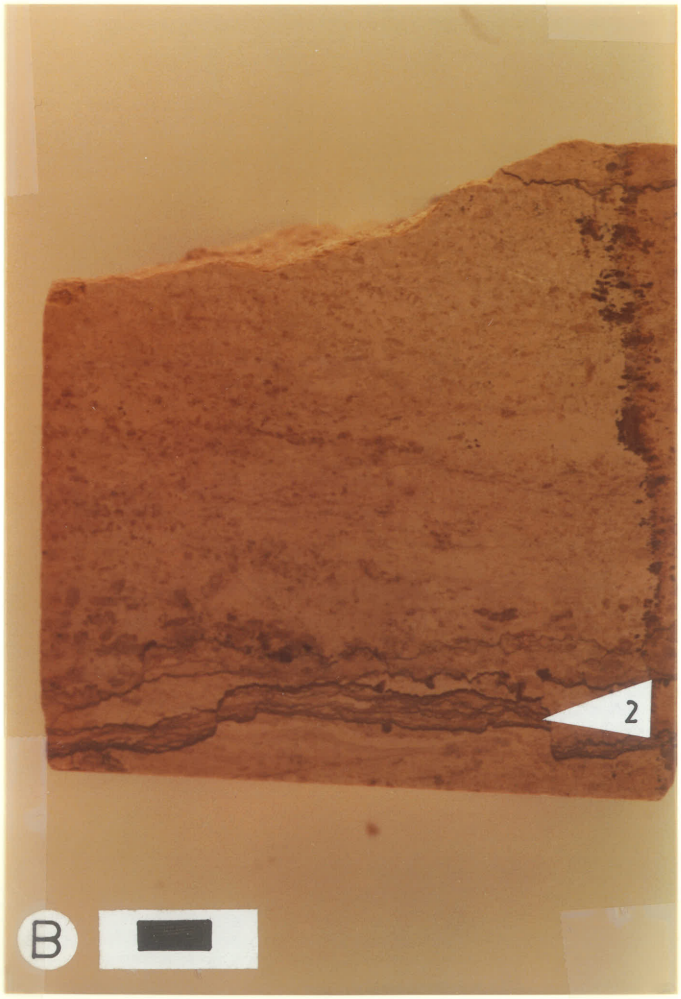
2
B

PLATE - 50

DIAGENESIS

A. Photograph showing an anastomosing swarm of fine clay seams (1) developed as a result of non-sutured grain solution style of pressure solution. Sample no. 5.11, polished core slab perpendicular to stratification. Bar scale equals 1 cm.

B. Photomicrograph showing a fracture (1) cutting across a gypsum crystal (2). Sample no. 4.51, thin section perpendicular to stratification, crossed nicols. Bar scale equals 0.5 mm.

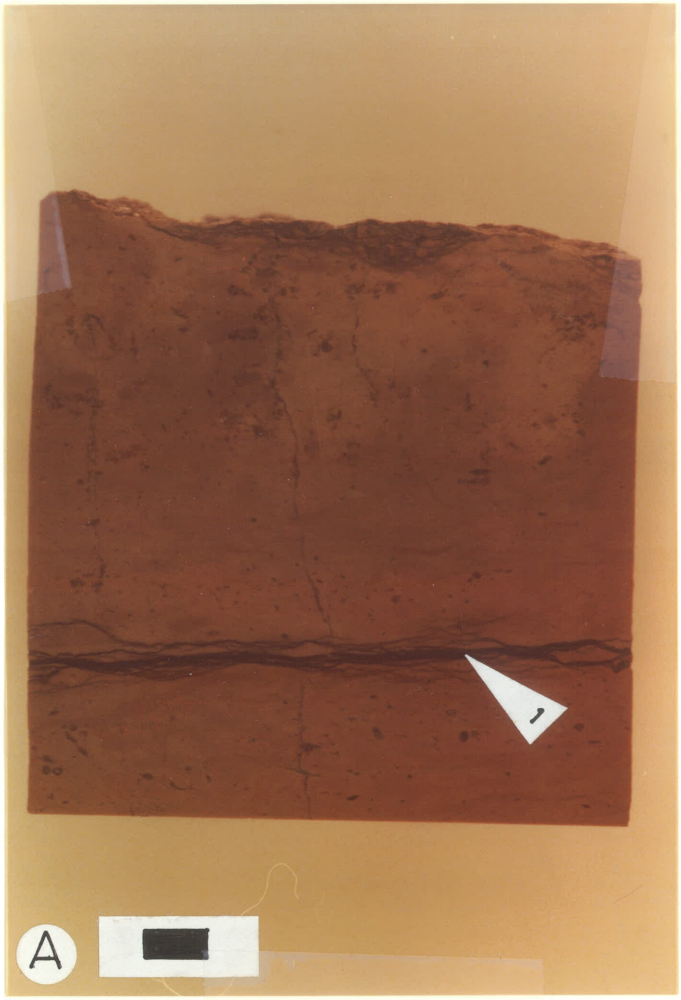
1
A

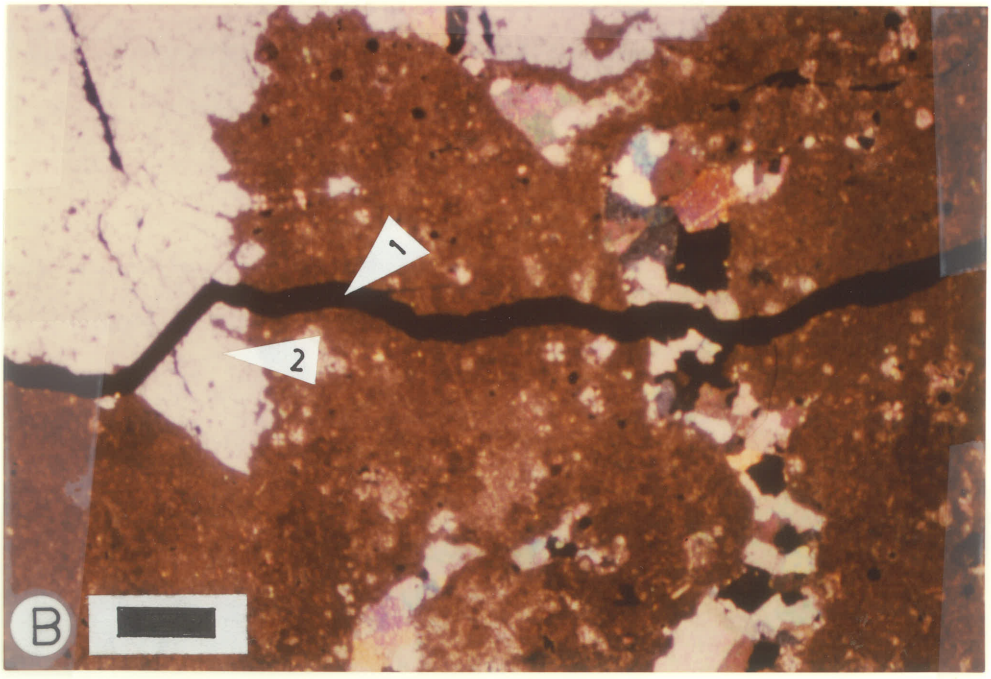
1
2
B

PLATE - 51

DIAGENESIS

Photomicrograph showing oil-stained anhydrite (1) in a modified interparticle pore of the bioclastic grainstone facies. Sample no. 1.61, thin section parallel to stratification. Bar scale equals 70 microns.

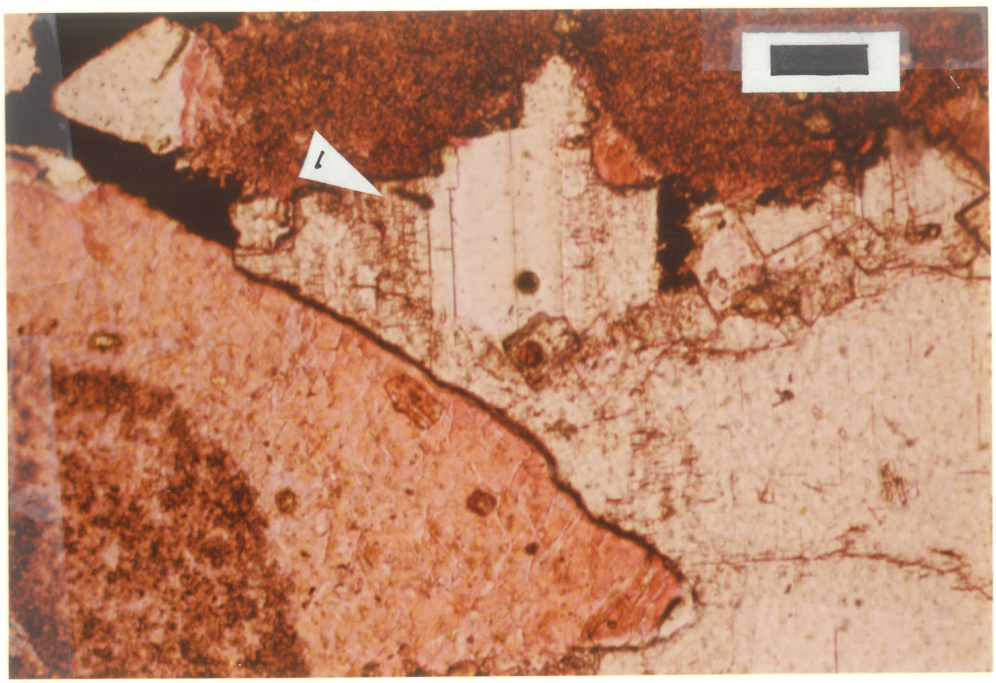
1

PLATE - 52

POROSITY

A. Photomicrograph of vadolite facies showing modified interparticle (1) and vuggy (2), and fracture (3) porosity. Sample no. 5.30, thin section perpendicular to stratification, crossed nicols. Bar scale equals 0.5 mm.

B. Photomicrograph of stromatolite subfacies showing vuggy pores (1). Sample no. 4.52, thin section perpendicular to stratification, crossed nicols. Bar scale equals 0.5 mm.

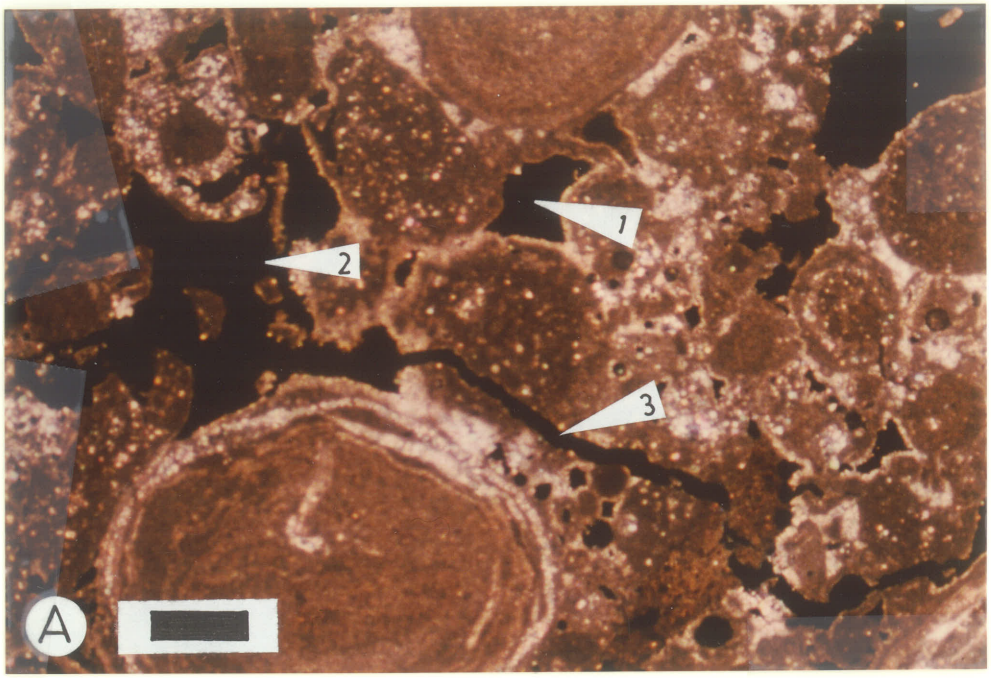
1
2
3
A

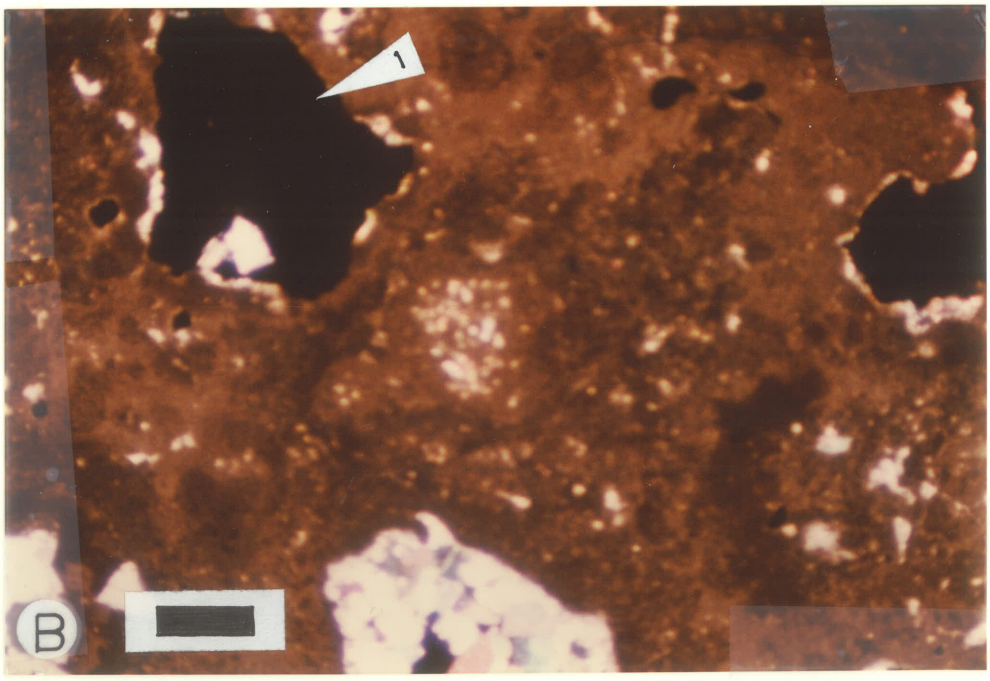
1
B

PLATE - 53

POROSITY

A. Photomicrograph shows oil-filled intercrystalline pores (1) associated with dolomitization in a thin band of rocks immediately below the altered zone. Sample no. 4.30, thin section perpendicular to stratification, crossed nicols. Bar scale equals 70 microns.

B. Photomicrograph showing vadomoldic pores (1). Sample no. 2.22, thin section parallel to stratification. Bar scale equals 0.5 mm.

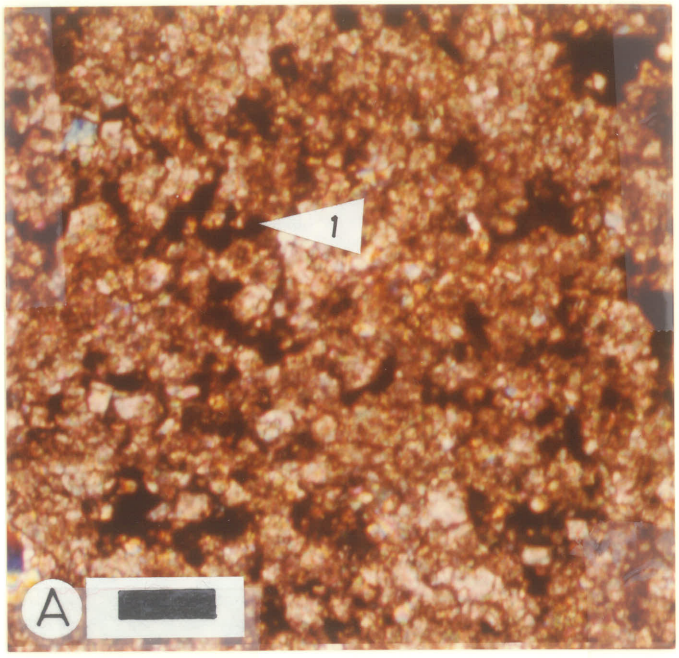
1
A

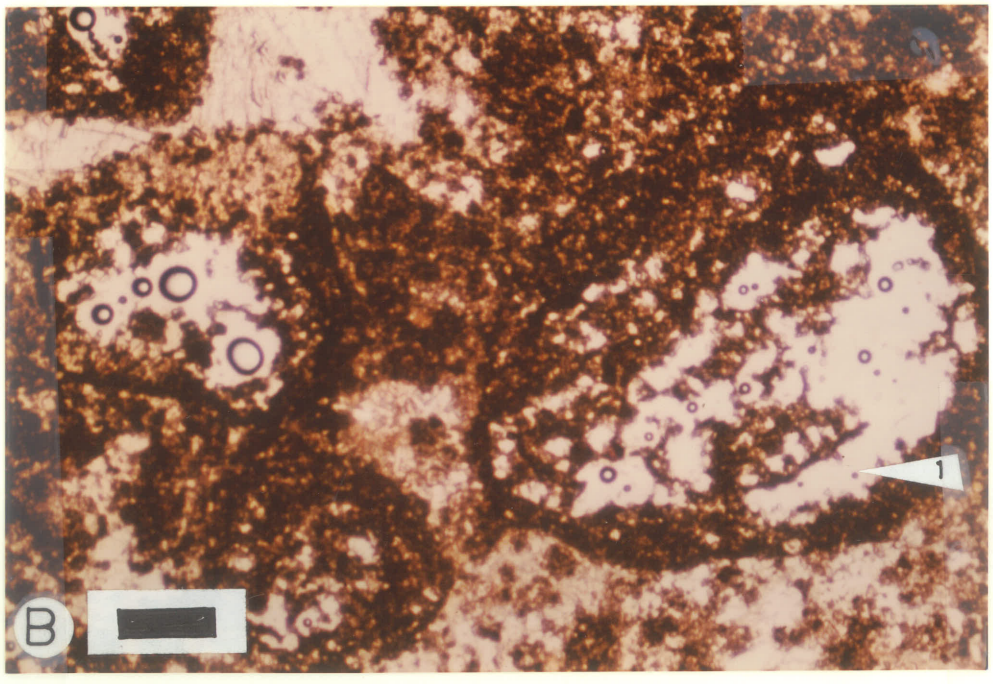
1
B

PLATE - 54

POROSITY

Photomicrograph showing biomoldic pore (1). Sample no. 2.44, thin section parallel to stratification, crossed nicols. Bar scale equals 30 microns.

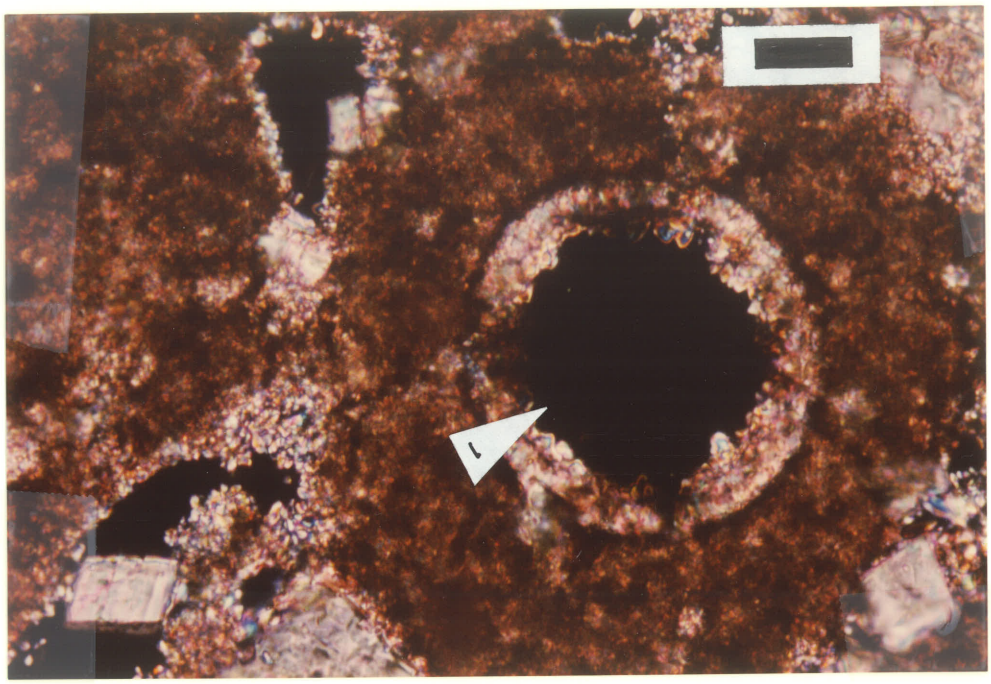

APPENDIX A

DESCRIPTION OF CORE SLABS

1 - 18 - 3 - 23W1

K.B. 1545 FT

Sample No.	Depth	Description
1.10	3209′ 11" - 3203′ 3"	Pre-Jurassic unconformity between upper Jurassic Amaranth red bed composed of anhydrite infilled green dolomitic silty shale and lower dolomitized cryptalgal laminae. The latter is a lithographic, grey buff anhydrite infilled dolostone. Vaguely preserved cryptalgal laminae observed. Porosity is < 1%.
1.11	3210′ 6" - 3210′ 9"	Lithographic, grey buff, anhydrite infilled with dolostone. Vaguely preserved cryptalgal laminae. Anhydrite infilled fractures present. Porosity is < 1%.
1.20	3211′ - 3211′ 2"	Upper part composed of lithographic grey buff, anhydrite infilled dolostone. Vaguely preserved cryptalgal laminae present. Porosity is < 1%.

		Lower part consists of grey white nodular anhydrite.
1.21	3211′ 4" - 3211′ 6"	Grey white nodular anhydrite.
1.31	3217′ - 3217′ 3"	Lithographic, grey buff, anhydrite infilled dolostone. Vaguely preserved cryptalgal laminae observed. Anhydrite infilled fracture present. Porosity is < 1%.
1.32	3225′ 11" - 3226′ 2"	Lithographic, grey buff, anhydrite infilled dolostone. Vaguely preserved cryptalgal laminae. Anhydrite infilled fracture present. Porosity is < 1%.
1.33	3227′ 4" - 3227′ 7"	Lithographic grey buff, anhydrite infilled dolostone. Vaguely preserved cryptalgal laminae observed. Anhydrite infilled fracture present. Porosity is < 1%.
1.40	3227′ 7" - 3227′ 9"	Erosional contact between upper dolomitized cryptalgal laminite and lower dolomitized peloidal grain-

		stone. The former is a lithographic, buff grey, anhydrite infilled dolostone. Vaguely preserved cryptalgal laminae present. Anhydrite infilled fracture observed. Porosity is ≈ 2.5%. The latter is a lithographic to sublithographic, grey buff, partially anhydrite infilled calcareous dolostone. The constituent particles are peloids. Anhydrite infilled fracture present. Oil stain observed.
1.41	3228′ 2" – 3228′ 5"	Sublithographic, grey buff, partially anhydrite infilled dolomitic limestone. Constituent particles are peloids. Vertical fracture with oil stain observed.
1.51	3230′ 3" – 3230′ 6"	Sublithographic, buff, partially anhydrite infilled dolomitic limestone. Constituent particles are bioclasts of sand size. Light oil stain present.

1.61	3235′ 1" - 3235′ 6"	Erosional contact between upper dolomitized bioclastic grainstone and lower dolomitized stromatolite. The former is a sublithographic, grey buff, partially anhydrite infilled dolomitic limestone. Constituent particles are bioclasts of sand size. Light oil stain present. The latter is a sublithographic, buff, partially anhydrite infilled dolomitic limestone. LLH type stromatolitic structure recognized. Irregular fenestrae as well as laminoid fenestrae between laminae of algal structure observed. Light oil stain present.
1.62	3240′ - 3240′ 2"	Earthy, buff white, massive, partially anhydrite infilled dolomitic limestone. Encrustation by algal filaments observed under microscope. Vertical desiccation cracks abundant. Stylolite present. Light oil stain observed.
1.71	3241′ 11"	Sublithographic, tan, massive,

	- 3242′ 1"	partially anhydrite infilled dolomitic limestone. Encrustation by algal filaments observed under microscope. Stylolite present.
1.72	3245′	Sublithographic to earthy, grey
	- 3246′ 3"	buff to buff white, partially anhydrite infilled limestone. Constituent particles are vadoids (peloid size through 4 mm). Light oil stain present.
1.81	3252′ 11"	Sublithographic, buff, partially
	- 3253′	anhydrite infilled dolomitic limestone. Constituent particles are vadoids (peloid size through 2 mm). Stylolite present.
1.82	3254′ 6"	Sublithographic, buff to grey buff,
	- 3254′ 10"	partially anhydrite infilled dolomitic limestone. Constituent particles are vadoids (peloid size through 4 mm). Associated vadose crusts observed. Stylolite present.
1.91	3258′ 1"	Sublithographic to earthy, buff,
	- 3258′ 4"	partially anhydrite infilled dolo-

		mitic limestone. Constituent particles are vadoids (peloid size through 2 mm). Associated vadose crusts observed. Stylolite present. Porosity ≈ 7.5%.
1.91a	3260′ 6" - 3260′ 8"	Lithographic, cream, partially anhydrite infilled dolomitic limestone. Cryptalgal laminae observed. Laminoid fenestrae abundant. Porosity ≈ 3%.
1.91b	3262′ 1" - 3262′ 3"	Erosional contact between upper dolomitized cryptalgal laminite and lower MC-2 bed. The former is a sublithographic, grey buff partially anhydrite infilled dolomitic limestone. Vaguely preserved cryptalgal laminae present. Porosity is < 1%.

3 - 20 - 3 - 28W1

K.B. 1553 FT

Sample No.	Depth	Description
2.11	3201′ - 3201′ 3"	Lithographic, grey buff, anhydrite infilled dolostone. Vaguely preserved cryptalgal laminae observed.
2.12	3208′ 4" - 3208′ 5"	Lithographic, grey buff, partially infilled dolostone. Constituent particles are vadoids (peloid size through 2 mm). Anhydrite infilled vertical fracture present. Light oil stain observed.
2.21	3210′ 5" - 3210′ 7"	Lithographic, grey buff, partially anhydrite infilled dolostone. Constituent particles are vadoids (peloid size through 2 mm). Associated vadose crusts observed.
2.22	3210′ 10" - 3211′	Lithographic, grey buff to brown, partially anhydrite infilled dolostone. Constituent particles are

vadoids (peloid size through 8 mm). Associated vadose crusts observed. Light oil stain present.

2.31	3212′ 7" - 3212′ 9"	Lithographic, buff, partially anhydrite infilled limestone. Constituent particles are vadoids (peloid size through 4 mm). Associated vadose crusts observed. Anhydrite infilled vertical fracture present.
2.32	3213′ 7" - 3213′ 9"	Lithographic, buff to grey buff, partially anhydrite infilled calcareous dolostone. Constituent particles are vadoids (peloid size through 2 mm). Associated vadose crusts present.
2.33	3215′ 7" - 3215′ 9"	Sublithographic, buff, partially anhydrite infilled dolomitic limestone. Constituent particles are vadoids (peloid size through 2 mm). Associated vadose crusts recognized. Anhydrite infilled vertical fracture present. Stylolite observed. Light oil stain present.

2.34	3216′ – 3216′ 4"	Lithographic, buff to grey, partially anhydrite infilled dolostone. Constituent particles are vadoids (peloid size through 4 mm). Associated vadose crusts present. Anhydrite infilled vertical fracture observed.
2.41	3218′ 7" – 3218′ 9"	Sublithographic, buff, partially anhydrite infilled dolomitic limestone. Constituent particles are vadoids (peloid size through 3 mm). Associated vadose crusts present. Stylolite observed. Light oil stain present.
2.42	3220′ 2" – 3220′ 4"	Gradational contact between upper dolomitized vadolite, and lower dolomitized cryptalgal laminite. The former is a sublithographic to earthy, buff white, partially anhydrite infilled dolomitic limestone. A few vadoids (peloid size through 1 mm) recognized. The latter is a sublithographic to earthy, buff white, partially anhydrite infilled dolomitic lime-

		stone. Vaguely preserved cryptalgal laminae observed. Stylolite present between the two facies. Light oil stain observed.
2.43	3220′ 8" - 3220′ 10"	Lithographic, grey buff, partially anhydrite infilled dolomitic limestone. Vaguely preserved cryptalgal laminae observed.
2.44	3225′ - 3225′ 2"	Sublithographic to earthy, cream, partially anhydrite infilled dolomitic limestone. Well preserved cryptalgal laminae observed. Irregular fenestrae present.

Z - 13 - 3 - 28W1

K.B. 1553 FT

Sample No.	Depth	Description
3.10	3236′ 9" - 3236′ 11"	Pre-Jurassic unconformity between upper Jurassic Amaranth red bed composed of rust red, anhydrite infilled, dolomitic siltstone, and lower lithographic to sublithographic, grey to buff grey, anhydrite infilled argillaceous dolostone. In the latter cryptalgal laminae observed; porosity is < 1%.
3.11	3237′ 2" - 3237′ 4"	Lithographic to sublithographic, grey to buff grey, anhydrite infilled argillaceous dolostone. Cryptalgal laminae observed. Porosity is < 1%.
3.12	3240′ - 3240′ 3"	Lithographic, grey buff, anhydrite infilled dolostone. Vaguely preserved cryptalgal laminae observed. Porosity is < 1%.

3.13	3243′ 9" - 3243′ 11"	Upper part composed of lithographic, grey buff, anhydrite infilled dolostone. Vaguely preserved cryptalgal laminae present. Porosity is < 1%. Lower part consists of grey nodular anhydrite.
3.20	3244′ 1" - 3244′ 3"	Upper part composed of grey nodular anhydrite. Lower part consists of lithographic to sublithographic, grey buff, partially anhydrite infilled calcareous dolostone. Vaguely preserved cryptalgal laminae present. Porosity is 5%. Oil bleeding observed.
3.21	3244′ 7" - 3244′ 10"	Earthy to sublithographic, tan, partially anhydrite infilled dolomitic limestone. Constituent particles are peloids. Porosity is 12.5%. Light oil stain present.
3.22	3252′ 2" - 3252′ 4"	Earthy to sublithographic, grey, partially anhydrite infilled dolomitic limestone. Constituent

		particles are peloids. Porosity is 7.5%. Oil stain observed.
3.31	3253′ 6" - 3253′ 8"	Earthy to sublithographic, buff, partially anhydrite infilled dolomitic limestone. Constituent particles are peloids. Stylolite observed. Porosity is 7.5%. Light oil stain present.
3.40	3256′ - 3256′ 3"	Erosional contact present between upper dolomitized peloidal grainstone, and lower dolomitized cryptalgal laminite. The former is a sublithographic, buff, partially anhydritized dolomitic limestone. Porosity is 5%. Light oil stain present. The latter is a lithographic, buff grey, partially anhydritized calcareous dolostone. Vaguely preserved cryptalgal laminae present. Porosity is 10%. Oil bleed in a band at top.
3.51	3258′ 10" - 3259′	Sublithographic to earthy, buff to tan, partially anhydrite infilled

calcareous dolostone. Vaguely preserved cryptalgal laminae observed. Porosity is 4%. Light oil stain present.

14 - 13 - 3 - 28W1

K.B. 1561 FT

Sample No.	Depth	Description
4.10	3240′ 3" - 3240′ 5"	Pre-Jurassic unconformity between upper Jurassic Amaranth red bed composed of rust red anhydrite infilled dolomitic siltstone, and lower grey nodular anhydrite.
4.21	3243′ 3" - 3243′ 5"	Lithographic, grey buff, anhydrite infilled dolostone. Vaguely preserved cryptalgal laminae observed. Porosity is < 1%.
4.22	3248′ 1" - 3248′ 3"	Lithographic, grey buff, anhydrite infilled dolostone. Vaguely preserved cryptalgal laminae observed. Porosity is < 1%.
4.23	3250′ 11" - 3251′ 2"	Lithographic, grey buff, anhydrite infilled dolostone. Vaguely preserved cryptalgal laminae observed. Porosity is < 1%.

4.30	3253′ 2" - 3253′ 4"	Lithographic, buff brown, partially anhydrite infilled calcareous dolostone. Vaguely preserved cryptalgal laminae observed. Anhydrite infilled fractures present. Porosity is 5%. Oil bleeding observed.
4.31	3254′ 7" - 3254′ 8"	Earthy to sublithographic, buff, partially anhydrite infilled dolomitic limestone. Vaguely preserved cryptalgal laminae present. Porosity is 7.5%. Light oil stain present.
4.40	3254′ 10" - 3255′	Earthy to sublithographic, buff, massive dolomitic limestone. Encrustation by algal filament observed under microscope. Vertical burrows present. Porosity is 4%. light oil stain observed.
4.41	3256′ - 3256′ 2"	Earthy to sublithographic, buff, partially anhydrite infilled dolomitic limestone. SH type stromatolitic structure recognized. Laminoid as well as irregular

		fenestrae present. Stylolite filled with dead oil observed. Porosity is 5%. Light oil stain present.
4.42	3258′ 2" - 3258′ 4"	Earthy to sublithographic, massive, partially anhydrite infilled limestone. Encrustation by algal filaments observed under microscope. Irregular fenestrae, and sheet cracks as well as vertical desiccation cracks present. Porosity is 7.5%. Light oil stain observed.
4.43	3260′ 8" - 3260′ 10"	Earthy to sublithographic, buff, partially anhydrite infilled dolomitic limestone. SH type stromatolitic structure observed. Laminoid as well as irregular fenestrae, and sheet cracks as well as vertical desiccation cracks present. Porosity is 5%. Light oil stain observed.
4.51	3262′ 2" - 3262′ 5"	Earthy to sublithographic, buff, partially anhydrite infilled calcareous dolostone. LLH type

		stromatolitic structure observed. Laminoid as well as irregular fenestrae, and sheet cracks as well as vertical desiccation cracks present. Porosity is 10%. Light oil stain observed.
4.52	3263′ 10" - 3264′	Earthy to sublithographic, buff, partially anhydrite infilled calcareous dolostone. Stromatolitic structure recognized. Laminoid fenestrae present. Porosity is 15%. Oil stain observed.

15 - 13 - 3 - 28W1

K.B. 1556 FT

Sample No.	Depth	Description
5.11	3237′ 3" - 3237′ 6"	Lithographic, buff grey, anhydrite infilled argillaceous dolostone. Vaguely preserved cryptalgal laminae observed. Swarm of fine clay seams present. Porosity is < 1%.
5.12	3243′ 10" - 3244′ 1"	Lithographic, grey buff, anhydrite infilled dolostone. Vaguely preserved cryptalgal laminae observed. Porosity is < 1%.
5.13	3247′ 7" - 3247′ 10"	Lithographic, light grey buff, anhydrite infilled dolostone. Vaguely preserved cryptalgal laminae observed. Anhydrite infilled fractures present. Porosity is < 1%.
5.21	3248′ 7" - 3248′ 9"	Earthy to sublithographic, buff, partially anhydrite infilled

calcareous dolostone. Vaguely preserved cryptalgal laminae observed. Porosity is ≈ 10%. Oil stain present.

5.30 3250′ - 3250′ 3" Erosional contact present between upper dolomitized cryptalgal laminite, and lower dolomitized pseudostromata.
The former is a sublithogrpahic, buff, partially anhydrite infilled dolomitic limestone. Porosity is ≈ 5%.
The latter is an earthy to sub-lithographic, massive, buff, partially anhydrite infilled dolo-mitic limestone. Vertical desiccation cracks observed. Porosity is ≈ 5%. Light oil stain present. Stylolite observed along the facies boundary.

5.31 3250′ 9" - 3250′ 11" Earthy to sublithographic, buff to grey buff, partially anhydrite infilled dolomitic limestone. LLH type stromatolitic structure recognized. Irregular as well as

laminoid fenestrae, and sheet cracks as well as vertical desiccation cracks observed. Porosity is ≈ 10%. Oil stain present.

5.32	3251′ 9″ – 3252′	Erosional contact present between upper dolomitized stromatolite, and lower dolomitized vadolite. The former is a sublithographic, buff to grey, partially anhydrite infilled dolomitic limestone. LLH type stromatolitic structure recognized. Irregular as well as laminoid, and sheet cracks as well as vertical desiccation cracks observed. Porosity is ≈ 5%. Light oil stain present. The latter is a sublithographic, grey buff, partially anhydrite infilled dolomitic limestone. Constituent particles are vadoids (peloid size through 1.5 mm). Porosity is ≈ 7.5%. Oil stain present.
5.33	3254′ 9″	Sublithographic, buff to buff grey,

	- 3254′ 11"	partially anhydrite infilled dolomitic limestone. Constituent particles are vadoids (peloid size through 1 cm). Associated vadose crusts observed. Porosity is ≈ 15%. Oil stain present.
5.34	3259′ 4"	Sublithographic to earthy, buff,
	- 3259′ 7"	partially anhydrite infilled dolomitic limestone. Constituent particles are vadoids (peloid size through 7 mm). Associated vadose crusts observed. Porosity is ≈ 10%. Oil stain present.

APPENDIX B

CORE ANALYSES DATA

CORE LABORATORIES-CANADA LTD.
REGINA SASKATCHEWAN

Company - KING RESOURCES COMPANY
Well - K-R ET AL PIERSON 1-18-3-28
Field - PIERSON, MANITOBA
Location - LSD 1-18-3-28 WI

Date Report - DECEMBER 10, 1965
Formation - MISSISSIPPIAN
D. Fluid - GYP BASE
Analysis - FULL DIAMETER

Page - 1 of 3
File - CNP-3-4229
Analysts - GP:DP
Cores - DIAMOND

SAMPLE NUMBER	DEPTH REPRESENTED FEET	FOOT. REPR.	PERMEABILITY TO AIR (HORIZONTAL) K MAX	K 90°	VERTICAL	PERM. × FEET	POROSITY PER CENT	POROSITY × FEET	DENSITY BULK	DENSITY GRAIN	VISUAL EXAMINATION
CORED INTERVAL 3206' - 3257'											
CORE NO. 1	3206' - 3257' (Rec. 50.4')										
-	3206.0-3228.7	22.7	-	-	-	-	-	-	-	-	Not analyzed by request
1	3228.7-3229.7	1.0	82.	49.	73.	82.0	18.0	18.00	2.24	2.73	Intergran.PPV.anhydrite, VF.
2	3229.7-3230.5	0.8	6.7	3.7	1.8	5.36	10.0	8.00	2.53	2.81	Intergranular,few SV.PPV.anh
3	3230.5-3231.3	0.8	6.8	6.5	3.6	5.44	9.8	7.84	2.51	2.78	Intergranular, SV.PPV.anhydr
4	3231.3-3232.0	0.7	15.	15.	0.11	10.5	6.9	4.83	2.64	2.83	Intergranular,PPV.anhydrite, shale breaks
5	3232.0-3233.0	1.0	123.	114.	0.69	123.0	15.3	15.30	2.30	2.71	Intergran.PPV.anhydrite, VF.
6	3233.0-3233.8	0.8	222.	222.	1.4	177.6	14.1	11.28	2.34	2.73	Intergranular,PPV. anhydrite
7	3233.8-3234.7	0.9	10.	7.5	0.29	9.0	7.1	6.39	2.59	2.78	Intergran.few SV.anhydrite,V
SS8	3234.7-3235.5	0.8	14.	0.2	0.1	11.2	6.5.	52.0	-	-	Intergranular
9	3235.5-3236.3	0.8	56.	42.	27.	44.8	12.9	10.32	2.50	2.87	Intergranular, PPV. anhydrit
10	3236.3-3237.3	1.0	292.	122.	15.	292.0	12.5	12.50	2.54	2.90	Intergranular, PPV. anhydrit
11	3237.3-3238.5	1.2	1.7	1.4	1.7	2.04	9.9	11.88	2.52	2.80	Intergranular,few SV.PPV.anh
12	3238.5-3239.4	0.9	1.7	1.6	0.92	1.53	11.8	10.62	2.48	2.81	Intergranular, PPV.
13	3239.4-3240.4	1.0	4.0	3.2	2.4	4.00	18.1	18.10	2.27	2.78	Intergranular, few PPV.
14	3240.4-3241.7	1.3	2.3	1.9	1.3	2.99	16.6	21.58	2.38	2.85	Intergranular, few PPV.
15	3241.7-3242.7	1.0	1.9	1.4	0.56	1.90	12.1	12.10	2.50	2.84	Intergran.few PPV.shale brea
16	3242.7-3243.5	0.8	31.	26.	19.	24.8	16.8	13.44	2.31	2.77	Intergranular, PPV. VF.stylo anhydrite
17	3243.5-3244.5	1.0	87.	13.	14.	87.0	19.0	19.00	2.22	2.74	Intergranular, PPV. VF.
18	3244.5-3245.4	0.9	16.	15.	13.	14.4	18.0	16.20	2.23	2.72	Intergranular, PPV.
19	3245.4-3246.4	1.0	49.	49.	8.6	49.0	14.8	14.80	2.34	2.74	Intergranular,SV,PPV.anhydri
20	3246.4-3247.3	0.9	25.	24.	2.8	22.5	12.1	10.89	2.43	2.76	Intergranular,SV.PPV.anhydri
21	3247.3-3248.1	0.8	15.	11.	0.12	12.0	8.9	7.12	2.52	2.77	Intergranular,SV.PPV.anhydri

CORE LABORATORIES-CANADA LTD.
REGINA SASKATCHEWAN

KING RESOURCES COMPANY
K-R ET AL PIERSON 1-18-3-28

SAMPLE NUMBER	DEPTH REPRESENTED FEET	FOOT. REPR.	PERMEABILITY TO AIR (HORIZONTAL) K MAX	K 90°	VERTICAL	PERM. × FEET	POROSITY PER CENT	POROSITY × FEET	DENSITY BULK	DENSITY GRAIN	VISUAL EXAMINATION
CORE NO. 1 CONT'D											
22	3248.1-3248.9	0.8	2.1	1.9	<0.01	1.68	7.2	5.76	2.57	2.77	Intergranular, PPV. anhydrite
23	3248.9-3249.8	0.9	0.57	0.54	<0.01	0.513	10.0	9.00	2.50	2.79	Intergranular,SV.PPV.anhydrite
24	3249.8-3250.8	1.0	1.2	0.85	<0.01	1.20	10.8	10.80	2.50	2.80	Intergranular,SV. PPV.
25	3250.8-3251.8	1.0	2.2	1.9	0.59	2.20	11.8	11.80	2.46	2.79	Intergranular, few SV. PPV.
26	3251.8-3252.7	0.9	2.2	1.5	3.5	1.98	11.7	10.53	2.50	2.84	Intergranular, PPV.
27	3252.7-3253.6	0.9	1.7	1.2	0.16	1.53	10.1	9.09	2.52	2.81	Intergranular,few SV. PPV.
28	3253.6-3254.5	0.9	0.97	0.91	<0.01	0.873	9.2	8.28	2.53	2.79	Intergranular, PPV.
29	3254.5-3255.6	1.1	0.67	0.48	0.25	0.737	9.7	10.67	2.54	2.81	Intergranular, PPV. stylolite
SS30	3255.6-3256.4	0.8	0.2	0.2	0.2	0.16	9.2	7.36	-	-	Intergranular
-	3256.4-3257.0	0.6	-	-	-	-	-	-	-	-	Lost core

PPV - Pin point vugs

SS - Small sample

SV - Small vugs

VF - Vertical fracture

CORE LABORATORIES-CANADA LTD.
REGINA SASKATCHEWAN

Company - KING RESOURCES COMPANY
Well - KR ET AL N PIERSON 3-20-3-28
Field - PIERSON, MANITOBA
Location - LSD 3-20-3-28 WIM

Date Report - SEPTEMBER 28, 1967
Formation - MISSISSIPPIAN
D. Fluid - GYP BASE
Analysis - FULL DIAMETER

Page - 1 of 2
File - CNP-3-5164
Analysts - GB HK
Core - DIAMOND CORES

SAMPLE NUMBER	DEPTH REPRESENTED FEET	FOOT. REPR.	PERMEABILITY TO AIR (HORIZONTAL) K MAX	K 90°	VERTICAL	PERM. × FEET	POROSITY PER CENT	POROSITY × FEET	DENSITY BULK	DENSITY GRAIN	RESIDUAL SATURATION OIL % PORE	RESIDUAL SATURATION TOTAL WATER % PORE	VISUAL EXAMINATIC
CORED INTERVAL 3197' - 3232'													
CORE NO, 1 3197' - 3232' (Rec. 35.0')													
1	3197.0-3202.9	5.9	<0.01	<0.01	<0.01	<0.01	1.1	6.49	2.86	2.89	0.0	69.2	1. A.
2	3202.9-3207.3	4.4	<0.01	<0.01	<0.01	<0.01	2.4	10.56	2.84	2.91	0.0	60.0	1. A.
3	3207.3-3209.7	2.4	<0.01	<0.01	<0.01	<0.01	1.8	4.32	2.85	2.90	0.0	86.6	1. A.
4	3209.7-3211.0	1.3	<0.01	<0.01	<0.01	<0.01	0.6	0.78	2.84	2.86	8.5	59.6	1. A.
5	3211.0-3212.0	1.0	<0.01	<0.01	<0.01	<0.01	1.1	1.10	2.81	2.84	Trace	83.1	1. A.
6	3212.0-3212.9	0.9	<0.01	<0.01	<0.01	<0.01	7.7	6.93	2.68	2.90	1.8	53.0	1. A. PPV.
7	3212.9-3213.8	0.9	<0.01	<0.01	<0.01	<0.01	1.6	1.44	2.76	2.81	0.0	60.6	1. A. PPV
SS8	3213.8-3214.1	0.3	109.	75.	31.	32.7	6.3	1.89	-	-	6.4	38.2	F.sand, A.
9	3214.1-3215.1	1.0	0.14	0.14	<0.01	0.140	2.0	2.00	2.74	2.80	0.0	69.3	1. A.
10	3215.1-3215.9	0.8	0.06	0.06	<0.01	0.048	8.6	6.88	2.46	2.69	Trace	54.4	1. A. PPV
11	3215.9-3216.9	1.0	0.10	0.10	<0.01	0.100	6.8	6.80	2.63	2.82	2.2	54.7	1. A. PPV
12	3216.9-3217.7	0.8	3.7	0.29	0.38	2.96	5.5	4.40	2.64	2.79	7.1	59.0	1. A. PPV
13	3217.7-3218.7	1.0	0.10	0.07	<0.01	0.100	8.9	8.90	2.64	2.90	0.0	70.0	1. A. PPV
14	3218.7-3219.7	1.0	0.18	0.16	<0.01	0.180	11.8	11.80	2.62	2.97	7.3	55.0	1. A. PPV
15	3219.7-3221.2	1.5	0.17	0.14	<0.01	0.255	10.2	15.30	2.50	2.78	0.0	64.4	1. A. VF.
16	3221.2-3222.7	1.5	0.19	0.06	0.11	0.285	9.9	14.85	2.52	2.80	0.0	68.8	1. A. VF. Few PPV.
SS17	3222.7-3222.9	0.2	2.7	2.5	1.5	0.54	13.1	2.62	-	-	19.8	26.7	1.
18	3222.9-3223.9	1.0	1.4	1.4	0.97	1.40	7.9	7.90	2.53	2.74	3.6	55.4	1. A. PPV
19	3223.9-3224.8	0.9	1.8	1.3	0.80	1.62	10.0	9.00	2.44	2.71	9.7	48.4	1. A. PPV
20	3224.8-3225.8	1.0	0.30	0.16	0.36	0.30	8.9	8.90	2.52	2.77	9.1	48.9	1. A. VF.
21	3225.8-3227.1	1.3	2.3	0.44	0.56	2.99	11.4	14.82	2.45	2.76	0.0	51.2	1. A. VF.
SS22	3227.1-3228.1	1.0	0.2	0.2	0.1	0.20	13.8	13.80	-	-	0.0	69.5	1.
SS23	3228.1-3228.8	0.7	0.3	0.3	0.2	0.21	8.7	6.09	-	-	0.0	59.8	1. A.

SAMPLE NUMBER	DEPTH REPRESENTED FEET	FOOT. REPR.	PERMEABILITY TO AIR HORIZONTAL K MAX	HORIZONTAL K 90°)	VERTICAL	PERM. × FEET	POROSITY PER CENT	POROSITY × FEET	DENSITY BULK	DENSITY GRAIN	RESIDUAL SATURATION OIL % PORE	RESIDUAL SATURATION TOTAL WATER % PORE	VISUAL EXAMINA
CORE NO. 1 (Cont'd.)													
SS24	3228.8-3229.6	0.8	<0.1	<0.1	<0.1	<0.1	3.1	2.48	-	-	Trace	71.0	I. A.
25	3229.6-3230.5	0.9	*	0.09	*	0.081	8.8	7.92	2.61	2.86	0.0	58.9	I. A. O
SS26	3230.5-3231.3	0.8	0.1	0.1	0.1	0.08	5.0	4.00	-	-	0.0	66.0	I. A.
SS27	3231.3-3232.0	0.7	0.2	0.1	0.1	0.14	8.6	6.02	-	-	0.0	81.2	I. A.

* - Broken or fractured core
SS. - Small sample
PPV. - Pin point vugs
VF. - Vertical fracture
OVF. - Open vertical fracture
I. - Intergranular
A. - Anhydrite

APPENDIX C

STATISTICAL DATA

DOLOMITE RHOMB SIZE IN MICRONS
FROM DIFFERENT DEPTH INTERVALS

(X1=3228.7-3229.7 FT, X2=3230.5-3231.3 FT
X3=3231.3-3232.0 FT, X4=3235.5-3236.3 FT
X5=3236.3-3237.3 FT, X6=3240.4-3241.7 FT
X7=3242.7-3243.5 FT, X8=3245.4-3246.4 FT
X9=3254.5-3255.6 FT, X10=3255.6-3256.4 FT)

OBS	X1	X2	X3	X4	X5	X6	X7	X8	X9	X10
1	22.08	49.06	22.08	24.53	44.15	34.34	44.15	26.98	19.62	22.08
2	73.58	24.53	39.25	19.62	19.62	26.98	19.62	68.68	53.96	17.17
3	24.53	41.70	26.98	36.79	61.32	19.62	41.70	29.43	24.53	53.96
4	31.89	19.62	31.89	41.70	36.79	49.06	34.34	24.53	44.15	31.87
5	19.62	29.43	34.34	24.53	31.89	17.17	24.53	49.06	29.43	24.53
6	49.06	31.89	19.62	19.62	36.79	56.42	53.96	24.53	63.77	73.58
7	44.15	26.98	26.98	36.79	36.79	24.53	31.89	39.25	31.89	17.17
8	49.06	36.79	41.70	22.08	49.06	73.58	12.26	19.62	31.89	31.89
9	78.49	34.34	36.79	31.89	34.34	51.51	19.62	56.42	49.06	17.17
10	24.53	17.17	29.43	34.34	24.53	44.15	68.68	41.70	22.08	41.70
11	22.08	80.94	73.58	39.25	73.58	36.79	73.58	98.11	34.34	44.15
12	49.06	49.06	31.89	31.89	49.06	17.17	24.53	73.58	36.79	17.17
13	53.96	24.53	17.17	29.43	34.34	19.62	26.98	31.89	29.43	19.62
14	19.62	22.08	24.53	41.70	49.06	31.89	17.17	41.70	17.17	49.06
15	29.43	24.53	26.98	22.08	66.23	78.49	53.96	34.34	41.70	17.17
16	31.89	19.62	44.15	29.43	73.58	24.53	31.89	24.53	22.08	56.42
17	34.34	36.79	34.34	17.17	36.79	36.79	24.53	53.96	24.53	24.53
18	46.60	39.25	24.53	51.51	31.89	26.98	22.08	31.89	44.15	51.51
19	36.79	31.89	22.08	24.53	34.34	44.15	29.43	78.49	36.79	34.34
20	19.62	26.98	36.79	22.08	26.98	36.79	36.79	24.53	29.43	61.32

DATA USED FOR CORRELATION MATRIX

OBS	DEPTH	IN	FEET	DOL	AN	PHAI	LMEAN	LSD	LKMAX	LK90	LKV
1	3228.7	TO	3229.7	56.66	10.00	18.0	3.55	0.43	4.41	3.89	4.29
2	3230.5	TO	3231.3	20.00	3.00	9.8	3.44	0.71	1.92	1.87	1.28
3	3231.3	TO	3232.0	15.00	3.00	6.9	3.42	0.33	2.71	2.71	-2.21
4	3235.5	TO	3236.3	5.00	3.00	12.9	3.36	0.10	4.03	3.74	3.30
5	3236.3	TO	3237.3	25.00	7.50	12.5	3.57	0.13	5.68	4.80	2.71
6	3240.4	TO	3241.7	35.00	17.50	16.6	3.53	0.45	0.83	0.64	0.26
7	3242.7	TO	3243.5	4.00	1.50	16.8	3.44	0.47	3.43	3.26	2.94
8	3245.4	TO	3246.4	20.00	5.25	14.8	3.67	0.46	3.89	3.89	2.15
9	3254.5	TO	3255.6	35.00	1.00	9.7	3.48	0.35	-0.40	-0.73	-1.39
10	3255.6	TO	3256.4	57.50	7.50	9.2	3.45	0.50	-1.61	-1.61	-1.61

NOTICE/AVIS

PAGE(S) Fig. 6, 10, 11, 12 IS/ARE EST/SONT filmed in sections

PLEASE WRITE TO THE AUTHOR FOR INFORMATION, OR CONSULT THE ARCHIVAL COPY HELD IN THE DEPARTMENT OF ARCHIVES AND SPECIAL COLLECTIONS, ELIZABETH DAFOE LIBRARY, UNIVERSITY OF MANITOBA, WINNIPEG, MANITOBA, CANADA, R3T 2N2.

VEUILLEZ ECRIRE A L'AUTEUR POUR LES RENSEIGNEMENTS OU VEUILLEZ CONSULTER L'EXEMPLAIRE DONT POSSEDE LE DEPARTEMENT DES ARCHIVES ET DES COLLECTIONS SPECIALES, BIBLIOTHEQUE ELIZABETH DAFOE, UNIVERSITE DU MANITOBA, WINNIPEG, MANITOBA, CANADA, R3T 2N2.

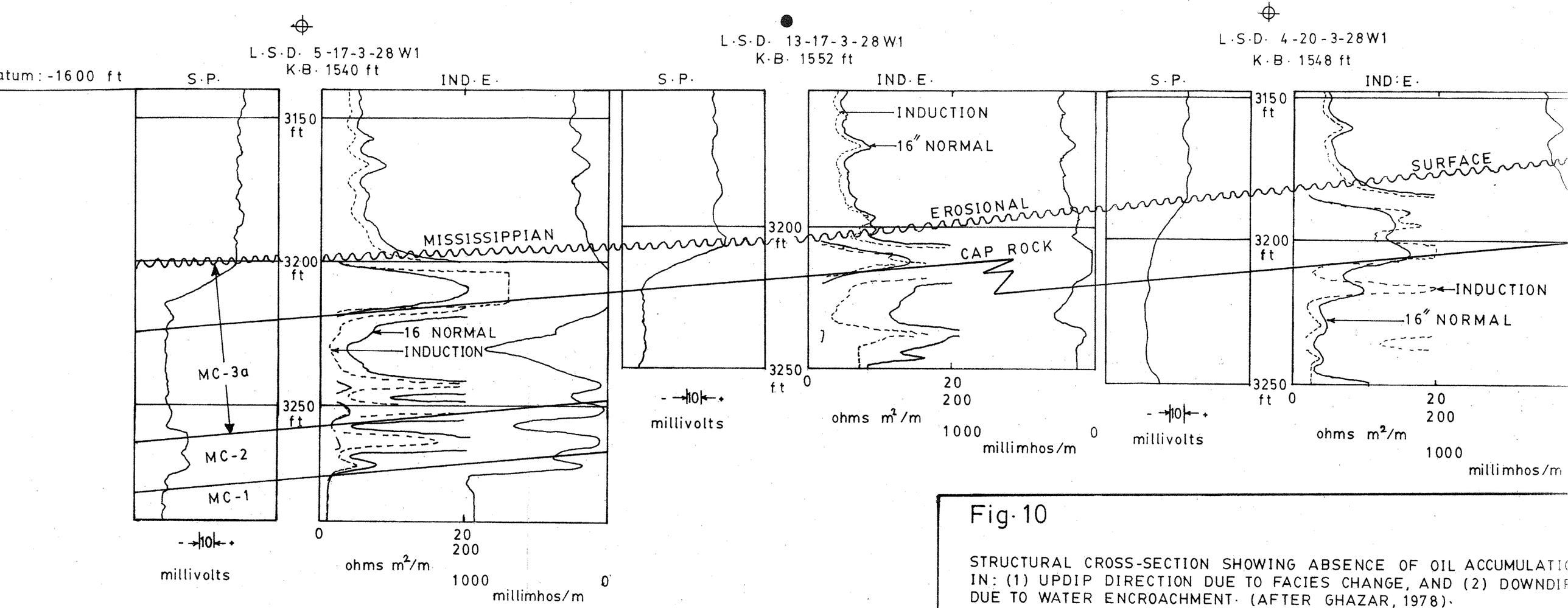

Fig·10

STRUCTURAL CROSS-SECTION SHOWING ABSENCE OF OIL ACCUMULATIO
IN: (1) UPDIP DIRECTION DUE TO FACIES CHANGE, AND (2) DOWNDI
DUE TO WATER ENCROACHMENT· (AFTER GHAZAR, 1978)·

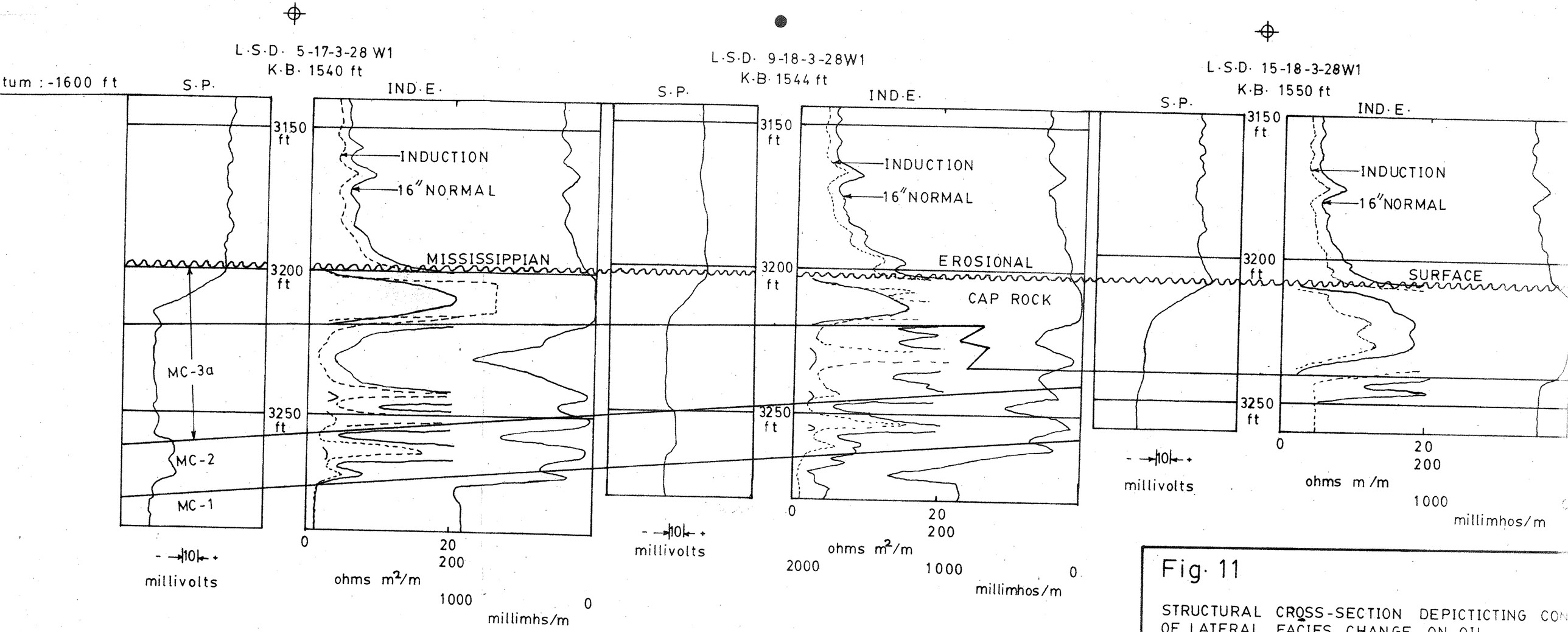

Fig· 11

STRUCTURAL CROSS-SECTION DEPICTICTING CO
OF LATERAL FACIES CHANGE ON OIL
ACCUMULATION·

L·S·D· 1-18-3-28 W1

PERMEABILITY TO AIR
(millidarcy)

1000 100 10 1

POROSITY

10% 20%

AMARANTH FOR.

3209' 2"

ALTERED ZONE

CL

K_{90}

K_{max}

K_v

S

P

CL

3262' 2"

MC-2

PERMEA
(
1000 100

Fig·12

LITHOLOGIC LOGS OF THE STUDIED DRILL CORES· ASSOCIATED POROSITY (ALL WELLS) AND PERMEABILITIES (TWO WELLS) ARE ALSO SHOWN·

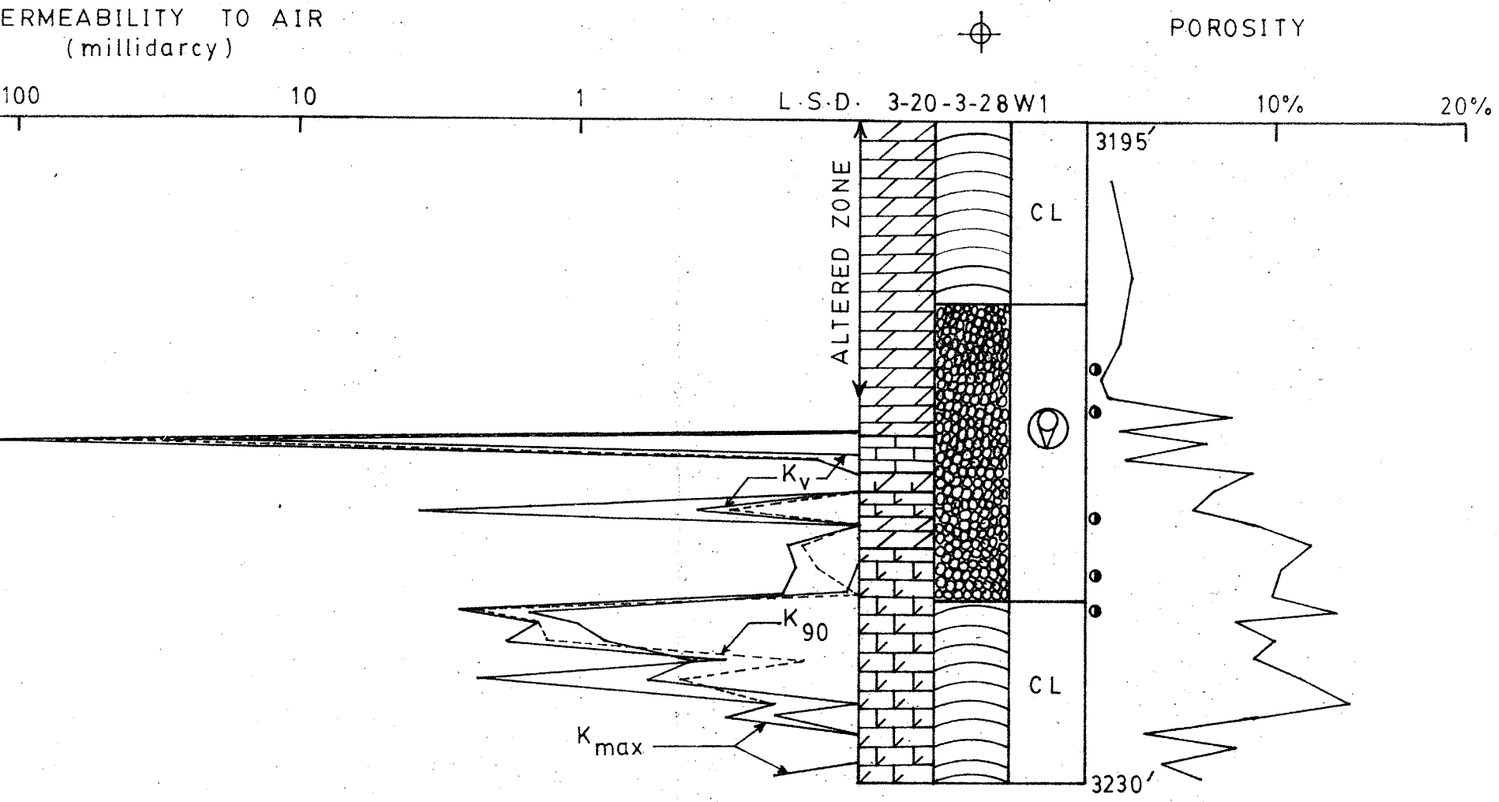
ERMEABILITY TO AIR
(millidarcy)
100
10
1
L·S·D· 3-20-3-28W1
POROSITY
10%
20%
3195′
ALTERED ZONE
CL
K_v
K_{90}
K_{max}
CL
3230′

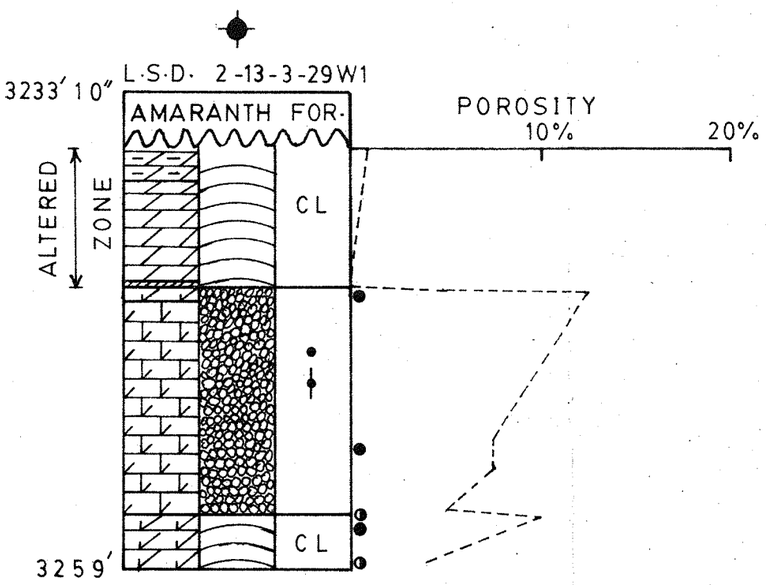
3233′10″
L·S·D· 2-13-3-29W1
AMARANTH FOR·
POROSITY
10%
20%
ALTERED ZONE
CL
CL
3259′

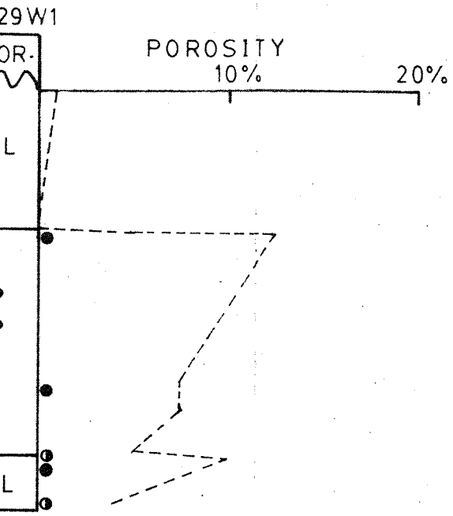
29W1
OR-
L
L
POROSITY
10%
20%

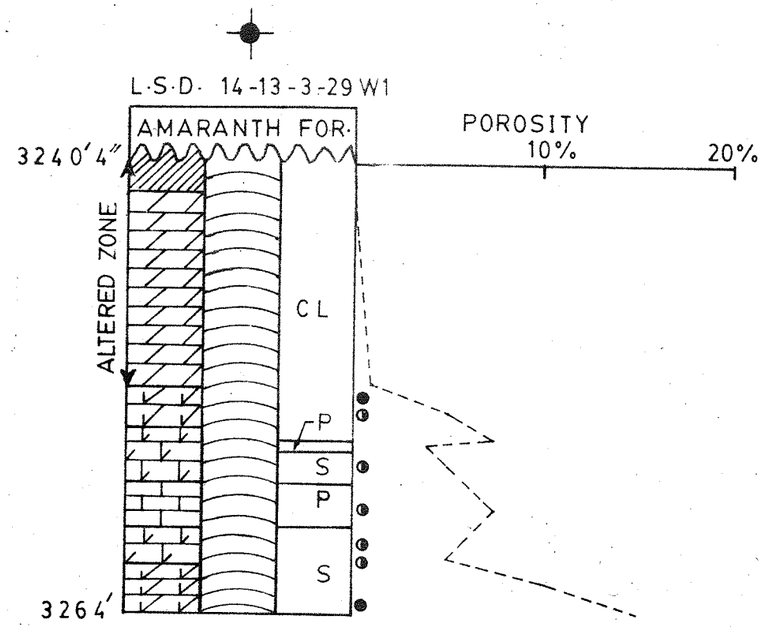
L·S·D· 14-13-3-29W1
AMARANTH FOR·
3240'4"
3264'
ALTERED ZONE
CL
P
S
P
S
POROSITY
10%
20%

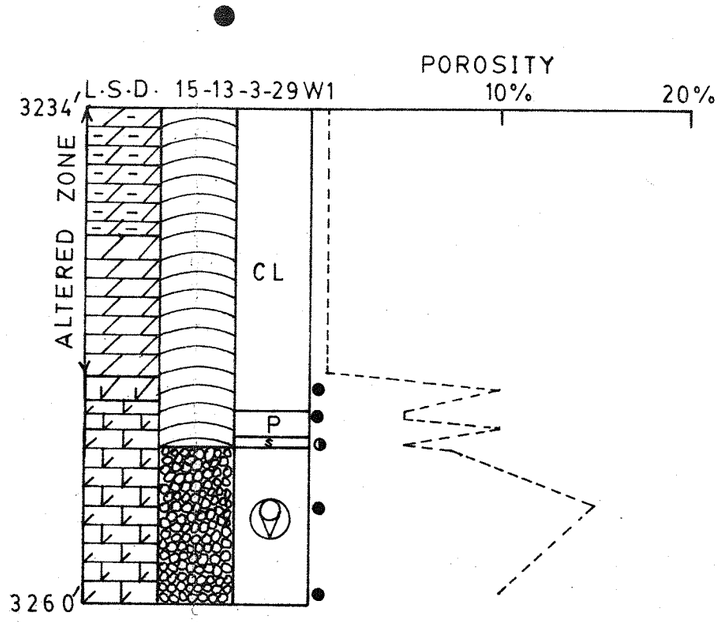
L·S·D· 15-13-3-29W1
3234'
3260'
ALTERED ZONE
CL
P
S
POROSITY
10%
20%

LEGEND

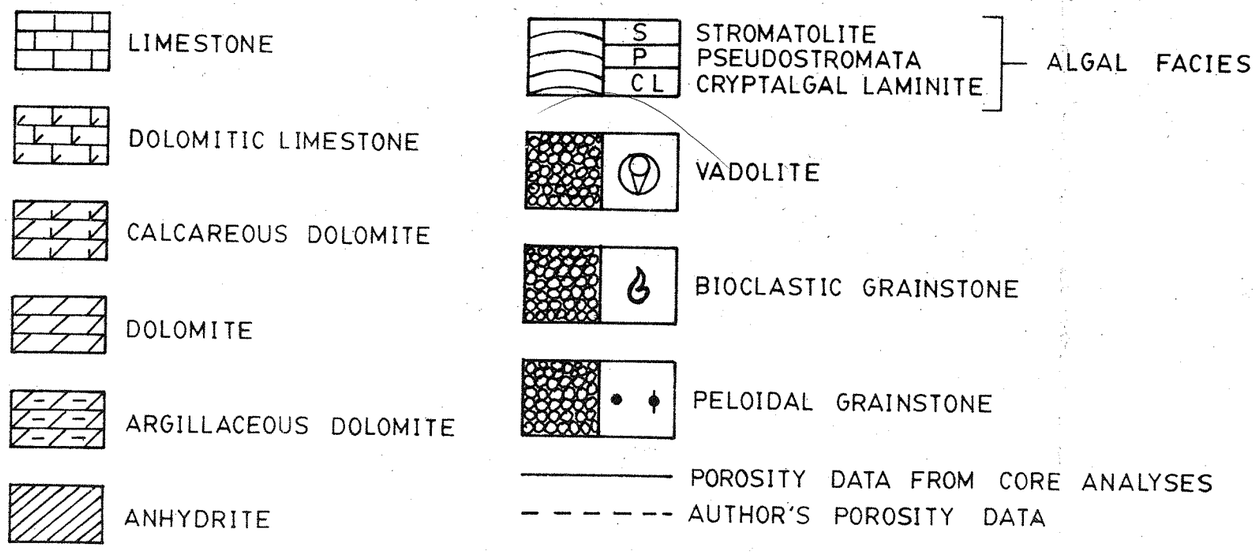
LIMESTONE
DOLOMITIC LIMESTONE
CALCAREOUS DOLOMITE
DOLOMITE
ARGILLACEOUS DOLOMITE
ANHYDRITE
S
P
CL
STROMATOLITE
PSEUDOSTROMATA
CRYPTALGAL LAMINITE
ALGAL FACIES
VADOLITE
BIOCLASTIC GRAINSTONE
PELOIDAL GRAINSTONE
POROSITY DATA FROM CORE ANALYSES
AUTHOR'S POROSITY DATA

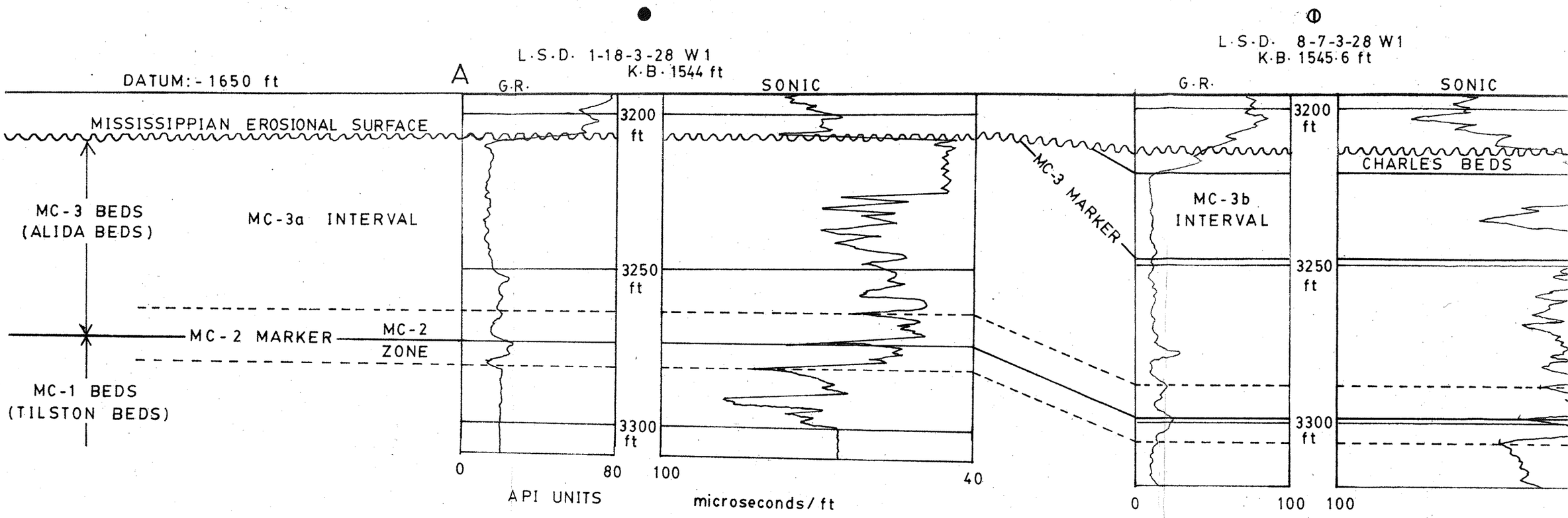

Fig· 6

STRUCTURAL CROSS-SECTION DEPICTING CORRELATION OF MISSION CANYON MEMBERS BETWEEN PIERSON AND WASKADA AREAS· (AFTER HALABURA, 1984, AND ROGERS, 1984) (SEE FIG·1 FOR LINE OF CROSS-SECTION)·

IND·E·

16″ NORMAL

INDUCTION

0/0 20
200

ohm m²/m

1000 0

millimhos/m

L·S·D· 14-20-2-28 W1
K·B· 1526 ft

S·P· G·R· IND·E·

3200 ft

3250 ft

Z—18″

3300

INDUCTION

3350 ft

-→|10|←+ millivolts

Radiation Intensity Increases

0 20
200

ohms m²/m

L·S·D· 1-22-2-28 W1
K·B· 1505·7 ft

S·P· E·LOG

3200 ft

3250 ft

3300 ft

64″ NORMAL

16″ NORMAL

-→|10|←+ millivolts

0 20
200

ohms m²/m

L·S·D· 1-11-2-28 W1
K·B· 1497 ft

S·P· | G·R· | SONIC | IND·E·

3150 ft
3200 ft
3250 ft
3300 ft
3350 ft

18" NORMAL
INDUCTION

- →|10|← +
millivolts

0 — 120
API UNITS

140 — 40/0
microseconds/ft

20 — 200
ohm m^2/m

L·S·D· 10-6-2-27W1
K·B· 1505 ft

S·P· | G·R· | SONIC

3200 ft
3250 ft
3300 ft

- →|10|← +
millivolts

0 — 150
API UNITS

140 — 40/0
microseconds/ft

L·S·D· 16-16-1-27 W1
K·B· 1497 ft

G·R·

NEUTRON

E·LOG

L·S·D· 7-16-1-26 W1
K·B· 1510 ft

S·P·

G·R·

3150 ft

3200 ft

3250 ft

3300 ft

3350 ft

16" NORMAL

64" NORMAL

AMPLIFIED 16" NORMAL

18'-8" LATERAL

EP
ION

-8

20
200

Radiation Intensity Increases

6

neutron counts/sec

406/0

20/0
200

20
200

ohm m^2/m

0←amplified 16 normal→4

3200 ft

3250 ft

-110+

0

120

millivolts

API UNITS

140

micr

L·S·D· 7-16-1-26 W1
K·B· 1510 ft

A´

E·LOG

16 " NORMAL

64" NORMAL

AMPLIFIED 16" NORMAL

18'-8" LATERAL

20/0 200

20 200

ohm m^2/m

16 normal → 4

S·P·

millivolts

G·R·

0 120

API UNITS

3200 ft

3250 ft

SONIC

140

microsecons/ft

IND·E·

INDUCTION

16" NORMAL

40/0

20 200

ohms m^2/m

2000 1000 0

3000 2000

millimhos/m